



International Workshop on
Microcavities & their applications
25th - 29th November 2024
Tūhura Otago Museum,
419 Great King Street,
Dunedin New Zealand 9016

This template originates from [LaTeXTemplates.com](https://www.latextemplates.com) & is based on the original version at:
https://github.com/maximelucas/AMCOS_booklet

Contents

About	7
WOMA	7
Organizing committee	7
Local organizing committee at University of Otago	7
Timetable	8
Monday, 25th November	8
Tuesday, 26th November	9
Wednesday, 27th November	10
Thursday, 28th November	11
Friday, 29th November	12
Abstracts – Monday 25th November	13
Kyungwon An - Recent progresses in single-atom superradiance	13
Qi-Tao Cao - Universal critical dynamics of non-equilibrium phase transition in photonic resonators	14
Li Ge - Novel resonances and exceptional points in non-Hermitian optical systems	16
Hugo Girin - Non-Euclidean Photonics with a Hyperbolic Surface: Experiments and Numerics	17
Síle Nic Chormaic - Emission Patterns from 2D and 3D Deformed Microcavities	19
Miro Erkintalo - Parametrically-driven cavity soliton frequency combs in pure-Kerr microresonators	20
Matthew Macnaughtan - Spontaneous Soliton Formation Under Pulsed-Pumping Conditions in a Coherently Driven Passive Kerr Resonator	22
Takasumi Tanabe - Mode-locking in coupled microresonators using exceptional point modulation .	24
Andrew Poon - Silicon Carbide Microresonators for Integrated Nonlinear and Quantum Photonic Applications	26
Kerry Vahala - New opportunities for high-Q integrated devices and systems	27
Abstracts – Tuesday 26th November	28
Lan Yang - Opportunities in Whispering-Gallery Microresonators: Fundamentals and Applications	28
Jan Wiersig - Spectral response strength of non-Hermitian optical systems at and near higher-order exceptional points	29
Nicholas Lambert - Using exceptional points for coherent control of a hybrid system	30
Luke Trainor - Optically detected spin state of erbium dopants in a whispering-gallery resonator .	32
Takao Aoki - Nanofiber Cavity Quantum Electrodynamics for Quantum Network	33
Wenjie Wan - Slow and Fast light in a microcavity	34
Min Wang - Taming Brillouin optomechanics using supermode microresonators	36
Guoping Lin - Harnessing Crystalline Anisotropy in Whispering Gallery Mode Resonators for Enhanced Nonlinear Optical Processes	38
Zaijun Chen - Photonic AI Computing using Coherent Microcavity Lasers	39
Xi Yang - Fast thermogenic detection with a microlaser	40
Abstracts – Wednesday 27th November	42
Yanne Chembo - Stochastic and quantum dynamics of microcombs	42
Qi-Fan Yang - A quantum perspective of Kerr microcombs	43
Jordan Wise - Tunable Non-Phaselocked Solitons in Pulse-Driven Passive Kerr Resonators Mediated by Stimulated Raman Scattering	45
Youling Chen - Directional light emission and nanoparticle detection based on WGM microcavities	47

Mallika Suresh - Multichannel THz upconversion in a LiNbO ₃ optical resonator	49
Andrey Matsko - Photonic Oscillators Involving Bulk Optical Cavities	51
Takahisa Harayama - Self-organization of lasing modes in chaotic billiard lasers	53
Chengcai Tian - Stimulated Raman lasing and second harmonic generation in lithium tetraborate whispering gallery mode resonators	54
Muhan Choi - Implementing Non-Euclidean Microcavity in 2D Flat space	56
Abstracts – Thursday 28th November	58
Beibei Li - Fully integrated, ultrahigh-sensitivity cavity optomechanical ultrasound sensors	58
Yongyong Zhuang - Whispering gallery mode resonator based on PMN-PT single crystal	60
Stuart Murdoch - Kerr solitons in fiber cavities – past and present	62
Wang Liao - All-optical injection Locking of Dissipative Breather Solitons in Microresonators	64
Baicheng Yao - Soliton Microcomb-based Point and Distributed Optical Fiber Sensors	66
Vahid Sandoghdar - Cavity-induced coupling of a handful of molecules	67
Christophe Pin - Singular field in the nanogap of a plasmonic multimer antenna excited by a circularly-polarized plane wave	68
Shui-Jing Tang - Microcavity vibrational spectroscopy for single-cell fingerprinting	70
Mengjie Yu - Ultrafast Nonlinear Photonics on Thin Film Lithium Niobate	72
Fangxin Zhang - Modular sub-Hertz linewidth laser self-injection-locked to a whispering-gallery-mode resonator	73
Abstracts – Friday 28th November	75
Martina Hentschel - Steering complex dynamics in anisotropic and coupled microcavities	75
Hui Cao - Nonlinear optical encoding with a linear scattering cavity	77
Julius Kullig - High-order exceptional points in systems of waveguide-coupled microring cavities	79
Gabriella Gardosi - PicoSNAP: towards the picometre-precise fabrication of WGM microresonators and their applications	81
Zhen Shen - Frequency conversion in optomechanical microresonators	82
Keiji Sasaki - Topological control of localized electric fields in plasmonic nanocavities	84
Dmitry Srekalov - Polarization entangled photons from a whispering gallery resonator	86
Suwan Sun - Radiofrequency Electrometry with an Electrooptic Whispering-Gallery-Mode Resonator	88
Zhi-Gang Hu - Picotesla-sensitivity microcavity optomechanical magnetometry	90
Poster Abstracts	92
Amal Jose - Hollow, Egg-Like Whispering Gallery Mode Resonator	92
Binbin Nie - Soliton microcombs in X-cut LiNbO ₃ microresonators	94
Boyi Xue - Dual-color Coherent Perfect Absorber	96
Farhan Azeem - Titanium doped Sapphire and Whispering Gallery Modes: An Effective Combination for Low Threshold Lasing and Amplification	98
Florian Lorenz - Structure of chaotic resonance modes in dielectric cavities	99
Jalaludeen Mohammed - Development of vector magnetometer based on hollow core whispering gallery resonators and nitrogen-vacancy centers in diamond	101
Jisung Seo - Toward Observation of Superradiance at an Exceptional Point of a Birefringent Fabry-Perot Cavity	103
Josh Christensen - Newton's rings interferometry for absolute distance calibration	105
Juman Kim - Birefringence EP in a high-finesse Fabry-Perot cavity	106
Junseo Ha - Spectrum of a superradiant laser with injected atomic coherence	108
Kang Xu - High-resolution microwave frequency identification via a hybrid microbottle cavity	110
Maika Mitogawa - Nonlinear Laser Dynamics of an Asymmetric Optical Microcavity	112
Quan-Xin Luo - Surface-acoustic-wave-assisted vibrational spectroscopy using an integrated mi- croresonator	114

Ramgopal Madugani - Precision Spectral and Spatial Optimisation of Whispering Gallery Modes in Microbubble Cavities	116
Rui-Qi Zhang - Chaos-enhanced chirality in optical microcavities	118
Samuel Begumya - Coupling of NV centers in diamond to adiabatically tapered optical nanofibers .	120
Seongju Lee - Resonant Mode Calculation in Large-scale 3-Mirror Ring Resonators via Transformation Optics	122
Shuai Wan - Soliton Microcombs in the High-Q Lithium Niobate Microresonators	124
Songyi Liu - Properties extraction of optical microcavity coupling system based on coupled mode theory-informed neural network	126
Wensong Yan - Enhancing Cavity Optomechanics by Magnetically-mediated Photothermal Effect .	128
Xiao-Chong Yu - Single-Molecule Optofluidic Microsensor with Interface Whispering Gallery Modes	130
Xiaomin Lv - Microwave-rate dark pulse microcombs in integrated LiNbO ₃ microresonators	132
Xing Jin - Microresonator-referenced soliton microcombs with zeptosecond-level timing noise	134
Yanwu Liu - Microresonator-based Vortex Spectroscopy	136
Yoshikazu Kuribayashi - Self-organized formation of nonlinear scar modes	138
Yupei Liang - Graphene-assisted mode locking of optomechanical combs in a microresonator	139
Ze Wang - Large-scale cluster quantum microcombs	141
Zhenzhong Hao - Efficient second and third harmonic generation in dual-layer lithium niobate resonator	143
Zongda Li - Desynchronisation dynamics of ultrashort dissipative Raman solitons	145

List of Participants **147**

Biographies of Invited Speakers **150**

Prof. Andrew Wing On Poon	150
Dr Andrey B. Matsko	151
Prof. Baicheng Yao	152
A/Prof. Beibei Li	153
Dr Dmitry V. Srekalov	154
Dr Gabriella Gardosi	155
A/Prof. Guoping Lin	156
Prof. Hui Cao	157
Prof. Jan Wiersig	158
Prof. Keiji Sasaki	159
Prof. Kerry J. Vahala	160
Prof. Kyungwon An	161
Prof. Lan Yang	162
Prof. Li Ge	163
Prof. Martina Hentschel	164
Asst. Prof. Mengjie Yu	165
A/Prof. Miro Erkintalo	166
Prof. Muhan Choi	167
Asst. Prof. Qi-Fan Yang	168
Dr Scott B. Papp	169
Asst. Prof. Shui-Jing Tang	170
Prof. Sile Nic Chormaic	171
A/Prof. Stuart Murdoch	172
Prof. Takahisa Harayama	173
Prof. Takao Aoki	174
Prof. Takasumi Tanabe	175
Prof. Vahid Sandoghdar	176
A/Prof. Wenjie Wan	177

Prof. Yanne Chembo	178
Prof. Youling Chen	179
Asst. Prof. Zaijun Chen	180
Useful Information	181
Partner Institutions & Sponsors	182

WOMA

International Workshop on Microcavities & their applications (WOMA) is a leading international conference series on optical microcavities and their applications. The 7th WOMA will be held in Aotearoa New Zealand at the University of Otago in Ōtepoti Dunedin during the 25th - 29th November 2024. This conference will be in person during spring on the South Island of New Zealand. Scholars around the world of the optical microcavity community will share & discuss their latest work & insights in this rapidly expanding field. The five-day Workshop will include invited talks, contributed talks, student poster presentations & social activities in Dunedin. Invited speakers include preeminent researchers in the field, Prof. Kerry Vahala (Caltech), Prof. Hui Cao (Yale), and Prof. Vahid Sandoghdar (Max Planck Institute for the Science of Light). Three Best Student Paper Awards will be awarded.

Organizing committee

A/Prof. Harald Schwefel
University of Otago
Dunedin, New Zealand

Prof. Warwick Bowen
University of Queensland
Brisbane, Australia

Prof. Yun-Feng Xiao
Peking University
Beijing, China



Local organizing committee at University of Otago

Dr Farhan Azeem
Researcher

Dr Nicholas Lambert
Research Fellow

Dr Florian Sedlmeir
Postdoctoral Fellow

Dr Mallika Suresh
Agnes-Blackie Research Fellow



Timetable

CT: Contributed Talk, IT: Invited Talk, FT: Feature Talk.

Monday, 25th November

8:30–9:40	Registration and Welcome remarks		
9:40–10:20	IT	Prof Kyungwon An Seoul National University, Seoul, Korea	Recent progresses in single-atom superradiance
10:20–10:40	CT	Mr Qi-Tao Cao Peking University, Beijing, China	Universal critical dynamics of non-equilibrium phase transition in photonic resonators
10:40–11:10	Morning tea		
11:10–11:50	IT	Prof Li Ge City University of New York, NY, USA	Novel resonances and exceptional points in non-Hermitian optical systems
11:50–12:10	CT	Mr Hugo Girin CNRS Paris-Saclay, Gif-sur-Yvette, France	Non-Euclidean Photonics with a Hyperbolic Surface: Experiments and Numerics
12:10–12:50	IT	Prof Sile Nic Chormaic OIST, Okinawa, Japan	Emission Patterns from 2D and 3D Deformed Microcavities
12:50–13:50	Lunch		
13:50–14:30	IT	A/Prof Miro Erkintalo University of Auckland, Auckland, New Zealand	Parametrically driven soliton frequency combs in pure Kerr resonators
14:30–14:50	CT	Mr Matthew Macnaughtan University of Auckland, Auckland, New Zealand	Spontaneous Soliton Formation Under Pulsed-Pumping Conditions in a Coherently Driven Passive Kerr Resonator
14:50–15:30	IT	Prof Takasumi Tanabe Keio University, Yokohama, Japan	Mode-locking in coupled microresonators using exceptional point modulation
15:30–16:00	Afternoon Tea		
16:00–16:40	IT	Prof Andrew Wing On Poon Hong Kong University of Science and Technology, Hong Kong	Silicon Carbide Microresonators for Integrated Nonlinear and Quantum Photonic Applications
16:40–17:30	FT	Prof Kerry Vahala California Institute of Technology, Pasadena, CA, USA	New opportunities for high- Q integrated devices and systems
17:30–19:00	Welcome reception & Poster session		

Tuesday, 26th November

9:00–9:40	IT	Prof Lan Yang Washington University in St Louis, St. Louis, MO, USA	Opportunities in Whispering-Gallery Microresonators: Fundamentals and Applications
9:40–10:20	IT	Prof Jan Wiersig Otto-von-Guericke-Universität Magdeburg, Magdeburg, Germany	Spectral response strength of non-Hermitian optical systems at and near higher-order exceptional points
10:20–10:40	CT	Dr Nicholas Lambert University of Otago, Dunedin, New Zealand	Using exceptional points for coherent control of a hybrid system
10:40–11:10	Morning tea		
11:10–11:50	IT	Dr Scott Papp NIST National Institute of Standards, Boulder, CO, USA	Nonlinear nanophotonics for quantum sensing and frequency combs
11:50–12:10	CT	Dr Luke Trainor University of Otago, Dunedin, New Zealand	Optically detected spin state of erbium dopants in a whispering-gallery resonator
12:10–12:50	IT	Prof Takao Aoki Waseda University, Tokyo, Japan	Nanofiber Cavity Quantum Electrodynamics for Quantum Network
12:50–13:50	Lunch		
13:50–14:30	IT	A/Prof Wenjie Wan Shanghai Jiao Tong University, Shanghai, China	Slow and fast light in a microcavity
14:30–14:50	CT	Ms Min Wang Key Lab of Optical Physics, Chinese Academy of Science, Beijing, China	Taming Brillouin optomechanics using supermode microresonators
14:50–15:30	IT	A/Prof Guoping Lin Harbin Institute of Technology, Shenzhen, China	Harnessing Crystalline Anisotropy in Whispering Gallery Mode Resonators for Enhanced Nonlinear Optical Processes
15:30–16:00	Afternoon Tea		
16:00–16:40	IT	Asst. Prof Zaijun Chen University of Southern California, Los Angeles, CA, USA	Photonic AI Computing using Coherent Microcavity Lasers
16:40–17:00	CT	Dr Xi Yang Peking University, Beijing, China	Fast thermogenic detection with a microlaser
17:00	Free evening		

Wednesday, 27th November

9:00–9:40	IT	Prof Yanne Chembo University of Maryland, College Park, MD, USA	Stochastic and quantum dynamics of microcombs
9:40–10:20	IT	Asst. Prof Qi-Fan Yang Peking University, Beijing, China	A quantum perspective of Kerr microcombs
10:20–10:40	CT	Mr Jordan Wise University of Auckland, Auckland, New Zealand	Tunable Non-Phaselocked Solitons in Pulse-Driven Passive Kerr Resonators Mediated by Stimulated Raman Scattering
10:40–11:10	Morning tea		
11:10–11:50	IT	Prof Youling Chen Institute of Semiconductors, CAS, Beijing, China	Directional light emission and nanoparticle detection based on WGM microcavities
11:50–12:10	CT	Dr Mallika Suresh University of Otago, Dunedin, New Zealand	Multichannel THz upconversion in a LiNbO ₃ optical resonator
12:10–12:50	IT	Dr Andrey Matsko JPL, NASA, USA	Photonic Oscillators Involving Bulk Optical Cavities
12:50–13:50	Lunch		
13:50–14:30	IT	Prof Takahisa Harayama Waseda University, Tokyo, Japan	Self-organization of lasing modes in chaotic billiard lasers
14:30–14:50	CT	Mr Chengcai Tian University of Otago, Dunedin, New Zealand	Stimulated Raman lasing and second harmonic generation in lithium tetraborate whispering gallery mode resonators
14:50–15:30	IT	Prof Muhan Choi Kyungpook National University, Daegu, Korea	Implementing Non-Euclidean Microcavity in 2D Flat space
15:30–16:00	Afternoon Tea		
18:00–21:00	Conference dinner at Larnach Castle (till late)		

Thursday, 28th November

Late Start			
9:40–10:20	IT	A/Prof Beibei Li Institute of Physics, Chinese Academy of Sciences, Beijing, China	Fully integrated, ultrahigh-sensitivity cavity optomechanical ultrasound sensors
10:20–10:40	CT	A/Prof Yongyong Zhuang Xi'an Jiaotong University, Xi'an, China	Whispering gallery mode resonator based on PMN-PT single crystal
10:40–11:10	Morning tea		
11:10–11:50	IT	Prof Stuart Murdoch University of Auckland, Auckland, New Zealand	Kerr solitons in fiber cavities - past and present
11:50–12:10	CT	Mr Wang Liao University of Auckland, Auckland, New Zealand	All-optical Injection Locking of Dissipative Breather Solitons in Microresonators
12:10–12:50	IT	Prof Baicheng Yao UESTC, Chengdu, China	Soliton Microcomb-based Point and Distributed Optical Fiber Sensors
12:50–13:50	Lunch		
13:50–14:30	IT	Prof Vahid Sandoghdar Max Planck Institute for the Science of Light, Erlangen, Germany	Cavity-induced coupling of a handful of molecules
14:30–14:50	CT	Dr Christophe Pin OIST, Okinawa, Japan	Singular field in the nanogap of a plasmonic multimer antenna excited by a circularly-polarized plane wave
14:50–15:30	IT	Asst. Prof Shui-Jing Tang Peking University, Beijing, China	Microcavity vibrational spectroscopy for single-cell fingerprinting
15:30–16:00	Afternoon Tea		
16:00–16:40	IT	Asst. Prof Mengjie Yu University of Southern California, Los Angeles, CA, USA	Ultrafast Nonlinear Photonics on Thin Film Lithium Niobate
16:40–17:00	CT	Dr Fangxing Zhang Peking University, Beijing, China	Modular sub-Hertz linewidth laser self-injection-locked to a whispering-gallery-mode resonator
17:00–19:00	Poster session		

Friday, 29th November

9:00–9:40	IT	Prof Martina Hentschel TU-Chemnitz, Chemnitz, Germany	Steering complex dynamics in anisotropic and coupled microcavities
9:40–10:20	IT	Prof Hui Cao Yale University, New Haven, CT, USA	Nonlinear optical processing with a linear multiple-scattering cavity
10:20–10:40	CT	Dr Julius Kullig Otto von Guericke University, Magdeburg, Germany	High-order exceptional points in systems of waveguide-coupled microring cavities
10:40–11:10	Morning tea		
11:10–11:50	IT	Dr Gabriella Gardosi Aston University, Birmingham, United Kingdom	PicoSNAP: towards the picometre-precise fabrication of WGM microresonators and their applications
11:50–12:10	CT	Asst. Prof Zhen Shen Key Lab of Quantum Information, CAS, Hefei, China	Frequency conversion in optomechanical microresonators
12:10–12:50	IT	Prof Keiji Sasaki Hokkaido University, Sapporo, Hokkaidô, Japan	Topological control of localized electric fields in plasmonic nanocavities
12:50–13:50	Lunch		
13:50–14:30	IT	Dr Dmitry Strekalov University of Otago, Dunedin, New Zealand	Polarization entangled photons from a whispering gallery resonator
14:30–14:50	CT	Ms Suwan Sun University of Adelaide, Adelaide, Australia	Radiofrequency Electrometry with an Electrooptic Whispering-Gallery-Mode Resonator
14:50–15:10	CT	Mr Zhi-Gang Hu Institute of Physics, Chinese Academy of Sciences, Beijing, China	Picotesla-sensitivity microcavity optomechanical magnetometry
15:30–16:00	Afternoon Tea		
16:00–17:00	Poster awards & Concluding remarks		

Recent progresses in single-atom superradiance

Kyungwon An

IT

Seoul National University, Seoul, Korea

A superradiant state is a phase-correlated quantum state of atoms capable of undergoing superradiance immediately without a time delay. We can prepare a superradiant state in an optical cavity by exciting N atoms in the same superposition of the ground and excited states with a common phase angle by using a nanohole array aperture. These correlated atoms generate superradiance in the cavity even when the mean number of intracavity atoms is much less than unity [1]. As an application, the superradiant state can be used to realize the long-sought superabsorption, the opposite of superradiance, by reversing the superradiance process in time through the phase control of the superradiant state [2]. Another application is a photonic quantum engine, where the atoms entering the cavity act as a heat reservoir and the photons are an engine medium exerting radiation pressure on the cavity mirrors. Our engine operates between a thermal state and a superradiant state of reservoir at the same reservoir temperature. In our experiment, the effective engine temperature rose up to 150,000K because of the large ergotropy transfer from the reservoir through superradiance, resulting in the engine efficiency as high as 98%, the highest ever achieved in quantum engines [3]. Moreover, our superradiant lasing does not exhibit the conventional laser threshold that would occur around unity mean photon number. We observed the coherent photon statistics even when the mean photon number was far less than unity. The superradiant lasing occurs with the mean photon numbers between $\beta = (g\tau)^2$ and $1/\beta$ with the coupling constant g and the interaction time τ . One can increase the dynamical range greatly by making $\beta \ll 1$, which is achieved by employing a high-speed high-density ion beam in a long cavity. Recent progresses toward a thresholdless macroscopic superradiant laser in this direction will be discussed.

References

- [1] Junki Kim et al., "Coherent single-atom superradiance", *Science* **359**, 662 (2018).
- [2] Daeho Yang et al., "Realization of superabsorption by time reversal of superradiance", *Nature Photonics* **15**, 272 (2021).
- [3] Jinuk Kim et al., "A photonic quantum engine driven by superradiance", *Nature Photonics* **16**, 707 (2022).

Universal critical dynamics of non-equilibrium phase transition in photonic resonators

Qi-Tao Cao^{1,*}, Yun-Feng Xiao¹

CT

¹ Frontiers Science Center for Nano-optoelectronics, New Cornerstone Science Laboratory, School of Physics, Peking University, 100871 Beijing, China

* caoqt@pku.edu.cn

Abstract: In this work, we report the non-equilibrium phase transition of laser fields in a photonic microresonator, of which the power-law scaling within the critical dynamics is experimentally revealed.

1. Introduction

Non-equilibrium is ubiquitous in optics and photonics, where the steady state arises from the driven-dissipative balance rather than thermal equilibrium. Various fundamental processes of light can be perceived as phase transitions in non-equilibrium, including laser generation, optical parametric oscillation, and more recent discoveries in non-Hermitian physics such as PT -symmetry breaking. Besides the rich phenomena inspiring essential physics studies, the switch between different optical states in non-equilibrium phase transitions (NEPTs) is crucial for cutting-edge applications typified by photonic computation and exotic energy transfer. In particular, use of nonlinear optical processes has demonstrated substantial potential in a range of emerging tasks, e.g. serving as a convolution core for machine learning or solving non-polynomial problems [1].

As a theoretical framework, the Kibble-Zurek mechanism (KZM) describes the non-equilibrium critical dynamics displayed by systems undergoing transitions between different physical phases within a finite timescale. Specifically, the KZM offers universal scaling laws of relaxation with finite ramping rates, which govern the transition dynamics even spanning from cosmological domain structures, atomic Bose-Einstein condensates, to superfluids and superconductors [2]. In the realm of photonics, understanding the non-equilibrium critical dynamics of light fields is essential as the time scaling law sets fundamental limits on the operation rate of the applications. However, it is challenging to observe the critical phenomena out of equilibrium in photonic systems, due to their fast dynamics and vulnerability to noise. Here we experimentally construct an NEPT in miniaturized photonic resonators, in which the light fields can transit between the two nearly degenerate lasing states with the opposite parities (Fig. 1A). Experimentally, the critical dynamics is observed in real-time during the transition process (Figs. 1B and C), and the power-scaling law of the transition time is demonstrated following the prediction by the KZM (Fig. 1D).

2. Methods and Results

The microlaser operated in this work is generated by optically pumping a spherical microresonator, which supports a pair of nearly degenerate supermodes with opposite parities, i.e., the anti-symmetric mode a_- and the symmetric mode a_+ . Due to the mode competition [3], only the mode with the smallest loss lases above the threshold (Fig. 1A), which can be utilized for ground-state searching. Here we study the transition of lasing state between two supermodes by dynamically controlling the losses κ_- and κ_+ of the supermodes [represented by a generalized parameter ϵ in Fig. 1B]. When ϵ ramps across the critical point ϵ_c with balanced losses $\kappa_+ = \kappa_-$, the lasing mode switches after the transient state. The relaxation time τ_r toward steady state diverges at the critical point ϵ_c (Fig. 1B), giving $\tau_r \propto |\epsilon - \epsilon_c|^{-\nu z}$ described by the KZM [2]. Here ν and z ($\nu, z > 0$) denote static and dynamic critical exponents, respectively. Therefore, when ramping across the NEPT with a fixed scanning speed u , the system dynamics can be classified into two regimes: The system is away from the critical point, so that the lasing state evolves adiabatically and remains at the supermode a_- or a_+ due to the faster relaxation rate $1/\tau_r$ (Fig. 1A, left and right panel). As the system approaches and crosses the critical point, the original lasing state begins to switch to the other supermode, but the reaction is too sluggish to follow the parameter ramping and becomes non-adiabatic due to the faster ramping rate u (middle panel). Hence, the transition time τ_t within the interaction can be obtained by the boundary of the non-adiabatic region (red circles in Fig. 1B), i.e., $\tau_t \propto u^{-\nu z/(1+\nu z)}$ [2].

We directly observe the real-time transition by monitoring the frequency detuning between the laser and a fixed probe light. As the control parameter scanned across the critical point, the signal of the a_+ mode diminishes, and the a_- laser emerges, presenting an evident intermediate transition process marked by the region between the dashed lines in Fig. 1C. The offset frequency ~ 75 MHz corresponds to the frequency difference between the probe light and the center frequency of the supermode laser. We find a power law dependence of the transition time, defined as the time in regime (2), on the ramp rate that matches the KZM prediction (Fig. 1D), with the exponent $(\nu z)/(1 + \nu z) = 0.49 \pm 0.03$. Interestingly, this measured critical exponent is consistent with that in NEPTs of exciton-polaritons, suggesting that the observed universal behavior may exist in general driven-dissipative systems. Nevertheless, topological defects, widely observed in phase transitions of condensed matter systems, do not exist in this specific NEPT process but can present in similar coupled resonator architecture. Therefore, we use the temporal relaxation, another universal behavior, to characterize the NEPT here.

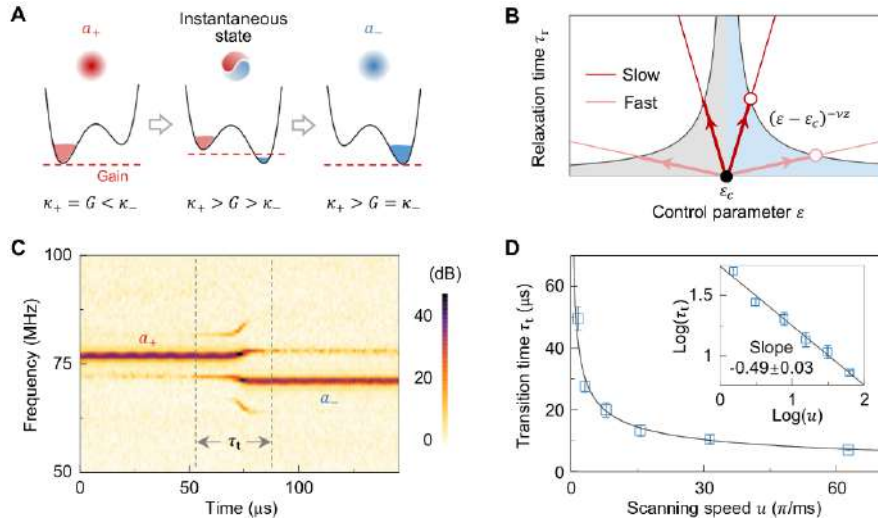


Fig. 1. **A**, Schematic transition of the optical field in a WGM microresonator from a_+ to a_- with the photon population, by ramping a control parameter across the critical point. Black curves: the effective potential of the nearly-degenerate supermodes; Red horizontal lines: optical gain rate G . **B**, The relaxation time τ_t relies on the distance to the critical point ϵ_c , depicted by the black curve. The red (pink) line represents the ramping of the control parameter with a slower (faster) speed. The thicker lines in the shaded area mark the transition process whose duration corresponds to the transition time τ_t . **C**, Measurement of the NEPT process from a_+ to a_- lasing. **D**, Scaling law of the transition time τ_t versus the ramp speed of the control parameter, with a double logarithmic plot (inset). Blue squares: the experimental data; black curve (line): the power (linear) fitting. The error bars represent the standard deviation of 5 measurements.

3. Summary

In summary, we have observed and harnessed the non-equilibrium phase transition of the coupled microlasers in a photonic resonator, by developing the RF readout and interference coupling technique. The critical phenomenon is revealed experimentally, and the scaling law of transition time predicted by the KZM is demonstrated, with the measured exponent νz to be about 1. This scaling imposes an upper limit for the convergence rate when similar photonic systems are used for ground state searching. Moreover, the universality of this time scaling is confirmed to be independent of the choice of parameters, as well as the increased system complexity, indicating the ability of its application in large networks. Moreover, the unveiled scaling law can provide universal guidance for understanding the fundamental time limit of the rapid switch of light fields, especially for the convergence rate of photonic computation, e.g., coherent Ising machines [1].

References

- [1] Inagaki, T. et al. A coherent Ising machine for 2000-node optimization problems. *Science* 354, 603 (2016).
- [2] Zurek, W. H. Cosmological experiments in superfluid helium? *Nature* 317, 505 (1985).
- [3] Zhang, P.-J., Ji Q.-X., Cao Q.-T., Wang H., Liu W., Gong Q., and Xiao Y.-F., Single-mode characteristic of a supermode microcavity Raman laser, *PNAS* 118(22), e2101605118 (2021).

Novel resonances and exceptional points in non-Hermitian optical systems

Li Ge^{1,2,*}

IT

¹ Department of Physics and Astronomy, College of Staten Island, City University of New York, New York, United States

² Graduate Center, City University of New York, New York, United States

* li.ge@csi.cuny.edu

Exceptional points (EPs) are a unique non-Hermitian phenomenon, where not only do the eigenvalues of an operator (the scattering matrix, the Hamiltonian, etc.) become degenerate but also the corresponding eigenstates become identical. In this talk, I will first discuss EPs with previously unexpected optical dispersion relations, i.e., at the center of a 2D Dirac cone [1]. In such a case, an imaginary gauge transformation also establishes the equivalence between certain non-Hermitian systems of two different types, namely, those with optical gain/loss and those featuring asymmetric couplings. In the presence of a non-Hermitian gauge field, we identified a new mechanism that enables strong model interactions and single-mode lasing in laser arrays [2]. Combining it with spin-orbital coupling, I will also discuss the underlying principle that led to the precise control of a micro-ring laser system emitting into a four-dimensional Hilbert space [3]. Lastly, I will talk about an active photonic resonance [4] that does not have an origin in a passive resonance, which ushered in new possibilities in the designing of laser cavities and other resonance structures. If time allows, I will touch on our recent work on robust non-Hermitian zero modes without a global symmetry [5] and a linear optical analogy of the fermionic Kitaev chain and Majorana bound states.

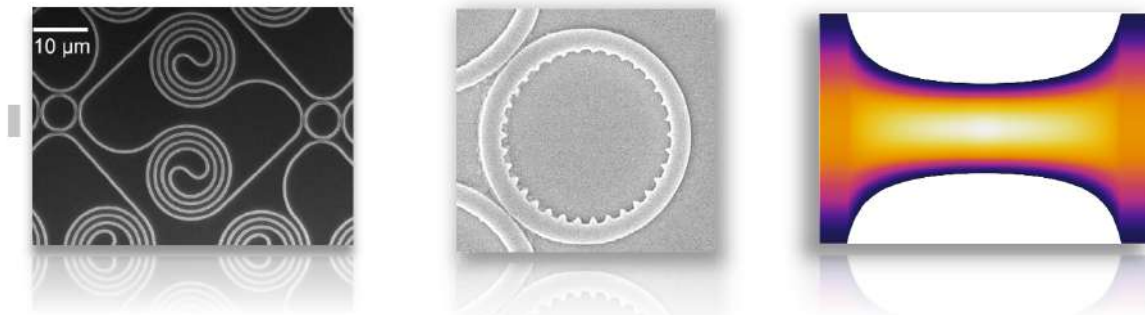


Fig. 1. (From left to right) A laser array with a non-Hermitian gauge field [2]; a ring resonator from a non-Hermitian photomolecule laser with spin-orbital coupling; a cavity hosting an active resonance [4].

References

- [1] Rivero, Feng, and Ge, Phys. Rev. Lett. 129, 243901 (2022).
- [2] Gao et al., Phys. Rev. Lett. 130, 263801 (2023).
- [3] Zhang et al., Nature 612, 246 (2022).
- [4] Rivero et al., Phys. Rev. Lett. 126, 163901 (2021).
- [5] Rivero et al., Phys. Rev. Lett. 131, 223801 (2023).

Non-Euclidean Photonics with a Hyperbolic Surface: Experiments and Numerics

H. Girin^{1,*}, *D. Decanini*¹, *X. Checoury*¹ and *M. Lebental*¹

CT

¹ Centre de Nanosciences et de Nanotechnologies, CNRS, Université Paris-Saclay, 10 Boulevard Thomas Gobert, Palaiseau, 91120, France.

* hugo.girin@c2n.upsaclay.fr

Abstract: Non-Euclidean Photonics on a hyperbolic surface is investigated in this paper. Both experimental and numerical results are developed for the case of dielectric tractoid microlasers fabricated with high optical quality by direct laser writing. © 2024 The Author(s)

1. Introduction

Hyperbolic surfaces are surfaces with a constant negative curvature. Theoreticians have intensively studied such surfaces over the last century. In particular, in the theory of quantum chaos, hyperbolic surfaces can exhibit strong chaoticity [1]. Literature is filled with relevant theoretical results about quantum chaos with hyperbolic surfaces. However, there are very few experimental works to validate those theoretical results. This paper reports experiments and numerics about a hyperbolic surface called the tractoid (cf. Fig. 1(a)). The tractoid is a 2D surface with a constant negative curvature embedded in \mathbb{R}^3 [2]. The lower boundary (blue line) is circular, and the top of tractoid goes to infinity.

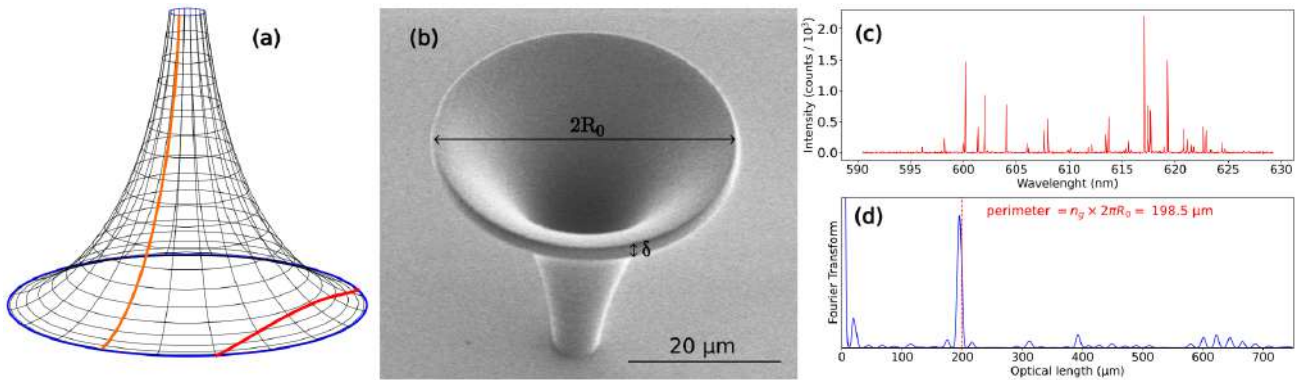


Fig. 1. (a) Tractoid surface with the lower circular boundary in blue. The orange line (the tractrix) and the red line are two geodesics. (b) SEM image of a tractoid microlaser with radius $R_0 = 20 \mu\text{m}$ and thickness $\delta = 2 \mu\text{m}$. (c) Experimental laser spectrum of a tractoid microlaser with $R_0 = 20 \mu\text{m}$ and $\delta = 1 \mu\text{m}$. (d) Normalized Fourier transform of the spectrum. The optical perimeter of the tractoid microlaser is indicated with a red dashed line, and n_g is the group index.

2. Tractoid microlasers and experimental results

Experiments are performed on tractoid microlasers fabricated with high optical quality by direct laser writing (cf. [3] for more information about the fabrication). The radius of the tractoid microlasers is $R_0 = 20 \mu\text{m}$, and the thickness δ can vary from 1 to $3 \mu\text{m}$. The top of the tractoids is cut perpendicularly to the rotational axis so that their size is not infinite (cf. Fig. 1(b)). The tractoid microlasers were pumped individually and with uniform intensity by a beam perpendicular to the substrate from a frequency-doubled Nd:YAG laser (532 nm, 500 ps, 10 Hz). Their emission was analyzed by a spectrometer with an overall resolution of 0.03 nm. A typical experimental spectrum of the tractoid microlaser is presented in Fig. 1(c). The spectrum is almost comb-like. As shown in [3], we expect modes to be localized along periodic geodesics (PGs). The length of the PG is linked to the spacing between two consecutive peaks. Therefore, the Fourier transform of this spectrum has been computed in Fig. 1(d). A single peak (and residual harmonics) is obtained, and its position is very close to the perimeter of the tractoid. It indicates that lasing modes are nothing but Whispering Gallery Modes (WGMs) propagating around the circular boundary of the tractoid.

3. Semiclassical study of the tractoid

To compare with experimental results, the tractoid has been studied analytically and numerically using a semiclassical approach (i.e., classical dynamics of rays and resolution of the wave equation). Miscellaneous results are quickly introduced in the following.

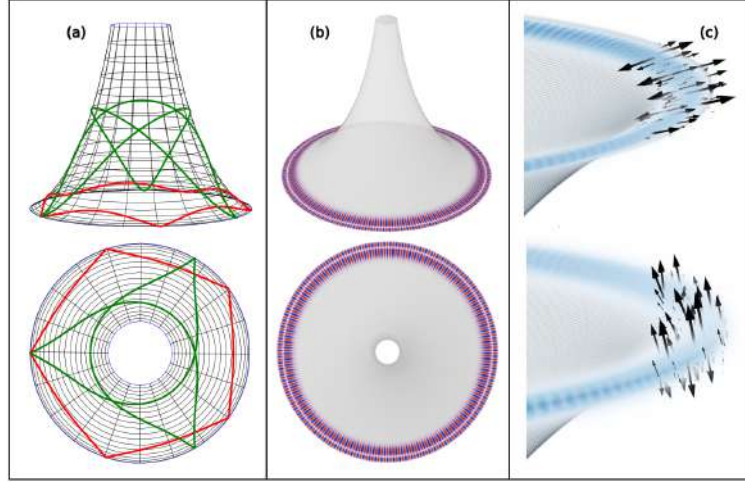


Fig. 2. (a) Different views of two PGs of the tractoid. (b) Different views of a single analytical scalar wavefunction. (c) Zoom on the right part of two different vectorial modes obtained by numerical Finite Difference Time Domain (FDTD). Black arrows indicate the electric field polarization. The upper mode is TE-polarized, whereas the bottom one is TM-polarized.

3.1 Ray dynamics

First, PGs of the tractoid have been classified. Every PG can be classified by the number of bounces on the circular boundary and the number of complete 2π -rotations around the surface (cf. Fig. 2(a)). Then, the stability of these PGs can be computed by using the monodromy matrix for the propagation over a distance t on a tractoid of radius R_0 , which is given by

$$\Pi(t) = \begin{pmatrix} \cosh\left(\frac{t}{R_0}\right) & R_0 \sinh\left(\frac{t}{R_0}\right) \\ \frac{1}{R_0} \sinh\left(\frac{t}{R_0}\right) & \cosh\left(\frac{t}{R_0}\right) \end{pmatrix} \quad (1)$$

After computations, the tractoid is marginally stable, as expected for systems with rotational symmetry.

3.2 Resolution of the wave equation

The scalar wave equation is the Helmholtz equation with a curvilinear Laplacian, which depends on the metric. It can be simplified using the rotational symmetry to separate the variables. The solution of this equation can be expressed using the *Modified Bessel function of Second Kind* K_m . Modes have been computed for Dirichlet boundary conditions and their wavefunction plotted in Fig. 2(b). Finally, the full vectorial wave equation was numerically solved using homemade FDTD simulations. The vectorial wavefunction of two modes has been plotted in Fig. 2(c). Modes belong to two distinct classes of polarization, TE-modes and TM-modes, as expected for flat surfaces.

4. Conclusion

To conclude, thanks to tractoid microlasers one has been able to have a first walk around experimental properties of quantum-like hyperbolic surfaces. Despite its constant negative curvatures, the tractoid is integrable due to its rotational symmetry. Therefore, the tractoid acts similarly to the disk with WG lasing modes and marginally stable dynamics. Nevertheless, this comparison between the disk and the tractoid may give rise to interesting asymptotic properties between the wavefunction of the disk (Bessel function) and the wavefunction of the tractoid (modified Bessel function).

References

- [1] R. Aurich, M. Sieber, and F. Steiner, “Quantum Chaos of the Hadamard-Gutzwiller Model” *Phys. Rev. Lett.* **61** (1988).
- [2] N. L. Balazs, A. Voro, “Chaos on the pseudosphere” *Physics Reports* **143**, 109–240 (1986).
- [3] Y. Song, M. Lebental et al. “Möbius Strip Microlasers: A Testbed for Non-Euclidean Photonics” *Phys. Rev. Lett.* **127**, 203901 (2021).

Emission Patterns from 2D and 3D Deformed Microcavities

Tom Rodemund^{1,2}, Shilong Li^{1,3}, Martina Hentschel², and Sîle Nic Chormaic^{1,*}

IT

¹ Okinawa Institute of Science and Technology Graduate University, Onna, Okinawa 904-0495 Japan

² Institute of Physics, Technische Universität Chemnitz, D-09107 Chemnitz, Germany

³ College of Information Science and Electronic Engineering, Zhejiang University, Hangzhou 310058, China

* sile.nicchormaic@oist.jp

Abstract: Here, we discuss mode-dependent chiral emissions that may appear from deformed cavities and the far-field directionality that results when two cavities are coupled to each other via their optical fields.

Studies on non-Hermitian physics [1] has gained popularity in relation to describing optical microcavities, resulting in interesting features, e.g. time-parity-symmetry in whispering gallery cavities [2]. When two passive, deformed optical cavities are coupled to each other, interesting dynamics are observable. Here, we consider the coupling of two deformed, dielectric microcavities and the nature of the near- and far-field emissions. The cavities are slightly deformed from a circular geometry, defined in terms of a parameter, ϵ . Using a Husimi function approach [3], we demonstrate mode-dependent chirality of the coupled system for the deformed cavities that does not appear for circular geometries [4].

Figure 1 illustrates the system under consideration. Initially, we focus on two identical deformed disks, with a Q-factor on the order of 10^4 for each cavity. These cavities demonstrate whispering gallery type modes, with the intensity varying around the circumference due to the deformation from the ideal circular profile. By varying the separation distance, D , we study the evolution of the eigenmodes for the coupled system and define a strong coupling regime when $D < \lambda/2$, where λ is the vacuum wavelength of the light. Experimental verification of the numerical results is desirable and will be a focus of future studies.

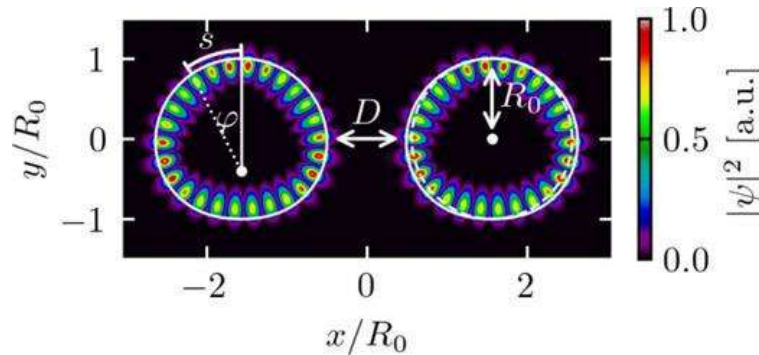


Figure 1: System of two coupled limaçon cavities, separated by a distance D , and R_0 is the mean radius. An even mode intensity distribution is illustrated for a distance $D = \lambda$. Reproduced from [4], with the permission of AIP Publishing.

References

- [1] C. M. Bender, “Making sense of non-Hermitian Hamiltonians,” *Rep. Prog. Phys.* 70, 947 (2007).
- [2] B. Peng, Ş. K. Özdemir, F. Lei, F. Monifi, M. Gianfreda, G. L. Long, S. Fan, F. Nori, C. M. Bender, and L. Yang, “Parity-time-symmetric whispering-gallery microcavities,” *Nat. Phys.* 10, 394 (2014).
- [3] M. Bosch, A. Behrens, S. Sinzinger, and M. Hentschel, “Husimi functions for coupled optical resonators,” *J. Opt. Soc. Am. A*, 38, 573 (2021).
- [4] T. S. Rodemund, S. Nic Chormaic, and M. Hentschel, “Coupled deformed microdisk cavities featuring non-Hermitian properties,” *Appl. Phys. Lett.* 124, 051107 (2024).

Parametrically-driven cavity soliton frequency combs in pure-Kerr microresonators

Miro Erkintalo^{1,2,*}, *Gregory Moille*^{3,4}, *Zongda Li*^{1,2}, *Miriam Leonhardt*^{1,2}, *David Paligora*^{1,2}, *Nicolas Englebert*⁵, *Francois Leo*⁵, *Julien Fatome*⁶ and *Kartik Srinivasan*^{3,4}

IT

¹ Department of Physics, University of Auckland, Auckland 1010, New Zealand

² The Dodd-Walls Centre for Photonic and Quantum Technologies, New Zealand

³ Joint Quantum Institute, NIST/University of Maryland, College Park, USA

⁴ Microsystems and Nanotechnology Division, National Institute of Standards and Technology, Gaithersburg, USA

⁵ Service OPERA-Photonique, Université libre de Bruxelles (U.L.B.), 50 Avenue F. D. Roosevelt, CP 194/5, B-1050 Brussels, Belgium

⁶ Laboratoire Interdisciplinaire Carnot de Bourgogne, UMR 6303 CNRS Université de Bourgogne, Dijon, France

* m.erkintalo@auckland.ac.nz

Abstract: We theoretically and experimentally show that bichromatic driving of pure-Kerr microresonators allows for the generation of parametrically driven cavity soliton frequency combs. We also discuss the solitons' existence and stability. © 2024 The Author(s)

Dissipative Kerr cavity solitons (CSs) are pulses of light that can persist indefinitely in dispersive Kerr resonators driven with continuous wave (CW) laser light [1]. They underpin the coherent and broadband optical frequency combs that can be generated in on-chip microresonators, which have found numerous applications from metrology to telecommunications. A key feature of such CSs is the fact that they are unique attractors: for any given set of system parameters, only a single type of soliton can exist. In addition, they form spectrally around the coherent laser that drives the cavity, and that driving field is accordingly part of the frequency comb associated with the soliton. These two features can be disadvantageous or altogether prohibitive for some applications.

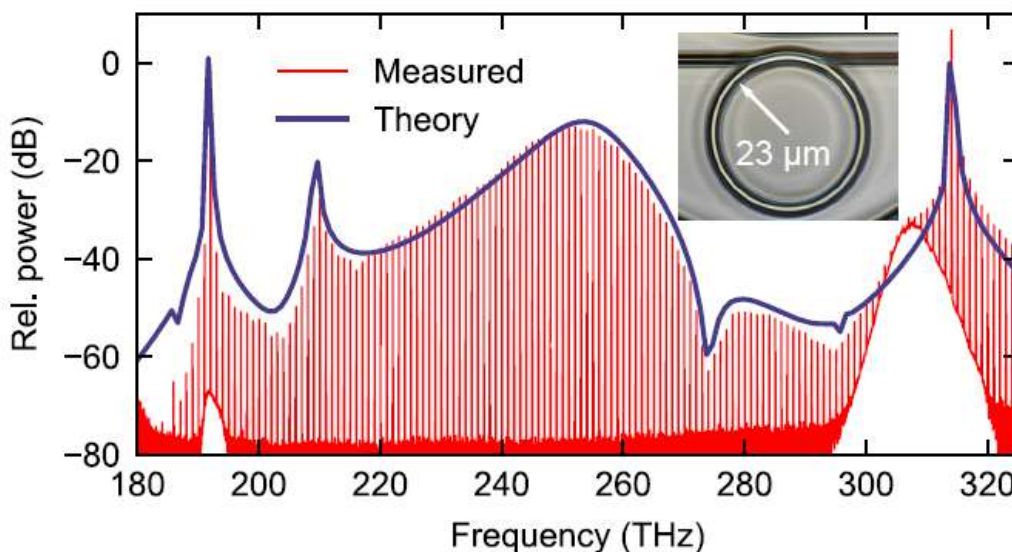


Fig. 1. Red curves show a coherent PDCS frequency comb spectrum generated in a silicon nitride microresonator (see inset for a micrograph). Blue curve shows results from numerical simulations [2].

We have recently unveiled – both theoretically and experimentally – a new paradigm of soliton generation

that can be reached in coherently-driven Kerr resonators [2]. Here, a judiciously dispersion-engineered resonator is driven with two monochromatic lasers with large frequency separation, giving rise to a cavity soliton frequency comb with carrier frequency in between the two inputs via parametric four-wave-mixing [Fig. 1]. In stark contrast to conventional Kerr CSs, these parametrically-driven cavity solitons (PDCSs) come in two different flavours with opposite phase, which could unlock altogether new applications requiring a binary degree of freedom. In this presentation, we will discuss the existence, stability, and characteristics of the parametrically-driven cavity solitons that can exist in Kerr resonators under conditions of bichromatic driving.

References

- [1] T. J. Kippenberg, A. L. Gaeta, M. Lipson, and M. L. Gorodetsky, “Dissipative Kerr solitons in optical microresonators,” *Science* **361** (2018).
- [2] G. Moille, M. Leonhardt, D. Paligora, N. Englebert, F. Leo, J. Fatome, K. Srinivasan, and M. Erkintalo, “Parametrically driven pure-Kerr temporal solitons in a chip-integrated microcavity,” *Nature Photonics* **18**, 617–624 (2024).

Spontaneous Soliton Formation Under Pulsed-Pumping Conditions in a Coherently Driven Passive Kerr Resonator

Matthew Macnaughtan^{1,2,*}, *Zongda Li*^{1,2}, *Yiqing Xu*^{1,2}, *Xiaoming Wei*³, *Zhongmin Yang*³, *Stéphane Coen*^{1,2}, *Miro Erkintalo*^{1,2}, and *Stuart Murdoch*^{1,2}

¹ Department of Physics, University of Auckland, Auckland, New Zealand

² The Dodd-Walls Centre for Photonic and Quantum Technologies, Auckland, New Zealand

³ School of Physics and Optoelectronics, South China University of Technology, Guangzhou 510640, People's Republic of China

* mmac848@aucklanduni.ac.nz

Abstract: We unveil a novel dynamical regime in which dissipative Kerr cavity solitons spontaneously emerge in a coherent, pulse-driven passive Kerr resonator. The regime is robust against perturbations, ensuring reliable and deterministic cavity soliton generation. © 2024 The Author(s)

Dissipative temporal cavity solitons (CSs), first observed in a fiber ring cavity in 2010 [1], are ultra-short localized pulses of light that can circulate indefinitely within an optical cavity without distortion. They have attracted particular attention in the context of optical microresonators, where they enable the realisation of coherent broadband optical frequency combs. Driven by the many potential applications of such frequency combs — from real-time spectroscopy [2] to ultra-fast ranging [3]—the applied potential of CSs is now beginning to be realised. Therefore, it is no surprise that over the past few years there has been a push towards tackling more practical issues, chief among these being the reliable and robust generation of CSs. For many cavity architectures, CS generation typically required the intracavity field to be either externally seeded [1] or subject to a parameter ramp that forces the field to undergo a substantial state change from modulation instability (MI) to a CS state [4]. Although such methods are known to work, they often require a prohibitive suite of equipment, as well as being susceptible to environmental perturbations or generating a random pattern of CSs at each realisation. More recently, efforts have been made towards injection-locking systems in which CSs can be generated through the use of Rayleigh scattering as a feedback mechanism [5]. Although such systems show promise in tiny microresonator setups, in macroscopic systems, Brillouin scattering may prove to be a compromising factor. In this contribution, we experimentally and numerically explore a pulse-driven passive Kerr resonator, identifying a new parameter regime where CSs can spontaneously emerge, thus eliminating the need for external seeding or parameter ramping through MI. Furthermore, we show that, in addition to single isolated soliton states, deterministic generation of complex CS bound states (molecules) can also be realised thanks to higher-order dispersion.

In our experiments, we use a 0.29-m-long dispersion-shifted fiber enclosed in a Fabry–Pérot (FP) system of two dielectric-coated fiber tips (yielding a free spectral range of 350 MHz and a finesse of 180). We drive our cavity with a train of picosecond pulses obtained from an electro-optic (EO) comb. The pump repetition rate, f_p , can be readily controlled by adjusting the clock frequency, allowing us to systematically control the desynchronisation, ΔT , between the pump repetition rate and the cavity roundtrip time. We actively stabilise our pump detuning, δ , via a Pound-Drever-hall technique. To numerically model our system, we make use of the Lugiato-Lefever equation (LLE) with higher-order dispersion and Raman scattering terms included [6]. For the measurements discussed below, we set the central wavelength of our pump to 1565 nm, putting us into the anomalous group-velocity dispersion (GVD) regime (the zero dispersion wavelength of our fiber is located at 1553 nm, and significant third- and fourth-order dispersive terms are also present).

In our first experiment, we demonstrate the spontaneous emergence of CSs. Specifically, we first ramp the cavity detuning (while maintaining the desynchronisation) through MI to values for which CSs exist, illustrating the conventional method for CS generation, then gradually increase the detuning till the intracavity field can no longer sustain a CS and collapses to the lower homogeneous steady-state (HSS). We then re-tune the detuning back to its initial value, observing the spontaneous generation of CSs in the absence of any external perturbation or MI. The experimentally measured spectral evolution is compiled into a pseudo-coloured map and displayed in Fig. 1(a), with Fig. 1(b) showing the simulated temporal evolution of the region outlined by the dashed white box in Fig. 1(a). Finally, Fig. 1(c) shows both an experimental (blue) and simulated (red) spectrum of the intracavity field taken from Fig. 1(a) at a detuning of 0.055 rad. Both Figs. 1(a) and (b) illustrate how, in the appropriate parameter region, a CS can spontaneously form out of the intracavity field under pulsed-pumping conditions. The physical mechanism that underpins the observed CS self-generation can be explained in terms of switching wave dynamics. Specifically, because the pump is inhomogeneous, each position along the intracavity field sees different driving conditions. This opens

up the possibility for spontaneous up-switching to occur at localised points along the intracavity pulse, effectively self-seeding CSs.

For our second experiment, we show how under this particular pulsed-pumping scheme, both singular and bound CS states can be reliably selected. To achieve this, we first tune into the fundamental CS state, then gradually change the pump desynchronisation, ΔT , until a bound state is achieved. Once such a state forms, we then reverse the desynchronisation until once again we generate the fundamental CS state. Figure 1(e) shows an experimentally acquired pseudo-coloured map of this process, with Fig. 1(d) showing the numerically simulated temporal result when using the same parameters as in (e). We can clearly observe deterministic switching between the fundamental CS state (with smooth spectral envelope) and bound states (that exhibit spectral interference).

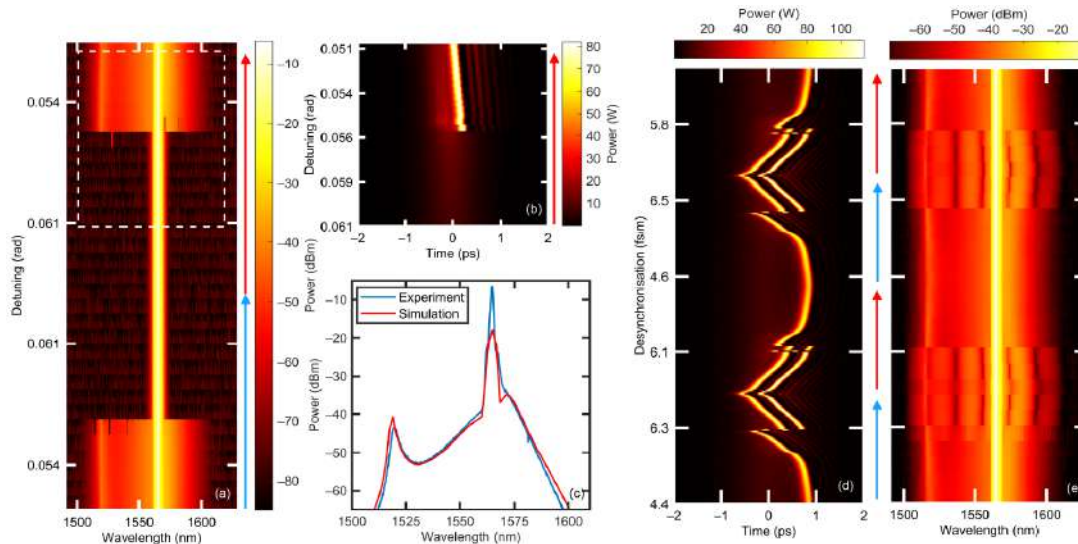


Fig. 1. (a) Experimentally measured spectra of spontaneous CS formation after the cavity is forced into the lower HSS via a detuning scan when driving with a picosecond driving pulse at a peak power of 2.3 W with $\Delta T = 4.4$ fs/m. (b) Numerically simulated temporal trace of the region outlined by the dashed white box in (a) under the same driving conditions. (c) Experimentally measured spectrum (blue) taken from (a) at a detuning $\delta = 0.055$ rad overlapped with a numerically simulated one (red). (e) Experimentally measured spectral map of bound and singular CS formation when changing the pump desynchronisation with $\delta = 0.068$ rad at a peak driving power of 3.2 W. (d) shows, using the same parameters in (e), the numerically simulated temporal evolution of the intracavity field when subjected to the same change in desynchronisation seen in (e). The red (blue) arrows beside the pseudo-coloured maps indicate when their respective parameters are decreasing (increasing).

In conclusion, by utilising a passive fiber based Fabry–Pérot setup, we have investigated through experimental and numerical methods both cavity soliton self-generation and deterministic bound state formation under coherent pulsed driving conditions. This work provides further insight into cavity soliton formation under pulsed driving, and hopes to further the push into efficient, robust, and reliable cavity architectures for future applications.

References

- [1] Leo, F., Coen, S., Kockaert, P., Gorza, S.P., Emplit, P., and Haelterman, M. (2010) “Temporal cavity solitons in one-dimensional Kerr media as bits in an all-optical buffer,” *Nature Photon.* **4** (7), 471–476.
- [2] Lucas, E., Lihachev, G., Bouchand, R., Pavlov, N.G., Raja, A.S., Karpov, M., Gorodetsky, M.L. and Kippenberg, T.J. (2018) “Spatial multiplexing of soliton microcombs,” *Nature Photon.* **12**, 699–705.
- [3] Trocha, P., Karpov, M., Ganin, D., Pfeiffer, M.H.P., Kordts, A., Wolf, S., Krockenberger, J., Marin-Palomo, P., Weimann, C., Randel, S., Freude, W., Kippenberg, T.J. and Koos, C. (2018) “Ultrafast optical ranging using microresonator soliton frequency combs,” *Science* **359**, 887–891.
- [4] Herr, T., Brasch, V., Jost, J. D., Wang, C. Y., Kondratiev, N. M., Gorodetsky, M. L. and Kippenberg, T.J. (2018) “Temporal solitons in optical microresonators,” *Nature Photon.* **8**, 145–152.
- [5] Lihachev, G., Weng, W., Liu, Chang, L., Guo, J., He, J., Wang, R.N., Anderson, M.H., Liu, Y., Bowers, J.E. and Kippenberg, T.J. (2022) “Platicon microcomb generation using laser self-injection locking,” *Nat Commun.* **13**, 1771.
- [6] Wang, Y., Anderson, M., Coen, S., Murdoch, S.G. and Erkintalo, M. (2018) “Stimulated Raman Scattering Imposes Fundamental Limits to the Duration and Bandwidth of Temporal Cavity Solitons,” *Phys. Rev. Lett.* **120**, 053902.

Mode-locking in coupled microresonators using exceptional point modulation

*Takasumi Tanabe**, *Riku Imamura*, and *Shun Fujii*

IT

Faculty of Science and Technology, Keio University, Yokohama, Japan

* takasumi@elec.keio.ac.jp

Abstract: We present a mode-locking technique using coupled microresonators near an exceptional point to achieve artificial saturable absorption without traditional materials. This efficient approach reduces power requirements, enabling compact, energy-efficient, high-repetition-rate pulsed lasers for integrated photonic applications.

In ultrafast photonics, mode-locked lasers are essential for spectroscopy, telecommunications, and high-precision measurements. Traditionally, passive mode-locking in these lasers depends on saturable absorbers (SAs), which can present challenges, particularly in small-scale lasers requiring extremely high Q factors for stability [1]. Here, we introduce an alternative mode-locking approach leveraging the unique properties of exceptional points (EPs) in coupled microresonator systems, effectively creating an artificial SA without the need for conventional materials [2]. This innovation simplifies system architecture and reduces power demands, marking significant progress in compact, on-chip pulsed laser technology.

Our design features two coupled microresonators: Cavity A, which provides gain, and Cavity B, with a higher loss, acting as a passive modulator. Using nonlinear Schrödinger equation modeling, we observe stable modelocking after multiple cavity roundtrips, generating a high-repetition-rate, Fourier-limited sech^2 pulse. A unique decoupling mechanism at pulse peaks ensures efficient loss modulation, effectively mimicking SA behavior. The system's proximity to the EP, where eigenfrequencies coalesce, enables significant modulation of system loss, achieving mode-locking without traditional SA materials. It allows Cavity B to function as an artificial SA, simplifying system design and lowering power requirements. This approach provides high stability at reduced operational power, making it ideal for energy-efficient, compact photonic systems.

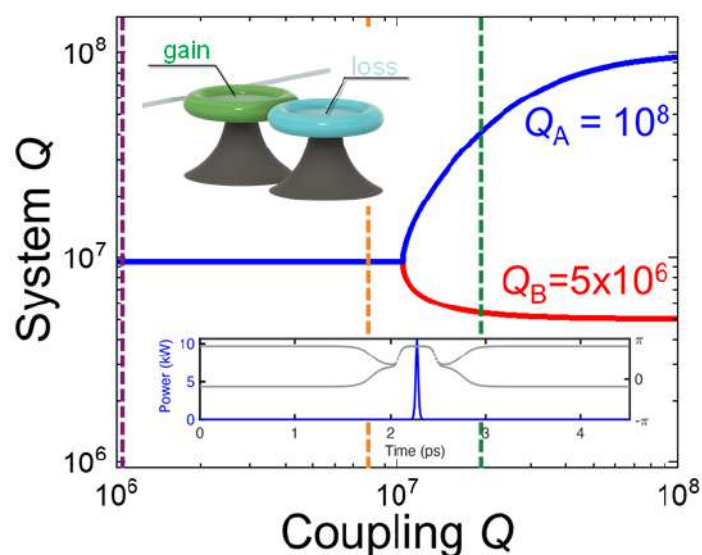


Figure 1: The system Q factor of a coupled microcavity system as a function of the coupling strength (Q_c). The intrinsic Q factors of Cavity A and Cavity B are 10^8 and 5×10^6 , respectively. The inset (bottom) displays the calculated waveforms (intensity and phase) within Cavity A, demonstrating the mode-locked pulse achieved through the coupled system.

Our work represents a paradigm shift in mode-locking technology by utilizing EP-induced modulation in coupled microresonators to create artificial saturable absorption, a potentially powerful approach for small modelocking lasers. This method enables efficient, stable, high-speed pulsing in a simplified, on-chip design.

The results are promising for integrated photonic systems where space and energy constraints are critical, opening avenues for experimental exploration and potentially impacting a broad range of applications that require ultrafast, low-power photonic devices.

References

- [1] T. S. L. P. Suzuki, A. Nakashima, K. Nagashima, R. Ishida, R. Imamura, S. Fujii, S. Y. Set, S. Yamashita, and T. Tanabe, "Design of a passively mode-locking whispering-gallery-mode microlaser," *J. Opt. Soc. Amer. B*, Vol. 38, No. 10, pp. 3172-3178 (2021).
- [2] R. Imamura, S. Fujii, A. Nakashima, and T. Tanabe, "Exceptional point proximity-driven mode-locking in coupled microresonators," *Opt. Express*, Vol. 32, No. 13, pp. 22280-22290 (2024).

This work was supported by SCOPE JP225003008 from MIC.

Silicon Carbide Microresonators for Integrated Nonlinear and Quantum Photonic Applications

*Andrew W. Poon**, *Qianni Zhang*, *Jiantao Wang*

IT

Photonic Device Laboratory, Department of Electronic and Computer Engineering, The Hong Kong University of Science and Technology, Clear Water Bay, Hong Kong, China

* eeawpoon@ust.hk

Abstract: We will introduce our recent progress in silicon carbide microresonators for integrated nonlinear and quantum photonic applications.

Integrated quantum photonic circuits enable quantum optical systems to be integrated on a chip. Microresonators constitute one fundamental building block that enables efficient photon-pairs to be generated at room temperature employing the second- and third-order optical nonlinearities. In this talk we will report our recent progress in using silicon carbide microresonators for integrated nonlinear and quantum photonic applications, including harmonic generation, photon-pair sources [1-2] and polarization entanglement [3]. We will share our perspectives on using such microresonator platforms as a building block for potentially high-dimensional and multipartite entangled quantum sources for quantum communications and quantum computing.

References

- [1] Li, J., Zhang, Q., Wang, J., & Poon, A. W. (2024). An integrated 3C-silicon carbide-on-insulator photonic platform for nonlinear and quantum light sources. *Communications Physics*, 7(1), 125.
- [2] Zhang, Q., Wang, J., & Poon, A. W. (2024). Silicon Carbide Microring Resonators for Integrated Nonlinear and Quantum Photonics Based on Optical Nonlinearities. *Photonics* 11 (8), 701.
- [3] Zhang, Q., Wu, K., & Poon, A. W. (2024). Polarization entanglement generation in silicon nitride waveguide-coupled dual microring resonators. *Optics Express*, 32(13), 22804-22816.

New opportunities for high-Q integrated devices and systems

*Kerry J. Vahala**

FT

T. J. Watson Laboratory of Applied Physics, California Institute of Technology, Pasadena, USA

* vahala@caltech.edu

The advent of ultra-low-loss (ULL) silicon nitride waveguides has transformed the high-Q microresonator landscape. With quality factors approaching 1 billion, ULL microresonators are fabricated in CMOS-compatible foundries, enabling both enhanced feature size control and high yield for microfabrication of sophisticated microresonator systems. Moreover, the photo- alvanic effect has introduced access to second-order nonlinearities within this platform—a capability typically restricted to non-centrosymmetric dielectric systems. I will discuss recent device and system advancements using ULL microresonator technology, including continuous dispersion control in state-of-the-art microcomb systems, ultra-high coherence visible light generation, and synthesis of record-low phase-noise microwave signals through optical frequency division.

Opportunities in Whispering-Gallery Microresonators: Fundamentals and Applications

*Lan Yang**

IT

Department of Electrical and Systems Engineering, Washington University, St. Louis, MO 63130, USA

* yang@seas.wustl.edu

Light-matter interactions form the foundation of numerous phenomena and processes in optical systems. High-Q microresonators and microlasers provide excellent platforms for both fundamental science and engineering applications. This talk will start with an introduction to diverse sensing mechanisms and strategies developed around high-Q microresonators. Various strategies, such as barcode technology based on collective behaviors of multiple resonances and AI-enhanced classification, will be introduced for sensing applications with resonators. Furthermore, our recent exploration of fundamental physics, including non-Hermitian physics in high-Q WGM resonators, have unraveled innovative strategies to achieve a new generation of optical systems enabling unconventional control of light flow. Examples including nonreciprocity in a parity-time (PT)-symmetry resonator system, loss engineering in a lasing system, directional lasing emission at an exceptional point (EP), and EP-enhanced sensing will be presented. To conclude, the applications of resonators in photonic integrated circuits (PIC) will be discussed. Our research discoveries just represent a glimpse of the potential of photonic resonators; there are still many exciting opportunities ahead for leveraging the enhanced light-matter interactions through resonant effects.

Spectral response strength of non-Hermitian optical systems at and near higher-order exceptional points

Jan Wiersig*

IT

Institut für Physik, Otto-von-Guericke-Universität Magdeburg, Postfach 4120, D-39016 Magdeburg, Germany

* jan.wiersig@ovgu.de

Abstract: Non-Hermitian systems with exceptional points exhibit a strongly enhanced response to perturbations and excitations. To characterize this response, we introduce the spectral response strength and various schemes to compute it.

1. Introduction

Exceptional points (EPs) are exotic spectral degeneracies in open wave and quantum systems with potential applications in optics and photonics [1]. At an EP of order n , exactly n eigenvalues (eigenfrequencies) and the related eigenstates (modes) of a non-Hermitian Hamiltonian \hat{H}_0 coalesce. When such a Hamiltonian is slightly perturbed, $\hat{H}_0 + \epsilon\hat{H}_1$, where $\epsilon > 0$ is the perturbation strength, the eigenvalues exhibit a strong spectral response $E_j - E_{\text{EP}} \propto \epsilon^{1/n}$. These large splittings have been exploited in experiments on sensing [2].

For an $m \times m$ Hamiltonian \hat{H}_0 , it was shown for the special case $m = n$, i.e., the Hilbert-space dimension equals the order of the EP, that the perturbation-induced splitting is bounded [3]

$$|E_j - E_{\text{EP}}|^n \leq \epsilon \|\hat{H}_1\|_2 \xi, \quad (0.1)$$

where $\|\cdot\|_2$ is the spectral matrix norm, $\xi := \|\hat{N}^{n-1}\|_2$ is the spectral response strength, and $\hat{N} := \hat{H}_0 - E_{\text{EP}}\mathbb{1}$. A large ξ indicates a strong spectral response, which is desirable e.g. for sensing applications.

2. Extension to arbitrary Hilbert-space dimension

We extend the theory of the spectral response strength to the general case $m \geq n$. A highly interesting result is that ξ diverges when a higher-order EP is approached in parameter space. An efficient and accurate numerical scheme based on residue calculus is presented.

3. Computation directly from wave simulations

We introduce a numerical method to compute the spectral response strength directly from wave simulations of photonic systems done with standard software such as COMSOL. The scheme is based on the behavior of the Petermann factors near an EP, see Refs. [5, 6].

4. Summary

The introduced spectral response strength characterizes EPs of arbitrary order by quantifying the spectral response of optical systems at such non-Hermitian degeneracies. Our theory is useful for the design of complex non-Hermitian photonic systems in general but in particular for sensing applications.

References

- [1] M.-A. Miri and A. Alù, “Exceptional points in optics and photonics,” *Science*, vol. 363, no. 6422, p. eaar7709, 2019.
- [2] W. Chen, Ş. K. Özdemir, G. Zhao, J. Wiersig, and L. Yang, “Exceptional points enhance sensing in an optical microcavity,” *Nature (London)*, vol. 548, pp. 192–196, 2017.
- [3] J. Wiersig, “Response strengths of open systems at exceptional points,” *Phys. Rev. Res.*, vol. 4, p. 023121, 2022.
- [4] J. Wiersig, “Moving along an exceptional surface towards a higher-order exceptional point,” *Phys. Rev. A*, vol. 108, p. 033501, 2023.
- [5] J. Wiersig, “Petermann factors and phase rigidities near exceptional points,” *Phys. Rev. Research*, vol. 5, p. 033042, 2023.
- [6] H. Schomerus, “Eigenvalue sensitivity from eigenstate geometry near and beyond arbitrary-order exceptional points,” *Phys. Rev. Res.*, vol. 6, p. 013044, 2024.

Using exceptional points for coherent control of a hybrid system

N. J. Lambert^{1,2,*}, *A. Schumer*³, *J. J. Longdell*^{1,2}, *S. Rotter*³ and *H. G. L. Schwefel*^{1,2} 

¹ Department of Physics, University of Otago, Dunedin, New Zealand

² The Dodd-Walls Centre for Photonic and Quantum Technologies, New Zealand

³ Institute for Theoretical Physics, Vienna University of Technology (TU Wien), A-1040 Vienna, Austria

* nicholas.lambert@otago.ac.nz

Abstract: Exceptional points are features of the eigenstates of coupled oscillators with competing loss and gain, at which both eigenvalues and eigenvectors coalesce. We use the topological properties of exceptional points for coherent control of magnon-polaritons. © 2024 The Author(s)

1. Introduction

Systems comprising two or more coupled oscillators display a rich variety of physical phenomena. There has been particular interest in the coupling of modes supported by different physical systems -so-called hybrid systems. These allow the characteristics of the coupled modes to be tuned by choosing appropriate subsystems. In particular, the coupling of quantum systems with microwave and optical cavities has proved fruitful [1], allowing new types of excitations to be created. For example, embedding ferromagnetic or antiferromagnetic materials in a microwave cavity results in excitations that are combinations of magnons and photons, termed magnon-polaritons. Magnons are a candidate system for quantum information processing due to their long excitation lifetimes and wide-ranging frequency tunability, and have allowed demonstrations of cavity-mediated coupling to qubits [2, 3], other magnon modes [4], and non-Hermitian physics [5]. However, coherent control of magnonic systems is challenging due to the difficulties of generating a rapidly changing magnetic field to tune the frequencies of the magnon modes. Here we demonstrate that the so-called exceptional point (EP) [6, 7], which emerges in the eigenstate manifold of coupled non-Hermitian oscillators, allows coherent control of magnon-polaritons. In particular, we show that encircling the EP allows excitations to be switched between modes, and traversing the EP permits deterministic preparation of a superposition of states.

However, coherent control of magnonic systems is challenging due to the difficulties of generating a rapidly changing magnetic field to tune the frequencies of the magnon modes. Here we demonstrate that the so-called exceptional point (EP) [6, 7], which emerges in the eigenstate manifold of coupled non-Hermitian oscillators, allows coherent control of magnon-polaritons. In particular, we show that encircling the EP allows excitations to be switched between modes, and traversing the EP permits deterministic preparation of a superposition of states.

2. Experiment

To implement coherent control using non-Hermitian physics, we require microwave resonators for which we have control over the centre frequency and loss/gain of microwave modes. We implement this using two resonators each comprising a loop of coplanar waveguide, with embedded amplifiers (providing gain) and IQ modulators (providing controlled loss and phase control via their I and Q voltages). Modes are travelling waves with an integer number of wavelengths around the loop. We also embed polished YIG spheres in the waveguides and achieve strong coupling between photons and magnons, and between the two microwave resonators.

Our objective is to carry out coherent manipulations of the magnon-polariton modes of the system within their lifetime ($\approx 0.5\mu$ s). We do this by exciting a particular mode, guiding the system through some trajectory in parameter space with carefully calibrated voltage waveforms on V_I and V_Q , and then observing the ringdown frequencies of the system.

3. Results

We demonstrate that a trajectory encircling an exceptional point allows transfer of energy between normal

modes, with the trajectory taking 75 ns. Circling must occur with the correct sense for switching to occur, and the sense is dependent on the target mode. We also study the effect of traversing through the exceptional point. Here, the effect of the generalised eigensystem on the evolution of the system must be considered, and we show that the time reversal symmetry of trajectories through the EP leads to robust preparation of the system in an equal superposition of magnon polariton modes. These results offer a pathway to novel coherent control of quantum hybrid systems.

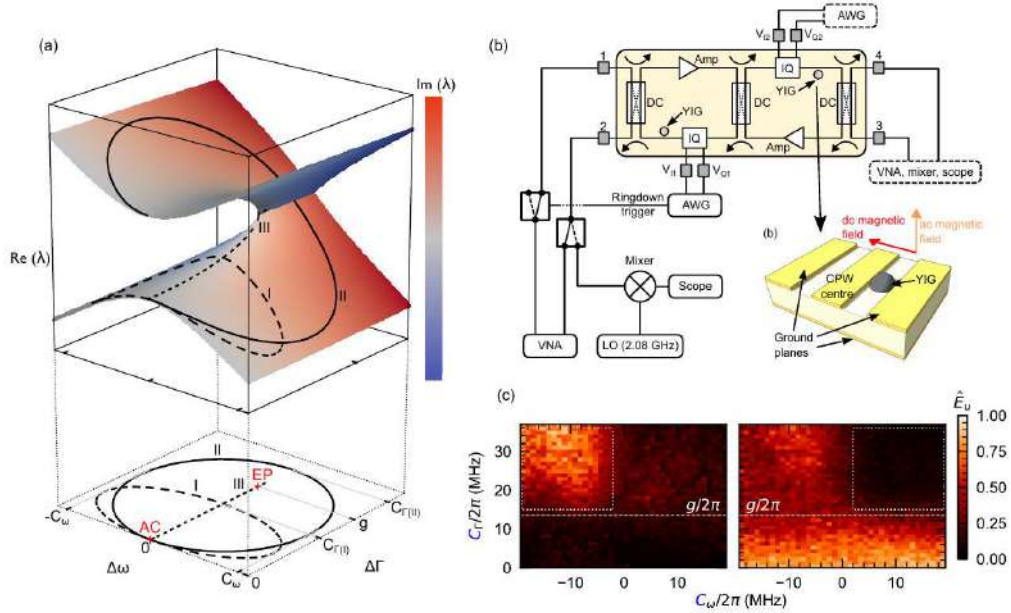


Fig. 1. (a) The eigenfrequencies of two non-Hermitian coupled resonators. The surface shows the real parts ($\text{Re}(\lambda)$) as a function of the angular frequency ($\Delta\omega$) and loss ($\Delta\Gamma$) detuning of the uncoupled resonators from degeneracy, and is coloured according to the imaginary parts ($\text{Im}(\lambda)$). For $\Delta\Gamma < g$ the real part of the eigenvalues exhibits an anticrossing as a function of $\Delta\omega$, and when $\Delta\Gamma > g$ the anticrossing is in the imaginary part. The two regimes are separated by the exceptional point (EP). Also shown are trajectories corresponding to: (I) an ellipse which does not enclose the EP; (II) an ellipse which does enclose the EP; (III) a trajectory from $\Delta\omega = \Delta\Gamma = 0$ through the EP and back to the starting point. (b) Schematic of the coupled resonators and readout electronics. (c) Relative population of state $|u\rangle$ as a function of C_ω and C_Γ for initial excitation of $|l\rangle$ (left) and $|u\rangle$ (right). Population transfer occurs for the parameter ranges marked by the white dotted boxes, where the EP is encircled with the correct chirality.

References

- [1] G. Kurizki, P. Bertet, Y. Kubo, K. Mølmer, D. Petrosyan, P. Rabl, and J. Schmiedmayer, "Quantum technologies with hybrid systems," *Proceedings National Academy Sciences* **112**, 3866-3873 (2015).
- [2] Y. Tabuchi, S. Ishino, A. Noguchi, T. Ishikawa, R. Yamazaki, K. Usami, and Y. Nakamura, "Coherent coupling between a ferromagnetic magnon and a superconducting qubit," *Science* **349**, 405-408 (2015).
- [3] D. Lachance-Quirion, S. P. Wolski, Y. Tabuchi, S. Kono, K. Usami, and Y. Nakamura, "Entanglement-based single-shot detection of a single magnon with a superconducting qubit," *Science* **367**, 425-428 (2020).
- [4] N. J. Lambert, J. A. Haigh, S. Langenfeld, A. C. Doherty, and A. J. Ferguson, "Cavity-mediated coherent coupling of magnetic moments," *Physical Review A* **93**, 021803 (2016).
- [5] D. Zhang, X.-Q. Luo, Y.-P. Wang, T.-F. Li, and J. Q. You, "Observation of the exceptional point in cavity magnonpolaritons," *Nature Communications* **8**, 1368 (2017).
- [6] R. El-Ganainy, K. G. Makris, M. Khajavikhan, Z. H. Musslimani, S. Rotter, and D. N. Christodoulides, "Non-Hermitian physics and PT symmetry," *Nature Physics* **14**, 11-19 (2018).
- [7] Ş. K. Özdemir, S. Rotter, F. Nori, and L. Yang, "Parity-time symmetry and exceptional points in photonics," *Nature Materials* **18**, 783-798 (2019).

Optically detected spin state of erbium dopants in a whispering-gallery resonator

*Luke S. Trainor**, *Li Ma*, *Gavin G. G. King*, *Harald G. L. Schwefel*, and *Jevon J. Longdell*

CT

Department of Physics, University of Otago, Dunedin, New Zealand
 The Dodd Walls Centre for Quantum and Photonic Technologies, New Zealand
 * luke.trainor@otago.ac.nz

Abstract: We demonstrate microwave-optical double resonance in an erbium-doped whispering-gallery resonator inside a microwave cavity. The resonances couple to the erbium ions and offer a strong nonlinearity with potential for quantum frequency conversion. © 2024 The Author(s)

Whispering-gallery resonators are well known for being monolithic optical cavities with high quality factors (Q) and low mode volumes. We present a cryogenic (4 K) erbium-doped resonator with an optical Q exceeding 10^8 only 10 GHz away from an erbium optical transition. This optical resonator is embedded in a microwave cavity, designed such that the magnetic field of the microwave resonance overlaps with the optical mode, see Fig. 1(a).

The erbium provides energy levels in the telecom domain at 1536 nm, as well as a microwave spin-state transition, both of which are tunable with an applied magnetic field. The optical modes in such a resonator are strongly coupled to collective transitions of the erbium ions. Fig. 1(b) shows an optical mode, which shows a coupling rate of $2\pi \times 0.85$ GHz to an erbium optical transition, which is tuned by magnetic field. The microwave resonator likewise allows us to probe the spin transition within the Zeeman-split ground state.

We present a scheme based on optically-detected magnetic resonance (ODMR) to better characterise the microwave-optical response of the device by measuring the microwave response of only those ions that lie within the optical mode volume [1]. Such a measurement allows us to characterise the system for possible future use of microwave-optical transduction, which will be useful to interconnect superconducting qubits through room temperature links.

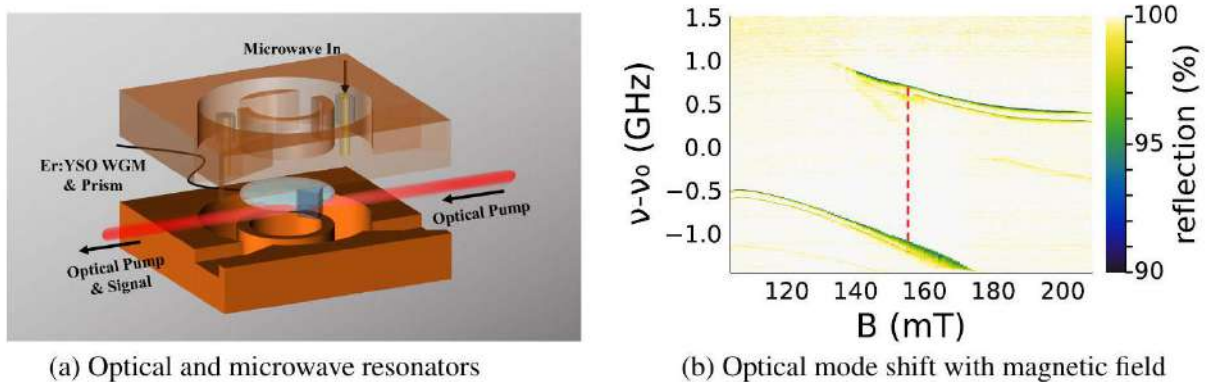


Fig. 1. (a) The erbium-doped Y_2SiO_5 whispering-gallery-mode resonator (Er:YSO WGM) sits in a copper microwave resonator. The setup is mounted inside a cryostat with a temperature of 4 K. An external magnetic field can be applied by a superconducting magnet. (b) An optical mode with a frequency of $\nu_0 \approx 195$ THz shows an avoided crossing of 1.7 GHz (red line) due to coupling to an erbium transition, which is tuned by the external magnetic field (B). Figures modified from [1].

References

[1] L. Ma, L. S. Trainor, G. G. G. King, H. G. L. Schwefel, and J. J. Longdell, "Optically detected magnetic resonance to characterize atomlike microwave-optical transducers," *Physical Review A*, vol. 107, p. 053514, May 2023. doi: 10.1103/PhysRevA.107.053514

Nanofiber Cavity Quantum Electrodynamics for Quantum Network

Takao Aoki*

IT

Department of Applied Physics, Waseda University, Tokyo, Japan

* takao@waseda.jp

Abstract: We present our development of high-finesse optical nanofiber cavities and experimental research on nanofiber cavity quantum electrodynamics systems for quantum network..

A quantum network, which consists of many quantum nodes connected by quantum channels, has a wide variety of applications from the implementation of quantum computation to fundamental studies on quantum many-body systems. Quantum nodes are required to be capable of storing and controlling local quantum information as well as to be efficiently interfaced with the quantum channels through which flying quantum information is transmitted. Fiber-coupled cavity quantum electrodynamics (QED) systems in the strong coupling regime are one of the most promising candidates for the quantum nodes. We present our experimental research on a nanofiber cavity QED system (Fig. 1) with a trapped single atom in the strong coupling regime [1], and the setting of coupled-cavities QED, where two nanofiber cavity QED systems are coherently connected by a meter-long low-loss channel in an all-fiber fashion [2,3], and development of high-finesse nanofiber cavities for achieving high cooperativity in nanofiber cavity QED [4-6]. We also show our recent progress on the development of nanofiber cavity QED systems with individually addressable multiple atoms trapped in an optical tweezer array on the nanofiber surface.

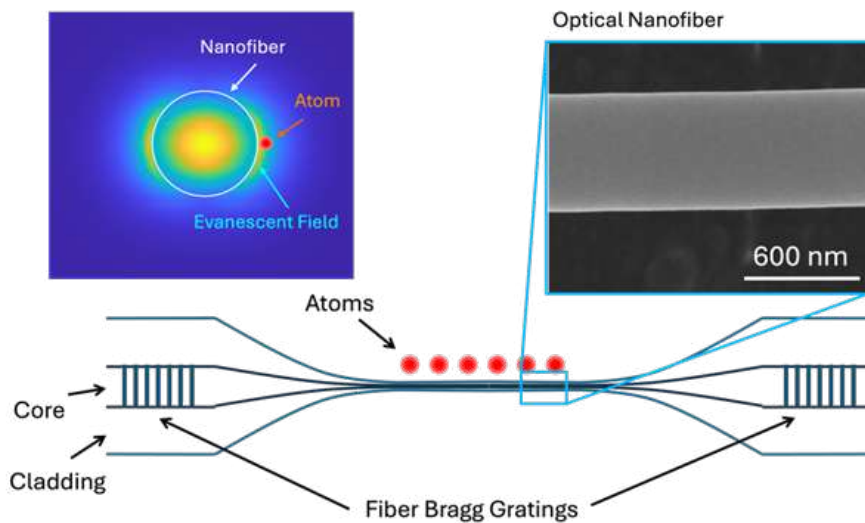


Fig. 1. Nanofiber cavity QED system with trapped atoms.

References

- [1] S. Kato and T. Aoki, Phys. Rev. Lett. 115, 093603 (2015).
- [2] S. Kato et al., Nature Communications 10, 1038 (2019).
- [3] D. White et al., Phys. Rev. Lett. 122, 253603 (2019).
- [4] S. K. Ruddell et al., Opt. Lett. 45, 4875 (2020).
- [5] S. Kato and T. Aoki, Opt. Lett. 47, 5000 (2022).
- [6] S. Horikawa et al., Rev. Sci. Instrum. 95, 073103 (2024).

Slow and Fast light in a microcavity

Wenjie Wan^{1,*}, Yicheng Zhu¹

IT

¹ University of Michigan-Shanghai Jiao Tong University Joint Institute, Shanghai Jiao Tong University, Shanghai 200240, China

* wenjie.wan@sjtu.edu.cn

Abstract: Fast and slow light is demonstrated experimentally in an optical microcavity through stimulated Brillouin scattering induced transparency and absorption. And the transition point between the fast and slow light reveals an intriguing stopped light.

1. Introduction

Light is the fastest information carrier with a tremendously large bandwidth, but hard to be stopped [1] or stored. In this work, we experimentally demonstrate a room-temperature stopped light scheme in an optical microcavity. Through nonlinear Brillouin scattering, a Parity-Time symmetry can be constructed by nonlinearly coupling an optical mode and an acoustic one. By effective detuning of the control beam, a critical transition between the slow-light and the fast-light regimes[2] exhibits its capability to stop light. Correspondingly, a separated light-storage experiment shows that the light pulse can be halted up to almost half a millisecond.

2. Stopped light near an exceptional point

In an optical microcavity, we excite a Brillouin acoustic field (green line in Fig. 1a) with a control light (blue line in Fig. 1a). Another signal light (red line in Fig. 1a) at the position of the low-frequency Stokes light obtain gain by injecting into microcavities. According to the Kramers-Kronig relationship, the group velocity of the signal light will increase. A parity-time symmetry can be constructed between the signal light and the acoustic field (Fig. 1b). Therefore, fine tuning of the frequency detuning or coupling strength of signal light can completely eliminate the group velocity of signal light and store light energy in the acoustic field.

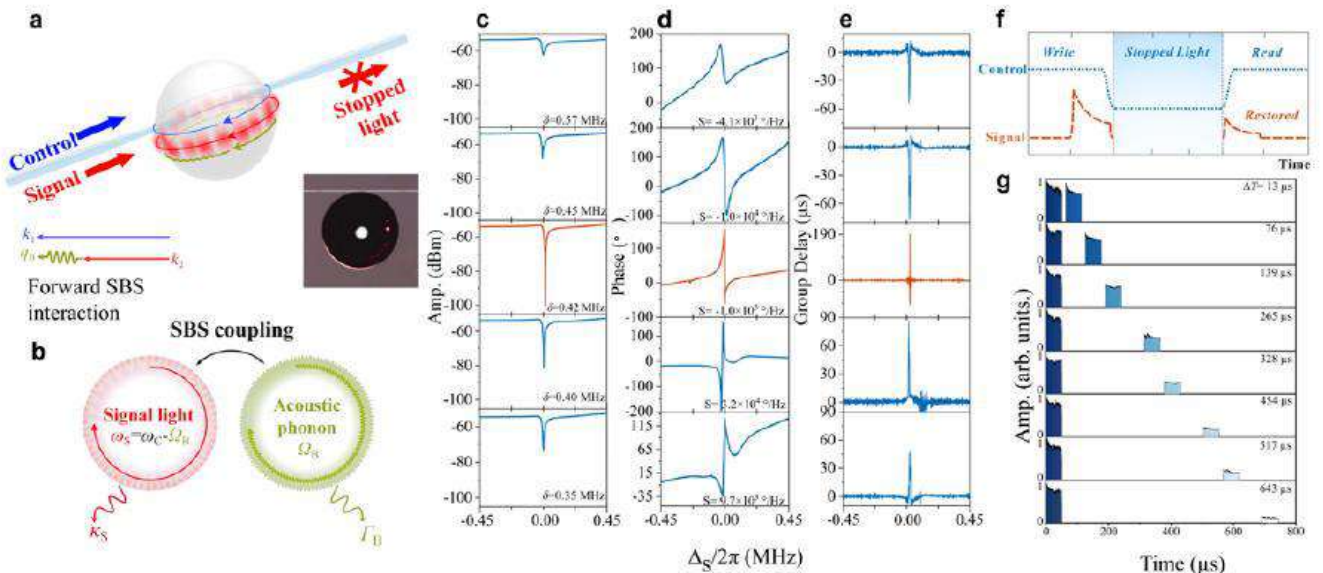


Fig. 1. a, Schematic diagram of stopped light through BSIA in a microsphere microcavity. b, PT symmetry is formed between photoacoustic modes. c-e, The transmission spectrum, phase, and group delay of signal light. f, Schematic diagram of optical storage principle using control light pulse and signal light pulse at the stopped light point. g, The experimental results of light storage at the stopped light point show that the maximum storage time can reach over 600 microseconds.

Fig. 1 c-e show the transmission spectrum, phase variation, and group delay of signal light when

adjusting the detuning of signal light. The phase slope and group delay indicate the transition of signal light from fast light to slow light. The red line represents the transition point. The phase slope and group delay of this point tend to infinity, corresponding to a group velocity of 0, which is the stopped light point. At this point, we will modulate both the control light and the signal light into pulses. Fig. 1 f shows the principle of light storage: controlling the light to turn on and off the acoustic field within one cycle, the signal light pulse transfers energy completely to the acoustic field at this point and is restored when the acoustic field is turned on again. The results of Fig. 1g show that the signal light pulse can still be recovered by the acoustic field after a time interval of up to 600 microseconds.

3. Summary

In summary, we have experimentally demonstrated a room-temperature stopped light scheme in an optical microcavity, utilizing the PT symmetry through stimulated Brillouin scattering. The transition from fast light to slow light indicates the generation of a stopped light point.

References

- [1] M. T. Goldzak, A. A. Mailybaev, and N. Moiseyev, Light Stops at Exceptional Points, *Phys. Rev. Lett.* **120**, 013901 (2018).
- [2] T. Qin, et. al. Fast- and slow-light-enhanced light drag in a moving microcavity, *Commun. Phys.* **3**, 118-125 (2020).

Taming Brillouin optomechanics using supermode microresonators

Min Wang,^{1,3,*} *Zhi-Gang Hu*,^{1,3} *Chenghao Lao*,^{1,2} *Yuanlei Wang*,^{1,2} *Wenjing Liu*,² *Qi-Fan Yang*,^{2,4,†} and *Bei-Bei Li*^{1,3,5,‡}

CT

¹ Beijing National Laboratory for Condensed Matter Physics, Institute of Physics, Chinese Academy of Sciences, Beijing 100190, China

² State Key Laboratory for Mesoscopic Physics and Frontiers Science Center for Nano-optoelectronics, School of Physics, Peking University, Beijing 100871, China

³ University of Chinese Academy of Sciences, Beijing 100049, China

⁴ Collaborative Innovation Center of Extreme Optics, Shanxi University, Taiyuan 030006, Shanxi, China

⁵ Songshan Lake Materials Laboratory, Dongguan 523808, Guangdong, China

*Presenting author; † leonardoyoung@pku.edu.cn; ‡ libeibei@iphy.ac.cn

Abstract: We have designed and fabricated a supermode microresonator to enhance Brillouin optomechanical coupling, and realized both phonon lasing and optomechanical strong coupling. This system exhibits a single-photon optomechanical coupling rate as high as 12.5 kHz.

1. Introduction

The enhanced photon-phonon interactions in high- Q microresonators [1-3] have accelerated the adoption of electrostrictive Brillouin scattering in nanophotonics. In these demonstrations, for efficient Brillouin scattering to occur, both the pump and scattered waves are essentially in resonance with the cavity modes. To satisfy such dual-resonance condition, it requires either precise control of the resonator size (usually at millimeter-to-centimeter scale) [1-3] to match one or multiple free spectral ranges (FSRs) of the resonator to the phonon frequency, or careful selection of a pair of optical modes whose frequencies and azimuthal numbers satisfy the energy and momentum conservation criteria [4, 5]. However, both strategies impose a fairly limited optomechanical coupling rate especially in the single-photon regime, due to the large cavity mode volume or reduced modal overlaps. Furthermore, in the former scenario, the Brillouin scattering would cascade which forbids high-power lasers or optomechanical strong coupling [6, 7].

In this work, we propose and demonstrate a supermode microresonator with nanometric Bragg gratings on the boundary, can significantly enhance Brillouin optomechanical coupling rates. By applying a periodic modulation to the boundary of the SiO₂ microresonator (Fig. 1(a)) in the form of $\alpha \cos(2m\phi)$ (with α and ϕ representing the modulation amplitude and azimuthal angle along the cavity boundary, respectively), strong coupling between the clockwise (CW) and counterclockwise (CCW) modes with azimuthal mode number m can be induced through Bragg scattering. As a result, the CW and CCW traveling-wave modes are hybridized into two standing-wave supermodes with a frequency splitting twice the coupling rate (β) [8]. In contrast to randomized defects, this modulation only impacts the mode with azimuthal mode number m , thus leaving other modes unperturbed. Controlling the value of α allows for the frequency splitting to match the frequency of the bulk acoustic phonons (Fig. 1(b)), which enables efficient Brillouin optomechanical coupling in a much smaller footprint. In this way, dual-resonance conditions in the same spatial modes are realized via Bragg scattering in a microresonator with a radius of 20 μm . A single-photon optomechanical coupling rate of $g_0/2\pi = 12.52\text{kHz}$ is achieved, which is more than one order of magnitude higher than previous works that use SiO₂ microresonators for Brillouin scattering [2-5]. Bi-directional phonon lasing (Fig. 1(c)) is demonstrated along with optomechanical strong coupling with a coupling rate of $G/2\pi > 100\text{MHz}$ (Fig. 1(d)).

2. Summary

In conclusion, we have demonstrated enhanced Brillouin optomechanical coupling using a supermode microresonator and realized both the phonon lasing and optomechanical strong coupling. Using this device we

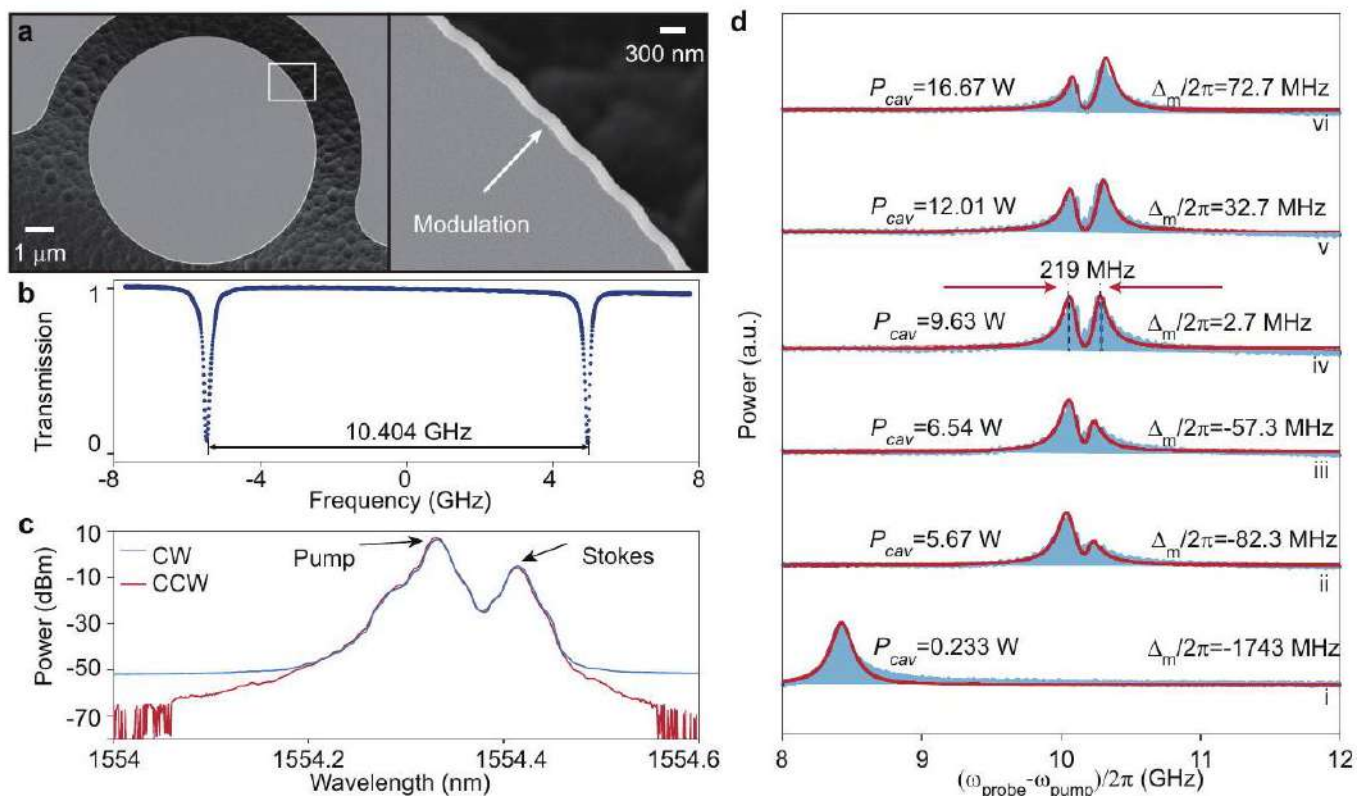


Fig. 1. **a**, Scanning-electron-microscope image of the SiO₂ microresonator (left), with a zoom-in view of the microresonator boundary shown on the right. **b**, Transmission spectrum of a SiO₂mi⁻ croresonator with $r_0 = 20\mu\text{m}$ and $\alpha \approx 12.6\text{ nm}$, where the target mode has a frequency splitting of $\Delta f = 10.404\text{GHz}$. **c**, Optical spectra of stimulated Brillouin scattering in both CW and CCW directions when the pump light is coupled into the higher-frequency split mode in the CW direction. **d**, Power spectra around the high-frequency split mode.

have achieved a single-photon optomechanical coupling rate of 12.52 kHz, which is more than one order of magnitude higher than the SiO₂ microresonators reported in previous works.

References

- [1] I. S. Grudinin, A. B. Matsko, L. Maleki, "Brillouin lasing with a CaF₂ whispering gallery mode resonator," *Phys. Rev. Lett.* **102**, 043902 (2009).
- [2] J. Li, H. Lee, T. Chen, K. J. Vahala, "Characterization of a high coherence, Brillouin microcavity laser on silicon," *Opt. Express* **20**, 20170-20180 (2012).
- [3] H. Lee, T. Chen, J. Li, K. Y. Yang, S. Jeon, O. Painter, K. J. Vahala, "Chemically etched ultrahigh-Q wedge-resonator on a silicon chip," *Nat. Photon.* **6**, 369-373 (2012).
- [4] M. Tomes, T. Carmon, "Photonic micro-electromechanical systems vibrating at X-band (11-GHz) rates," *Phys. Rev. Lett.* **102**, 113601 (2009).
- [5] G. Enzian, M. Szczykulska, J. Silver, L. Del Bino, S. Zhang, I. A. Walmsley, P. Del'Haye, M. R. Vanner, "Observation of Brillouin optomechanical strong coupling with an 11 GHz mechanical mode," *Optica* **6**, 7-14 (2019).
- [6] R. O. Behunin, N. T. Otterstrom, P. T. Rakich, S. Gundavarapu, D. J. Blumenthal, "Fundamental noise dynamics in cascaded-order Brillouin lasers," *Phys. Rev. A* **98**, 023832 (2018).
- [7] R. Pant, E. Li, D.-Y. Choi, C. Poulton, S. J. Madden, B. Luther-Davies, B. J. Eggleton, "Cavity enhanced stimulated Brillouin scattering in an optical chip for multiorder stokes generation," *Opt. Lett.* **36**, 3687-3689 (2011).
- [8] J. Zhu, S. K. Ozdemir, Y.-F. Xiao, L. Li, L. He, D.-R. Chen, L. Yang, "On-chip single nanoparticle detection and sizing by mode splitting in an ultrahigh-Q microresonator," *Nat. Photon.* **4**, 46-49 (2010).

Harnessing Crystalline Anisotropy in Whispering Gallery Mode Resonators for Enhanced Nonlinear Optical Processes

Guoping Lin*

IT

School of Physics, Harbin Institute of Technology, Shenzhen 518055, China

* guoping.lin@hit.edu.cn

Abstract: Wide-range cyclic phase matching for second-harmonic generation and broadband stimulated Brillouin scattering in crystalline resonators are explored. Both approaches leverage orientation-dependent wave velocities along circular paths, showcasing the versatility of anisotropic WGMRs in nonlinear optics.

1. Introduction

Whispering gallery mode resonators (WGMRs) have emerged as powerful platforms for nonlinear optics, offering high Q-factors and small mode volumes. While the general properties of WGMRs have been extensively studied, research on how crystal anisotropy affects WGM resonances and subsequent nonlinear processes is limited. This is especially true for phase matching in nonlinear effects, where the interplay between crystal orientation and the circular geometry of WGMRs can lead to unique and potentially beneficial phenomena.

Our research has focused on exploiting the crystalline anisotropy in these resonators to enhance different nonlinear optical processes. We review two significant developments in this aspect: second-harmonic generation (SHG) in x-cut BBO WGMRs [1] and stimulated Brillouin scattering (SBS) in z-cut MgF₂ WGMRs [2]. These studies demonstrate how strategic crystal axis orientation can be used to achieve broadband operation in nonlinear processes, a highly desirable feature for many applications.

2. Methods and discussion

In x-cut BBO WGMRs, a unique phenomenon for TM polarized whispering gallery modes was observed. It was observed that for TM polarized modes, the light wave velocity continuously changes along its path due to the crystal orientation. Due to the crystal orientation, the wave velocity of light continuously changes along its path within the resonator. This is equivalent to a continuous variation of the refractive index along the circumference. Remarkably, despite this variation, high-Q TM polarized WGMs still exist in the resonator. For second-harmonic generation, this refractive index variation affects the phase matching condition. While it might be expected to decrease conversion efficiency, we found that it actually broadens the phase matching bandwidth, leading to "widerange cyclic phase matching". [1]. This wide-range operation in a single device is a significant advantage for practical applications.

For z-cut MgF₂ WGMRs, it was found that the velocity of phonons along the circular path of photons exhibits a path-dependent variation by solving the Christoffel equation. This variation leads to a significant broadening of the Brillouin gain spectrum. A hundredfold increase in Brillouin gain bandwidth compared to conventional systems was observed [2]. This broadband effect is attributed to the continuous change in phase matching conditions along the resonator path, similar to the SHG case but involving acoustic waves.

In both cases, the anisotropic properties of the crystals, combined with the circular geometry of the resonators, lead to a periodic modulation of relevant parameters along the circumference. For SHG, this results in cyclic phase matching, while for SBS, it leads to an increased Brillouin gain bandwidth. This approach offers a versatile method for designing broadband nonlinear optical devices based on crystalline WGMRs. Future research could explore other crystal orientations and materials to further optimize these effects. The success of these studies could lead to potential applications in areas such as optical frequency combs, quantum optics, and precision sensing.

References

- [1] G. Lin, J. U. Fürst, D. V. Strekalov and N. Yu, "Wide-range cyclic phase matching and second harmonic generation in whispering gallery resonators," *Appl. Phys. Lett.* **103**, 181107 (2013).
- [2] G. Lin, J. Tian, T. Sun, Q. Song and Y. K. Chembo, "Hundredfold increase of stimulated Brillouin-scattering bandwidth in whispering-gallery mode resonators," *Photon. Res.* **11**, 917-924 (2023).

Photonic AI Computing using Coherent Microcavity Lasers

Zaijun Chen*

IT

Ming Hsieh Department of Electrical and Computer Engineering, University of Southern California, Los Angeles, CA 90089, USA

* zaijunch@usc.edu

Abstract: Space-time-wavelength multiplexing using microcavity laser arrays and lithium niobate photonics allows multidimensional tensor processing with 405,000 neural parameters. Parallel analog computing achieves 7 femtomoles per operation (140 TOP/W) and high-density integration (6 TOPS/mm²).

Deep neural networks (DNNs) are transforming the field of information processing, but their exponential growth poses challenges for conventional hardware. Existing computing bottlenecks with CMOS electronics are induced by electronic wires, which lead to on-chip thermal dissipation and capacitive resistance limiting the computing energy efficiency and clockrates. Optical neural networks (ONNs) have emerged as a promising solution, offering high clock rates, parallelism, and low-loss data transmission. However, ONNs still face hurdles, including high energy consumption, low compute density, and latency due to inefficient electro-optic digital-analog conversion, device footprints, and high optical power. I will present our time-multiplexed neuromorphic architectures [1–5] to overcome the above-mentioned computing challenges in photonics. We experimentally demonstrated photonic logics using photoelectric multiplication with homodyne detection and phase-controlled vertical-cavity surface-emitting laser (VCSEL) arrays. We further scale up the system by incorporating on-chip integration with wavelength-multiplexed VCSELs and thin film lithium niobate photonics. High-speed optical modulation allows temporal neural activation with 10 billion parameters per device per second, enabling future scaling of optical systems. Our approaches indicate a path towards trillions of operations per second with space-time-wavelength 3D data streaming and parallelism, making it highly scalable for machine learning models. These innovations enable advancements in AI hardware, accelerating tasks such as training large language models, real-time decision-making, and complex simulations, while pushing the boundaries of computing efficiency.

References

- [1] Z. Chen et al., *Deep Learning with Coherent VCSEL Neural Networks*, Nat. Photonics **17**, 723 (2023).
- [2] A. Sludds et al., *Delocalized Photonic Deep Learning on the Internet's Edge*, Science **378**, 270 (2022).
- [3] R. Davis III, Z. Chen, R. Hamerly, and D. Englund, *RF-Photonic Deep Learning Processor with Shannon-Limited Data Movement*, <http://arxiv.org/abs/2207.06883> (2023).
- [4] S. Ou, A. Sludds, R. Hamerly, K. Zhang, H. Feng, E. Zhong, C. Wang, D. Englund, M. Yu, and Z. Chen, *Hypermultiplexed Integrated Tensor Optical Processor*, <http://arxiv.org/abs/2401.18050> (2024).
- [5] R. Hamerly, A. Sludds, S. Bandyopadhyay, Z. Chen, Z. Zhong, L. Bernstein, and D. Englund, *Netcast: Low-Power Edge Computing With WDM-Defined Optical Neural Networks*, <https://ieeexplore.ieee.org/abstract/document/10539183> (2024).

Fast thermogenic detection with a microlaser

*Xi Yang*¹, *Shui-Jing Tang*² and *Yun-Feng Xiao*^{1,2,3,4,*}

CT

¹ Frontiers Science Center for Nano-optoelectronics and State Key Laboratory for Mesoscopic Physics, School of Physics, Peking University, Beijing 100871, China

² National Biomedical Imaging Center, Peking University, Beijing 100871, China

³ Collaborative Innovation Center of Extreme Optics, Shanxi University, Taiyuan 030006, China

⁴ Peking University Yangtze Delta Institute of Optoelectronics, Nantong 226010, China

* yfxiao@pku.edu.cn

Abstract: We develop a microcavity laser cellular thermometer with a temporal resolution of 3.92 ms, enabling the thermal dynamics analysis of the interaction of DMSO and water and monitoring the temperature variation of living cell.

1. Introduction

Real-time monitoring of cellular temperature dynamics is essential to reveal their fundamental cellular signaling, and even clinical diagnosis and therapy. Over the past decades, many promising approaches to cellular temperature sensing have been developed, including fluorescence, thermocouple, Raman spectroscopy, and photoacoustic imaging. Among the numerous technologies, thermocouple probes with the scales of sub-micrometers have been fabricated to determine intracellular temperature variation, showing a temporal resolution of 1 s [1]. Nanoscale thermometries including fluorescent polymers, quantum dots, and green fluorescent proteins have been developed to map the temperature distribution within a living cell [2]. Nitrogen-vacancy centres have been applied to measure the intracellular thermal conductivity [3]. However, most of these methods are limited by their poor temporal resolution because their low brightness requires long integration times.

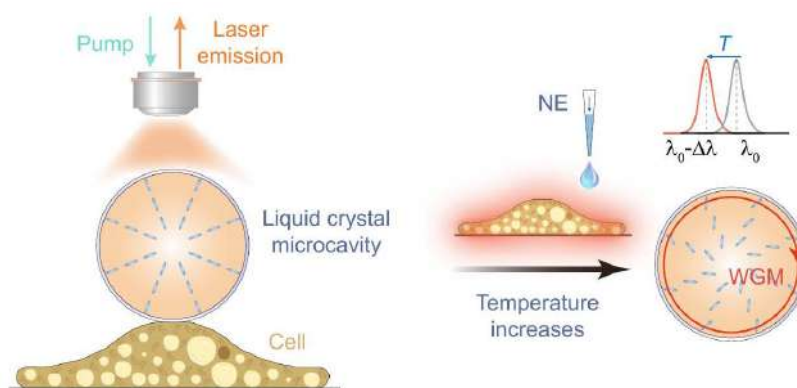


Fig. 1. Concept of microcavity laser-based cellular thermometry. The chemical stimuli induced cellular temperature increase and the blueshift of the lasing wavelength.

3. Summary

In summary, we have experimentally demonstrated a room-temperature stopped light scheme in an optical microcavity, utilizing the PT symmetry through stimulated Brillouin scattering. The transition from fast light to slow light indicates the generation of a stopped light point.

2. Results

The schematic diagram of the liquid-crystal microcavity laser-based cellular thermometer is illustrated in Figure 1, in which the liquid-crystal microcavity laser is fabricated by filling a glass capillary with dye-doped nematic liquid crystal. When the dye-doped liquid-crystal microcavity is pumped by a 532 nm pulsed laser, multiple WGMs are excited to achieve laser emission (Fig. 1). The lasing spectrum depends highly on the

refractive index of the optical microcavity [4], which can be tuned by the temperature of living cell. By adding norepinephrine (NE), the heat production from the mitochondria will boost the temperature of the cell. This will increase the local temperature of the optical microcavity through heat conduction and induce the decrease of refractive index of optical microcavity due to the negative thermo-optic coefficient of liquid crystal, inducing a blueshift of the lasing wavelength (Fig. 1).

In order to characterize the temporal resolution of the proposed thermometry and achieve local temperature measurement, silver coated polystyrene microsphere is stucked on the outer surface of the optical microcavity and is heated by a 1550 nm laser. By applying a square wave modulation, the temporal resolution of microcavity laser can be evaluated, and the corresponding temporal evolution of the lasing wavelength of the microlaser is shown in Fig. 2a. The temporal resolution is measured about 3.92 ms by using the exponential fitting (Fig. 2b), which is about three orders of magnitude higher than other technologies. This enables the proposed thermometry to explore the fast thermal dynamic analysis of the interaction of DMSO and water. Finally, the thermometer was applied for the measurement of cellular temperature.

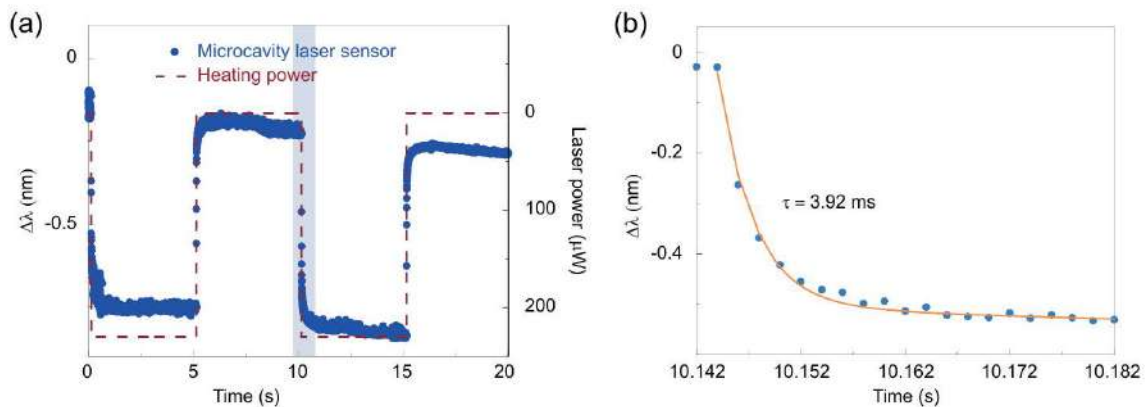


Fig. 2. (a) Time series of the $\Delta\lambda$ in a square-wave input of laser power with a periodicity of 100 mHz. (b) Thermal response time through exponential fitting.

3. Summary

In summary, we have experimentally demonstrated a room-temperature stopped light scheme in an optical microcavity, utilizing the PT symmetry through stimulated Brillouin scattering. The transition from fast light to slow light indicates the generation of a stopped light point.

References

- [1] Changling Wang, Ruizhi Xu, Wenjuan Tian, Xiaoli Jiang, Zhengyu Cui, Meng Wang, Huaming Sun, Kun Fang, and Ning Gu. Determining intracellular temperature at single-cell level by a novel thermocouple method. *Cell research*, 21(10):1517-1519, 2011.
- [2] Jiajia Zhou, Blanca Del Rosal, Daniel Jaque, Seiichi Uchiyama, and Dayong Jin. Advances and challenges for fluorescence nanothermometry. *Nature methods*, 17(10):967-980, 2020.
- [3] M Suzuki. In situ measurements of intracellular thermal conductivity using heater-thermometer hybrid diamond nanosensors. *Sci. Adv.*, 7(3).
- [4] Xi Yang, Shui-Jing Tang, Jia-Wei Meng, Pei-Ji Zhang, You-Ling Chen, and Yun-Feng Xiao. Phase-transition microcavity laser. *Nano Letters*, 23(7):3048-3053, 2023.

Stochastic and quantum dynamics of microcombs

Yanne Chembo^{1,2,*}

IT


¹ Department of Electrical and Computer Engineering, University of Maryland at College Park, College Park, MD, USA

² Institute for Research in Electronics and Applied Physics (IREAP), University of Maryland at College Park, College Park, MD, USA

* ykchembo@umd.edu

Kerr optical frequency combs are expected to play a major role in photonic technology, with applications related to spectroscopy, sensing, aerospace, and communication engineering. Here, we present some of the latest advances for the understanding of their stochastic and quantum dynamics.

A quantum perspective of Kerr microcombs

*Qi-Fan Yang*¹, *Xing Jin*¹, *Zhe Lv*¹, *Lu Yao*¹, *Ze Wang*¹, *Kangkang Li*¹, and *Yue Wang*¹ 

¹State Key Laboratory for Artificial Microstructure and Mesoscopic Physics and Frontiers Science Center for Nano-optoelectronics, School of Physics, Peking University, Beijing 100871, China

* leonardoyoung@pku.edu.cn

Abstract: We study quantum effects in Kerr microcombs, including quantum-limited timing noise and large-scale entanglement encoded on continuous quantum variables. © 2024 The Author(s)

An optical frequency comb is a coherent, bidirectional link between optical and microwave signals, consisting of a set of equally spaced lasers. The realization of these combs in optical microresonators—particularly those generated through Kerr nonlinearities—offers a chip-based solution for a wide range of applications, from precision metrology to telecommunications. While the classical dynamics of Kerr microcombs are well-described by the Lugiato-Lefever equation, the quantum properties of these systems have often been overlooked. In this study, we present our recent findings on the suppression of quantum-limited timing noise in bright soliton microcombs. Furthermore, we demonstrate the generation of correlated non-classical light in Kerr microresonators, leading to the largest-scale entanglement achieved on photonic chips.

The theoretical framework originates from the Lugiato-Lefever equation, modified to include quantum fluctuations:

$$\frac{\partial A}{\partial t} = i\frac{D_2}{2}\frac{\partial^2 A}{\partial \phi^2} + i|A|^2 A - \frac{\kappa}{2}A - i\delta\omega A + \sqrt{\frac{\kappa_{\text{ext}}P_{\text{in}}}{\hbar\omega_0}} + F_q(\phi, t) \quad (1)$$

Here, $A(t, \phi)$ represents the slowly-varying envelope of the optical field at time t and angular position ϕ , studied in a reference frame rotating with the free spectral range (FSR) of the microresonator. The parameters κ and κ_{ext} denote the total and external damping rates of the comb-forming mode family, respectively, while δ_0 is the pump-resonator detuning. The nonlinear coupling coefficient, $g = \hbar\omega_0^2 n_2 D_1 / 2\pi n_0 A_{\text{eff}}$, depends on the linear (n_0) and nonlinear (n_2) refractive indices and the effective mode area A_{eff} . The pump power is represented by P_{in} . Quantum fluctuations are introduced as a Langevin force F_ϕ , satisfying the following correlation function [1]:

$$\langle F_q(\phi_1, t_1) F_q^\dagger(\phi_2, t_2) \rangle = 2\pi\kappa\delta(\phi_1 - \phi_2)\delta(t_1 - t_2) \quad (2)$$

Numerical simulations based on these equations can be performed using the split-step Fourier Transform method. Under certain conditions, analytical solutions are also feasible [1]. Our first set of results addresses the quantum-limited timing jitter of soliton microcombs, a fundamental noise constraint intrinsic to these systems [2]. Solitons interact stochastically with the vacuum electromagnetic field through various loss channels in the microresonator, as predicted by theory [1] and confirmed in experimental studies [3–5]. We have demonstrated that by exploiting dispersive wave dynamics in multimode microresonators, this quantum-limited timing jitter can be suppressed to unprecedented levels. The viscous force generated by these dispersive waves effectively reduces the stochastic motion of the solitons, establishing a new fundamental noise limit for soliton microcombs. These findings provide a pathway for the coherence engineering of soliton microcombs within the quantum regime, offering significant implications for synthesizing ultralow-noise microwave and optical signals. In parallel, high-quality-factor (Q) optical microresonators present a compact and scalable platform for generating squeezed light [6]. Unlike traditional tabletop optical parametric oscillators, the large FSR of microresonators allows for the resolution of individual quantum modes. Bipartite squeezing has been

demonstrated in microresonators pumped monochromatically via Kerr nonlinearity, forming a comb-like structure referred to as a squeezed quantum microcomb [6]. However, creating continuous-variable (CV) cluster states involving multiple frequency quantum modes remains a challenge. In our second study [7], we replace the classical components of microcombs with correlated quantum light to produce cluster quantum frequency combs, which provide extensive quantum resources for measurement-based quantum computation and multi-user quantum networks. We propose and experimentally generate cluster quantum microcombs within an on-chip optical microresonator driven by chromatic lasers. Through resonantly enhanced four-wave mixing processes, we deterministically establish quantum correlations—such as squeezing—among the continuous quantum variables of 60 modes. By tuning the pump lasers, we can reconfigure the cluster structures into one- and two-dimensional lattices. Our results demonstrate the largest-scale cluster states with unprecedented levels of raw squeezing from a photonic chip, paving the way for a compact and scalable platform for computational and communicational tasks with quantum advantages.

References

- [1] A. B. Matsko and L. Maleki, “On timing jitter of mode locked Kerr frequency combs,” *Opt. Express* **21**, 28862–28876 (2013).
- [2] X. Jin, Z. Lv, L. Yao, Q. Gong, and Q.-F. Yang, “Self-suppressed quantum-limited timing jitter and fundamental noise limit of soliton microcombs,” *Phys. Rev. Lett.* **133**, 073801 (2024).
- [3] D. Jeong, D. Kwon, I. Jeon, I. H. Do, J. Kim, and H. Lee, “Ultralow jitter silica microcomb,” *Optica* **7**, 1108–1111 (2020).
- [4] C. Bao, M.-G. Suh, B. Shen, K. S. Afak, A. Dai, H. Wang, L. Wu, Z. Yuan, Q.-F. Yang, A. B. Matsko et al., “Quantum diffusion of microcavity solitons,” *Nat. Phys.* **17**, 462–466 (2021).
- [5] C. Lao, X. Jin, L. Chang, H. Wang, Z. Lv, W. Xie, H. Shu, X. Wang, J. E. Bowers, and Q.-F. Yang, “Quantum decoherence of dark pulses in optical microresonators,” *Nat. Commun.* **14**, 1802 (2023).
- [6] Z. Yang, M. Jahanbozorgi, D. Jeong, S. Sun, O. Pfister, H. Lee, and X. Yi, “A squeezed quantum microcomb on a chip,” *Nat. Commun.* **12**, 4781 (2021).
- [7] Z. Wang, K. Li, Y. Wang, X. Zhou, Y. Cheng, B. Jing, F. Sun, J. Li, Z. Li, Q. Gong et al., “Chip-scale generation of 60-mode continuous-variable cluster states,” arXiv preprint arXiv:2406.10715 (2024).

Tunable Non-Phaselocked Solitons in Pulse-Driven Passive Kerr Resonators Mediated by Stimulated Raman Scattering

Jordan J. Wise,^{1,2,*} *Zongda Li*,^{1,2} *Yiqing Xu*,^{1,2} *Miro Erkintalo*,^{1,2} *Stéphane Coen*,^{1,2} and *Stuart Murdoch*^{1,2}

CT

¹ Department of Physics, University of Auckland, New Zealand

² Dodd-Walls Centre for Photonic and Quantum Technologies, New Zealand

* jordan.wise@auckland.ac.nz

Abstract: Enabled by Raman scattering, a passive optical cavity driven with pulses desynchronised from the cavity's roundtrip time supports spontaneous generation of nonphaselocked solitons centred at optical frequencies more than 15 THz below the pump frequency. © 2024 The Author(s)

1. Introduction and Background

Externally driven passive optical cavities are a commonly used platform for the generation of ultrashort solitons. Pulsed driving enables us to control where within a resonator solitons can exist [1]. Loss within optical cavities means that a soliton sustained through pulsed driving must necessarily have the same repetition rate as its driving pulse. Changing the repetition rate of our driving pulses therefore changes the repetition rate, and consequently the velocity, of our solitons [1]. In practice, a soliton achieves this change in velocity by shifting its centre frequency. While solitons formed in passive resonators typically have the same centre frequency as their driving field, it has recently been shown that Raman scattering can be leveraged to enable the generation of solitons more than 10 THz away from the centre frequency of their driving field [2]. In this work, we explore a regime in which solitons form more than 15 THz below the centre frequency of their pump and are not locked in phase to their driving field.

2. Methods

Our experimental setup is based around a 0.5 m Fabry-Pérot cavity (1m roundtrip) constructed from Corning MetroCor non-zero dispersion-shifted optical fibre ($\gamma = 2.6 \text{ W}^{-1} \text{ km}^{-1}$, $\beta_2 = 7.150 \text{ ps}^2 \text{ km}^{-1}$ and $\beta_3 = 0.136 \text{ ps}^3 \text{ km}^{-1}$ at an operating wavelength of 1562.5 nm) butt-coupled to a dielectric mirror at each end. Cavity finesse is approximately 175. We coherently drive our resonator with a train of 5 ps pulses. Detuning is fixed at $\delta_0 \approx 0$ using a continuous-wave control beam with polarisation orthogonal to that of the main beam.

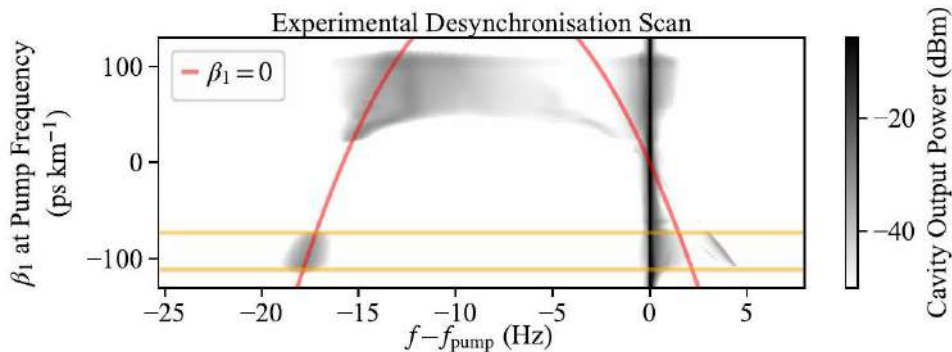


Fig. 1. Output spectra of a passive optical resonator driven with pulses desynchronised from the roundtrip time of the cavity by different amounts. The red lines indicate the optical frequencies at which the repetition rate of the input pulses is matched to the roundtrip time of the cavity. The orange lines indicate the desynchronisation values for which non-phaselocked solitons exist.

3. Results and Discussion

Scanning the repetition rate of our input pulses across a wide range of values, we find that, in addition to

the range of positive β_1 values for which soliton generation has previously been described [2], there is also a small range of negative β_1 values which result in the spontaneous generation of solitons more than 15 THz below the centre frequency of the pump (see Figs. 1 and 2). We note that this range coincides with the range of desynchronisation values for which a switching wave appears around the centre frequency of the pump (see Fig. 1). The relationship between this switching wave and the existence of solitons remains under investigation.

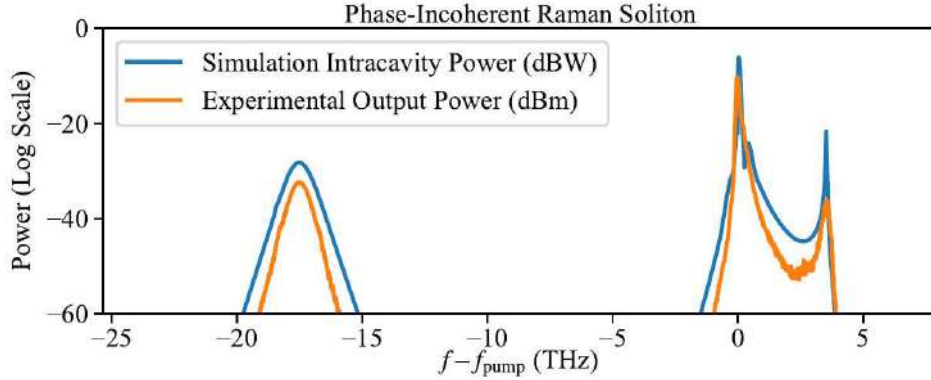


Fig. 2. Simulated and experimental optical spectra of a non-phaselocked Raman soliton.

Because the solitons which form under this regime have the same repetition rate as their pump, the frequency combs corresponding to the pump and the soliton have the same frequency spacing. However, unlike many other solitons sustained on pulsed backgrounds [1,2], they do not have the same carrier envelope offset frequency as their pump, meaning that the pump and soliton beat against each other. In the time domain, this manifests as a time-varying pattern of amplitude modulation across the soliton (see Fig. 3).

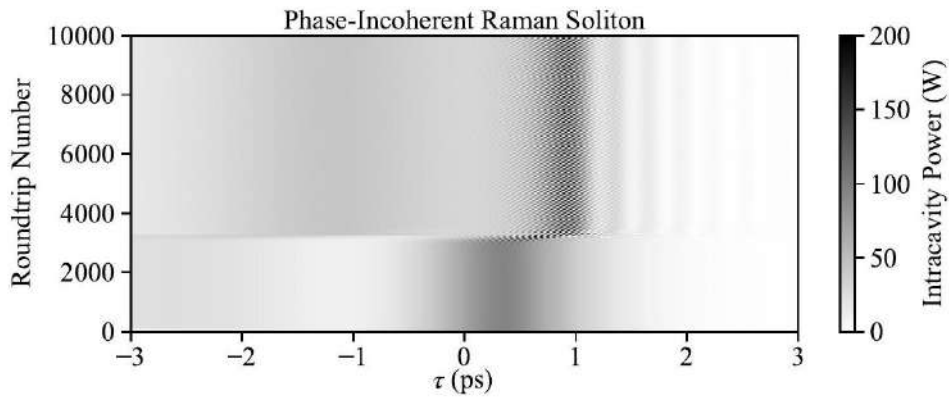


Fig. 3. Simulated temporal evolution of a non-phaselocked Raman soliton.

4. Conclusions and Future Work

Driving a passive optical resonator with pulses whose period is desynchronised from its roundtrip time at the centre frequency of the pump enables the generation of non-phaselocked Raman solitons. In future work we will investigate the relationship between switching wave structures appearing around the pump and the existence of non-phaselocked Raman solitons

References

- [1] E. Obrzud, S. Lecomte, and T. Herr, "Temporal solitons in microresonators driven by optical pulses," *Nature Photonics*, vol. 11, no. 9, pp. 600-607, 2017.
- [2] Z. Li, Y. Xu, S. S. Shamailov, X. Wen, W. Wang, X. Wei, Z. Yang, S. Coen, S. G. Murdoch, and M. Erkintalo, "Ultrashort dissipative Raman solitons in Kerr resonators driven with phase-coherent optical pulses," *Nature Photonics*, vol. 18, pp. 46-53, 2022.

Directional light emission and nanoparticle detection based on WGM microcavities

Wei Wang, Yong-Zhen Huang, and Youling Chen*

IT

State Key Laboratory of Integrated Optoelectronics, Institute of Semiconductors, Chinese Academy of Sciences, Beijing 100083, China

* ylchen@semi.ac.cn

Abstract: A deformed circular-side triangular microresonator is fabricated. Unidirectional light emission is experimentally demonstrated, which changes drastically upon the binding of a nanoparticle, predicting applications in electrically pumped, portable and highly sensitive far-field detection of nanoparticles.

1. Introduction

Whispering-gallery mode (WGM) optical microcavities have found a wide range of applications such as highly sensitive bio/chemical sensing, and microlasers. However, light emission is isotropic in a traditional WGM microlaser. To realize efficient extraction and collection of light, the emission should be tailored. Highly directional light emission has been reported in microcavities with defects or boundary deformation. The Q factors reduced drastically for cavities with defects. Semiconductor polygonal microcavities represent another kind of deformed microcavity. Directly connected with a waveguide, directional output has been reported with semiconductor polygonal microcavities, benefiting the integration with other optoelectronic devices.

2. Experimental results

For the widely adopted cavity material of AlGaInAs quantum wells, a waveguide-connected deformed circular-side triangular microresonator (CTM) is designed and fabricated, as illustrated in Fig. 1.

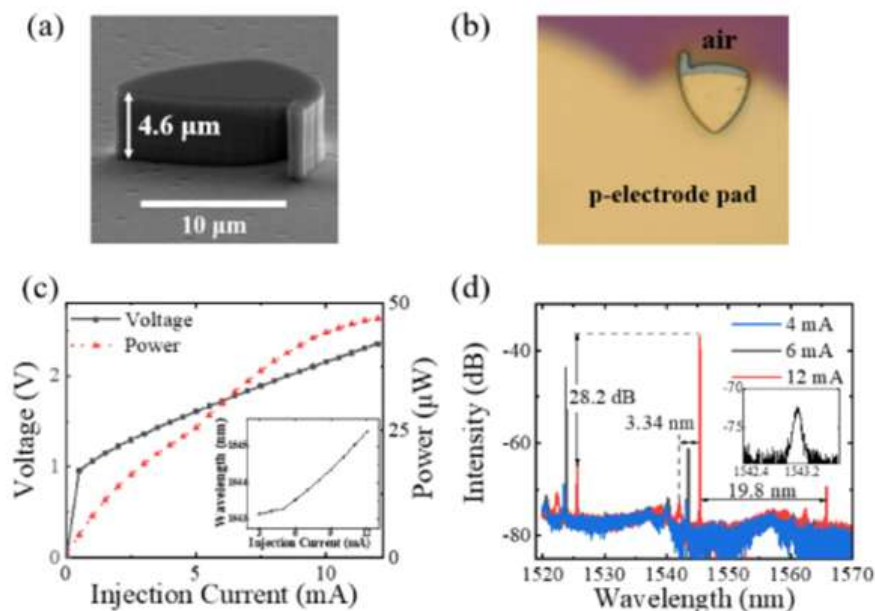


Fig .1. (a) SEM image of the circular side triangular microlaser after ICP etching. (b) Microscopic image of the CTM with p-electrode. (c) Integral ball output power and voltage versus continuous-wave injection current. The inset shows the wavelength of the main lasing mode versus the injection current. (d) Lasing spectra at injection currents of 4, 6, and 12 mA. The inset shows the detailed spectra at 4 mA near the wavelength of 1543.15 nm.

The far field light emission pattern is illustrated in Fig. 2. Fig. 2 (b) is the detailed experimental far field pattern for $I = 12$ mA. Unidirectional light emission from arc side 1 with a divergence angle of about 38°

is obtained. Slight deviation between the simulation and experimental far field emission patterns may be induced by the unavoidable roughness during the fabrication process.

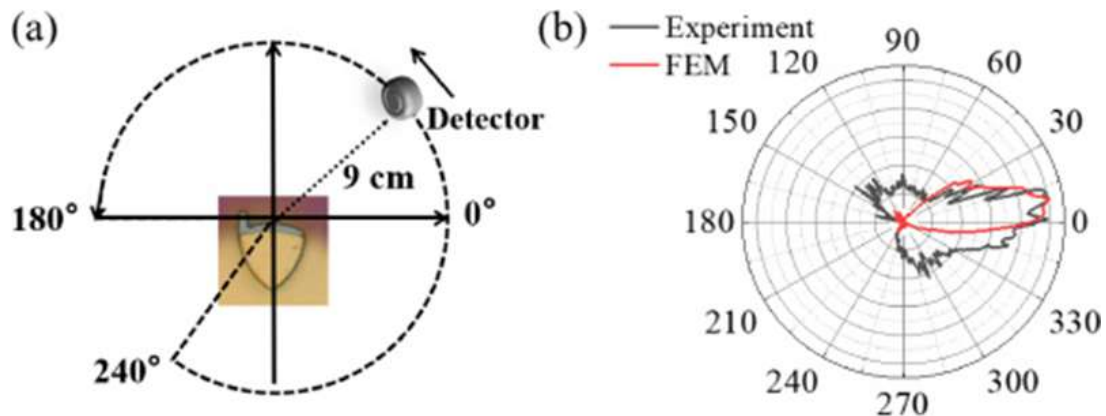


Fig. 2. (a) Schematic diagram of the experimental far field light emission test. (b) Experimental (black) and theoretical (red) far field pattern at the injection current of 12 mA.

3. Summary

Unidirectional light emission with chirality close to 1 is experimentally reported in the far-field pattern with a divergence angle of 38° . Numerical simulation predicts sharp change of the far-field emission pattern upon the adsorption of nanoparticles. Direct integration of the triangular microresonator and the waveguide provides a convenient and robust scheme not only for unidirectional light emission but also for far-field nanoparticle detection based on chirality. The advantages of electrical pumping, simple structure, and low-cost may greatly inspire the development of integrated portable sensing devices.

References

- [1] W. Wang, Y. L. Chen, et al. "Unidirectional light emission in a deformed circular-side triangular microresonator," *Opt. Express* 31, 14560 (2023).
- [2] Z. Z. Shen, M. Tang, Y. L. Chen, and Y. Z. Huang, "Unidirectional emission and nanoparticle detection in a deformed circular square resonator," *Opt. Express* 29, 1666 (2021).

Multichannel THz upconversion in a LiNbO₃ optical resonator

Mallika Suresh^{1,2,*}, *Florian Sedlmeir*^{1,2}, *Dominik W. Vogt*^{1,3}, and *Harald G. L. Schwefel*^{1,2}

CT

¹ Dodd-Walls Centre for Photonic and Quantum Technologies, New Zealand

² Department of Physics, University of Otago, Dunedin 9016, New Zealand

³ Department of Physics, University of Auckland, Auckland 1010, New Zealand

* mallika.suresh@otago.ac.nz

Abstract: We present multichannel nonlinear optical upconversion of THz signals around 0.16 THz in a lithium niobate disk microresonator. This scheme demonstrates the upconversion of six non-resonant THz signals using a resonantly enhanced continuous-wave optical pump.

1. Introduction

Nonlinear frequency mixing in electro-optic crystalline whispering gallery mode resonators (WGMR) has been explored and discussed for a couple of decades now [1]. Such platforms have been used to shift signals from the microwave (e.g. 10 GHz [2] and 80 GHz [3]) up to the optical domain, i.e., "upconversion" via sum-frequency generation (SFG) and difference-frequency generation (DFG). Here, we demonstrate the upconversion of signals that are an octave higher than previously demonstrated [3].

2. Experimental setup

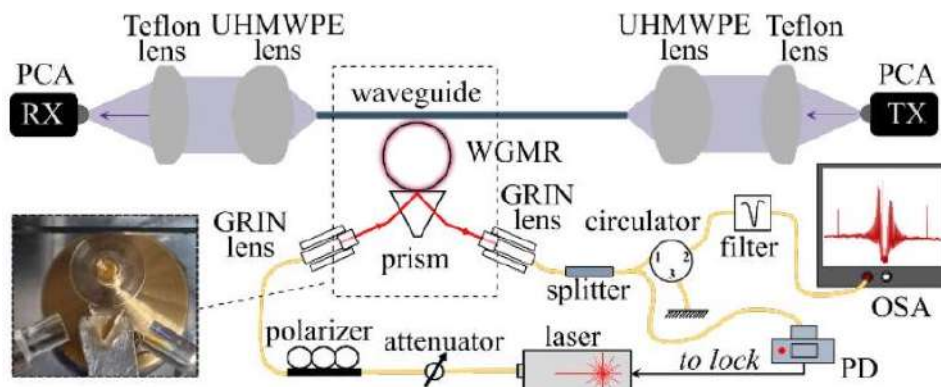


Fig. 1. Sketch of experimental set-up showing the terahertz and optical sections (inset: a photo of the LiNbO₃ WGMR, silicon waveguide, diamond prism and GRIN lenses).

The WGMR used here is a LiNbO₃ disk with the crystal optic axis along the rotational axis, with a thickness of $163.6\mu\text{m}$ and radius of 2.23mm . The experimental setup [Fig. 1] for the upconversion has two parts for each frequency domain involved. In the optical domain, a continuous-wave tunable diode laser ($\sim 192\text{THz}$) from Toptica Photonics is used. The laser light is coupled in and out of the WGMR via two graded-index (GRIN) lenses and a diamond prism. The light emerging from the outcoupling GRIN lens is split with 10% of the signal being sent to a photodiode (PD) and the remaining 90% being sent via a filter to an optical spectrum analyser (OSA). The filter is used to decrease the outcoupled pump power being sent to the high-sensitivity OSA. A frequencydomain TeraScan system with photoconductive antennae (PCA) from Toptica Photonics was used as the source of THz radiation for upconversion. Ultra-high-molecular-weight polyethylene (UHMWPE) lenses are used to couple the radiation to and from a silicon rod waveguide.

3. Results and discussion

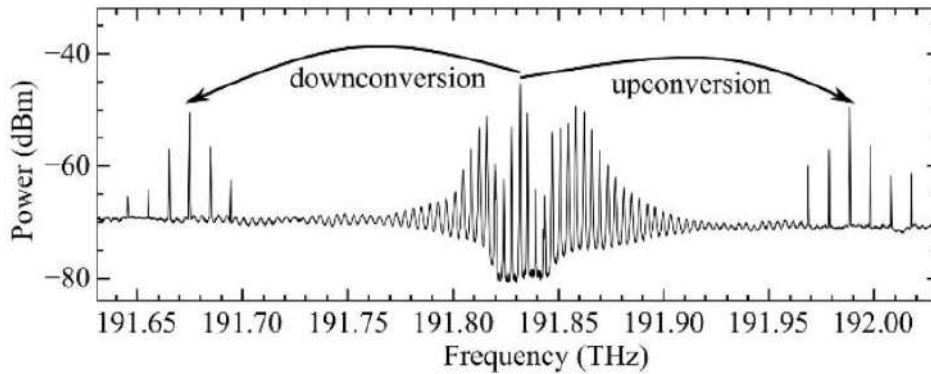


Fig. 2. Optical spectrum showing upconverted peaks from 0.137 THz to 0.186 THz on either side of the pump.

The plot shown in Fig. 2 depicts 6 channels of upconversion as can be seen by the SFG and DFG of frequencies from 0.137 THz to 0.186 THz observed as the sidebands on either side of the pump. These spectra are captured by the "Maximum Hold" function of the Finisar 1500S OSA as the TeraScan system is scanned and each pair of peaks appears when the system reaches the respective THz frequency. The resolution of the OSA is 150 MHz, which is much larger than the expected bandwidth of the upconverted signal mode (approx. 1.4 MHz). These optical signals are integer multiples of the free spectral range of the optical mode. This indicates that the upconverted signal in each case is generated in an optical WGMR mode - so both the pump and upconverted signal are resonant in the WGMR.

The THz radiation being upconverted overlaps with the optical mode but is not resonant in the disk, like that proposed in [4]. This broadens the range of frequencies being upconverted as the phase-matching requirements for all-resonant upconversion would allow only one frequency to be upconverted.

References

- [1] V. S. Ilchenko, A. A. Savchenkov, A. B. Matsko, and L. Maleki, "Whispering-gallery-mode electro-optic modulator and photonic microwave receiver," *J. Opt. Soc. Am. B* **20** (2003).
- [2] A. Rueda et al., "Efficient microwave to optical photon conversion: an electro-optical realization," *Optica* **3** (2016).
- [3] G. S. Botello et al., "Sensitivity limits of millimeter-wave photonic radiometers based on efficient electro-optic upconverters," *Optica* **5**, (2018).
- [4] D. Strekalov et al., "W-Band Photonic Receiver for Compact Cloud Radars," *Sensors* **22** (2022).

Photonic Oscillators Involving Bulk Optical Cavities

Anatoliy Savchenkov¹, Wei Zhang¹, Vladimir Itchenko¹, and Andrey Matsko^{1,*},

IT

¹ Jet Propulsion Laboratory, MS 298, California Institute of Technology, Pasadena, California 91109-8099, USA

* andrey.b.matsko@jpl.nasa.gov

Abstract: Recent advances in generation of low noise microwave (from X- to W-band) and optical signals using self-injection locked semiconductor lasers as well as high-Q monolithic optical cavities integrated on the same platform are discussed. © 2024 California Institute of Technology. Government sponsorship acknowledged.

1. Introduction

High-Q optical microcavities are essential for stabilizing and creating low noise both optical and microwave sources. The performance of the devices is primarily impacted by a few parameters of the cavities, including their quality (Q-) factor, geometrical volume, nonlinearity, and thermal sensitivity. The high-Q factor enables reduction of the phase noise of the active devices involving the cavity but also reduces the threshold of various nonlinear processes that can be observed in the cavity and can be both useful and detrimental, depending on the application. The geometrical volumes of the cavity and the cavity modes impact the vibration sensitivity of the system as well as its fundamental thermodynamic stability. Additionally, it influences the nonlinear response of the cavity and impacts the density of the cavity spectrum. The nonlinearity enables generation of optical frequency combs but also results in exchange between the amplitude and phase noise of the system. The thermal sensitivity, including thermo-refraction and thermo-expansion properties of the cavity, impacts the thermal stability of the cavity-based system but also enables tuning of the cavity spectrum.

To create a low noise stable oscillator based on an optical cavity one has to involve a high-Q device, with low thermal and optical nonlinearity, high mode volume, small overall volume, and clean optical spectrum. Some of the requirements are contradictory and a significant effort is needed to optimize the space of the parameters. In this presentation we discuss a few applications of the optical cavities to create optimized high performance lasers and microwave photonic oscillators [1 – 4].

2. Lasers and Laser-based Microwave Oscillators

Optical resonators are optical metrological instruments benefiting from highly isolated environment. The cavity structure defines the needed degree of isolation. For instance, to achieve peak performance of empty Fabry-Perot (FP) cavities, they has to be placed in high-vacuum enclosure. The selection of the cavity host materials and mirrors is also critically important. Monolithic FP resonators are emerging as promising alternative to traditional designs because of these reasons. The optimization of the cavity design is an ongoing activity. We recently demonstrated a monolithic FP resonator with less than 5cc volume and 2×10^5 finesse and used it for a laser stabilization [2,3]. We demonstrated less than 20 Hz integral laser linewidth and 7×10^{-14} relative frequency stability measured from 0.1 s to 0.3 s averaging time. This is the highest spectral purity and stability demonstrated to date in the context of monolithic reference resonators. By locking two separate lasers to distinct modes of the same resonator using a Pound-Drever-Hall (PDH) technique, a 96 GHz microwave signals were generated with phase noise -100dBc/Hz at 10 kHz frequency offset, achieving orders of magnitude improvement if compared with the other microwave photonic synthesizer involving stabilized lasers.

We also demonstrated simultaneous self-injection locking (SIL) [5] of two semiconductor lasers to high-order modes of a stand-alone monolithic non-confocal FP cavity [3]. The lasers were used to generate a low noise microwave signal on a fast photodiode. The overall improvement of the laser spectral purity exceeds 80 dB. The observed single sideband phase noise of X - to Ka-band signals is at the -110dBc/Hz level (the SIL technique was more effective than the PDH technique) and is limited by the fundamental thermorefractive noise of the cavity. The demonstrated cavity-laser configuration can be tightly packaged and is promising for

generation of high frequency RF signals as well as for referencing optical frequency combs. The compact monolithic FP resonator is promising for applications in spectrally-pure, high frequency microwave photonic references as well as optical clocks and other metrological devices.

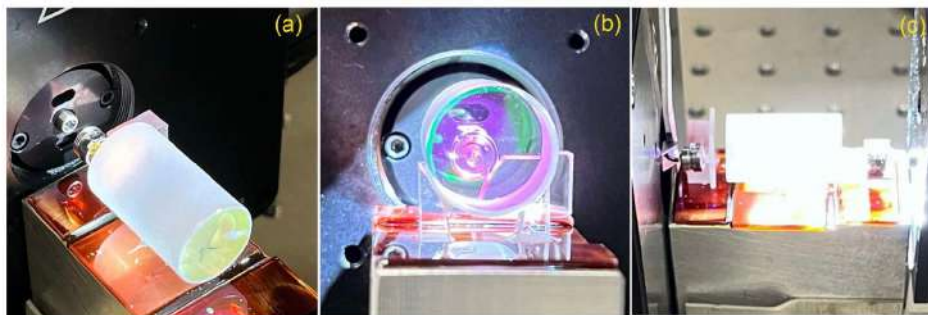


Fig. 1. The Fabry-Perot cavity coupled to one (a,b) and two (c) distributed feedback (DFB) lasers. Panels (a) and (b) show different projections of the cavity and one of the lasers. The opposite side of the cavity is open and its far field can be analyzed with the near-infrared camera. In panel (b) a front window of the DFB TO-can laser is visible through the mirrors of the cavity (the mirrors are reflective in the C-band only). Panel (c) depicts two lasers coupled to the same cavity. A rugged aluminum frame hosts the Thorlabs thermally controlled laser diode mount (a black case with white "laser danger" mark), a Fabry-Perot cavity (a white cylinder in the middle), and the coupling lens which matches the laser field with the high order mode of the cavity. The optical phase between the laser and the cavity is not controlled. No optical isolators are used. The optical elements are permanently mounted with a UV curable epoxy to a matched glass plates.

3. Kerr Comb Microwave Photonic Oscillators

Kerr comb microwave photonic oscillators are among the best in generation of spectrally pure microwave signals on a chip [6,7]. We recently shown that using a Kerr comb generated in a MgF_2 WGM resonator with Q-factor exceeding 10^9 one can generate W-band microwave frequency signals with phase noise approaching $-120\text{dBc}/\text{Hz}$ at 10 kHz frequency offset [4]. The observation paves the way towards realization of the miniature microwave photonic frequency generators and synthesizers at higher carrier frequencies. If compared with previous demonstrations by proper scaling of the phase noise, the phase noise demonstrated here is a few dB lower at 10 kHz offset and has comparable characteristics at lower and higher spectral frequencies. To our knowledge, this is the best phase noise achieved in the free running Kerr frequency comb microwave photonic oscillators.

Acknowledgments

The research was carried out at the Jet Propulsion Laboratory, California Institute of Technology, under a contract with the National Aeronautics and Space Administration (80NM0018D0004).

References

- [1] I. Kudelin, W. Groman, Q.-X. Ji, J. Guo, M. L. Kelleher, D. Lee, T. Nakamura, C. A. McLemore, P. Shirmohammadi, S. Hanifi, H. Cheng, N. Jin, L. Wu, S. Halladay, Y. Luo, Z. Dai, W. Jin, J. Bai, Y. Liu, W. Zhang, C. Xiang, L. Chang, V. Iltchenko, O. Miller, A. Matsko, S. M. Bowers, P. T. Rakich, J. C. Campbell, J. E. Bowers, K. J. Vahala, F. Quinlan, S. A. Diddams, "Photonic chip-based low-noise microwave oscillator," *Nature* **627**, 534-539 (2024).
- [2] W. Zhang, E. Kittlaus, A. Savchenkov, V. Iltchenko, L. Yi, S. B. Papp, A. Matsko, "Monolithic optical resonator for ultrastable laser and photonic millimeter-wave synthesis," *Commun. Phys.* **7**, 177 (2024).
- [3] A. Savchenkov, W. Zhang, V. Iltchenko, and A. Matsko, "Robust self-injection locking to a non-confocal monolithic Fabry-Perot cavity," *Opt. Lett.* **49**, 1520-1523 (2024).
- [4] A. Savchenkov, D. Strekalov, V. Ilchenko, M. Toennies, N. Majurec, R. Ahmed, A. Matsko, "Low noise W-band photonic oscillator," *IEEE J. Sel. Top. Quantum Electron.* **30**, 2100309 (2024).
- [5] W. Liang, V. S. Ilchenko, A. A. Savchenkov, A. B. Matsko, D. Seidel, and L. Maleki, "Whispering-gallery-mode-resonator-based ultranarrow linewidth external-cavity semiconductor laser," *Opt. Lett.* **35**, 2822-2824 (2010).
- [6] A. A. Savchenkov, A. B. Matsko, D. Strekalov, M. Mohageg, V. S. Ilchenko, and L. Maleki, "Low threshold optical oscillations in a whispering gallery mode CaF_2 resonator," *Phys. Rev. Lett.* **93**, 243905 (2004).
- [7] W. Liang, D. Eliyahu, V.S. Ilchenko, A.A. Savchenkov, A.B. Matsko, D. Seidel, L. Maleki, "High spectral purity Kerr frequency comb radio frequency photonic oscillator," *Nature Commun.* **6**, 7957 (2015).

Self-organization of lasing modes in chaotic billiard lasers

*Takahisa Harayama**

IT

Department of Applied Physics, School of Advanced Science and Engineering, Waseda University, 3-4-1 Okubo, Shinjuku-ku, Tokyo 169-8555, Japan

* harayama@waseda.jp

Abstract: I will show self-organized formation of lasing modes in three cases: Uniform and selective pumping in fullychaotic billiard lasers, and partially-chaotic asymmetric billiard lasers.

First, I will show the universal single-mode lasing in fully-chaotic billiard lasers: At least one single-mode lasing state is stable, whereas all multi-mode lasing states are unstable, when the external pumping power is sufficiently large and the billiard size is much larger than the wavelength. These phenomena arise from the combination of two different nonlinear effects of mode-interaction due to the active lasing medium and deformation of the billiard shape.

Second, by numerical simulation of a fully-chaotic billiard laser with the selective pumping where the pumping region is limited to the narrow area covering a short unstable periodic ray orbit, I will show that the resonance wave functions cooperate to localize the light intensity of the stationary lasing state along the periodic ray orbit in the self-organized manner that realizes an optimal intensity pattern for getting the external pumping energy efficiently. In spite of no scars in cold cavity resonance modes, locking of the resonance modes enables the localization along the short unstable periodic ray orbit. We call this localized stationary lasing mode “nonlinear scar mode” in order to make it distinguished from a cold cavity linear scar mode.

Finally, I will show clockwise (CW) and counter-clockwise (CCW) chiral lasing modes as the locked state of a chiral pair of non-orthogonal resonance modes in a partially-chaotic billiard laser. From the view-point of laser dynamics, I will explain that the only the CW or CCW chiral mode becomes a stable lasing state at the exceptional point.

References

- [1] M. You, D. Sakakibara, K. Makino, Y. Morishita, K. Matsumura, Y. Kawashima, M. Yoshikawa, M. Tonosaki, K. Kanno, A. Uchida, S. Sunada, S. Shinohara, and T. Harayama, “Universal Single-Mode Lasing in Fully Chaotic Billiard Lasers,” *Entropy* **5**, 1648 (2022).
- [2] M. Matogawa, Y. Kuribayashi, Y. Suzuki, M. You, S. Shinohara, S. Sunada, and T. Harayama, “Nonlinear laser dynamics of a non-orthogonal chiral pair,” *Applied Physics Letters* **123**, 231104 (2023).

Stimulated Raman lasing and second harmonic generation in lithium tetraborate whispering gallery mode resonators

Chengcai Tian^{1,2,3}, *Florian Sedlmeir*^{1,2}, *Petra Becker*⁴, *Ladislav Bohatý*⁴, *Richard Blaikie*^{1,2,3}
and *Harald G. L. Schwefel*^{1,2,*}

CT

¹ The Dodd-Walls Centre for Photonic and Quantum Technologies, New Zealand

² Department of Physics, University of Otago, Dunedin 9016, New Zealand

³ The MacDiarmid Institute for Advanced Materials and Nanotechnology, Wellington 6012, New Zealand

⁴ Institute of Geology and Mineralogy, Sect. Crystallography, Zùlpicher Str. 49 b, 50674 Köln, Germany

* harald.schwefel@otago.ac.nz

Abstract: We investigate the relatively uncommon, but promising lithium tetraborate (LB4) as host material for whispering-gallery mode resonators since it has a high transparency in the visible and UV regime, strong Raman gain, and second order nonlinearities.

1. Introduction

Whispering gallery mode resonators (WGMRs) crafted from low-loss dielectric materials, such as lithium tetraborate (LB4) [1,2], exhibit exceptional confinement of light near the surface through total internal reflection. This allows for remarkably high Q factors and compact mode volumes, making them suitable for enhancing nonlinear effects [1], such as stimulated Raman lasing and second harmonic generation (SHG). Up to now LB4 has not been widely used as WGMR, besides recent impressive results of SHG by Fürst et al. [2]. Here, we report the fabrication of a millimeter sized x - and z -cut LB4 WGMRs, with Q factor (2×10^9 at 517 nm) in z -cut WGMRs. The Raman gain of LB4 is about 1.8 cm/GW [3], two orders of magnitude larger than that of silica [4] and we can report cascaded stimulated Raman scattering (SRS). Moreover, its second-order ($\chi^{(2)}$) nonlinear coefficients d_{31} and d_{33} are 0.5 pm/V and 3 pm/V, respectively [5]. Using cyclic phase matching [6], a broadband SHG at 258 nm 397 nm, and 780 nm in x -cut LB4 WGMRs can be observed.

2. Results

We fabricated our LB4 WGMR from a (001)-orientated LB4 wafer, grown by some of us [3]. A precursor disc was first drilled out of this wafer using a hollow brass drill bit and water-based 30 μ m diamond slurry. Subsequently, the disc was shaped on an air-bearing lathe via single-point diamond turning [7]. After cutting, the preliminary WGMR was polished using different-size diamond slurry. The resulting z -cut LB4 WGMR has a major radius $R = 2.97 \text{ mm} \pm 0.01 \text{ mm}$ and a minor radius $r = 2.30 \text{ mm} \pm 0.01 \text{ mm}$. The x -cut WGMR has a major radius of $1.45 \text{ mm} \pm 0.01 \text{ mm}$ and a minor radius of $0.90 \text{ mm} \pm 0.01 \text{ mm}$.

2.1 Cascaded Raman scattering in z -cut WGMRs

Cascaded SRS peaks with wavenumber difference about 720 cm^{-1} up to fourth order are observed in a z -cut WGMR on a spectrometer (Oceanoptics) when excited by a tunable laser at 517 nm. The spectrum is shown in Fig. 1(a). The saturated peak in Fig. 1(a) is the pump laser. The SRS peaks are located at 537.1 nm, 558.8 nm, 582.4 nm, and 608.2 nm, respectively. The inset in Fig. 1 (a) shows a photograph of the cascaded SRS signal captured with a USB camera after the optical grating. Fig. 1 (b) shows the first order SRS intensity changes with the absorbed power, indicating the threshold is about 0.69 mW.

2.2 SHG in x -cut WGMRs

In an x -cut WGMR made from uniaxial crystals with its optic axis lying within the plane of the equator, cyclic phase matching takes advantage of oscillating refractive index of the transverse-magnetic (TM) mode [8]. This spatial refractive index modulation in an x -cut WGMR allows negative uniaxial crystals, such as BBO [6] and here LB4, to achieve broadband phase matching within the transparency window of the nonlinear materials [6]. Our x -cut LB4 WGMRs have quality (Q) factors in the order of 10^7 at all pump wavelength. Exploiting a cubic z -cut LB4 prism as a second outcoupling prism, selective outcoupling of SHG is achieved [9]. which improves the SHG conversion efficiency by a factor of two, and detect SHG signals at 780 nm, 397 nm and 258 nm. Table 1 summarizes the Q factors and conversion efficiency of SHG in our LB4 WGMRs.

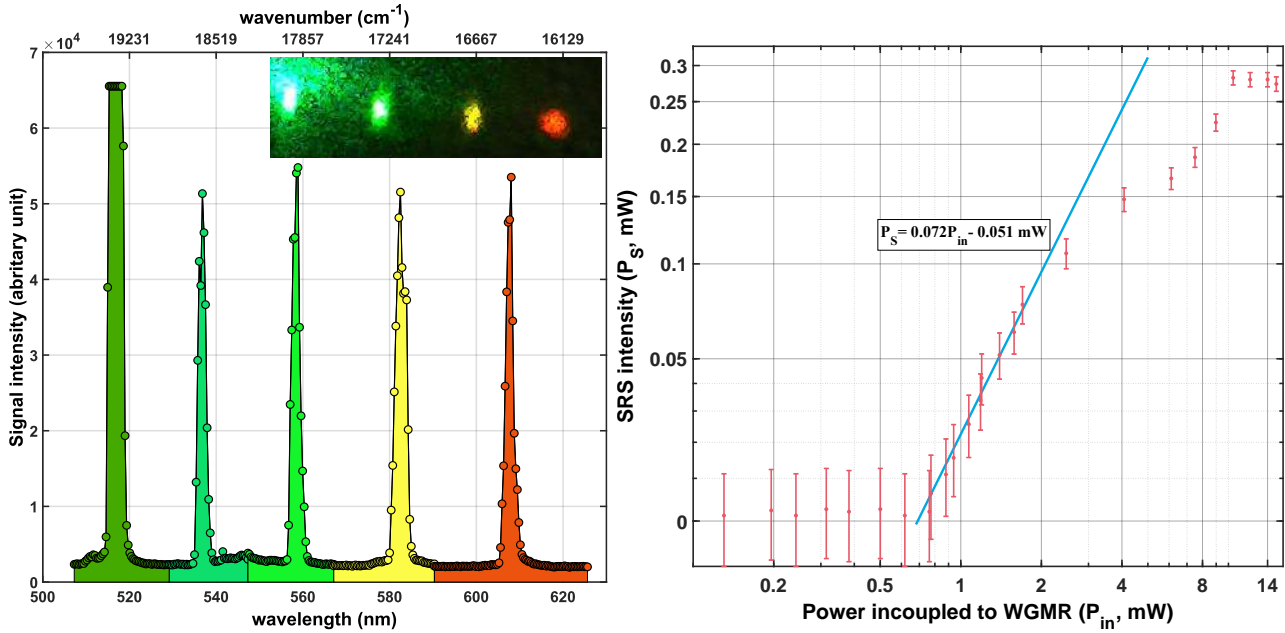


Fig. 1. Left panel: Cascaded SRS in LB4 WGMR under critical coupling. Inset: the four SRS signals after the optical grating, of which the first two orders are saturated in the center due to the high absorbed pump power (7 mW). Right Panel: First order SRS intensity changes with the absorbed power in fundamental mode (dots with 5% error bar), the inserted dashed line is the fitting curve when the pump is larger than the threshold $P_{th,s}$, of which the slope is the slope efficiency of SRS.

Table 1: Summary of second harmonic (SH) generation for three different pump wavelengths: maximum incident pump power (P_p^{max}), maximum second harmonic (SH) power (P_{SH}^{max}), the Q factor of the pump mode, and conversion efficiency (P_{SH}/P_p^2) per mW incident pump power

wavelength (nm)	Q factor ($\times 10^7$)	P_p^{max} (mW)	P_{SH}^{max} (μ W)	SH wavelength (nm)	P_{SH}/P_p^2 (%/mW)
1560	4.8	1.05	0.19	780	0.016
795	2.0	7.83	10.51	397	0.021
517	6.7	10.49	133.60	258	0.129

References

- [1] D. V. Strekalov, C. Marquardt, A. B. Matsko, H. G. Schwefel, and G. Leuchs, "Nonlinear and quantum optics with whispering gallery resonators," *J. Opt.* **18**, 123002 (2016).
- [2] J. U. Fürst, H. Breunig, P. Becker, J. Liebertz, and L. Bohaty, "Second-harmonic generation of light at 245 nm in a lithium tetraborate whispering gallery resonator," *Opt. Lett.* **40**, 1932–1935 (2015).
- [3] A. Kaminskii, L. Bohaty, P. Becker, J. Liebertz, H. Eichler, and H. Rhee, "Stimulated Raman scattering and cascaded nonlinear laser ($\chi^{(3)} + \chi^{(2)}$) effects in tetragonal non-centrosymmetric $\text{Li}_2\text{B}_4\text{O}_7$ single crystals," *Laser Phys. Lett.* **3**, 519 (2006).
- [4] R. Stolen and E. Ippen, "Raman gain in glass optical waveguides," *Appl. Phys. Lett.* **22**, 276–278 (1973).
- [5] D. Kasproicz, J. Kroupa, A. Majchrowski, E. Michalski, M. Drozdowski, and J. Žmija, "Elastic and nonlinear optical properties of lithium tetraborate," *Cryst. Res. Technol. J. Exp. Ind. Crystallogr.* **38**, 374–378 (2003).
- [6] G. Lin, J. U. Fürst, D. V. Strekalov, and N. Yu, "Wide-range cyclic phase matching and second harmonic generation in whispering gallery resonators," *Appl. Phys. Lett.* **103** (2013).
- [7] F. Sedlmeir, "Crystalline whispering gallery mode resonators," Ph.D. thesis, Friedrich-Alexander-Universität Erlangen-Nürnberg (FAU) (2016).
- [8] J. Fürst, B. Sturman, K. Buse, and I. Breunig, "Whispering gallery resonators with broken axial symmetry: Theory and experiment," *Opt. Express* **24**, 20143–20155 (2016).
- [9] F. Sedlmeir, M. R. Foreman, U. Vogl, R. Zeltner, G. Schunk, D. V. Strekalov, C. Marquardt, G. Leuchs, and H. G. Schwefel, "Polarization-selective out-coupling of whispering-gallery modes," *Phys. Rev. Appl.* **7**, 024029 (2017).

Implementing Non-Euclidean Microcavity in 2D Flat space

Muhan Choi^{1,*}, *Inbo Kim*², *Yong-Hoon Lee*²

IT

¹ School of Electronic and Electrical Engineering, Kyungpook National University, Daegu 41566, Republic of Korea

² Digital Technology Research Center, Kyungpook National University, Daegu 41566, Republic of Korea

* muhan@knu.ac.kr

Abstract: Non-Euclidean optical microcavities are demonstrated as flat photonic devices using transformation optics. Although the devices have a planar structure, they possess the optical characteristics of non-Euclidean microcavity resonators.

Introduction

Recently, due to advancements in fabrication technologies, research into 2D optical resonators implemented in topologically curved spaces (non-Euclidean microcavity) has been actively studied [1,2]. These studies are not only of great significance in theoretical physics but could also potentially lead to dramatic improvements in photonic devices by tailoring the properties of the topological spaces in which the devices are embedded. However, although fabricating devices on topologically curved substrates is useful as a testbed for understanding the properties of 2D resonators on curved surfaces, it is practically difficult to apply these devices in industrial applications since most commercial photonic devices are implemented on flat substrates using semiconductor fabrication technologies.

Here, we have demonstrated non-Euclidean microcavities characterized in 2D curved space, implemented as flat photonic devices using transformation optics. [3-6]. Although the devices have a planar structure, they possess the optical characteristics of non-Euclidean microcavity resonators.

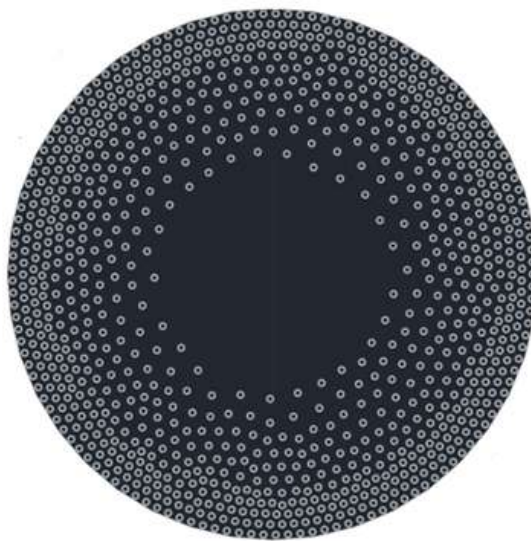


Fig. 1. Schematic of non-Euclidean optical microcavity demonstrated as flat photonic devices.

References

- [1] Y. Song, Y. Monceaux, S. Bittner, K. Chao, H. M. Reynoso de la Cruz, C. Lafargue, D. Decanini, B. Dietz, J. Zyss, A. Grigis, X. Checoury, and M. Leblental, "Möbius strip microlasers: a testbed for non-Euclidean photonics," *Physical Review Letters*, 127(20), 203901 (2021).
- [2] Y. Wang, Y. Ren, X. Luo, B. Li, Z. Chen, Z. Liu, F. Liu, Y. Cai, Y. Zhang, J. Liu and F. Li, "Manipulating cavity photon dynamics by topologically curved space," *Light: Science & Applications*, 11(1), 308 (2022).
- [3] J. B. Pendry, D. Schurig, and D. R. Smith, "Controlling electromagnetic fields," *Science* 312, 1780–1782 (2006).

- [4] U. Leonhardt, "Optical conformal mapping," *Science* 312, 1777–1780 (2006).
- [5] Y. Kim, S.-Y. Lee, J.-W. Ryu, I. Kim, J.-H. Han, H.-S. Tae, M. Choi, and B. Min, "Designing whispering gallery modes via transformation optics," *Nat. Photonics* 10, 647–652 (2016).
- [6] Y.-H. Lee, H. Park, I. Kim, S.-J. Park, S. Rim, B.J. Park, M. Kim, Y.Kim, M.-K Kim, W. S. Han, H. Kim, H. Park, and M. Choi, "Shape-tailored whispering gallery microcavity lasers designed by transformation optics," *Photon. Res.* 11, A35-A43 (2023).

Fully integrated, ultrahigh-sensitivity cavity optomechanical ultrasound sensors

Xuening Cao^{1,2}, Hao Yang^{1,2}, Min Wang^{1,2}, Zu-Lei Wu^{1,2}, Qi-Fan Yang³ and Beibei Li^{1,2,*}

¹ Beijing National Laboratory for Condensed Matter Physics, Institute of Physics, Chinese Academy of Sciences, Beijing 100190, China

² University of Chinese Academy of Sciences, Beijing 100049, China

³ State Key Laboratory for Artificial Microstructure and Mesoscopic Physics and Frontiers Science Center for Nano-optoelectronics, School of Physics, Peking University, Beijing 100871, China

* libeibei@iphy.ac.cn

Abstract: We demonstrate a fully integrated, ultrahigh-sensitivity optomechanical ultrasound sensor using a SiO₂ membrane with a Si₃N₄ ring resonator embedded inside. An ultrasound sensitivity of 9.6nPaHz^{-1/2} has been achieved in the water environment. © 2024 The Author(s)

1. Introduction

Ultrasound sensing is widely adopted in various applications, including medical imaging, non-destructive testing, underwater acoustics, and industrial process monitoring. Conventional ultrasound transducers, typically based on piezoelectric materials, have been widely used in these applications. However, these transducers face challenges in terms of miniaturization, integration, and sensitivities, which restrict their applications in scenarios that require compactness and high resolutions. Recently, ultrasound sensors based on optical microcavities have been developed, which provide the advantages of high sensitivities, broad bandwidth, low power consumption, and chip-integration capabilities to meet the needs of a wide range of applications [1]. Currently, researchers have obtained noise equivalent pressures (NEP) on the order of $\mu\text{PaHz}^{-1/2}$ using optical microcavities. However, most of these highly sensitive microcavity ultrasound sensors necessitate tapered fiber coupling, which brings considerable challenges in integration and mass production [2-4]. Furthermore, on-chip integrated optical microcavity ultrasound sensors have been developed, but their substrate limits their mechanical response, resulting in NEPs at the mPa Hz^{-1/2} level [5-7].

In this work, we propose and demonstrate a novel integrated, high-sensitivity optomechanical ultrasound sensor (Figs. 1a-1c) consisting of a suspended SiO₂ membrane and an embedded Si₃N₄ microring resonator. The device is fabricated using CMOS-compatible processes including electron-beam lithography (EBL) and reactive ion etching (RIE) to fabricate the Si₃N₄ microring in the front side, and deep-RIE to etch the silicon underneath the microring. Due to the mechanical resonance enhanced response of the SiO₂ membrane and the optical resonance enhanced readout sensitivity of the high-*Q* Si₃N₄ microring resonator, this sensor achieved a NEP of 9.6nPaHz^{-1/2} in the water environment (Fig. 1d). We further apply the sensor for ultrasound imaging in water, achieving a spatial resolution of 1.34 mm (Fig. 1e). This fully integrated, high-sensitivity ultrasound sensor opens new possibilities for a range of applications such as underwater ultrasound imaging, photoacoustic imaging, etc.

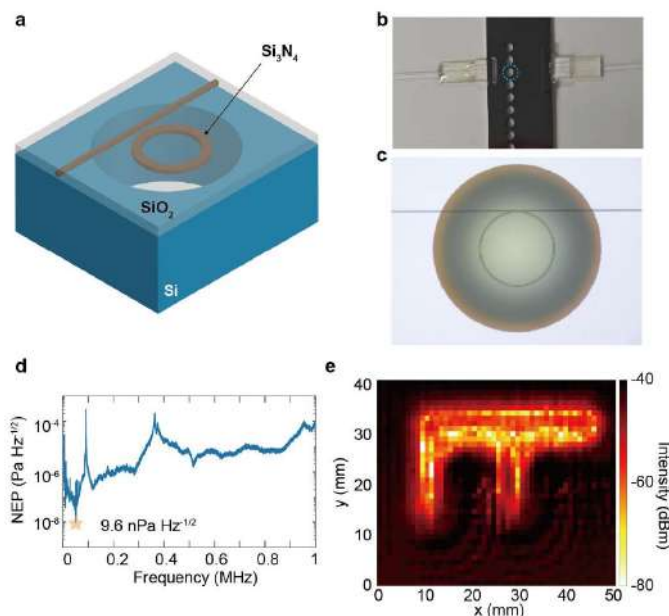


Fig. 1. **a**, Schematic of the integrated ultrasound sensor. **b**, Photograph of the encapsulated sensor. **c**, Optical microscope image of the suspended membrane with an embedded microring. **d**, NEP spectrum of the ultrasound sensor in water. **e**, Demonstration of the ultrasound imaging of the sample in water.

References

- [1] X. Cao, H. Yang, Z.-L. Wu, and B.-B. Li, "Ultrasound sensing with optical microcavities," *Light Sci. Appl.* **13**, 159 (2024).
- [2] S. Basiri-Esfahani, A. Armin, S. Forstner, and W. P. Bowen, "Precision ultrasound sensing on a chip," *Nat. Commun.* **10**, 132 (2019).
- [3] H. Yang, Z.-G. Hu, Y. Lei, X. Cao, M. Wang, J. Sun, Z. Zuo, C. Li, X. Xu, and B.-B. Li, "High-sensitivity aircoupled megahertz-frequency ultrasound detection using on-chip microcavities," *Phys. Rev. Appl.* **18**, 034035 (2022).
- [4] H. Yang, X. Cao, Z.-G. Hu, Y. Gao, Y. Lei, M. Wang, Z. Zuo, X. Xu, and B.-B. Li, "Micropascal-sensitivity ultrasound sensors based on optical microcavities," *Photon. Res.* **11**, 1139-1147 (2023).
- [5] W. J. Westerveld, M. Mahmud-Ul-Hasan, R. Shnaiderman, V. Ntziachristos, X. Rottenberg, S. Severi, and V. Rochus, "Sensitive, small, broadband and scalable optomechanical ultrasound sensor in silicon photonics," *Nat. Photonics* **15**, 341-345 (2021).
- [6] J. Pan, Q. Li, Y. Feng, R. Zhong, Z. Fu, S. Yang, W. Sun, B. Zhang, Q. Sui, J. Chen, Y. Shen, and Z. Li, "Parallel interrogation of the chalcogenide-based micro-ring sensor array for photoacoustic tomography," *Nat. Commun.* **14**, 3250 (2023).
- [7] R. Shnaiderman, G. Wissmeyer, O. Ülgen, Q. Mustafa, A. Chmyrov, and V. Ntziachristos, "A submicrometre silicon-on-insulator resonator for ultrasound detection," *Nature* **585**, 372-378 (2020).

Whispering gallery mode resonator based on PMN-PT single crystal

Yongyong Zhuang^{1,}, Liu Yang¹, Yifan Zhang¹, Hao Zhang¹, Xin Liu¹, Qingyuan Hu¹, Y. J. Zhang², S. Y. Zhang², P. Del'Haye², Xiaoyong Wei¹, Zhuo Xu¹*

CT

¹ Electronic Materials Research Laboratory, Key Laboratory of the Ministry of Education & International Center for Dielectric Research, School of Electronic Science and Engineering, Faculty of Electronic and Information Engineering, Xi'an Jiaotong University, Xi'an, China

² Max Planck Institute for the Science of Light, Staudtstrasse 2, Erlangen, Germany

* xiaozhuang235@163.com

Abstract: Electro-optic and inverse piezoelectric effects are used to achieve effective regulation of the resonance frequencies of PMN-PT based WGMR and the modulation efficiency up to 0.16GHz/V, which is ten times that of LN.

1. Introduction

The resonance frequency of whispering gallery mode resonators (WGMRs) is a significant parameter of the resonator. We report the fabrication of PMN-PT optical resonators, which is polarized by high-temperature methods to decrease the number of domain walls in [001]-oriented PMN-PT crystal. Additionally, we also have proposed a scheme that uses the electro-optic (EO) and inverse piezoelectric effects of tetragonal PMN-PT to achieve resonance frequency tuning in the WGMR. When applying an electrical field on the PMN-PT resonator, the frequency detuning is flexibly controlled by changing the refractive index and the size of the resonator. Notably, compared with LN resonator, we find the frequency tuning range of PMN-PT resonator is ten times than that of LN resonator. Moreover, the asymmetric phenomenon appears in different wavelength scan directions, and a hysteresis phenomenon appears when applied a huge voltage, which are caused by the photorefractive effect. Our work shows that PMN-PT is a potential platform material for the application of frequency-tunable and electro-optic modulation devices.

2. Results

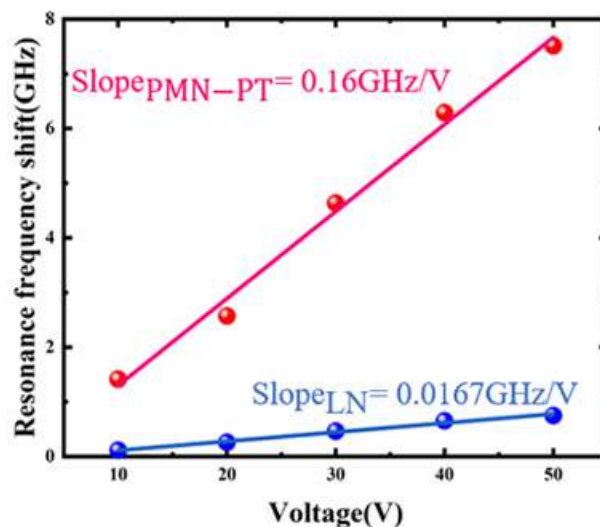


Fig. 1. Induced resonance frequency shift of the PMN-PT(LN) resonator as a function of the applied voltage, where the experimental data are shown as red (blue) points, and the pink (blue) line is a linear fitting, with a slope of 0.159GHz/V (0.0167GHz/V).

3. Summary

The resonance frequency can be controlled by applying an electric field to the surface of the resonator. The asymmetrical resonance modes and a hysteresis phenomenon caused by photorefractive effects have been observed in PMN-PT resonators. Excellent EO and inverse piezoelectric effects enable PMN-PT resonators to have greater resonance frequency tuning capability under low power consumption, which makes it widely used in the field of frequency tunable devices.

References

- [1] Liu X, Tan P, Ma X, et al, "Ferroelectric crystals with giant electro-optic property enabling ultracompact Q-switches," *Science*, 376 (6591):371, (2022).
- [2] Qiu C R, Wang B, Zhang N, et al, "Transparent ferroelectric crystals with ultrahigh piezoelectricity," *Nature*, 577 (7790):350, (2020).

Kerr solitons in fiber cavities – past and present

Stuart G. Murdoch^{1,2,*}

IT

¹ Department of Physics, University of Auckland, Auckland, New Zealand

² The Dodd-Walls Centre for Photonics and Quantum technologies, New Zealand

* s.murdoch@auckland.ac.nz

Abstract: We review the history and future prospects for the generation of Kerr cavity solitons in passive optical fiber cavities.

The temporal cavity soliton (CS) was first demonstrated in 2010 in a macroscopic fiber cavity [1]. The demonstration of CSs in optical microresonators followed in 2014 [2], sparking a surge of interest in these remarkable nonlinear dissipative optical structures [3]. In this talk, we discuss how measurements of CS properties and interactions are often simpler in macroscopic fiber cavities and share some notable results (refer to Figure 1). We will also evaluate the performance of fiber cavities with dimensions approaching those of an optical microresonator which facilitate the generation of CS combs with GHz line-spacings.

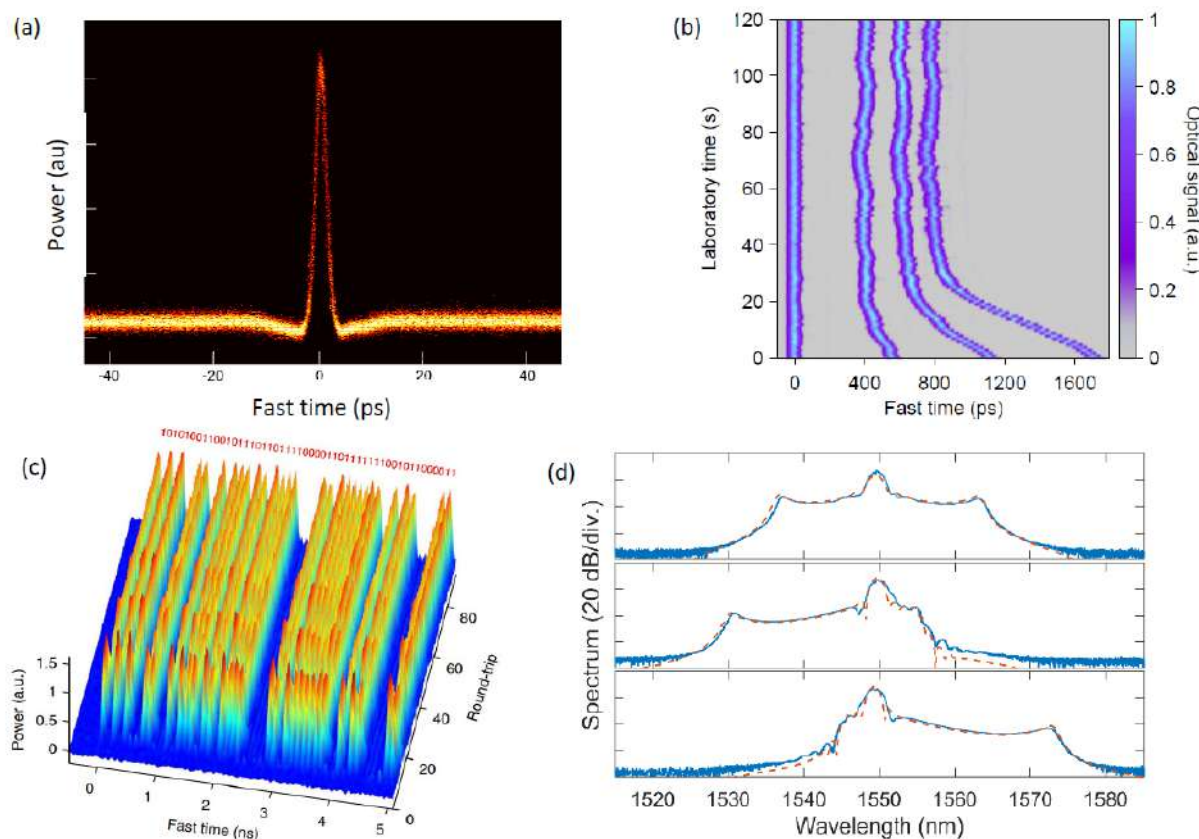


Fig. 1. (a) Direct measurement of a temporal CS in a fiber cavity using a ps resolution optical sampling scope [4], long-range ultra-weak interaction between adjacent CSs measured over 2 minutes [5], 4700 optical bits stored as CSs circulating in a fiber cavity [4]. Pulse-driven normal-dispersion switching wave combs measured at different desynchronizations in sub-meter length fiber cavity [6].

References

- [1] Leo F, Coen S, Kockaert P, Gorza SP, Emplit P, Haelterman M. Temporal cavity solitons in one-dimensional Kerr media as bits in an all-optical buffer. *Nature Photonics* **4** 471-6 (2010).
- [2] Herr T, Brasch V, Jost JD, Wang CY, Kondratiev NM, Gorodetsky ML, Kippenberg TJ. Temporal solitons in optical microresonators. *Nature Photonics* **8** 145-52 (2014).

- [3] Lugiato LA, Prati F, Gorodetsky ML, Kippenberg TJ. From the Lugiato–Lefever equation to microresonator-based soliton Kerr frequency combs. *Philosophical Transactions of the Royal Society A* **376** 20180113 (2018).
- [4] Jang JK, Erkintalo M, Schröder J, Eggleton BJ, Murdoch SG, Coen S. All-optical buffer based on temporal cavity solitons operating at 10 Gb/s. *Optics letters* **41** 4526-9 (2016).
- [5] Jang JK, Erkintalo M, Murdoch SG, Coen S. Ultraweak long-range interactions of solitons observed over astronomical distances. *Nature Photonics* **7** 657-63 (2013).
- [6] Xu Y, Sharples A, Fatome J, Coen S, Erkintalo M, Murdoch SG. Frequency comb generation in a pulse-pumped normal dispersion Kerr mini-resonator *Optics Letters*. **46** 512-5 (2021).

All-optical injection Locking of Dissipative Breather Solitons in Microresonators

Wang Liao^{1,2,*}, Stuart Murdoch^{1,2}, Stéphane Coen^{1,2}, Gregory Moille^{3,4}, Kartik Srinivasan^{3,4}
and Miro Erkintalo^{1,2}

CT

¹ Department of Physics, University of Auckland, New Zealand

² The Dodd-Walls Centre for Photonics and Quantum technologies, New Zealand

³ Joint Quantum Institute, NIST/University of Maryland, College Park, MD, USA

⁴ Microsystems and Nanotechnology Division, NIST, Gaithersburg, MD, USA

* wang.liao@auckland.ac.nz

Abstract: We experimentally and numerically show that oscillation frequency of dissipative breather solitons generated in a chip-integrated microresonator can be all-optically synchronized to an injected reference laser. © 2024 The Author(s)

Temporal cavity solitons are localized pulses of light that circulate indefinitely around a coherently driven nonlinear optical cavity. Their experimental realization in optical microresonators sparks persistent interest because they are associated with broadband and coherent optical frequency combs. Temporal cavity solitons also display rich nonlinear dynamics, including oscillatory instability. Specifically, under suitable conditions, the solitons' characteristics (e.g. pulse width and energy) exhibit periodic oscillations. Such oscillating solitons are often called temporal dissipative breathers, and they are related to Hopf bifurcations [1]. Temporal dissipative breathers were first observed in a fibre ring resonator [2], and then in microresonators [3, 4].

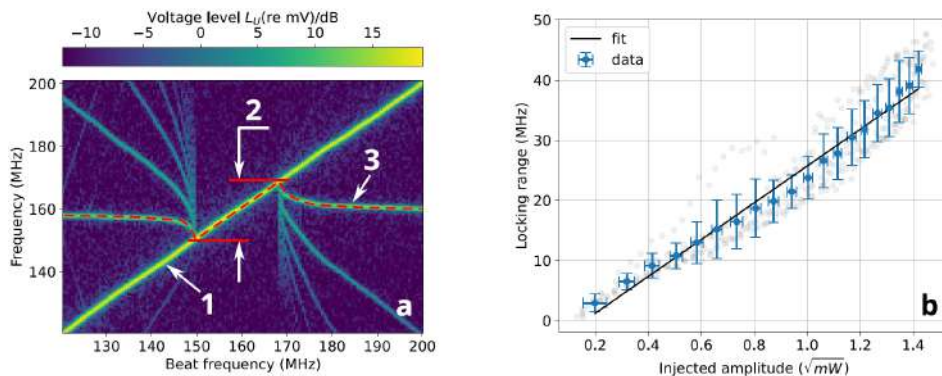


Fig. 1. Data from the experiment on the injection locking of breathing solitons. a A spectrogram shows the first harmonic component of the soliton breather locked to the beat between the injected laser and the driving laser: 1 — Beat signal between the driving laser and the injected laser; 2 — The locking range; 3 — Breather's breathing first harmonic signal. b Locking range dependence on injected laser amplitude (the square root of the power).

Recent research shows that the repetition rate of a stable temporal cavity soliton can be synchronized to an external reference laser [5,6]. In these studies, the frequency of the reference laser injected into the microresonator is placed sufficiently close to one of the soliton frequency comb lines, resulting in the entrainment of that comb line to the reference laser. Thus, the comb line spacing becomes pinned by the driving laser and the reference laser. This causes the repetition rate to be synchronized together with a reduction in the phase noise through optical frequency division. Interestingly, stable temporal solitons are not the only localized structures that can be synchronized: recent experiments show that the oscillating frequency of a dissipative breather can be synchronized by electrooptic modulation of the driving power [7]. However, because the free-spectral range of typical chip-integrated microresonators ranges from tens of GHz to THz, direct electro-optic modulation of the cavity driving field can only probe synchronization dynamics around the driven mode. An all-optical scheme is required to achieve and explore synchronization around frequency comb lines other than the driven mode, which could potentially reap the benefits of optical frequency division. However, to the best of our knowledge, the synchronization of dissipative breathers to an externally injected reference laser has

not yet been studied.

In this work, we demonstrate the first experimental realization of the all-optical dissipative breather synchronization in microresonators by directly injecting a secondary reference laser into the microresonator. We show experimentally that the breather's oscillating frequency is entrained when the frequency of the reference laser is brought sufficiently close to the optical (breather) sidebands around comb lines, thus enabling the control of the breathing frequency. Our experiments are performed using a Si_3N_4 microring resonator with an FSR of 1 THz. We drive the resonator at 1552 nm to generate a coherent frequency comb state that exhibits periodic oscillations with a frequency of about 160 MHz. We then inject a second ("reference") laser into the resonator to explore synchronization. Figure 1(a) shows the spectrogram measured when sweeping the injected reference laser across the breather's first harmonic component near the driving laser frequency. As can be seen, when sufficiently close to the breather's natural oscillation frequency of 160 MHz, the harmonic component is entrained to the injected laser (emphasized by the red dashed line). We also experimentally investigated the dependence of the locking range on the injected laser power, and found that the locking range increases linearly with the square root of the injected laser power (i.e., the "injected amplitude"). Figure 1(b) shows the linear trend between the injected laser amplitude and the breather injection locking range. To demonstrate the capability of synchronization at comb lines that are not directly driven, we swept the injected laser across the comb line frequency at 1569 nm. To probe whether the synchronization of the breathing frequency affects the frequency of the comb line (and hence the soliton repetition rate), we utilized the method of optical heterodyne detection by mixing the output light from the microresonator with a third laser whose frequency was close to the comb line frequency of interest. Figure 2 shows the spectrogram obtained from the heterodyne measurement, where f_0 is the comb line frequency of 191 THz. The spectrogram shows clearly the synchronization of both the low- and high-frequency breather sidebands (labeled by A and C respectively) as well as the comb line itself (labeled by B).

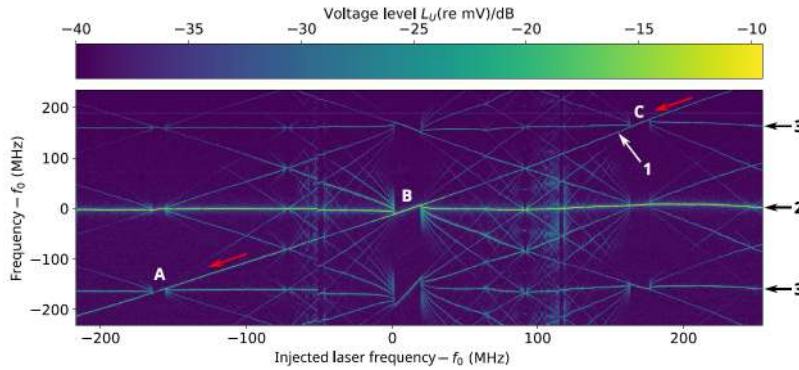


Fig. 2. Heterodyne measurement: 1 — Injected laser trace; 2 — Comb line at 1569 nm; 3 — Breather's optical sidebands. The red arrow points to the direction of the injected laser sweep.

In conclusion, we have shown that the oscillation frequency of dissipative breather solitons can be synchronized to an external injected laser in a microresonator when the injected laser is near the driving laser or comb line frequencies.

References

- [1] F. Leo, S. Coen, P. Kockaert, S.-P. Gorza, P. Emplit, and M. Haelterman, "Temporal cavity solitons in one-dimensional kerr media as bits in an all-optical buffer," *Nature Photonics*, vol. 4, no. 7, pp. 471–476, 2010.
- [2] F. Leo, L. Gelens, P. Emplit, M. Haelterman, and S. Coen, "Dynamics of one-dimensional kerr cavity solitons," *Optics express*, vol. 21, no. 7, pp. 9180–9191, 2013.
- [3] C. Bao, J. A. Jaramillo-Villegas, Y. Xuan, D. E. Leaird, M. Qi, and A. M. Weiner, "Observation of fermi-pasta-ulam recurrence induced by breather solitons in an optical microresonator," *Physical review letters*, vol. 117, no. 16, p. 163901, 2016.
- [4] E. Lucas, M. Karpov, H. Guo, M. Gorodetsky, and T. J. Kippenberg, "Breathing dissipative solitons in optical microresonators," *Nature communications*, vol. 8, no. 1, p. 736, 2017.
- [5] G. Moille, J. Stone, M. Chojnacky, R. Shrestha, U. A. Javid, C. Menyuk, and K. Srinivasan, "Kerr-induced synchronization of a cavity soliton to an optical reference," *Nature*, vol. 624, no. 7991, pp. 267–274, 2023.
- [6] T. Wildi, A. Ulanov, N. Englebert, T. Voumard, and T. Herr, "Sideband injection locking in microresonator frequency combs," *APL photonics*, vol. 8, no. 12, 2023.
- [7] S. Wan, R. Niu, Z.-Y. Wang, J.-L. Peng, M. Li, J. Li, G.-C. Guo, C.-L. Zou, and C.-H. Dong, "Frequency stabilization and tuning of breathing solitons in Si_3N_4 microresonators," *Photonics Research*, vol. 8, no. 8, pp. 1342–1349, 2020.

Soliton Microcomb-based Point and Distributed Optical Fiber Sensors

Baicheng Yao*

IT

Key Laboratory of Optical Fibre Sensing and Communications (Education Ministry of China), University of Electronic Science and Technology of China, Chengdu, 611731, China

* yaobaicheng@uestc.edu.cn

Optical sensing is crucial for information acquisition, forming the foundation of an optical information networks. High-performance light sources are essential for effective sensing systems, and determine the sensing configurations. The stability of the light source directly impacts the sensor's signal-to-noise ratio, while its multi-channel capability fundamentally enhances the information capacity of a sensing system. Soliton microcavity optical frequency combs have shown remarkable potential in communication and metrology applications due to their broad bandwidth, high coherence, natural wavelength division multiplexing, and excellent integration capabilities. Our recent studies demonstrate that microcavity based soliton frequency combs are also ideal light sources for driving both point and distributed fiber sensors, significantly enhancing their functionality and performance [1,2]. In chemical sensing, we achieved selective single-molecule detection of multispecies gas by locking symbiotic Kerr and Stokes solitons in a graphene-sensitized whispering-gallery mode microcavity [3]. For fiber optic distributed sensing, dual soliton combs were used to excite Rayleigh scattering in long-distance fibers, enabling high energy frequency division injection and ultra-sensitive acoustic sensing with a sensitivity of $560 \text{ f}\epsilon/\text{Hz}^{1/2}$ [4]. This approach also extends the sensing distance and resolves coherent fading issues found in traditional single-frequency driving schemes. Additionally, by discretizing the soliton comb across the entire chip, we demonstrated its ability to drive over 20 fiber optic microphone arrays simultaneously, achieving free-space localization of sound signals and high-precision passive detection of targets such as drones [5].

References

- [1] B. Yao*, et al. Interdisciplinary advances in microcombs: bridging physics and information technology. **eLight** 10.1186/s43593-024-00071-9 (2024).
- [2] B. Yao* & Y.-F. Xiao*, et al. Soliton Microcombs Multiplexing Using Intracavity-Stimulated Brillouin Lasers. **Phys. Rev. Lett.** 130, 153802 (2024).
- [3] B. Yao*, et al. Coherently parallel fiber-optic distributed acoustic sensing using dual Kerr soliton microcombs. **Science Advances** 1, eadf8666 (2024).
- [4] B. Yao*, et al. Multispecies and individual gas molecule detection using Stokes solitons in a graphene over-modal microresonator. **Nature Comm.** 12, 6716 (2021).
- [5] B. Yao*, et al. On-chip dual-microcomb based fiber-optic acoustic mapper. **Nature, in review** [Research Square: 10.21203/rs.3.rs-4234821/v1] (2024).

Cavity-induced coupling of a handful of molecules

*Vahid Sandoghdar**

IT

Max Planck Institute for the Science of Light, Staudtstr. 2, 91058 Erlangen, Germany

* vahid.sandoghdar@mpl.mpg.de

Over the past two decades, we have achieved a high degree of mastery in studying fundamental nano-optical interactions between single molecules and single photons. These include controlled coherent experiments in the near field, far-field demonstration of efficient extinction, various nonlinear measurements as well as single-molecule strong coupling in a microcavity. More recently, we have pursued projects, in which we examine the cooperative coherent interaction of several well-controlled individual molecules via a common photonic mode. In this talk, I present results from two different platforms, involving an open Fabry-Perot microcavity and a microdisc resonator in a chip-based integrated circuit.

Singular field in the nanogap of a plasmonic multimer antenna excited by a circularly-polarized plane wave

Christophe Pin^{1,*}, *Keiji Sasaki*^{2,‡}

CT

¹ Light-Matter Interactions for Quantum Technologies Unit, Okinawa Institute of Science and Technology Graduate University, Onna, Okinawa 904-0495, Japan

² Research Institute for Electronic Science, Hokkaido University, Kita 20, Nishi 10, Kita-ku, Sapporo, Hokkaido, 001-0021, Japan

* christophe.pin@oist.kp, ‡ sasaki@es.hokudai.ac.jp

Abstract: By breaking the rotational symmetry of a plasmonic multimer antenna, we demonstrate that a singular field localized in a nanogap can be excited by an incident circularly polarized plane wave either resonantly or non-resonantly.

1. Introduction

Since Nye and Berry in 1974 [1] and Allen et al. in 1992 [2], phase singularities of electromagnetic waves and optical vortex beams have been extensively studied and have enabled the demonstration of a remarkable range of new phenomena. For instance, Laguerre-Gaussian beams have been employed to manipulate and rotate micro- and nanoparticles, helically shape materials [3], control the chirality of chiral crystals [4], excite exciton-polariton vortices and optically-forbidden electronic transitions [5], and generate a superfluid flow [6]. However, the diffraction limit prevents us from focusing free-space optical vortex beams below the microscale (in the visible and near-infrared wavelength range). To enhance the light-matter interactions between singular electromagnetic fields and nanomaterials, molecules, or atoms, optical vortices must be confined on a nanoscale. Deep-subwavelength light focusing may be achieved by exciting the localized surface plasmon resonances of a plasmonic nanogap antenna. It was previously shown that an optical nanovortex, i.e. a confined singular field, is generated in the nanogap of a plasmonic multimer nanostructure excited by an optical vortex beam, provided that the multimer nanostructure is composed of a sufficient number of metal particles [7].

2. Results and discussion

We demonstrate here that an optical nanovortex may be directly generated when two interlocked plasmonic multimer nanostructures with a π -phase-shifted optical response are excited by an incident circularly polarized plane wave. For instance, two interlocked trimer nanostructures composed of nanorods with respectively red-shifted and blue-shifted dipole resonances make it possible to form a nanovortex field when excited by circularly polarized light with an intermediate wavelength. In this scenario, the weak, non-resonant excitation of both kinds of out-of-phase dipole resonators introduces the phase difference needed to obtain a phase singularity in the electric field localized in the central nanogap.

Designing a resonant nanovortex antenna with similar dipole resonators would require a 3D assembly of nanorods, adding complexity to the fabrication process. To avoid such difficulty, a 2D resonant nanovortex antenna may alternatively be designed by combining short and long nanorods with their respective dipole and longitudinal quadrupole resonances tuned to the same wavelength. Although the longitudinal quadrupole resonance cannot be directly excited by the incident plane wave, it is indirectly excited via evanescent coupling with the dipole resonators. The phase shift introduced by this indirect coupling leads to the generation of a phase singularity in the evanescent field confined in the central nanogap (see Figure 1).

3. Summary

In this work, we have shown that an optical nanovortex confined in the nanogap of a plasmonic multimer antenna can be directly excited by an incident circularly polarized plane wave. Whereas a non-resonant optical nanovortex may be obtained by using two interlocked multimer antenna with respectively red-shifted

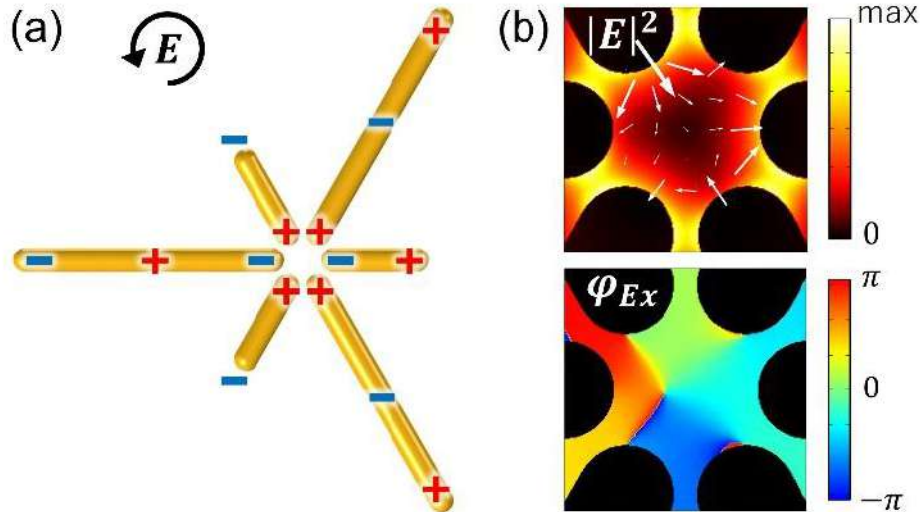


Fig. 1. (a) 2D nanovortex antenna composed of two interlocked gold trimer nanostructures (nanorod lengths: 440 nm and 175 nm; resonant wavelength: 890 nm). The resonant excitation of both dipole and longitudinal quadrupole modes generates a quadrupole-like charge distribution around the central nanogap. (b) Electric field intensity and phase distributions of the singular field generated in the nanogap under circularly polarized plane wave excitation.

and blue-shifted dipole resonances, resonant nanovortex antenna made of only dipole resonators require a complex 3D architecture. Alternatively, a 2D resonant nanovortex antenna may be obtained by combining dipole and longitudinal quadrupole resonators.

Acknowledgments

This work was supported by JSPS KAKENHI (Grants JP16H06506, JP18H03882, JP18H05205, and JP21H04657 to KS and JP20K15145, JP22H01923, and JP23H04571 to CP), and JSPS KAKENHI Grant-in-Aid (No. JP23H04571 to CP) for Transformative Research Areas (A) "Revolution of Chiral Materials Science using Helical Light Fields" from the Japan Society for the Promotion of Science (JSPS).

References

- [1] J. F. Nye and M. V. Berry, "Dislocations in wave trains," *Proceedings of the Royal Society of London A* 336, 165-190 (1974).
- [2] L. Allen et al., "Orbital angular momentum of light and the transformation of Laguerre-Gaussian laser modes," *Physical review A* 45, 8185 (1992).
- [3] T. Omatsu et al., "A new twist for materials science: the formation of chiral structures using the angular momentum of light," *Advanced Optical Materials* 7, 1801672 (2019).
- [4] A. C. Cheng et al., "Enantioselectivity in Chiral Crystallization Driven by the Canonical and Spin Momentum Forces of Optical Vortex Beams," *Journal of Physical Chemistry C* 128, 4314-4320 (2024).
- [5] G. F. Quinteiro Rosen et al., "Interplay between optical vortices and condensed matter," *Review of Modern Physics* 94, 035003 (2022).
- [6] A. Ramanathan et al., "Superflow in a toroidal Bose-Einstein condensate: an atom circuit with a tunable weak link," *Physics Review Letters* 106, 130401 (2011).
- [7] Y. Sunaba et al., "Nano-shaping of chiral photons," *Nanophotonics* 12, 2499-2506 (2023).

Microcavity vibrational spectroscopy for single-cell fingerprinting

Shui-Jing Tang*

IT

National Biomedical Imaging Center, College of Future Technology, Peking University, Beijing, China

* sjtang@pku.edu.cn

Abstract: Natural vibrations of mesoscopic particles – including most biological cells – have remained hidden from existing technologies. Here we demonstrated the real-time measurement of natural vibrations of single mesoscopic particles using an optical microresonator, extending the reach of vibrational spectroscopy to the megahertz-gigahertz frequency window.

It is first discovered by Pythagoras that the vibrations of strings are drastically enhanced at certain frequencies, which forms the basis of our tone system. Such natural vibrations ubiquitously exist in objects regardless of their size scales and are widely utilized to derive their species, constituents, and morphology. For example, molecular vibrations at terahertz rate have become the most common fingerprints for the identification of chemicals and structural analysis of large biomolecules. Recently, natural vibrations of particles at the mesoscopic scale have received growing interest, since this category includes a wide range of functional particles, as well as most biological cells and viruses. Extending the concept of vibrational spectroscopy to the mesoscopic world enables interrogating structures and mechanical properties of particles in a non-destructive way[1]. However, natural vibrations of mesoscopic particles – including most biological cells – have remained hidden from existing technologies[2]. These particles with sizes ranging from 100 nm to 100 μm are expected to vibrate faintly at megahertz to gigahertz rates[3]. This frequency regime could not be resolved by current Raman and Brillouin spectroscopies due to strong Rayleigh-wing scattering, while the performances of piezoelectric techniques that are widely exploited in macroscopic systems degrade significantly at frequencies beyond a few megahertz.

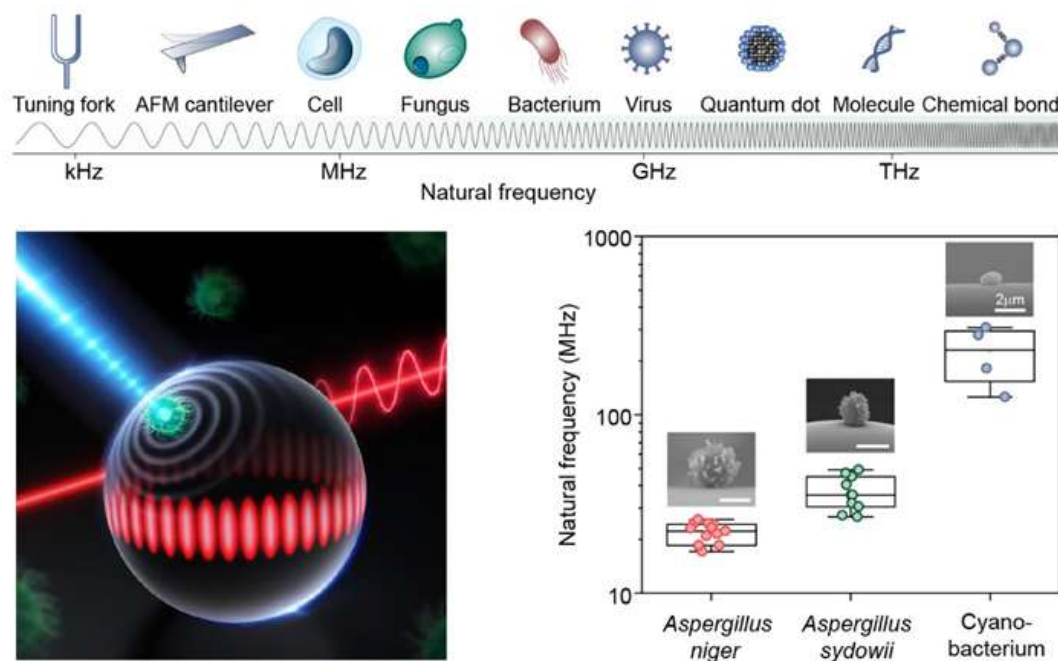


Fig. 1. Top: Natural frequencies of representative objects across different scales. Bottom left: Artist's view of microresonator-enabled single-particle vibrational spectroscopy. Bottom right: Measured natural frequencies of three types of microbial cells.

Here, we demonstrated the real-time measurement of natural vibrations of individual mesoscopic particles using

an optical microresonator, extending the reach of vibrational spectroscopy to the megahertz-gigahertz frequency window[4]. Conceptually, the vibrational modes of the particles are stimulated photoacoustically by laser pulse absorption, and coupled to optical resonances by stimulating acoustic waves within the microresonator. With the formation of whispering galleries through total-internal-reflections, the microresonator offers high-Q optical resonances that respond to acoustic waves in real time[5]. The concept of microcavity vibrational spectroscopy (MVS) was verified by measuring mesoscopic particles with different constituents, sizes, and internal structures, showing an unprecedented signal-to-noise ratio of 50 dB and detection bandwidth over 1 GHz. Using this new technology, we have further demonstrated biomechanical fingerprinting of the species and living states of microorganisms at the single-cell level. Specifically, we used MVS to measure three types of microorganisms, cyanobacteria, *Aspergillus sydowii*, and *Aspergillus niger*, in the atmospheric environment. It was observed that microorganisms of the same species exhibited bunched natural frequencies, forming unique fingerprints due to the highly defined and stable morphology of certain biological species. Additionally, the spectral information, including natural frequencies and mechanical quality factors, provides a measure of the viscoelastic properties of cells.

References

- [1] J. Zhou et al. "Single-particle spectroscopy for functional nanomaterials", *Nature* 579, 41 (2020).
- [2] E. Gil-Santos et al. "Optomechanical detection of vibration modes of a single bacterium", *Nat. Nanotech.* 15, 469 (2020).
- [3] S. Wheaton et al. "Probing the Raman-active acoustic vibrations of nanoparticles with extraordinary spectral resolution", *Nat. Photon.* 9, 68 (2015).
- [4] S.-J. Tang et al. "Single-particle photoacoustic vibrational spectroscopy using optical microresonators", *Nat. Photon.* 17, 951 (2023).
- [5] J. Meng et al. "Dissipative acousto-optic interactions in optical microcavities", *Phys. Rev. Lett.* 129, 073901 (2022).

Ultrafast Nonlinear Photonics on Thin Film Lithium Niobate

Mengjie Yu^{1,2,*}

IT

¹ Department of Electrical and Computer Engineering, University of Southern California, Los Angeles, CA 90089, United States

² Department of Electrical Engineering and Computer Science, University of California, Berkeley, CA 94720, United States

* mengjie.yu@berkeley.edu

Abstract: Lithium niobate (LN) is an excellent nonlinear photonic material due to its large electro-optic (EO) coefficient, second order ($\chi^{(2)}$) and Kerr ($\chi^{(3)}$) nonlinearity, along with a wide optical transparency window. Thanks to the recent advances in nanofabrication technology, monolithic LN waveguides with high optical confinement and ultralow linear loss has been achieved, which was critical to the success of the silicon-based platform in the past decade. Highly efficient and controllable light-matter interactions can be achieved using optical, electrical, or mechanical waves at extremely compact footprints. In this talk, I will review our recent developments of 1) optical frequency combs, 2) generation and measurement of ultrafast optical waveforms, and 3) mid infrared optics on thin-film LN nonlinear platform. Combination of multiple nonlinearities of LN unlocks ultrabroadband electromagnetic spectrum from microwave to mid-infrared. Lastly, I will discuss the potential of LN photonic platform for scaling up and accelerating classical and quantum technologies in sensing, photonic computing, and communication networks.

Modular sub-Hertz linewidth laser self-injection-locked to a whispering-gallery-mode resonator

Fangxin Zhang^{1,*}, *Ziji Cai*^{1,2}, *Bowen Ruan*¹

CT

¹ Peking University Yangtze Delta Institute of Optoelectronics, Nantong, China

² Peking University, Beijing, China

* Fangxing.Zhang@ydioe.pku.edu.cn

Abstract: We propose a modular Self-injection locking laser to address packaging difficulty and diode degeneration problem in SIL lasers. By stabilizing whispering-gallery-mode resonator and active control, 0.93 Hertz linewidth and 7*24 hours mode-hopping-free operation are achieved.

1. Introduction

Self-injection locking (SIL) technology is an efficient technique to stabilize laser by utilize an external resonator, which is used to reduce phase noise and frequency noise [1,2]. People tried package the external resonator and DFB in a small box to improve robustness, Liang et al. reported a heterogeneously integrated, chip-scale diode laser stabilized by SIL to a crystalline whispering-gallery-mode (WGM) microresonator [3]. Although the those WGM-SILs demonstrate exceptional performance in terms of ultra-low frequency noise and compact form factor, its hybrid package structure necessitates intricate precision micro-assembly and chip packaging techniques. Furthermore, the degradation of the laser module resulting from the aging of the laser diode, which typically has a lifespan around tens thousands hours, should not be disregarded. A direct solution to these disadvantages is to construct SIL laser in a modular manner, with every component packaged as a replaceable module and connected to others by fiber. Hertz-level linewidth has been attained [4] by adopting an all-fiber add-drop configuration, using feedback of MgF₂ WGM resonator to stabilize a multi-longitudinal mode fiber laser. However, the locking phase affected by the microresonator resonant frequency and the round-trip time from laser to microresonator, was susceptible to ambient disturbance, which impacts its long-term stability.

In this work, we assembled a modular SIL laser, and each component is packaged as a replaceable fiber compatible module implemented. By utilizing Rayleigh feedback from the WGM resonator and active control to the feedback phase delay, the multi-longitudinal mode fiber laser achieves stabilization, resulting in a 0.5 Hertz linewidth and long-term stability output.

2. Experiment & Results

Experimentally, we assembled a modular SIL laser with a commercial laser diode (Box Optronics Tech, BFLD-1550-10SM-FA2-N0) and a homemade packaged resonator device in Fig.1(a). The resonator is formed on a millimeter-sized silica rod, which is packaged in a copper box with polyetheretherketone liner (shown in the inset of Fig. 1(b)). The quality factor of the resonator after packaging is 4×10^8 , determined by characterizing the resonant linewidth in Fig. 1(b). Pump light coupled into the resonator through a fiber taper, and the random inhomogeneities in the resonator induce Rayleigh backscattering, which injected into the laser diode, serving as optical feedback. The fiber between the diode and the resonator is packaged, to isolate the ambient thermal and mechanical perturbation and keep the phase delay stable. These three modules (diode, fiber, and resonator) are fixed in an aluminum box, and thermoelectric coolers are placed under the fiber and resonator module. The instantaneous linewidth of the laser is 0.5 Hz. The phase noise of our modular SIL is 60dB lower than free-running DFB, also lower than NKT E15, which is shown in Fig. 1(c). To further reduce the influence of environment disturbance, we monitor the system operation state through the output power and apply feedback control to the phase delay. With initial parameters tuned to the optimal point, the output power rise indicates the deviation from the optimal caused by unknown perturbation. The photodetector records the power increase and sends the signal to a servo controller, changing the temperature of the fiber module, thus pull the system back to the optimal state. The long-term stability of the laser is

significantly improved by the implementation of this feedback control. In the test duration of 7*24 hours, no mode hopping is observed.

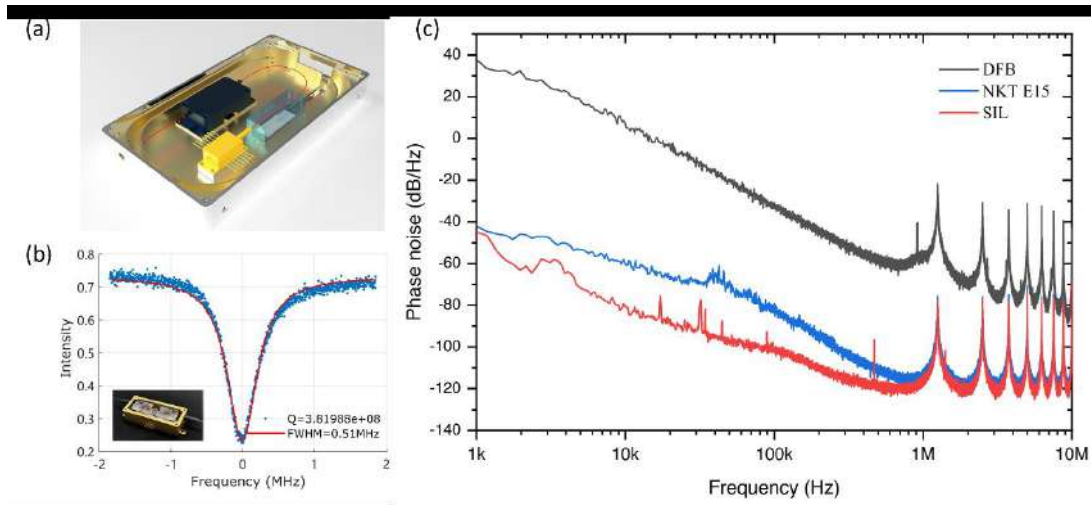


Fig. 1. (a) Schematic of the modular SIL laser. The inset shows the package structure of the resonator. (b) Characterization of the resonator Q-factor after packaging. (c) The phase noise of the modular SIL laser and compared to DFB and NKT E15.

Designing a resonant nanovortex antenna with similar dipole resonators would require a 3D assembly of nanorods, adding complexity to the fabrication process. To avoid such difficulty, a 2D resonant nanovortex antenna may alternatively be designed by combining short and long nanorods with their respective dipole and longitudinal quadrupole resonances tuned to the same wavelength. Although the longitudinal quadrupole resonance cannot be directly excited by the incident plane wave, it is indirectly excited via evanescent coupling with the dipole resonators. The phase shift introduced by this indirect coupling leads to the generation of a phase singularity in the evanescent field confined in the central nanogap (see Figure 1).

3. Summary

In this work, we have shown that an optical nanovortex confined in the nanogap of a plasmonic multimer antenna can be directly excited by an incident circularly polarized plane wave. Whereas a non-resonant optical nanovortex may be obtained by using two interlocked multimer antenna with respectively red-shifted and blue-shifted dipole resonances, resonant nanovortex antenna made of only dipole resonators require a complex 3D architecture. Alternatively, a 2D resonant nanovortex antenna may be obtained by combining dipole and longitudinal quadrupole resonators.

Acknowledgments

This work was supported by JSPS KAKENHI (Grants JP16H06506, JP18H03882, JP18H05205, and JP21H04657 to KS and JP20K15145, JP22H01923, and JP23H04571 to CP), and JSPS KAKENHI Grant-in-Aid (No. JP23H04571 to CP) for Transformative Research Areas (A) "Revolution of Chiral Materials Science using Helical Light Fields" from the Japan Society for the Promotion of Science (JSPS).

References

- [1] Dahmani, B., L. Hollberg, and R. Drullinger. "Frequency stabilization of semiconductor lasers by resonant optical feedback." *Optics Letters* 12.11 (1987)
- [2] Li, H., and N. B. Abraham. "Power spectrum of frequency noise of semiconductor lasers with optical feedback from a high-finesse resonator." *Applied physics letters* 53.23 (1988)
- [3] Liang, W., et al. "Ultralow noise miniature external cavity semiconductor laser." *Nature communications* 6.1 (2015)
- [4] Ji, Jingru, et al. "Narrow linewidth self-injection locked fiber laser based on a crystalline resonator in add-drop configuration." *Optics Letters* 47.6 (2022)

Steering complex dynamics in anisotropic and coupled microcavities

Lukas Seemann¹, Angelika Knothe², and Martina Hentschel^{1,*},

IT

¹ Institute of Physics, Technische Universität Chemnitz, D-09107 Chemnitz, Germany

² Institut für Theoretische Physik, Universität Regensburg, D-93040 Regensburg, Germany

* martina.hentschel@physik.tu-chemnitz.de

Abstract: The progress in the fabrication of mesoscopic microcavities for both light and electrons opens new methods to control and steer their dynamics. Here, we focus on anisotropic cavities, realizable in metamaterials or bilayer graphene, and coupled microsystems. © 2024 The Author(s)

Mesoscopic systems for electrons and photons do not only open the path to new applications such as microcavity lasers, but at the same time have proven to be rich and interesting model systems for the field of quantum chaos or testing ray-wave correspondence that allowed for a deeper understanding of their dynamics. A system class studied intensively over the past decades are graphene systems [1], where ray-wave correspondence in Dirac fermion optics was confirmed [2].

Bilayer graphene systems allow to incorporate anisotropies into the system, namely via the trigonal warping of the Fermi line that occurs for suitable choices of parameters. This is illustrated in Fig. a). The flat side of the Fermi line indicate the preferred propagation directions, that form triangular orbits as indicated in Fig. b). As a consequence, the Poincaré surface of section develops new features, even for a circular cavity. The anisotropy destroys the whispering gallery modes that dominate the dynamics in isotropic microdiscs, as shown in Fig. c). Here the trajectory intensity was taken into account by accounting for the electronic properties of bilayer graphene and deducing generalized Fresnel coefficients [3]. The formation of islands corresponding to the triangular orbits is clearly visible, while the whispering-gallery orbits eventually are lost in the chaotic sea.

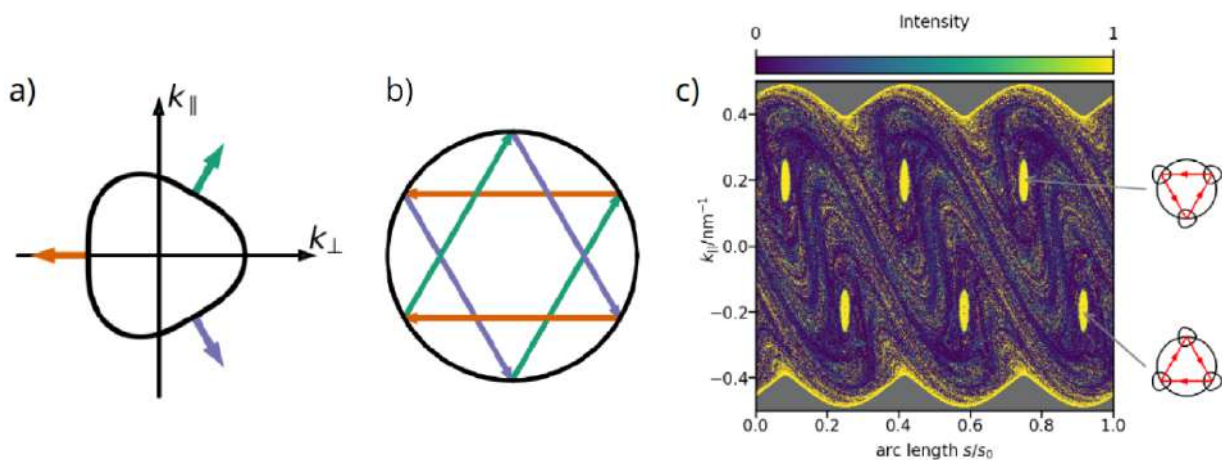


Fig. 1. The presence of anisotropies converts the phase space of a circular cavity into a mixed dynamics. a) Triangularly warped Fermi line typical for bilayer graphene. b) Trajectories built from the three preferred propagation directions. c) Intensity-weighted Poincaré surface of section for an open Fermion optics billiard of circular geometry realized in bilayer graphene.

An interesting subject is to study the interplay between deviations from the circular geometry in real and in phase space, by investigating deformed microdisks subject to different degrees of anisotropy [4]. We will illustrate how the phase space can be fine-tuned by controlling the external parameters available in bilayer graphene. For example, we find that Whispering-gallery modes can be stabilized by the formation of larger islands in the Poincaré surface of section under certain conditions.

In an outlook, we will briefly discuss the impact of anisotropies in optical mesoscopic systems. We will also introduce how the dynamics of photons can be controlled in coupled cavities [5] over surprisingly large distances between them.

References

- [1] Himadri Chakraborti, Cosimo Gorini, Angelika Knothe, Ming-Hao Liu, Péter Makk, Francois D. Parmentier, David Perconte, Klaus Richter, Preden Roulleau, Benjamin Sacépé, Christian Schönonenberger, and Wenmin Yang. Electron quantum optics in graphene, 2024.
- [2] Jule-Katharina Schrepfer, Szu-Chao Chen, Ming-Hao Liu, Klaus Richter, and Martina Hentschel. Dirac fermion optics and directed emission from single- and bilayer graphene cavities. *Physical Review B*, 104(15):155436, October 2021.
- [3] Lukas Seemann, Angelika Knothe, and Martina Hentschel. Gate-tunable regular and chaotic electron dynamics in ballistic bilayer graphene cavities. *Phys. Rev. B*, 107:205404, May 2023.
- [4] Lukas Seemann, Angelika Knothe, and Martina Hentschel. Steering internal and outgoing electron dynamics in bilayer graphene cavities by cavity design, 2024.
- [5] Tom Simon Rodemund, Síle Nic Chormaic, and Martina Hentschel. Coupled deformed microdisk cavities featuring non-Hermitian properties. *Applied Physics Letters*, 124(5):051107, 01 2024.

Nonlinear optical encoding with a linear scattering cavity

Hui Cao*

IT

Department of Applied Physics, Yale University, New Haven, Connecticut, USA

* hui.cao@yale.edu

Abstract: We exploit the passive nonlinear mapping inside a multiple-scattering cavity for rapid optical information processing. High-order structural nonlinearity fosters the generation of low-dimensional latent feature space and facilitates strong data compression to enhance computing performance.

1. Introduction

Optical information processing and computing can potentially offer enhanced performance, scalability and energy efficiency. However, achieving nonlinearity—a critical component of computation—remains challenging in the optical domain. Here we introduce a design that leverages a multiple-scattering cavity to passively induce optical nonlinear random mapping with a continuous-wave laser at a low power. Each scattering event effectively mixes information from different areas of a spatial light modulator, resulting in a highly nonlinear mapping between the input data and output pattern. We demonstrate that our design retains vital information even when the readout dimensionality is reduced, thereby enabling optical data compression. This capability allows our optical platforms to offer efficient optical information processing solutions across applications. We demonstrate our design’s efficacy across tasks, including classification, image reconstruction, keypoint detection and object detection, all of which are achieved through optical data compression combined with a digital decoder. In particular, high performance at extreme compression ratios is observed in real-time pedestrian detection. Our findings open pathways for novel algorithms and unconventional architectural designs for optical computing.

2. Multiple-scattering cavity

2.1 Structural nonlinearity

We investigate the nonlinear mapping between a reconfigurable disordered potential and emerging light of a multiple-scattering cavity. Note that the multiple-scattering-induced nonlinear mapping is fundamentally different from the conventional nonlinear optics based on intrinsic material response. At low optical power where the intrinsic nonlinear material response is negligible, the output field depends linearly on the input field. However, due to multiple scattering of light, the output field has a nonlinear dependence on the scattering potential. Such nonlinear mapping is realized experimentally with an integrating sphere with rough inner wall (Fig. 1). One of the opening is covered by a switchable digital mirrors device (DMD), which provides reconfigurable scattering potential. A continuous-wave, linearly polarized laser is coupled into the integrating sphere. Input light is scattered multiple times inside the integrating sphere by the rough wall and the switchable micromirrors. The outputs light from the third opening is directed to camera, which records the speckle intensity pattern for a specific DMD configuration. The change of output speckle pattern due to variation of scattering structure is nonlinear, this is called structural nonlinearity [1]. Such nonlinearity can be easily tuned experimentally by varying the modulation area on the DMD. A larger area have higher chance of interacting with light, experiencing more light scattering, leading to higher order nonlinearity.

2.2 Computing tasks

Increasing nonlinear order facilitates data compression [2]. One example is the keypoint detection in human faces, which has applications in facial recognition, emotion detection, and other human-computer interaction systems. We record 16 output speckle grains to achieve a compression ratio of 576:1 in Fig. 2a. Another example is the real-time video analytics, using the benchmark dataset known as Caltech Pedestrian, including real-time video recordings (Fig. 2b). Using our multiple-scattering cavity, we can compress the video and use only 25 speckle grains to encode each frame. Then we train a light-weight digital decoder to detect and track pedestrians with high accuracy [2].

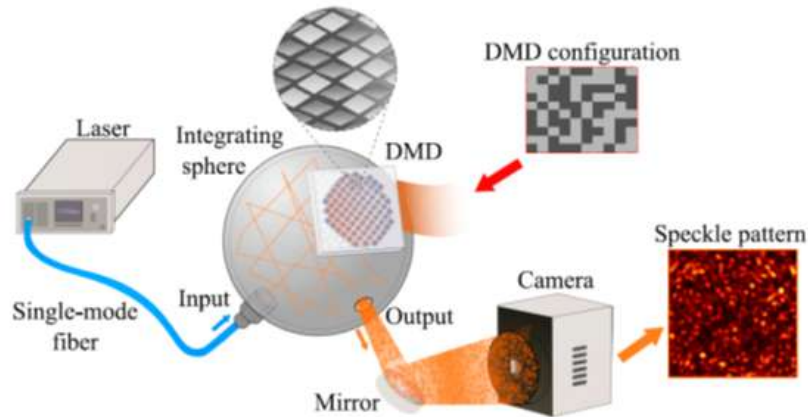


Fig. 1. Experimental setup. A frequency-tunable continuous-wave fiber laser is coupled via a single-mode fiber to an integrating sphere with an inner static rough boundary. A two-dimensional (2D) digital-mirror-array (DMD) covers one of the sphere’s ports. Light is scattered multiple times inside the integrating sphere by its static boundary and the reconfigurable mirror array. Through a small opening, light leaks out of the cavity, and its intensity pattern is recorded by a digital camera.

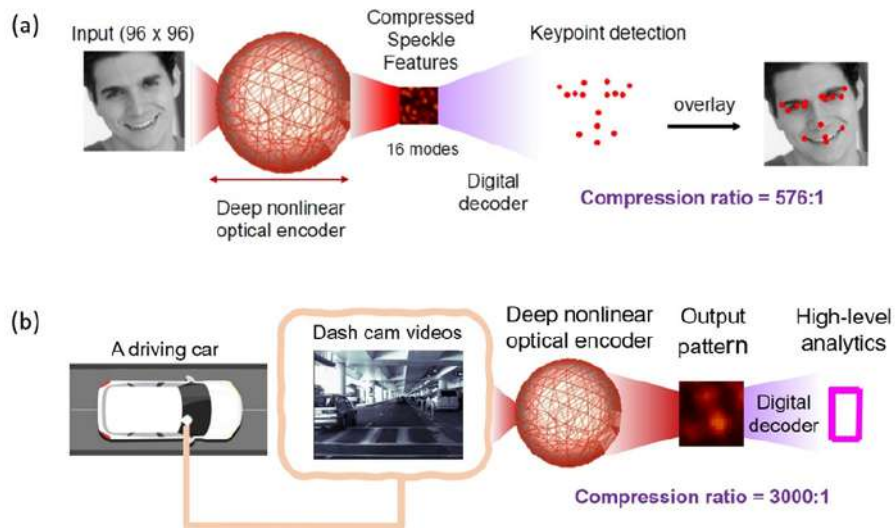


Fig. 2. Nonlinear optical encoding using the multiple-scattering cavity to perform computing tasks of keypoint detection in human faces in (a), and real-time video analytics in (b).

3. Summary

We have leveraged multiple scattering of light in a passive cavity to achieve high-order nonlinear response at low power. It is used for implementation of optical neural network and data compression. Our multiple-scattering cavity serves as an optical nonlinear encoder with optimal and adjustable nonlinearity for various computing tasks. We demonstrate the enhancement of computing performance in optical image classification, image reconstruction, keypoint detection, and object detection.

References

- [1] Y. Eliezer, U. Rührmair, N. Wisiol, S. Bittner, H. Cao. “Tunable nonlinear optical mapping in a multiple-scattering cavity”. Proc. Natl. Acad. Sci. vol. 120, e2305027120 (2023).
- [2] F. Xia, K. Kim, Y. Eliezer, S. Han, L. Shaughnessy, S. Gigan, H. Cao. “Nonlinear Optical Encoding Enabled By Recurrent Linear Scattering”. Nat Photon. DOI: 10.1038/s41566-024-01493-0.

High-order exceptional points in systems of waveguide-coupled microring cavities

Julius Kullig^{1,*} *Daniel Grom*¹ *Jan Wiersig*¹

CT

¹ Institut für Physik, Otto-von-Guericke-Universität Magdeburg, Postfach 4120, D-39016 Magdeburg, Germany

* julius.kullig@ovgu.de

Abstract: We study waveguide-coupled microrings at higher-order EPs under generic and non-generic perturbations leading to interesting cavity-selective behavior. Intuitive analysis of the modes is given by a graph-theoretical approach. © 2024 The Author(s)

1. Introduction

Optical microcavities are ideally suited to study non-Hermitian physics of open systems [1]. One among the plethora of interesting effects in these systems are exceptional points (EPs) [2]. EPs are points in the parameter space marking a special type of degeneracy where two or more eigenvalues (frequencies) and simultaneously the involved eigenstates (modes) coalesce. The order of an EP represents the number of coalescing eigenvalues and eigenstates. For practical relevance is not only the EP itself but also the system's behavior in its vicinity. If an EP of order N is perturbed in a generic way the eigenvalues split according to the N th complex root [3]. This splitting is always larger compared to the linear splitting of a conventional degeneracy if the perturbation is small enough. On the one hand, this property gives rise to interesting sensing applications but on the other hand it results in tight error margins on fabrication tolerances of EP-based sensors. To circumvent this challenge the concepts of EP-surfaces has been introduced [4]. The idea is to make the EP immune to changes of certain parameters that correspond to fabrication and at the same time keep the EP-enhanced sensitivity to desired detectable perturbations.

In our work we iterate the ideas of Refs. [4,5] to construct intuitively a higher-order EP within an EP-surface [6]. We show that systems of waveguide-coupled microrings allows for a cavity-selective sensing scheme based on generic and non-generic perturbations. We analyze the eigenvalue braiding and give a graph-theoretical approach to the EP-based sensing.

2. EPs in waveguide-coupled microrings

Microring cavities exhibit degenerate pairs of clockwise (CW) and counter-clockwise (CCW) propagating waves. Via attached waveguides a coupling between the CW and CCW waves of different cavities can be introduced in an unidirectional way which can already lead to EPs [5]. With an additional asymmetric coupling introduced via a mirror at one waveguide end the order of the EP can be increased. A mode in such a setup is shown in Fig 1a. Here, six modes according to the (C)CW propagating waves in the three microrings coalesce into a single eigenstate that is a purely CCW wave in the most lower cavity.

2.1 Cavity-selective sensing

If the system in Fig. 1a is perturbed by a test-particle (TP) the eigenfrequencies Ω_i , $i = 1, \dots, 6$, diverge according to a six-order-root when the radius r_{TP} of the TP is increased. This splitting can be quantified by $\Delta\Omega = \max_{i,j} |\Omega_i - \Omega_j|$. As shown in Fig. 1b the generic behavior is observed when the most lower cavity is perturbed by the TP. Contrary, if the middle or upper cavity is perturbed by the TP a scaling of $\Delta\Omega$ is given by a fourth-order and a square-root. Thus the strength of the splitting is cavity selective.

2.2 Eigenvalue braids

A TP is a natural but also a non-generic perturbation to the system: A TP targets a single cavity at a specific angular position φ_{TP} along the microring's circumference. Hence, moving the TP along the microring results in a quasi-periodic perturbation according to the azimuthal mode number of the involved modes. This leads to an interesting interchange of eigenvalues, so-called eigenvalue braids, as shown in Fig. 2a-c.

2.3 Graph-theoretical description

The behavior of the eigenvalues under a given (TP) perturbation can be understood intuitively from a graphtheoretical point of view that reveals the relevant paths of light in the system [7]. Each CW and CCW propagating wave in the microrings represents a node in a graph whereas the waveguides and the TP-perturbation give rise to directed links between these nodes. Searching for the longest closed path in this directed graph gives the scaling behavior of the splitting $\Delta\Omega$.

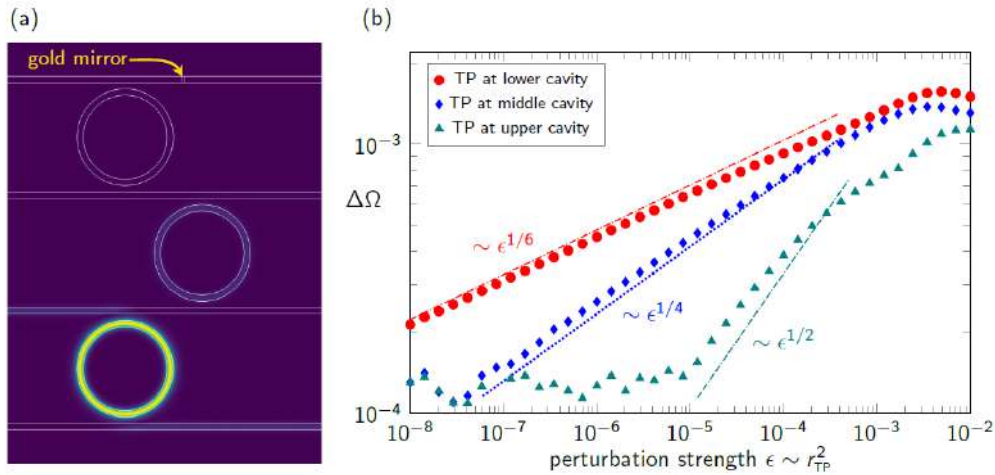


Fig. 1. (a) Mode pattern in a setup of three waveguide-coupled microrings at an EP of order six. A gold mirror is placed at the upper waveguide, right to the cavity. (b) The corresponding frequency splitting $\Delta\Omega$ is shown for a test-particle perturbation at the (red dots) lower, (blue diamonds) middle, and (green triangles) upper cavity.

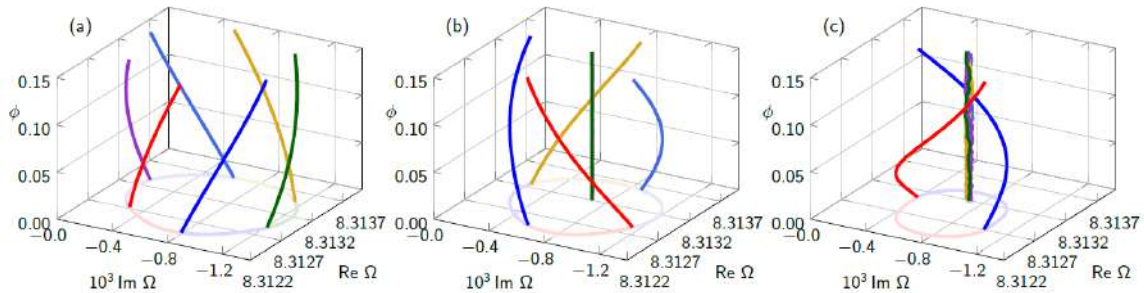


Fig. 1. (a-c) Eigenvalue braids for the setup shown in Fig 1a with a TP moved along the circumference of a microring. The TP is placed at the (a) lower, (b) middle, or the (c) upper cavity.

References

- [1] H. Cao and J. Wiersig, “Dielectric microcavities: Model systems for wave chaos and non-Hermitian physics,” *Rev. Mod. Phys.* **87**, 61–111 (2015).
- [2] M.-A. Miri and A. Alù, “Exceptional points in optics and photonics,” *Science* **363**, eaar7709 (2019).
- [3] T. Kato, *Perturbation Theory for Linear Operators* (Springer, New York, 1966).
- [4] Q. Zhong, J. Ren, M. Khajavikhan, D. N. Christodoulides, Ş. K. Özdemir, and R. El-Ganainy, “Sensing with exceptional surfaces in order to combine sensitivity with robustness,” *Phys. Rev. Lett.* **122**, 153902 (2019).
- [5] X.-Y. Wang, F.-F. Wang, and X.-Y. Hu, “Waveguide-induced coalescence of exceptional points,” *Phys. Rev. A* **101**, 053820 (2020).
- [6] J. Kullig, D. Grom, S. Klemmt, and J. Wiersig, “Higher-order exceptional points in waveguide-coupled microcavities: perturbation induced frequency splitting and mode patterns,” *Photon. Res.* **11**, A54–A64 (2023).
- [7] D. Grom, J. Kullig, J. Wiersig, and M. Röntgen, “Graph-theoretical approach to the eigenvalue spectrum of perturbed higher-order exceptional points,” (in preparation).

PicoSNAP: towards the picometre-precise fabrication of WGM microresonators and their applications

Gabriella Gardosi^{1,*}, *Misha Sumetsky*¹

IT

Aston institute of photonic technologies, Aston university, Birmingham, UK

* g.gardosi3@aston.ac.uk

We report recent advancements in the development of picometer-precise SNAP technology crucial for a range of important optical, microwave, and industrial applications. Techniques include CO₂ laser annealing, femtosecond laser inscription, slow cooking, and fibre bending.

Frequency conversion in optomechanical microresonators

Zhen Shen*, Chun-Hua Dong

CT

Key Lab of Quantum Information, University of Science and Technology of China, Hefei, Anhui 230026, China
* shenzhen@ustc.edu.cn

Abstract: Here, we develop a hybrid platform consisting of a magnomechanical cavity and an optomechanical cavity. By harnessing the excellent tunability of magnons, we have achieved tunable microwave-optical conversion and phonon interference.

1. Introduction

Mechanical degrees of freedom, which have often been overlooked in various quantum systems, have been studied for applications ranging from quantum information processing to sensing. Here, we develop a hybrid platform consisting of a magnomechanical cavity [1] and an optomechanical cavity, which are coherently coupled by the straightway physical contact. The phonons in the system can be manipulated either with the magnetostrictive interaction or optically through the radiation pressure. Together with mechanical state preparation and sensitive readout, we demonstrate the microwave-to-optical conversion with an ultrawide tuning range up to 3 GHz. In addition, we observe a mechanical motion interference effect, in which the optically driven mechanical motion is canceled by the microwave-driven coherent motion. Manipulating mechanical oscillators with equal facility through both magnonic and photonic channels enables new architectures for signal transduction between the optical, microwave, mechanical, and magnetic fields [2].

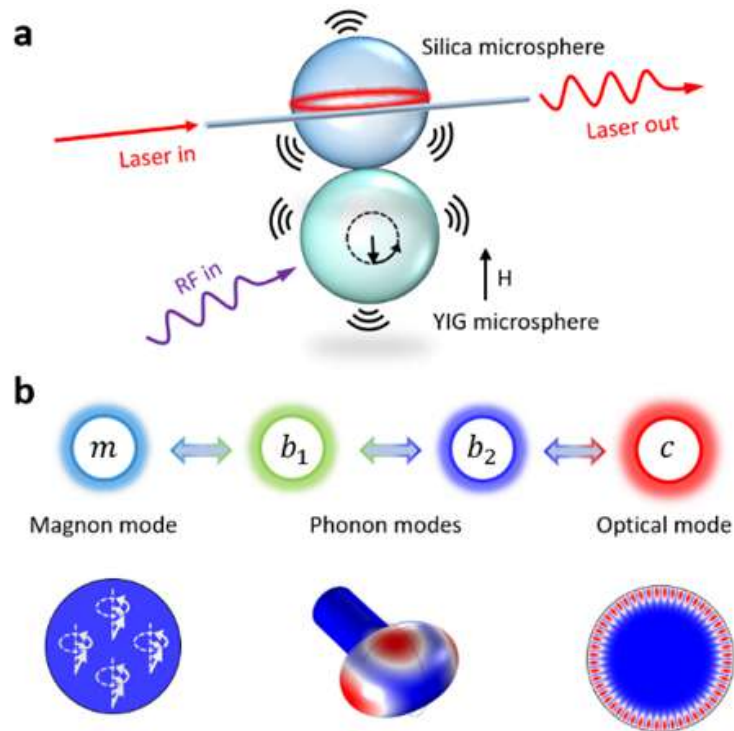


Fig. 1. (a) Schematic of the device that consists of a YIG and a silica microsphere, which both support the mechanical modes excited by the magnetostrictive interaction through magnons or the radiation pressure induced by the circulating optical fields. Based on the straightway physical contact, the localized mechanical modes establish direct coupling. (b) Schematic of the coupling between magnons, phonons, and photons and an intuitive illustration of the magnon, phonon, and photon mode.

2. Methods and results

The device used in our experiment, including the key components of the single-crystal YIG microsphere and silica microsphere, is schematically shown in Fig. 1(a). The YIG microsphere supports a uniform magnon mode with an external magnetic field H and the magnon can couple with mechanical modes through

magnetostrictive interaction, which allows us to excite phonons in YIG microsphere by microwaves. Meanwhile the optical and mechanical modes in the silica microcavity can be coupled through radiation pressure. Due to the direct contact of the microcavities, the localized mechanical modes establish direct coupling, which also induces the interaction between the magnons and photons. Our system enables new architectures for signal transduction between the optical, and mechanical domains based on coherent coupling between photons, phonons, and magnons, as shown in Fig. 1(b).

When the laser drive fixed at one mechanical frequency below the cavity resonance, the optomechanical interaction can convert the coherent phonons into photons, thus achieving microwave-to-optical conversion. Here, we fix the frequency of microwave signal to convert the phonon mode and the power of optical carrier. Figure 2(a) plots the conversion efficiency as a function of the microwave drive power. As the microwave drive power increases, the enhancement of the magnomechanical interaction leads to stronger mechanical motion and higher conversion efficiency. The maximum conversion efficiency achieved in the experiment is approximately 10^{-5} . Figure 2(b) shows measured conversion efficiency for drive-resonance detunings varying from -12.2 MHz to -18.2 MHz, which can be achieved only by changing the bias magnetic field to tune the magnon resonance. The data demonstrates the important role of the magnon in the conversion process. Since the external magnetic field can tune the frequency of the magnon, this corresponds to the tunable microwave-to-optical conversion. By tuning the magnon frequency and the relevant microwave drive to match drive-resonance detuning, we can realize 4 GHz – 7 GHz microwave conversion as shown in Fig. 2(c), providing a great tenability compared to the previous scheme. **3. Summary**

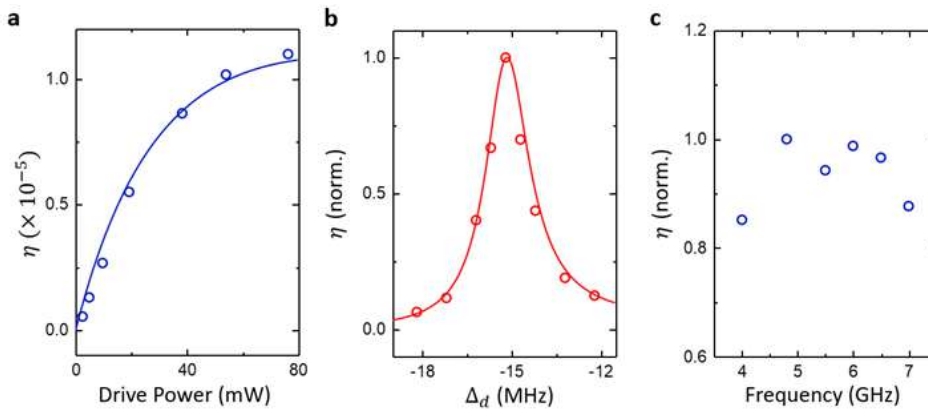


Fig. 2. (a) The microwave-to-optical conversion efficiency as a function of the microwave drive power. (b) The normalized conversion efficiency versus drive-resonance detunings. (c) The conversion efficiency as a function of the microwave signal frequency (normalized to the efficiency of 4.8 GHz).

In summary, we have presented a magno-optomechanical platform in which a magnomechanical cavity is in physical contact with an optomechanical cavity. Several effects have been demonstrated, including the mechanical state sensitive readout and preparation with desired amplitude and phase, microwave-to-optical conversion with tuning range up to 3 GHz, and the mechanical motion interference effect. Considering the easily reached strong magnon-photon coupling in microwave cavities, phonon manipulation and microwave-to-optical conversion can be achieved with lower power consumption. Our hybrid platform will find applications in various fields, such as tunable slow light or delay lines in both microwave and optical domains, and quantum signal transduction and sensing for quantum networks.

References

- [1] G.-T. Xu#, M. Zhang#, Y. Wang, Z. Shen*, G.-C. Guo, C.-H. Dong*, “Magnonic frequency comb in the magnomechanical resonator,” *Phys. Rev. Lett.* 131, 243601 (2023).
- [2] Z. Shen#, G.-T. Xu#, M. Zhang#, Y.-L. Zhang, Y. Wang, C.-Z. Chai, C.-L. Zou, G.-C. Guo, and C.-H. Dong*, “Coherent coupling between phonons, magnons and photons,” *Phys. Rev. Lett.* 129, 243601 (2022).

Topological control of localized electric fields in plasmonic nanocavities

Keiji Sasaki^{1,*}, *Christophe Pin*²

IT

¹ Research Institute for Electronic Science, Hokkaido University, Sapporo, Japan

² Okinawa Institute of Science and Technology, Okinawa, Japan

*sasaki@es.hokuda.ac.jp

Abstract: We present the unique topological properties of the localized fields formed by tailored plasmonic nanocavities. We show that the metal multimer nanocavity irradiated with circularly polarized beam generates the nano-vortex field with the half-integer angular momenta. We also demonstrate that the transverse spin loop can be generated around the nanocavity, which results in forming the electric-field-spin skyrmion textures.

We have developed “optical nanoshaping” technique that can realize confining optical fields into nanocavity beyond the diffraction limit and controlling the amplitude, phase, and polarization distribution of the nanolocalized fields. We designed the tailored plasmonic nanocavities composed of metal multimer surrounding a nano-sized gap. The plasmonic nanocavities make it possible to localize the optical vortex fields into the gap spaces with conserving the high-order orbital and spin angular momenta. Here, we present the unique topological properties of the nano-localized plasmonic fields formed by metal multimer nanocavities. We show that the nanomultimer irradiated with circularly polarized beam generates the nano-vortex field with the half-integer total angular momenta corresponding to monopole, tripole, tetrapole, etc. which are categorized to Möbius strip states (Fig. 1). We applied this topological plasmonic fields to chiral crystallization from achiral compounds and succeeded in achieving giant crystal enantiomeric excess of sodium chlorate and ethylenediamine sulfate (Table 1). We also demonstrate that the transverse spin loop can be generated around the nanocavity (Fig. 2), and the energy flow simultaneously appears due to the spin-momentum locking effect, which results in forming the electric-field-spin skyrmion textures above and below the nanocavity. This nanoscale photonic spin skyrmion field is applicable to generation and control of magnetic skyrmion in ferromagnetic, ferrimagnetic, and antiferromagnetic materials.

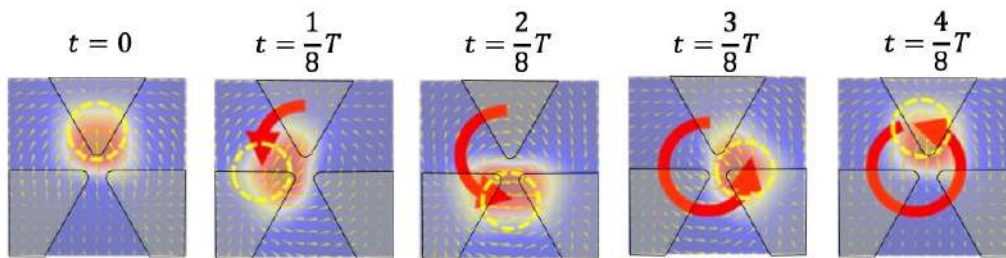


Fig. 1. Spontaneous intensity distributions of localized nano-vortex field. T is the time of optical one cycle.

Table 1: Summary of d - and l -crystal generation numbers under G and LG laser beam irradiations, accompanied by the crystal enantiomeric excess (CEE) values.

	r -CP	l -CP	r -CP, r -OV	l -CP, l -OV
d -crystal	18	8	7	18
l -crystal	7	17	18	7
Total trial	25	25	25	25
CEE (%)	44	-36	-44	44

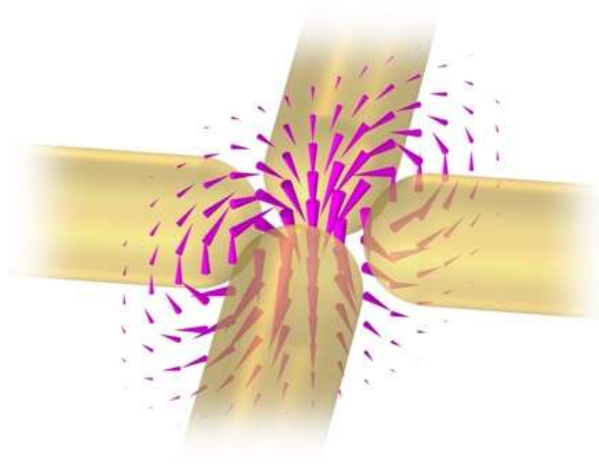


Fig. 2. Transverse electric spin loop formed around plasmonic tetramer nanocavity.

References

- [1] Y. Sunaba, M. Ide, R. Takei, K. Sakai, C. Pin, K. Sasaki, “Nano-shaping of chiral photons,” *Nanophotonics* 12, 2499 (2023).
- [2] H. Fujiwara, K. Sudo, Y. Sunaba, C. Pin, S. Ishida, K. Sasaki, “Spin-orbit angular-momentum transfer from a nanogap surface plasmon to a trapped nanodiamond,” *Nano Letters* 21, 6268 (2021).
- [3] A.-C. Cheng, C. Pin, Y. Sunaba, T. Sugiyama, K. Sasaki, “Nanoscale helical optical force for determining crystal chirality,” *Small* 2024, 2312174 (2024).

Polarization entangled photons from a whispering gallery resonator

Sheng-Hsuan Huang,^{1,2,*} Thomas Dirmeier,^{1,2} Golnoush Shafiee,^{1,2} Kaisa Laiho,³ Dmitry V. Strekalov,¹ Gerd Leuchs,^{1,2} Christoph Marquardt^{1,2}

IT

¹ Max Planck Institute for the Science of Light, Erlangen, Germany

² Department of Physics, Friedrich-Alexander-Universität, Erlangen, Germany

³ German Aerospace Center, Institute of Quantum Technologies, Ulm, Germany

* strekalov@yahoo.com

Abstract: We implement the interferometric approach to the generation of polarization-entangled photon pairs using a nonlinear whispering gallery mode resonator. The generated states are shown to span the $|\Phi^\pm\rangle$ Bell states and violate the Clauser–Horne–Shimony–Holt inequality by more than six standard deviations.

Whispering gallery mode (WGM) resonators provide an advantageous platform in nonlinear and quantum optics owing to their high quality factor and small mode volume. They found numerous applications in technology as well as in research science, see e.g. the review [1]. In particular, such resonators were successfully used for generating quantum optical states, such as single- or two-mode squeezed light, or heralded single photons [2–4] via parametric down conversion (PDC) of light. One remarkable aspect of these quantum light sources is that they can be easily interfaced with atomic [5] or solid state optical transitions such as may be used in qubits implementations. This aspect is enabled by the central wavelength and linewidth wide tunability of the WGM photon sources. It makes their further development especially appealing in quantum information field, particularly targeting generation of the polarization-entangled photon pairs.

Polarization entanglement has been one of the most productive discoveries in experimental quantum optics. It enabled a plethora of important results, such as Bell’s inequalities violations, several quantum cryptography protocols, quantum teleportation, and more. Generating polarization-entangled photon pairs matching narrow-line atomic or solid state optical transition would be a next big step forward. But this task is difficult and may even appear impossible at a first glance. Indeed, the WGM polarization is rigidly determined by the boundary conditions, and in most cases either lies in the equatorial plane of the resonator, or is perpendicular to it. Polarization entanglement, on the other hand, requires both polarization basis states to be accessible for each PDC signal and idler mode.

We circumvent this problem by using the interferometric approach to polarization entanglement, when the quantum mechanical amplitudes comprising the entangled state are generated separately and combined in an interferometric setup [6]. This approach may involve two different but coherently pumped PDC crystals [7], or two opposite pump directions within the same crystal [8]. The latter approach can be easily adapted to a WGM resonator, where the counter-propagating clockwise (cw) and counter-clockwise (ccw) WGMs are degenerate in frequency and perfectly matched in mode geometry.

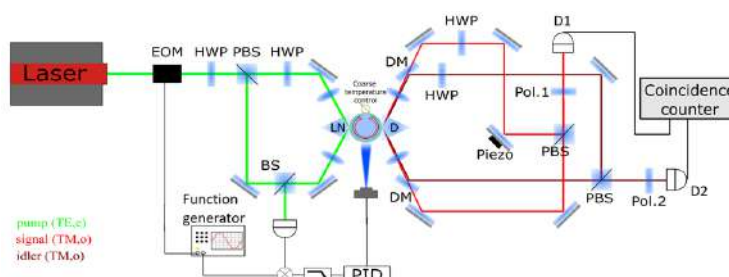


Fig. 1. The experiment diagram.

A diagram of our experiment leveraging this approach is shown in Fig. 1. Here a lithium niobate WGM resonator is pumped in both cw and ccw directions, and the horizontally polarized nondegenerate signal and idler photon pairs are also emitted in two directions. The signals are separated from the idlers by dichroic mirrors (DM). The cw signal and idler polarizations are rotated from horizontal to vertical with half-wave plates (HWP), and then combined with the ccw signal and idler on polarizing beam splitters (PBS). A state of the photon pair emerging from the PBSs is

$$|\Phi\rangle = \frac{1}{\sqrt{2}} \left(|HH\rangle + e^{i\varphi} |VV\rangle \right)$$

where H and V represent the horizontal and vertical polarization, respectively, and the phase Φ depends on the relative

phase of the two pump beams and on the signal and idlers propagation path lengths. This phase is a priori unknown, but it can be controlled with the piezo-actuated mirror in one of the signal beams, see Fig. 1. With this control, we produce Bell's $|\Phi^+\rangle$ and $|\Phi^-\rangle$ states

$$|\Phi^+\rangle = \frac{(|HH\rangle + |VV\rangle)}{\sqrt{2}} \quad \text{and} \quad |\Phi^-\rangle = \frac{(|HH\rangle - |VV\rangle)}{\sqrt{2}}$$

identified by minimizing the coincidence rate with the polarizers Pol.1 and Pol.2 set at $\theta_{i,s} = \pm 45^\circ$ to the V and H directions. The polarization entanglement is then demonstrated by measuring a nonlocal polarization correlation function while co- and counter-rotating the signal and idler polarizers, as shown in Fig. 2a). This is the same measurement that is traditionally used for the polarization entanglement demonstration. Importantly, in order to claim the quantum entanglement as opposed to a classical correlation, the single counting rates by both detectors D1 and D2 must remain constant during the polarizers rotation. We have verified this to be the case, see Figs. 2b) and c).

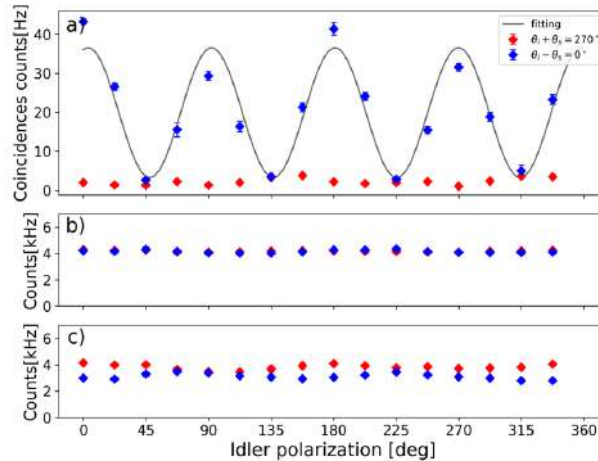


Fig. 2. Demonstration of the polarization entanglement by recording the coincidence rate as a function of the polarizers' orientation. The single counting rates remain constant.

In order to further prove its functionality, we used our polarization entanglement source to demonstrate a violation of the Clauser–Horne–Shimony–Holt's inequality [9]. This was done in two ways. In a direct way, the CHSH observable S was constructed by measuring the coincidence rate at the optimum set of the polarizers angles $\theta_{i,s}$ and the classical boundary $S < 2$ was tested. Alternatively, we derived the inferred violation from the interference fringe visibility. In both approaches the magnitude of the classical realism violation exceeded six standard deviations.

Finally, we would like to point out that a version of the setup in Fig.1 can be used for studying the higher-order quantum optical phenomena, such as generation of heralded photon pairs, or of four-photon entangled states. Considering the high efficiency of the WGM-based PDC sources, the expected four-photon rate can be relatively high. More importantly, the long coherence length of the generated photons will allow for construction of desired four-photon states via the interferometric approach, similarly to the technique reported here. Our progress in this direction will be reported elsewhere.

References

- [1] D. V. Srekalov et al., Nonlinear and quantum optics with whispering gallery resonators, *J. Opt.* **18**, 123002 (2016).
- [2] J. U. Furst et al., Quantum Light from a Whispering-Gallery-Mode Disk Resonator, *Phys. Rev. Lett.* **106**, 113901 (2011).
- [3] M. Fortsch et al., A versatile source of single photons for quantum information processing, *Nat. Commun.* **4**, 1818 (2013).
- [4] A. Otterpohl et al., Squeezed vacuum states from a whispering gallery mode resonator, *Optica* **6**, 1375 (2019).
- [5] G. Schunk et al., Interfacing transitions of different alkali atoms and telecom bands using one narrowband photon pair source, *Optica* **2**, 773 (2015).
- [6] S.-H. Huang et al., Polarization-entangled photons from a whispering gallery resonator, *npj Quantum Inf.* **10**, 85 (2024).
- [7] P. G. Kwiat et al., Ultrabright source of polarization-entangled photons, *Phys. Rev. A* **60**, R773 (1999).
- [8] T. Kim et al., Phase-stable source of polarization-entangled photons using a polarization Sagnac interferometer, *Phys. Rev. A* **73**, 012316 (2006).
- [9] J. F. Clauser et al., Proposed Experiment to Test Local Hidden-Variable Theories, *Phys. Rev. Lett.* **23**, 880 (1969).

Radiofrequency Electrometry with an Electrooptic Whispering-Gallery-Mode Resonator

Suwan Sun^{1,2}, *Hairun Guo*¹, *Andre N. Luiten*¹, and *Wenle Weng*^{1,*}

CT

¹ Institute for Photonics and Advanced Sensing (IPAS), University of Adelaide, SA 5005, Australia

² Key Laboratory of Specialty Fiber Optics and Optical Access Networks, Joint International Research Laboratory of Specialty Fiber Optics and Advanced Communication, Shanghai University, Shanghai 200444, China

*wenle.weng@adelaide.edu.au

Abstract: We develop a radiofrequency electric-field sensor utilizing a lithium niobate whispering-gallery-mode microresonator. Being antenna-free, the detection sensitivity of the sensor is enhanced by the piezoelectric resonances of the microresonator. Our theoretical derivation and experimental tests show that the detection sensitivity can be maintained even the electric-field signal frequency is out of the optical resonance bandwidth, as long as the sensitivity is limited by the laser frequency noise. © 2024 The Author(s)

1. Introduction

Recently, microwave electric-field sensors based on photonic-integrated-circuit microresonators have been demonstrated [1]. Using the Pockels effect in lithium niobate (LN) for electric-to-optic transduction and the Pound-Drever-Hall (PDH) technique for signal detection, the developed sensors have achieved an unprecedented detection sensitivity of $5.2\mu\text{V}/(\text{m}\sqrt{\text{Hz}})$ with the resonant enhancement of dipole antenna. Despite of this excellent performance, several related issues need to be further investigated to bring out the full potential of this opticalmicroresonator-based scheme. While it is intuitive that increasing the quality factor (Q) of the optical microresonator can improve the sensitivity, the prevailing belief is that the sensing bandwidth would be compromised because according to the conventional practice the frequency of the microwave electric field should be within the optical resonance bandwidth. Therefore it is interesting to see if the sensitivity can be maintained or even improved at a frequency out of the optical resonance bandwidth. In addition, the use of antenna for signal enhancement not only increases the footprint of the device (especially for relatively low frequency ranges) but may also distort the electric field to be detected. As such, the performance of antenna-free sensors needs to be investigated to complete the study of the microresonator-based electric-field sensors.

In this work, we develop an antenna-free electric-field sensor that mainly detects radiofrequency (RF) electricfield signals with a frequency below 10 MHz. The sensor is based on an ultrahigh- Q crystalline LN microresonator whose Pockels effect and piezoelectric resonances are harnessed to convert the electric-field signal into optical frequency generation. While the ultra-narrow optical resonance bandwidth of the microresonator significantly improves the signal sensitivity of the PDH technique, the sensor is capable to perform electrometry at frequencies out of the optical resonance bandwidth.

2. Experiment and results

Figure 1 (a) shows a photo of the crystalline LN microresonator. With surface polishing, the under-coupled bandwidth of the optical resonances can reach ~ 1 MHz, corresponding to an intrinsic Q of 2×10^8 . Using the copper sheet on top of the microresonator and the supporting post as the electrodes, RF electric-field signal derived from a function generator is applied to the microresonator. Figure 1 (b) shows the electric-field strength simulated by finite-element method. Due to the geometry of the electrodes, the electric-field strength at the location of the optical mode is only around 8% of U_0/d , where U_0 is the voltage difference between the electrodes and d is the thickness of the microresonator, showing that for free-space sensing applications the sensitivity can be improved over the results in our experiments by more than one order of magnitude. Figure 1 (c) presents the laser-frequencyswept spectrogram of an optical resonance with varied applied RF frequency. Around the modulation frequency of 4 MHz we observe prominent modulation sidebands, indicating that the electric-to-optic transduction is enhanced by the piezoelectric resonances.

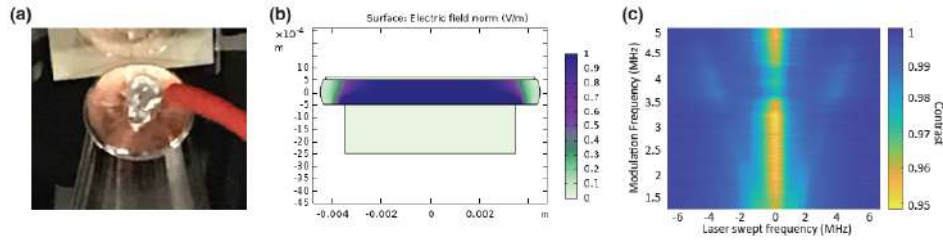


Fig. 1. (a) A photo of the LN microresonator. (b) Finite-element-method simulation of electric-field strength. (c) Laser-frequency-swept spectrogram of a modulated optical resonance.

The experimental setup is depicted in Fig. 2 (a). A 1550-nm laser is frequency-locked to an optical resonance of the microresonator via PDH technique with a low servo control bandwidth of ~ 100 Hz. Figure 2 (b) shows the resonance spectroscopy and the PDH error signal. The error signal is sent into a Fourier spectrum analyzer to characterize the signal strength and the noise floor at the frequency of the applied RF electric field. Figure 2(c) shows the signal when the applied electric field is at 3.9 MHz and of a peak-to-peak amplitude of 10 mV. The noise floor, which is currently limited by the photodetector noise, is corresponding to a detection limit the signal amplitude of $100 \mu\text{V}$. Taking into account the sensitivity reduction due to the electrodes, this result shows that a resolution of $10 \mu\text{V}/(\text{m}\sqrt{\text{Hz}})$ can be achieved. We also use an additional modulator to add artificial laser frequency noise. We find that the frequency noise and the detected signal amplitude are suppressed equally when the signal frequency is higher than the optical resonance bandwidth. As a result, the signal-to-noise ratio (SNR) is maintained as long as the noise floor is dominated by the laser frequency noise. This result is corroborated by our theoretical analysis.

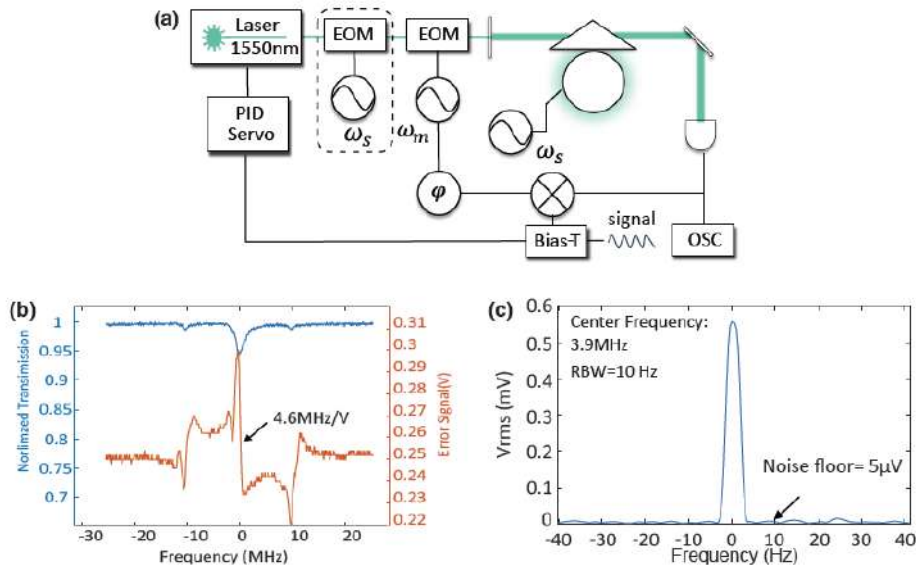


Fig. 2. (a) Experimental setup. (b) Transmission spectrum of a resonance and the corresponding PDH error signal. (c) Sensing signal spectrum obtained by an electrical spectrum analyzer using a resolution bandwidth (RBW) of 10 Hz.

3. Summary

In conclusion, we have demonstrated a RF electric-field sensor based on a LN microresonator. We show that when the noise floor is limited by the laser frequency noise the sensing resolution would not be compromised by increasing the signal frequency beyond the optical resonance bandwidth. This result can be used in combination with piezoelectric-resonance enhancement to increase both the sensitivity and the sensing bandwidth for economical sensors that are built with low-cost lasers.

References

[1] X. Ma, Z. Cai, C. Zhuang, X. Liu, Z. Zhang, K. Liu, B. Cao, J. He, C. Yang, C. Bao, and Z. Rong, "Integrated microcavity electric field sensors using Pound-Drever-Hall detection," *Nat. Commun.* **15**, 1386 (2024).

Picotesla-sensitivity microcavity optomechanical magnetometry

Zhi-Gang Hu^{1,2,†}, *Yi-Meng Gao*^{1,2}, *Jian-Fei Liu*^{1,2}, *Yong-Chang Lau*^{1,2}, *Jian-Wang Cai*^{1,2}, and *Bei-Bei Li*^{1,2,3,*}

¹ Beijing National Laboratory for Condensed Matter Physics, Institute of Physics, Chinese Academy of Sciences, Beijing 100190, China

² University of Chinese Academy of Sciences, Beijing 100049, China

³ Songshan Lake Materials Laboratory, Dongguan 523808, Guangdong, China

† huzhigang20@mailsucas.ac.cn

* libeibei@iphy.ac.cn

Abstract: We have realized a high-sensitivity cavity optomechanical magnetometer by depositing a thin film of FeGaB magnetostrictive material onto a SiO₂ microdisk resonator and achieved a peak sensitivity of 1.68 pT/Hz^{1/2}.

1. Introduction

High-sensitivity magnetometers play a crucial role in many applications, including nuclear magnetic resonance, magnetocardiography, mineral exploration, nondestructive inspection, magnetic induction tomography, and current detection. Currently, the state-of-the-art magnetometers are based on superconducting quantum interference devices (SQUIDS), with exceptional sensitivity at the fT/Hz^{1/2} level. However, their reliance on cryogenic systems has resulted in elevated operational costs and limited applications. Recently, various magnetometers that can work at room temperature have been developed, such as atomic magnetometers, diamond nitrogen-vacancy color center magnetometers, and microcavity optomechanical magnetometers [1-3]. Microcavity optomechanical magnetometers have recently been developed by incorporating magnetostrictive materials into high-*Q* whispering gallery mode (WGM) optical microcavities, which offer advantages of miniaturization and low power consumption; ease of on-chip integration; high sensitivity and broad bandwidth. In these magnetometers, the magnetic field induces strain in the magnetostrictive material, which can drive the mechanical motion of the microcavity and result in a change in the radius of the microcavity. This radius change shifts the optical resonance, resulting in a periodic change in the intracavity field. Consequently, the magnetic field can be optically read out, with its sensitivity enhanced by both the optical and mechanical resonances. Cavity optomechanical magnetometers have been demonstrated by embedding the magnetostrictive material Terfenol-D particles into high-*Q* WGM microcavities, and achieved a peak sensitivity of 26 pT/Hz^{1/2}. However, their fabrication process is rather complicated, hindering the mass-production and reproducible fabrication. Previous studies have also successfully achieved mass-produced and reproducible microcavity optomechanical magnetometers by sputter coating Terfenol-D thin films into high-*Q* WGM microcavities [4]. However, the sensitivity was limited to 585 pT/Hz^{1/2}, over 20 times inferior to those using Terfenol-D particles [5].

In this work, we have successfully developed a mass-produced and high-sensitivity microcavity optomechanical magnetometers by sputter coating thin films of a new magnetostrictive material, FeGaB, onto high-*Q* microdisk cavities. We derive the expression of sensitivity of the magnetometers using the intensity modulation mechanism and study how various parameters affect the sensitivity (Fig. 1a). We have made several key improvements experimentally to enhance the device performance compared to previous works. Firstly, we replace the magnetostrictive material Terfenol-D with FeGaB, as FeGaB exhibits superior soft magnetic properties [6], including lower coercivity, lower saturation magnetic field, and a larger maximum piezomagnetic coefficient. Secondly, we conduct comprehensive simulations to explore the relationship between the sensitivity and the geometric parameters of the FeGaB films and SiO₂ microdisks. Subsequently, we fabricate magnetometers with varying microdisk radii. Thirdly, we optimize the optical frequency detuning between the incident laser and the optical mode, minimizing the contribution of the shot noise to the total noise. Lastly, microdisk cavities are used in this work, offering improved reproducibility compared with microtoroids used in earlier studies (Fig. 1b–1c). Remarkably, we achieve a peak sensitivity of 1.68 pT/√Hz at 9.52 MHz using a magnetometer with a SiO₂ microdisk radius of 355 μm and a thickness of 1 μm, along with a FeGaB film radius of 330 μm and a thickness of 1.3 μm (Fig. 1d–1e). This sensitivity surpasses previous mass-produced microcavity optomechanical magnetometers by over two orders of magnitude. Furthermore, we explore a proof-of-concept application by detecting a pulsed magnetic field signal, simulating corona current detection in high-voltage transmission lines (Fig. 2a–2c). These findings demonstrate the potential of our fabricated high-sensitivity magnetometers for various practical applications, such as magnetic induction tomography and corona current detection.

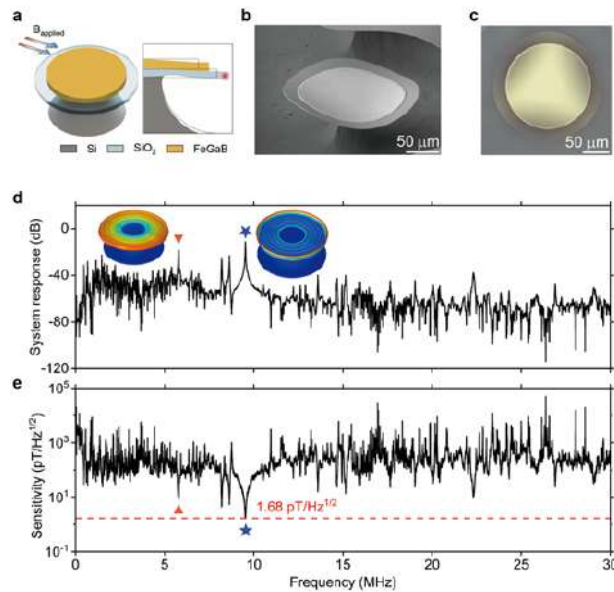


Fig. 1. **a c**, Schematic, scanning electron microscope image, optical microscope of the magnetometer, respectively. **d**, System response of the magnetometer. **e**, Sensitivity spectrum of the magnetometer.

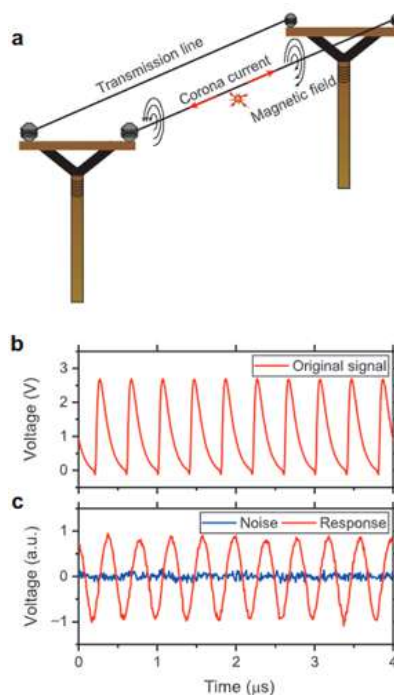


Fig. 2. **a**, Schematic of corona current monitoring through magnetic field detection. **b**, Original voltage signal generated by the arbitrary function generator to simulate the corona current. **c**, Response of the magnetometer with a microdisk radius of 205 μm. The red (blue) curve shows the alternate current component of the optical transmission with (without) the signal.

References

- [1] S. Forstner et al., "Cavity optomechanical magnetometer," *Phys. Rev. Lett.* **108**, 120801 (2012).
- [2] S. Forstner et al., "Ultrasensitive optomechanical magnetometry," *Adv. Mater.* **26**, 6348 (2014).
- [3] C. Yu et al., "Optomechanical magnetometry with a macroscopic resonator," *Phys. Rev. Appl.* **5**, 044007 (2016).
- [4] B.-B. Li et al., "Invited article: Scalable high-sensitivity optomechanical magnetometers on a chip," *APL Photonics* **3**, 120806 (2018).
- [5] B.-B. Li et al., "Ultrabroadband and sensitive cavity optomechanical magnetometry," *Photonics Res.* **8**, 1064 (2020).
- [6] C. Dong et al., "Characterization of magnetomechanical properties in FeGaB thin films," *Appl. Phys. Lett.* **113**, 262401 (2018).

Hollow, Egg-Like Whispering Gallery Mode Resonator

Amal Jose^{1,*}, *Ramgopal Madugani*¹, and *Sile Nic Chormaic*¹

¹ Okinawa Institute of Science and Technology Graduate University, Onna, Okinawa 904-0495, Japan

* amal.jose@oist.jp

Abstract: We fabricated a three-dimensional egg-shaped hollow structure in silica using a CO₂ laser. These structures can support WGMs around 1550 nm and might be valuable for studying mode filtering, spin-orbit interactions of light, and directional emission. © 2024 The Author(s)

1. Introduction

Whispering gallery mode resonators (WGMR) are structures where light circulates through total internal reflection. One factor that affects the ability to store light is the circular symmetry that maintains a constant angle of incidence during propagation. WGMRs are extensively researched to understand different phenomena that require tight confinement of light [1] and for the fabrication of various sensors [2]. Recently, it has been theoretically and experimentally elucidated that whispering gallery modes can exist in certain structures where the symmetry is broken [3]. Investigations of such structures have revealed the possibility of directional emission [4–6], intermodal interactions, and the spin-orbit interaction of light [7]. These phenomena cannot be easily observed in a symmetric WGM resonator.

2. Results and Discussion

Asymmetry in whispering gallery mode resonators can be broadly classified into two types: asymmetry introduced to an otherwise perfectly symmetric structure [8] and asymmetric structures. In this study, we created an asymmetric structure capable of sustaining WGMs. Unlike 2D structures, such as deformed microdisks [9] or limaçon [10] cavities, our structure is a 3D egg-like shape made from a tapered hollow capillary by creating an uneven expansion. The expansion rate was controlled by fabricating a smaller microbubble initially, using a focussed dual beam CO₂ laser setup [11], followed by blocking one beam to attain an egg profile (see Fig. 1). The 3D resonators have an additional axis of confinement compared to deformed microdisk and limaçon structures, with the potential to achieve higher Q-factor modes. The thin anisotropic walls may open the way to study direction-dependent sensitivity and emission in 3D structures. Additionally, the hollow structure is beneficial for storing materials and conducting studies requiring material isolation [12].

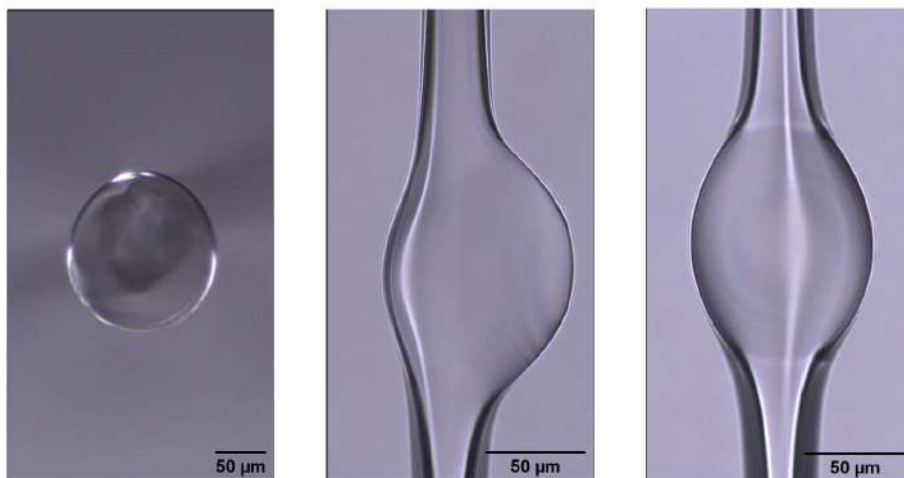


Fig. 1. Left: cross-section view; Middle: side view; Right: top view of the hollow egg-like whispering gallery mode resonator. The profile of the egg-like shape is achieved by inducing a nonuniform expansion in an initially symmetric microbubble resonator.

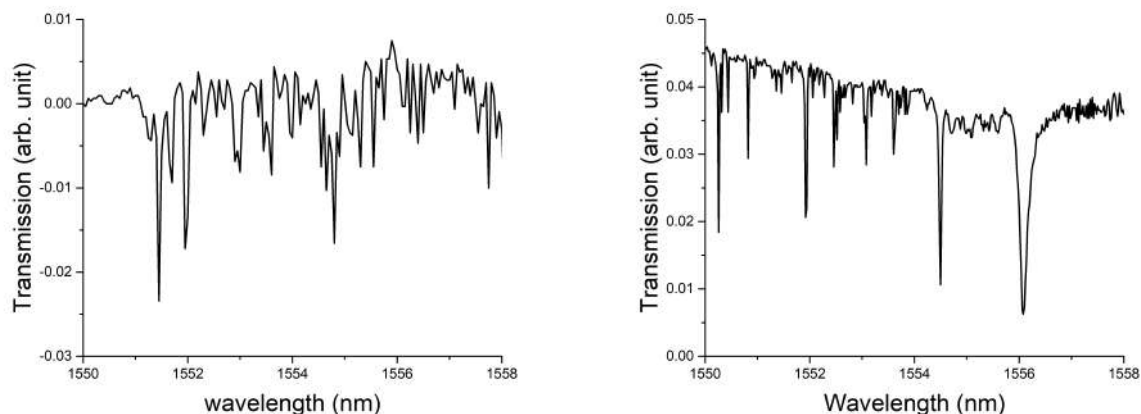


Fig. 2. Transmission spectrum through the tapered fibre while tuning the laser from 1550 nm to 1558 nm. Left: symmetric resonator; Right: asymmetric resonator. Note: the hollow egg-like resonator is comparatively bigger than the initial symmetric one, as it has to be expanded further on one side to introduce the asymmetry.

The resonator was characterized before and after introducing asymmetry by coupling a 1550 nm tunable laser using a tapered fibre (see Fig. 2). In our fabrication method, one can adjust the ratio between the radius of curvature of the asymmetric bulge and its symmetric counterpart. This adjustment allows for tuning of the asymmetry and the potential to achieve mode filtering and selection.

3. Conclusion

We have demonstrated soliton microcomb generation on X-cut TFLN. Building on this, alongside recent advancements in heterogeneously integrated lasers [7] and high-speed photodetectors [8] on TFLN, we propose a photonic chip that integrates all essential optical components for optical clocks (Fig. 1f). Clock lasers are stabilized to atomic transitions or ultrastable cavities using the Pound-Drever-Hall technique, facilitated by the integrated phase modulator. While most atomic transitions for optical clocks are at visible wavelengths, the system can interface with mature microcomb technologies at near-infrared wavelengths via a periodically-poled LiNbO₃ (PPLN) waveguide. Another PPLN waveguide enables the detection of the carrier-envelope offset frequency, which can be stabilized by feedback to the electrodes on the microresonator. Consequently, the photodetected repetition frequency of the soliton microcomb serves as the clock output.

References

- [1] L. Yang, Y. Zhuang, Y. Zhang, Y. Zhang, S. Zhang, Z. Xu, P. Del’Haye, and X. Wei, “Electromagnetically induced transparency-like effect in a lithium niobate resonator via electronic control,” *Photonics Res.* **11**, 773–779 (2023).
- [2] J. M. Ward, Y. Yang, F. Lei, X.-C. Yu, Y.-F. Xiao, and S. Nic Chormaic, “Nanoparticle sensing beyond evanescent field interaction with a quasi-droplet microcavity,” *Optica* **5**, 674–677 (2018).
- [3] L. Ma, S. Li, V. M. Fomin, M. Hentschel, J. B. Götte, Y. Yin, M. Jorgensen, and O. G. Schmidt, “Spin-orbit coupling of light in asymmetric microcavities,” *Nat. communications* **7**, 10983 (2016).
- [4] C. Yan, J. Shi, P. Li, H. Li, and J. Zhang, “Limaçon-shaped micro-cavity lasers with directional emission and its performance,” *Opt. & Laser Technol.* **56**, 285–289 (2014).
- [5] J. Kreismann and M. Hentschel, “The optical möbius strip cavity: Tailoring geometric phases and far fields,” *Europhys. Lett.* **121**, 24001 (2018).
- [6] Y. Song, Y. Monceaux, S. Bittner, K. Chao, H. M. Reynoso De La Cruz, C. Lafargue, D. Decanni, B. Dietz, J. Zyss, A. Grigis *et al.*, “Möbius strip microlasers: a testbed for non-euclidean photonics,” *Phys. Rev. Lett.* **127**, 203901 (2021).
- [7] J. Kreismann and M. Hentschel, “Spin-orbit interaction of light in three-dimensional microcavities,” *Phys. Rev. A* **102**, 043524-1–043524-13 (2020).
- [8] M. Ding, G. Senthil Murugan, G. Brambilla, and M. N. Zervas, “Whispering gallery mode selection in optical bottle microresonators,” *Appl. Phys. Lett.* **100** (2012).
- [9] A. Behrens, M. Bosch, P. Fesser, M. Hentschel, and S. Nic Chormaic, “Fabrication and characterization of deformed microdisk cavities in silicon dioxide with high Q-factor,” *Appl. Opt.* **59**, 7893–7899 (2020).
- [10] J. Kreismann, S. Sinzinger, and M. Hentschel, “Three-dimensional limaçon: Properties and applications,” *Phys. Rev. A* **95**, 011801 (2017).
- [11] A. Watkins, J. Ward, Y. Wu, and S. Nic Chormaic, “Single-input spherical microbubble resonator,” *Opt. letters* **36**, 2113–2115 (2011).
- [12] A. Jose, R. Madugani, R. S. Kalra, and S. Nic Chormaic, “Magnetospirillum bacteria sensing using a microbubble wgm resonator,” in *Nonlinear Optics and its Applications 2024*, vol. 13004 (SPIE, 2024), pp. 6–8.

Soliton microcombs in X-cut LiNbO₃ microresonators

Binbin Nie^{1,†}, *Xiaomin Lv*^{1,2,†}, *Chen Yang*^{1,†}, *Rui Ma*³, *Kaixuan Zhu*¹, *Ze Wang*¹, *Yanwu Liu*¹, *Zhenyu Xie*¹, *Xing Jin*¹, *Guanyu Zhang*¹, *Du Qian*¹, *Zhenyu Chen*³, *Qiang Luo*³, *Shuting Kang*³, *Guowei Lv*^{1,4,5}, *Qihuang Gong*^{1,4,5}, *Fang Bo*^{3,*}, and *Qi-Fan Yang*^{1,4,5,*}

¹ State Key Laboratory for Artificial Microstructure and Mesoscopic Physics and Frontiers Science Center for Nano-optoelectronics, School of Physics, Peking University, Beijing, 100871, China

² Hefei National Laboratory, Hefei, 230088, China

³ Nankai University, Tianjin, 300071, China

⁴ Collaborative Innovation Center of Extreme Optics, Shanxi University, Taiyuan, 030006, China

⁵ Peking University Yangtze Delta Institute of Optoelectronics, Nantong, 226010, China

† These authors contributed equally to this work.

* bofang@nankai.edu.cn; leonardoyoung@pku.edu.cn

Abstract: We demonstrate the generation of transverse-electric-polarized soliton microcombs with 25 GHz repetition rate and 200 nm spectral span in an integrated X-cut LiNbO₃ microresonator. © 2024 The Author(s)

1. Introduction

Recently, the development of high-quality-factor (high-Q) optical microresonators has spawned chip-based optical frequency combs, known as microcombs [1], which promise miniaturized instrumentation of time keeping [2], ranging [3], and spectroscopy [4]. Despite their realizations on various material platforms such as silica, Si₃N₄, and MgF₂, achieving full comb functionality on photonic chips necessitates co-integration with high-speed modulators and efficient frequency doublers, which are monolithically available on X-cut thin-film lithium niobate (TFLN).

LiNbO₃ has long been exploited for frequency doubling and electro-optic modulation, whose performance is recently leveraged by the thin-film lithium niobate (TFLN) technology due to the improved confinement of optical and electric fields. To access the highest second-order nonlinear coefficient ($d_{33} = -27$ pm/V) and electro-optic coefficient ($\gamma_{33} = 30.9$ pm/V) of LiNbO₃, the optical and electric fields should be both polarized parallel to the optical axis, which can be readily implemented for transverse-electric-polarized (TE-polarized) optical modes on X-cut TFLN. However, soliton microcombs are elusive on X-cut TFLN due to the strong Raman response associated with extraordinary light. Instead, Raman lasing is commonly observed in this configuration [5].

In this work, we tailor the portion between ordinary and extraordinary light in LiNbO₃ microresonators to suppress stimulated Raman scattering on X-cut TFLN. Microwave-rate (25 GHz) soliton microcombs with 200 nm spectral span are generated in TE modes with a continuous-wave pump laser. Our demonstration provides a route for chip-scale integration of the entire optical system of optical clocks.

2. Results

We first characterize the polarization-dependence of the Raman response of an X-cut TFLN chip using Raman spectroscopy (Fig. 1 a). The Raman spectra contain multiple peaks corresponding to different vibrational modes, with intensities decreasing as the pump polarization transitions from parallel (extraordinary light) to perpendicular (ordinary light) to the optical axis. For instance, the peak intensities of vibrational modes A(TO)₁ and A(TO)₄ are reduced to 40% and 20%, respectively (Fig. 1b). Thus, incorporating more ordinary light in the modes of LiNbO₃ microresonators can significantly mitigate the Raman effect, which is the key to our design.

To increase the portion of ordinary light, we use racetrack microresonators instead of ring microresonators. The majority of the modes are confined in the straight waveguides, which are oriented along the optical axis to maximize the portion of ordinary light. The soliton-generating microresonators are fabricated from a 600-nm-thick LiNbO₃ layer atop a 4.7- μ m-thick silica layer, following established procedures [6]. The design of the microresonator is shown in Fig. 1c. The free-spectral-range (FSR) of the microresonator is approximately 25 GHz. A bus waveguide with a top width of 1 μ m is coupled to the microresonator at the Euler bend. The transmitted spectrum shows an intrinsic Q factor up to 3 million within the telecommunication C-band (Fig. 1d). In experiment, soliton microcombs are generated with continuous-wave laser pumping, whose optical spectrum is shown in Fig. 1e. The spectrum spans more than 200 nm, following a sech²-shaped spectral envelope with deviations caused by mode-crossings.

3. Conclusion

We have demonstrated soliton microcomb generation on X-cut TFLN. Building on this, alongside recent advancements in heterogeneously integrated lasers [7] and high-speed photodetectors [8] on TFLN, we propose a photonic chip

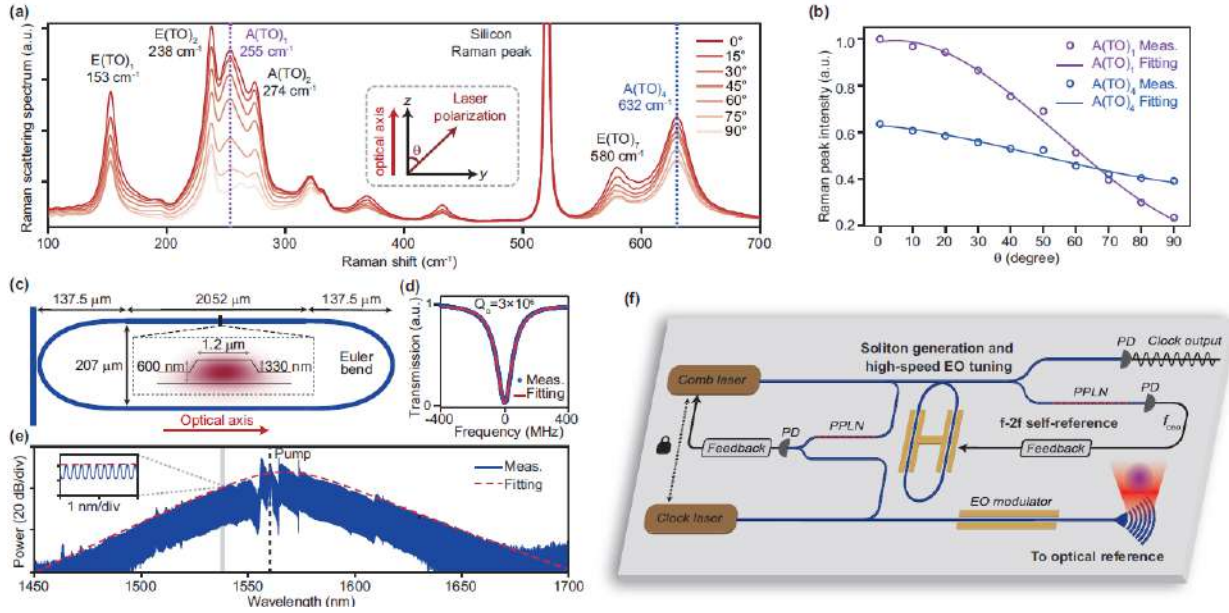


Fig. 1. (a) Polarization-dependent Raman spectra of X-cut TFLN, with the angle between the pump laser polarization and the optical axis varying from 0° to 90°. (b) Raman peak intensity of vibrational modes A(TO)₁ and A(TO)₄ as a function of the angle between the pump laser polarization and the LN optical axis. (c) Design of the microresonator (not to scale). The cross-sectional geometry with the profile of the TE fundamental mode is provided in the inset. (d) Typical transmission spectrum of a fundamental TE mode. (e) Optical spectrum of the soliton microcomb. The dashed red line represents sech^2 fitted soliton spectral envelope. The left inset shows the zoom-in views of soliton comb lines. (f) Conceptual illustration of an integrated optical clock on X-cut TFLN. PPLN: periodically-poled lithium niobate; PD: photodetector.

that integrates all essential optical components for optical clocks (Fig. 1f). Clock lasers are stabilized to atomic transitions or ultrastable cavities using the Pound-Drever-Hall technique, facilitated by the integrated phase modulator. While most atomic transitions for optical clocks are at visible wavelengths, the system can interface with mature microcomb technologies at near-infrared wavelengths via a periodically-poled LiNbO₃ (PPLN) waveguide. Another PPLN waveguide enables the detection of the carrier-envelope offset frequency, which can be stabilized by feedback to the electrodes on the microresonator. Consequently, the photodetected repetition frequency of the soliton microcomb serves as the clock output.

References

- [1] T. J. Kippenberg, R. Holzwarth, and S. A. Diddams, “Microresonator-based optical frequency combs,” *Science* **332**, 555–559 (2011).
- [2] Z. L. Newman, V. Maurice, T. Drake, J. R. Stone, T. C. Briles, D. T. Spencer, C. Fredrick, Q. Li, D. Westly, B. R. Ilic et al., “Architecture for the photonic integration of an optical atomic clock,” *Optica* **6**, 680–685 (2019).
- [3] M.-G. Suh and K. J. Vahala, “Soliton microcomb range measurement,” *Science* **359**, 884–887 (2018).
- [4] M.-G. Suh, Q.-F. Yang, K. Y. Yang, X. Yi, and K. J. Vahala, “Microresonator soliton dual-comb spectroscopy,” *Science* **354**, 600–603 (2016).
- [5] M. Yu, Y. Okawachi, R. Cheng, C. Wang, M. Zhang, A. L. Gaeta, and M. Lončar, “Raman lasing and soliton mode-locking in lithium niobate microresonators,” *Light. Sci. Appl.* **9**, 9 (2020).
- [6] X. Lv, B. Nie, C. Yang, R. Ma, Z. Wang, Y. Liu, X. Jin, K. Zhu, Z. Chen, D. Qian et al., “Broadband microwave-rate dark pulse microcombs in dissipation-engineered LiNbO₃ microresonators,” arXiv preprint arXiv:2404.19584 (2024).
- [7] A. Shams-Ansari, D. Renaud, R. Cheng, L. Shao, L. He, D. Zhu, M. Yu, H. R. Grant, L. Johansson, M. Zhang et al., “Electrically pumped laser transmitter integrated on thin-film lithium niobate,” *Optica* **9**, 408–411 (2022).
- [8] X. Guo, L. Shao, L. He, K. Luke, J. Morgan, K. Sun, J. Gao, T.-C. Tzu, Y. Shen et al., “High-performance modified uni-traveling carrier photodiode integrated on a thin-film lithium niobate platform,” *Photon. Res.* **10**, 1338–1343 (2022).

Dual-color Coherent Perfect Absorber

Boyi Xue¹, Wenjie Wan^{1,*}

¹ University of Michigan-Shanghai Jiao Tong University Joint Institute, Shanghai Jiao Tong University, Shanghai 200240, China

* wenjie.wan@sjtu.edu.cn

Abstract: We observed a dual-color CPA in a whispering-gallery-mode microcavity, which enables perfect absorption of both the incoming fundamental wave and its second harmonic through nonlinear interference, breaking the linear boundary of CPA into multi-frequency domain.

1. Introduction

Coherent perfect absorbers (CPA) play a crucial role in various interdisciplinary areas. The ability of CPA to perfectly absorb any incoming wave without re-emitting solely lies on the interference-enhanced absorption in a lossy cavity, leading to a “blackhole” singularity in the spectrum [1,2]. One critical quest of CPAs is to pursue the broadband/multi-channel perfect absorption across the spectra. Nonlinearity might be the key to tackling the problem. Though “colored” CPAs have been theoretically predicted through nonlinear processes like optical parametric oscillation [3], the experiment still remains elusive. In this work, we demonstrate a dual-color CPA in a single WGM microcavity, enabling simultaneous complete absorption of incoming waves at two frequencies. The DC-CPA phenomenon arises from the nonlinear coupling between a fundamental wave (FW) mode and its second harmonic (SH). This results in destructive interference for both modes. Moreover, the coherent control of transmission can be realized by tuning the relative phase and intensity between these two input waves.

In this work, we tailor the portion between ordinary and extraordinary light in LiNbO₃ microresonators to suppress stimulated Raman scattering on X-cut TFLN. Microwave-rate (25 GHz) soliton microcombs with 200 nm spectral span are generated in TE modes with a continuous-wave pump laser. Our demonstration provides a route for chip-scale integration of the entire optical system of optical clocks.

2. Dual-Color Coherent Perfect Absorber

2.1 Theory The schematic illustration of the DC-CPA concept is depicted in Fig. 1a. A second-order nonlinear microcavity is coupled to a tapered fiber. Two input lasers (α and β) are launched into the system. We consider the weak nonlinear coupling condition, where the nonlinear coupling G can be assumed as a small constant. Under this crucial condition, only the weak SH wave will be influenced during the nonlinear coupling process. The FW will remain critically coupled in the weak coupling regime, while the relatively weak SH wave will also become perfectly absorbed due to the total destructive interference among the out-coupled SH light, the nonlinearly converted SH, and the residual SH transmission [4].

We adopt the S-matrix approach employed in the original one-port CPA [1], and describe our DC-CPA system utilizing the electromagnetic scattering matrix (S-matrix):

$$\begin{pmatrix} \alpha_{\text{out}} \\ \beta_{\text{out}} \end{pmatrix} = S(\omega) \begin{pmatrix} \alpha_{\text{in}} \\ \beta_{\text{in}} \end{pmatrix} = \begin{pmatrix} 1 - \frac{i\gamma_{c1}\delta_2}{\delta_1\delta_2 - 2|G|^2} & \frac{i\sqrt{\gamma_{c1}\gamma_{c2}}G}{\delta_1\delta_2 - 2|G|^2} \\ \frac{2i\sqrt{\gamma_{c1}\gamma_{c2}}G^*}{\delta_1\delta_2 - 2|G|^2} & 1 - \frac{i\gamma_{c2}\delta_1}{\delta_1\delta_2 - 2|G|^2} \end{pmatrix} \begin{pmatrix} \alpha_{\text{in}} \\ \beta_{\text{in}} \end{pmatrix}$$

DC-CPA occurs at the zeros of the S-matrix, leading to the vanishing of the total output in response to an input signal aligned with the corresponding eigenvector of S . When the eigenvalue equals zero, its corresponding eigenfrequency will be purely real when $G \approx 6.37$ MHz, as simulated in Fig. 1b. This is the CPA condition. Then, by choosing proper phase and intensity relationships between the two input waves, DC-CPA could be achieved.

2.2 Observation of dual-color CPA

In the experiment, we first launch the FW laser, select a mode suitable for second harmonic generation and make it and make it critically coupled. The corresponding SH mode is observed to be under coupled. The cavity temperature is tuned using a thermoelectric cooler (TEC) to ensure double resonance. Then, we adjust the power Of these two input modes, while maintaining their relative phase fixed at $\pi/2$. The DC-CPA phenomenon is observed when the

input power of FW and SH are equal to $78.96 \mu\text{W}$ and 116.4 nW , respectively, corresponding to a relative amplitude $\beta_{\text{in}}/\alpha_{\text{in}} = 0.0384$. The transmission spectrum is visualized in Graph C of Fig. 1e, revealing that the transmission rate approaches zero at the DC-CPA point. Graphs A, B, D, and E represent the output spectra when the input signal deviates from the eigenchannel of the S-matrix, exhibiting substantial deviations from the CPA effect. The experimental data for normalized transmittance at zero detuning is illustrated in Fig. 1d. The obtained results exhibit a remarkable alignment with the theoretical predictions.

The absorption behavior of DC-CPA is highly sensitive to the relative phase of the inputs. To investigate the behavior of phase modulation, we conducted measurements on the transmittance for both the FW and SH modes around the zero-detuning point as a function of the relative phase. While the FW remains unaffected, the SH signal exhibits sinusoidal oscillations in phase with $\Delta\phi$, as shown in Fig. 1c, resembling an optical modulator.

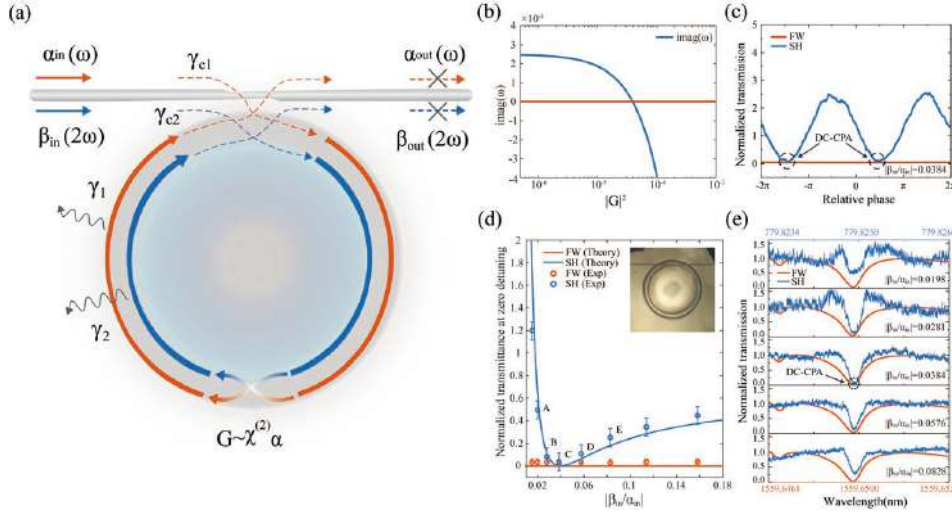


Fig. 1. Illustration of dual-color CPA effect. (a) Schematic diagram of nonlinear coupling between two modes in a tapered fiber coupled microcavity. (b) Imaginary part of ω for the zeros of the S-matrix is plotted as a function of $2G$. (c) Transmission rate of FW and SH at zero detuning as a function of relative phase. (d) Normalized transmittance at zero detuning under CPA condition, plotted as a function of $\beta_{\text{in}}/\alpha_{\text{in}}$. Phase difference is fixed at $\Delta\phi = \pi/2$. (e) Experimentally obtained transmission spectra with different values of $\beta_{\text{in}}/\alpha_{\text{in}}$, corresponding to A–E in (a). The DC-CPA point is marked in curve C.

3. Summary

We demonstrated the dual-color coherent perfect absorption in a single microcavity with second-order nonlinearity, where the FW mode and SH mode can be perfectly absorbed simultaneously. This significant advancement expands the scope of research on coherent perfect absorption into the nonlinear regime, enabling coherent control of two signals at distinct wavelengths. Given that this absorption behavior is highly sensitive to both the power and relative phase of the input waves, our system holds great promise for constructing an all-optical modulator in a cost-effective and compact form. These findings pave the way for numerous applications including all-optical computing and quantum information processing.

References

- [1] Y. D. Chong, L. Ge, H. Cao, and A. D. Stone, Coherent perfect absorbers: time-reversed lasers, *Phys. Rev. Lett.* **105**, 053901 (2010).
- [2] W. Wan, Y. Chong, L. Ge, H. Noh, A. D. Stone, & H. Cao, Time-reversed lasing and interferometric control of absorption, *Science* **331**, 889-892 (2011).
- [3] S. Longhi, Time-reversed optical parametric oscillation, *Phys. Rev. Lett.* **107**, 033901 (2011).
- [4] J. Hou, J. Lin, J. Zhu, G. Zhao, Y. Chen, F. Zhang, Y. Zheng, X. Chen, Y. Cheng, L. Ge, and W. Wan, Self-induced transparency in a perfectly absorbing chiral second-harmonic generator, *Photonix* **3**, 22 (2022).

Titanium doped Sapphire and Whispering Gallery Modes: An Effective Combination for Low Threshold Lasing and Amplification

Farhan Azeem^{1,2,*}, *Luke S. Trainor*^{1,2}, *Ang Gao*^{3,4}, *Maya Isarov*⁵, *Dmitry V. Strekalov*^{1,2}, and *Harald G. L. Schwefel*^{1,2}

¹ Department of Physics, University of Otago, 730 Cumberland Street, Dunedin 9016, New Zealand

² The Dodd-Walls Centre for Photonic and Quantum Technologies, New Zealand.

³ MOE Key Laboratory of Weak-Light Nonlinear Photonics, TEDA Institute of Applied Physics and School of Physics, Nankai University, Tianjin, 300457, China

⁴ State Key Laboratory for Artificial Microstructure and Mesoscopic Physics, School of Physics, Peking University, Beijing, 100871, China

⁵ School of Electrical Engineering & Telecommunications, University of New South Wales, Australia.

* fazeem13@ku.edu.tr

Abstract: Titanium-doped sapphire (Ti:sapphire) has long been a prevalent gain medium in the solid-state laser industry, valued for its broadband gain properties and sustained performance over more than three decades. Recently, we demonstrated a Ti:sapphire laser utilizing the whispering gallery mode (WGM) resonator platform. Here, we summarize our findings, detailing lasing and amplification in the first high-quality Ti:sapphire whispering-gallery laser (WGL).

In this work, we introduce a high-quality Ti:sapphire WGM resonator, characterized by a low lasing threshold and high slope efficiency. Amplification is also readily achievable [1,2]. By evanescently coupling a green pump laser to the WGM resonator, we observe single-mode lasing at pump powers as low as 14.2 mW. Additionally, we achieved multi-mode lasing and report laser slope efficiencies of 34%. The four-level gain system is directly observed by simultaneously coupling to a near-infrared mode at 795 nm, which results in a notable linewidth decrease with increase in the green pump power, as shown in Fig.1(c).

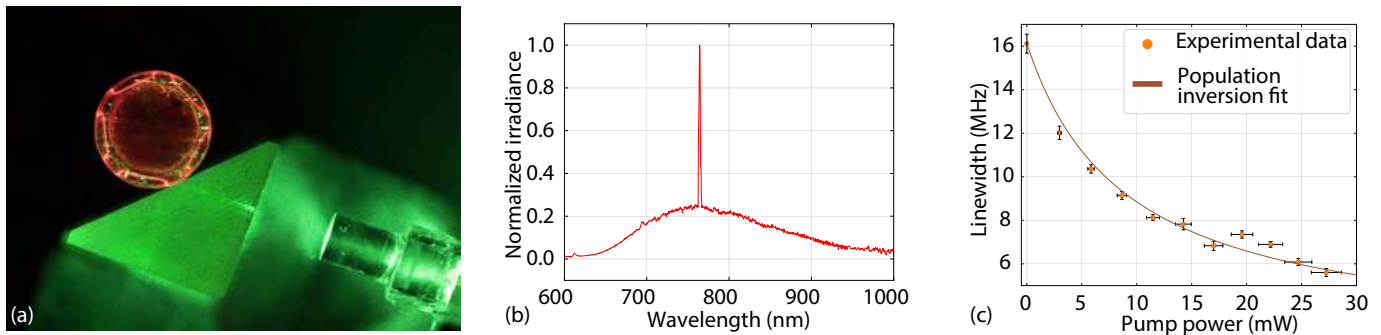


Fig. 1. (a) Photograph showing fluorescence in the titanium-doped sapphire whispering gallery mode (WGM) resonator. (b) Single-mode lasing: by adjusting polarization and coupling, lasing on different laser lines can be selectively achieved. (c) Amplification: the gain narrows the linewidth of a concurrently coupled near-infrared laser.

References

[1] F. Azeem, L. S. Trainor, A. Gao, M. Isarov, D. V. Strekalov, and H. G. L. Schwefel, *Ultra-Low Threshold Titanium-Doped Sapphire Whispering-Gallery Laser*, *Advanced Optical Materials* 10, 2102137 (2022).

Structure of chaotic resonance modes in dielectric cavities

Florian Lorenz¹, Jan Robert Schmidt¹, and Roland Ketzmerick¹

¹ Institute of Theoretical Physics, TU Dresden, 01062 Dresden, Germany

Abstract: We explain the structure of chaotic resonance modes with arbitrary lifetimes in dielectric cavities in the limit of geometric optics. It is given by a multifractal measure from ray dynamics. © 2024 The Author(s)

1. Introduction

According to a factorization conjecture [1, 2, 3], the multifractal structure of chaotic resonance modes is given by a product of (i) a conditionally invariant measure from ray dynamics with a smoothed spatial density and (ii) universal exponentially distributed fluctuations. We present progress on the construction of the first factor, i.e., the correct conditionally invariant measures for resonance modes with arbitrary lifetimes [4].

2. Wave-ray correspondence

For the limaçon-shaped dielectric cavity, we show that ray dynamics is able to describe resonance states with an arbitrary lifetime. This is demonstrated for modes with TM- and TE polarization. Numerical verification is performed far in the semiclassical regime ($nkR \approx 10^4$), see Fig. 1. In contrast to a previous approach [2], we find that the chaotic resonance modes, in the limit of geometric optics, converge towards these conditionally invariant measures [4]. This is quantified using the Jensen-Shannon divergence.

3. Conditionally invariant measures

We explain how to construct the correct conditionally invariant measures [4]. To this end we generalize the matrix approximation of the Perron-Frobenius operator, generating coarse-grained conditionally invariant measures of various lifetimes. Among all measures with the same lifetime we determine the one relevant for resonance states by locally demanding closeness to uniformity.

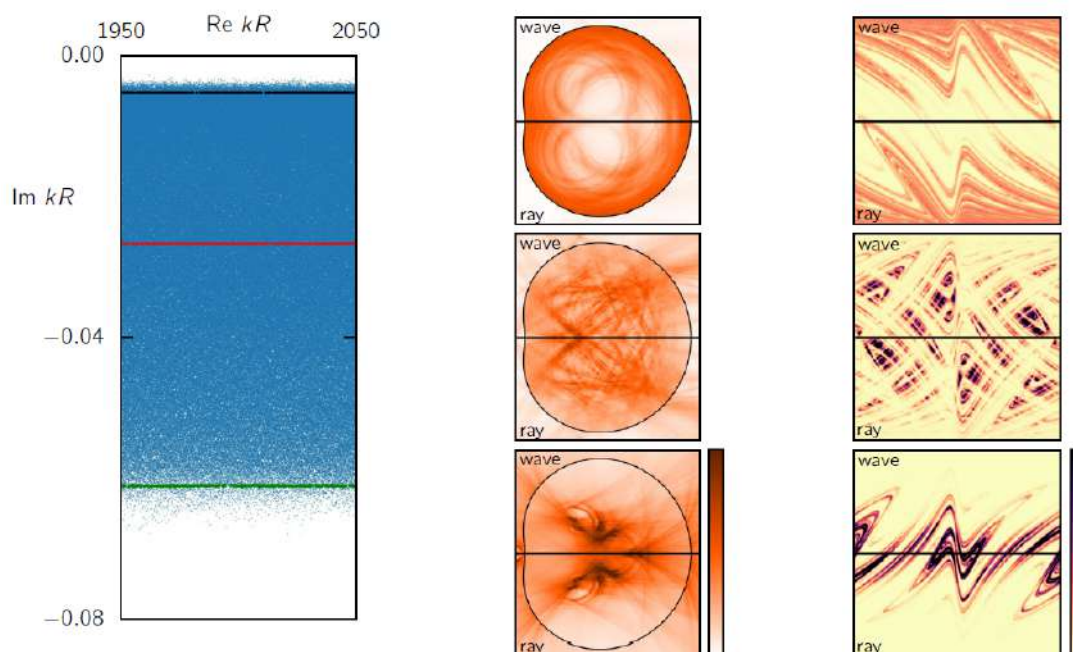


Fig. 1. Left: Spectrum of 379,492 antisymmetric TM polarized modes of limaçon cavity with $n = 3.3$. Highlighted are 400 poles nearest to three different lifetimes, respectively. Middle: Waveray comparison in position space between average wave structure (upper half) and ray-dynamical measure (lower half) for the three marked lifetimes. Right: Wave-ray comparison in boundary phase space.

References

[1] K. Clauß, F. Kunzmann, A. Bäcker, and R. Ketzmerick, *Universal intensity statistics of multifractal resonance states*, *Phys.*

Rev. E **103**, 042204 (2021).

[2] R. Ketzmerick, K. Clauß, F. Fritsch, and A. Bäcker, *Chaotic resonance modes in dielectric cavities: Product of conditionally invariant measure and universal fluctuations*, *Phys. Rev. Lett.* **129**, 193901 (2022).

[3] J. R. Schmidt and R. Ketzmerick, *Resonance states of the three-disk scattering system*, *New J. Phys.* **25**, 123034 (2023).

[4] R. Ketzmerick, F. Lorenz, and J. R. Schmidt, *in preparation*.

Development of vector magnetometer based on hollow core whispering gallery resonators and nitrogen-vacancy centers in diamond

Jalaludeen Mohammed^{1,*}, *Samuel Begumya*¹, *Ke Tian*¹, *Shilong Li*^{1,2}, and *Sile Nic Chormaic*¹

¹ Light-Matter Interactions for Quantum Technologies Unit, Okinawa Institute of Science and Technology Graduate University, Onna, Okinawa 904-0495, Japan

² Department of Information Science and Electronic Engineering, Zhejiang University, Zhejiang, 310027, China

* mohammedzia.jalaludeen@oist.jp

Abstract: Magnetometry based on optically detected magnetic resonance using nitrogen-vacancy centers in diamond coupled to whispering gallery modes of a hollow core optical microresonator is explored in this work.

1. Introduction

Nitrogen vacancy (NV) centers in diamond have gained significant attention in the past decade owing to their unique quantum properties, such as room temperature stable single-photon source and magnetic field sensing at the nanometer scale [1]. The NV-center in diamond is an atomic-scale defect in a diamond lattice with a substitutional nitrogen atom next to a lattice vacancy. The electronic ground level of the NV-center is a spin triplet system, $m_s = 0, \pm 1$. The spin sublevels $m_s = \pm 1$ are nearly degenerate and have a zero-field separation of 2.87 GHz from the $m_s = 0$ sublevel. These ground-level spin states can be manipulated using microwave photons, and the spin state can be optically read through state-dependent fluorescence. The NV-centers are optically pumped non-resonantly using a 532 nm laser, producing broadband fluorescent photons from 600–800 nm with a zero-phonon line (ZPL) at 637 nm. When a microwave field is frequency scanned across the NV center, a reduction in fluorescence intensity can be observed at 2.87 GHz, corresponding to the zero-field splitting energy. However, when an external magnetic field is applied, the degeneracy between the ground states $m_s = \pm 1$ is lifted. As a result, two intensity minima can be observed upon microwave frequency scanning. The splitting of these levels is proportional to the strength of the external magnetic field and is 56 MHz/mT for weak magnetic fields. However, the full potential of NV-center based magnetic sensors, specifically at the single molecule level, still needs to be improved and is explored in many laboratories [2, 3].

Optical cavities possessing ultra-high quality factors have proven to be an effective method to enhance the sensitivity limit of an optical sensor [4]. Whispering gallery mode (WGM) microcavities are an excellent class of optical microcavities that provide ultra-high quality factors. Therefore, integrating NV centers with a WGM cavity should help further enhance the magnetic field sensitivity limit. Several attempts have been made to incorporate NV centers with WGM cavities [5, 6] but these have yet to result in a significant improvement in terms of performance. Existing methods use WGM cavity geometries which are bulky, with their feature size being much larger than the optical wavelength. As a result, the interaction of the WGM field with the external NV-center is weak, resulting in reduced performance. In this work, NV-centers were coupled to a hollow microbubble microresonator [7, 8], where the wall thickness of the resonator was of the order of the optical wavelength used, thus enhancing the light-matter interaction.

2. Model and discussion

Figure 1 shows a schematic of the magnetometer system based on the NV-center in diamond and microbubble resonator. The microbubble was fabricated using borosilicate glass capillary with 350 μm outer and 250 μm inner diameters. The resonator was made by first tapering the glass capillary by heating it with a CO₂ laser while simultaneously pulling it. Once the taper reached a few tens of micrometers, the tapering process was stopped. The tapered capillary was again exposed to laser radiation to soften a section of the capillary, which was simultaneously pressurized internally by allowing nitrogen gas to flow through the capillary to form the microbubble. The final diameter of the microbubble was controlled by adjusting the laser power. In this experiment, a microbubble of diameter 100 μm was fabricated. 70 nm nanodiamond particles containing 2.5 ppm NV-centers were used to couple to the microbubble resonator. A small amount of diamond stock was used to make a suspension with suitable dilution. A tiny aliquot of the diluted suspension was drop-cast on to the surface of the microbubble. Once the droplet landed on the resonator's surface, the solvent evaporated rapidly, depositing nanodiamond particles. The presence of NV-centers was confirmed by monitoring it in real time through a fluorescence widefield imaging system.

After the deposition, the fluorescence from NV-centers to the microbubble was detected using an optical nanofiber scanned along the microbubble axis. As a result of the coupling of fluorescence to the optical modes of the microbubble, a modification of the characteristic spectral shape of the NV-center diamond was observed as shown in Figure 2.

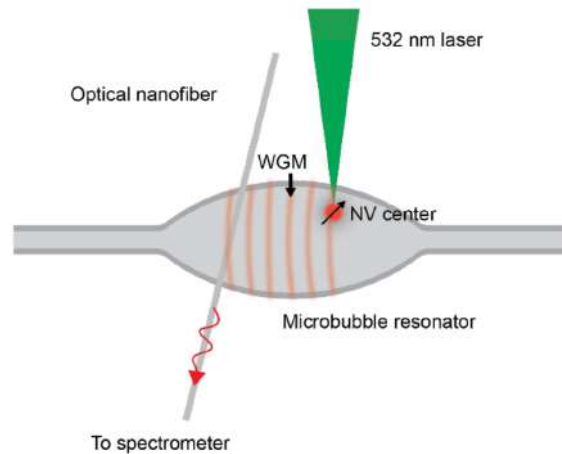


Fig. 1. Microbubble–NV-center based magnetometer. Nanodiamond particles containing NV-centers are attached to the surface of a microbubble microresonator. The fluorescence from the NV centers coupled to the optical modes of the microresonator was detected using an optical nanofiber and analyzed using a spectrometer.

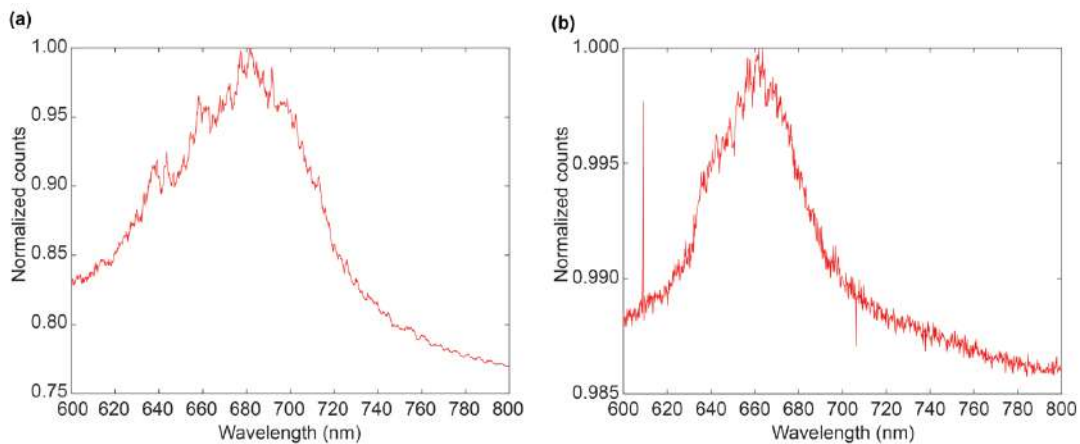


Fig. 2. NV center spectrum. The fluorescence spectra of NV-centers when attached to (a) an optical nanofiber and (b) a microbubble microresonator.

3. Conclusion

In this work, nanodiamond particles containing NV centers were coupled to a hollow core microbubble resonator. The effects of optical modes on the NV-center are characterized through fluorescence spectrum measurements, and a modification in spectral behavior was observed.

References

- [1] G. Balasubramanian et al., Nanoscale imaging magnetometry with diamond spins under ambient conditions, *Nature* **455**, 2008.
- [2] S. Magaletti et al., Magnetic sensitivity enhancement via polarimetric excitation and detection of an ensemble of NV centers, *Sci. Rep.* **14**, 11793, 2024.
- [3] Z. Wang et al., Picotesla magnetometry of microwave fields with diamond sensors, *Sci. Adv.* **10**(32), 2022.
- [4] D. Yu et al., Whispering-gallery-mode sensors for biological and physical sensing, *Nat. Rev. Methods Primers* **1**(83), 2021.
- [5] Y. Ruan et al., Atom–Photon Coupling from Nitrogen-vacancy Centres Embedded in Tellurite Microspheres, *Sci. Rep.* **5**, 11486, 2015.
- [6] S. Schietinger et al., Coupling single NV-centres to high-Q whispering gallery modes of a preselected frequency-matched microresonator, *J. Phys. B: At. Mol. Opt. Phys.* **42**, 114001, 2009.
- [7] M. Z. Jalaludeen et al., Structural characterization of thin-walled microbubble cavities, *Photonics Res.* **11**(8), 2023.
- [8] J. Yu et al., A tellurite glass optical microbubble resonator, *Opt. Express* **28**(22), 2020

Toward Observation of Superradiance at an Exceptional Point of a Birefringent Fabry-Perot Cavity

Jisung Seo, Juman Kim and Kyungwon An*

Department of Physics and Astronomy, Seoul National University, Seoul 08826, Korea

* kwan@phya.sun.ac.kr

Abstract: We have fabricated a pump-cavity assembly supporting pump-cavity phase matching and adjustable interaction between two polarization modes of a Fabry-Perot cavity to form an exceptional point (EP) for investigation of fluctuations at EP through superradiance.

1. Introduction

It is shown that lasing linewidth is increased by the Petermann factor near an EP due to enhanced fluctuations [1]. Such enhanced fluctuations would also affect the superradiance process, where atomic correlation responsible for superradiance is induced by fluctuations. If superradiance is made to occur in a cavity mode near an EP, the delay time, pulse width and peak power of superradiance would thus change [2].

Previously, we have observed superradiance with a beam of two-level atoms interacting with a Fabry-Perot cavity [3]. If we can achieve EP with a Fabry-Perot cavity, we can readily perform superradiance experiment with it. One cannot have EP in an ideal Fabry-Perot cavity, but it is shown that EP's of two linearly polarized modes can be formed in a Fabry-Perot by installing a pair of waveplates and a pair of Brewster windows inside and by finely tuning the angles of them independently [4].

We have designed and fabricated a stable cavity-pump assembly based on this idea. This assembly can be incorporated into the existing setup of a high-speed, high-density atomic ion beam to induce superradiance and measure the effect of enhanced fluctuations near an EP.

2. Theory and results

2.1 Jones matrix and EP formation

Consider a pair of waveplates with their fast axes along the $\hat{\epsilon}_i$ direction ($i=1,2$), creating a phase difference of ϵ_i with

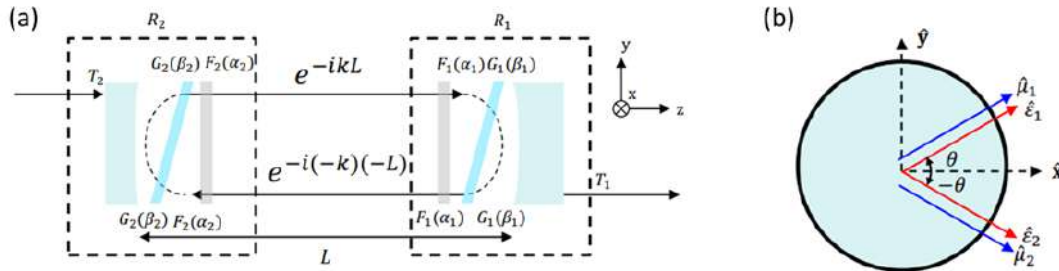


Fig. 1. Schematic of a cavity composed of mirrors, a pair of waveplates F_i with angle of α_i to the x-axis and a pair of Brewster windows G_i with angle of β_i to the x-axis.

respect to the perpendicular direction, and a pair of Brewster windows, causing a loss difference of e^μ between the direction of $\hat{\mu}_i$ and its perpendicular direction in a Fabry-Perot formed by two mirrors with reflectivity r_1 and r_2 .

Let us group a mirror with a waveplate and a Brewster window as one unit of reflection and denote its Jones matrix as R_i , which can be written as $R_i = r_i F_i(\alpha_i) G_i(\beta_i) F_i(\alpha_i)$ with F_i being the Jones matrix of the waveplate and G_i that of the Brewster window. After N round trips, the Jones matrix of the whole system can be described as $T_1 \sum (R_1 R_2 e^{-2ikL})^N T_2$. By assuming $\alpha_i = \beta_i = \theta_i$, diagonalizing $R_1 R_2$, and letting $\tilde{\mu} = \mu_1 + \mu_2$, $\tilde{\epsilon} = \epsilon_1 + \epsilon_2$, $\Delta\epsilon = \epsilon_1 - \epsilon_2$, $\Delta\mu = \mu_1 - \mu_2$, $a = \tilde{\mu} + i\tilde{\epsilon}$, $b = \Delta\mu + i\Delta\epsilon$, we have

$$R_1 R_2 = r_1 r_2 e^{-\frac{a}{2}} \begin{pmatrix} \cosh b \sin^2 2\theta + \cos 2\theta (e^a \cos^2 \theta - e^{-a} \sin^2 \theta) & -\cosh a \sin 2\theta \cos 2\theta + \sin 2\theta (e^b \cos^2 \theta - e^{-b} \sin^2 \theta) \\ \cosh a \sin 2\theta \cos 2\theta + \sin 2\theta (e^b \sin^2 \theta - e^{-b} \cos^2 \theta) & \cosh b \sin^2 2\theta - \cos 2\theta (e^a \sin^2 \theta - e^{-a} \cos^2 \theta) \end{pmatrix}. \quad (1)$$

The eigenvalues λ_\pm of $R_1 R_2$ are obtained as

$$\lambda_\pm = \cosh b \sin^2 2\theta + \cosh a \cos^2 2\theta \pm \sqrt{\sinh^2 a \cos^2 2\theta + (-\cosh^2 a \cos^2 2\theta + \cosh^2 b \sin^2 2\theta + 2 \cosh a \cosh b \cos^2 2\theta - 1) \sin^2 2\theta}. \quad (2)$$

The EP condition is satisfied when $\lambda_+ = \lambda_-$. If two $\lambda/4$ waveplates are used and a Brewster window is installed on only one side, we obtain $\epsilon_1 = \epsilon_2 = \frac{\pi}{2}$, $\mu_2 = 0$, $a = \mu_1 + i\pi$, and $b = \mu_1$. The EP condition in this case is simplified to

$$\tanh^2 \mu_1 = \sin^2 4\theta. \quad (3)$$

2.2 Cavity-Pump Assembly

In order to observe superradiance, the phases of the pump laser and the cavity mode should match each other. The cavity-pump phase matching involves aligning the pump beam parallel to the traveling-wave cavity mode. The traveling-wave interaction is made possible by tilting the atomic beam slightly from the normal incidence to the cavity axis [5]. Parallelogram-shaped prisms are utilized to position the pump beam just in front of the cavity mode. The pump beam's diameter should be similar to that of the cavity mode to achieve effective Guoy-phase matching.

The pump beam, delivered through a single-mode optical fiber, is made to have an elliptical cross-section

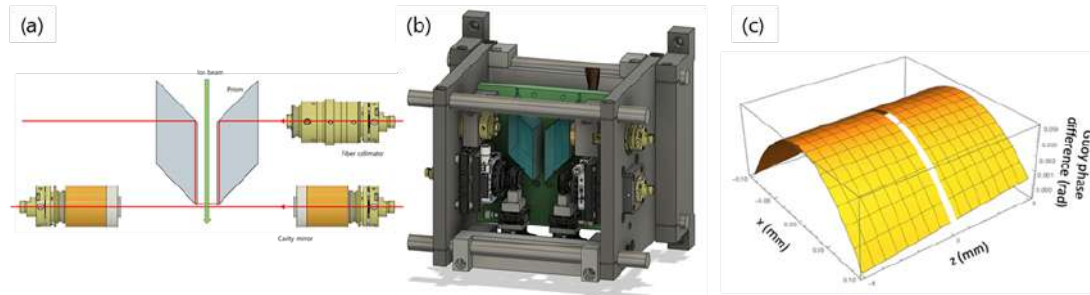


Fig. 2. (a) and (b) The schematic and the design of the cavity-pump assembly capable of satisfying the phase matching condition for superradiance. The pump beam and the cavity mode have similar mode waists while parallel to each other. (c) The Guoy phase difference between the pump beam and the cavity mode. Under the given experimental conditions, the expected Guoy phase difference between the pump beam and the cavity mode is less than 5 mrad, sufficiently satisfying the required phase matching for superradiance.

in front of the cavity mode. The ion beam passes through the minor axis of the ellipse, while the major axis aligns with the cavity mode's transverse direction. A slit is used to limit the atomic beam to cavity mode's central region, achieving a small Guoy phase difference between the pump beam and the cavity mode for sufficient cavity-pump phase matching. The pump beam optics and the prisms as a whole are mounted on a nanometer-precision 5-axis aligner to achieve parallelism with respect to the cavity mode. In this manner, our pump-cavity system can be incorporated into the existing setup of a high-speed, high-density atomic ion beam to induce superradiance and measure the effect of enhanced fluctuations near an EP.

3. Summary

EP's can be achieved in a Fabry-Perot cavity by incorporating a pair of waveplates and a pair of Brewster window inside and by adjusting them independently. We have designed and fabricated an FP-type cavity-pump assembly based on this idea. We will first investigate EP's in our pump-cavity assembly and then integrate it into a high-speed high-density ion beam apparatus to study the interaction between the EP mode and the atoms, inducing superradiance at the EP mode. We will investigate how the properties of superradiance change around the EP, which would enhance our understanding on the nature of fluctuations at the EP. **References**

- [1] J. Kim, et al, "Practical lineshape of a laser operating near an exceptional point", *Sci. Rep.* 11, 6164 (2021).
- [2] M. Gross and S. Haroche, "Superradiance: An essay on the theory of collective spontaneous emission", *Phys. Rep.* **93**, 301-396 (1982).
- [3] J. Kim et al., "Coherent single-atom superradiance", *Science* 359, 662 (2018).
- [4] J. F. Bisson, "Single-mode lasers using parity-time-symmetric polarization eigenstates", *Phys. Rev. A* **102**, 043522 (2020).
- [5] Wonshik Choi et al., "Observation of sub-Poisson photon statistics in the cavity-QED microlaser", *Phys. Rev. Lett.* **96**, 093603 (2006); Hyun-Gue Hong et al., "Spectrum of the Cavity-QED Microlaser: Strong Coupling Effects in the Frequency Pulling at Off Resonance", *Phys. Rev. Lett.* **109**, 243601 (2012).

Newton's rings interferometry for absolute distance calibration

Josh T. Christensen^{1,2,*}, *Farhan Azeem*^{1,2}, *Luke S. Trainor*^{1,2}, *Dmitry V. Strekalov*^{1,2} and *Harald G. L. Schwefel*^{1,2}

¹ Department of Physics, University of Otago, 730 Cumberland Street, Dunedin, New Zealand

² The Dodd-Walls Centre for Photonic and Quantum Technologies, New Zealand

* chrjo748@student.otago.ac.nz

Abstract: An absolute distance calibration between a prism and a whispering gallery mode resonator was achieved via Newton's rings interferometry, this enables detailed studies of mode profiles as well as a useful technique for beam alignment. © 2024 The Author(s)

1. Introduction

We present an application of Newton's rings used to measure the distance between a coupling prism and a whispering gallery mode resonator (WGMR) [1]. Three narrowband colour channels were used to illuminate these rings, which provided an absolute distance scale without the need for the resonator and coupling prism to come into contact. We demonstrate this method to be effective at measuring coupler separation distances to sub-nanometer precision, that further allow us to study the profile of modes coupled to the WGMR. Furthermore, this method is shown to provide an excellent beam alignment technique for coupling WGMR and prisms.

We follow up from our previous work [2] to demonstrate contact-free determination of the absolute distance between a WGMR and a prism by photographing the Newton's rings with illumination from an RGB diode, as seen in Figure 1. The captured image is decomposed into its R, G and B colour channels, Newton's rings phases of each channel are extracted and the differences between the respective colour channels' phases are studied to provide an absolute distance scale.

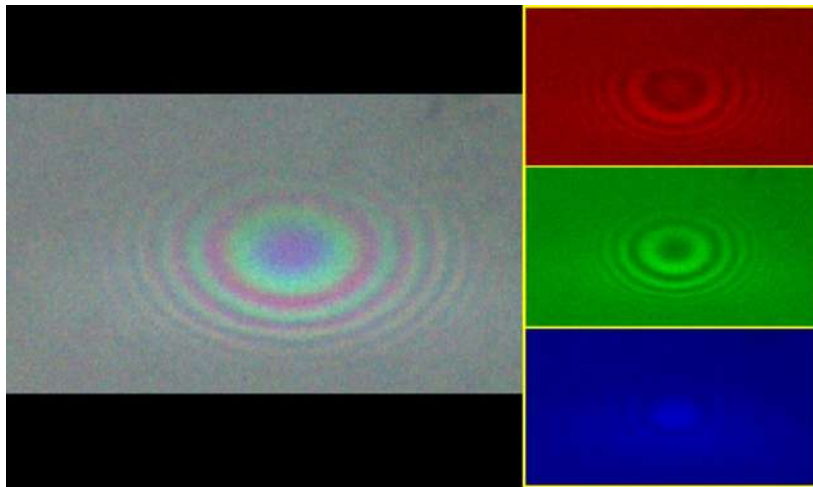


Fig. 1. Newton's rings are observed at the interface between a coupling prism and WGMR when illuminated by an RGB diode. The R, G, and B colour channels are then digitally extracted, shown as the right insets, and the respective phase of the Newton's rings are used to determine the absolute distance between coupler and resonator.

This work aims to further investigations into the mode profiles of whispering gallery modes that require accurate distance measurements, as well as to provide a method of beam alignment in prism-WGMR systems.

References

- [1] Luke S. Trainor, Florian Sedlmeir, Christian Peuntinger, and Harald G.L. Schwefel, "Selective Coupling Enhances Harmonic Generation of Whispering-Gallery Modes", *Phys. Rev. Applied* 9, 024007 (2018).
- [2] Josh T. Christensen, Farhan Azeem, Luke S. Trainor, Dmitry V. Strekalov, and Harald G. L. Schwefel, "Distance calibration via Newton's rings in yttrium lithium fluoride whispering gallery mode resonators," *Opt. Lett.* 47, 6053-6056 (2022).

Birefringence EP in a high-finesse Fabry-Perot cavity

Juman Kim¹, Jisung Seo¹, and Kyungwon An^{1,*}

¹ Department of Physics and Astronomy, Seoul National University, Seoul 08826, Korea.

* kwan@phya.snu.ac.kr

Abstract: We explore the birefringence exceptional points (EP's) in a high-finesse Fabry-Perot cavity arising from the interaction between two linearly polarized modes due to the intrinsic birefringence in the dielectric coating of the supermirrors.

1. Introduction

Supermirrors, widely used in optical gyroscopes, ring-down spectroscopy and cavity quantum electrodynamics experiments, possess intrinsic birefringence and dichroism due to anisotropy arising from the polishing and coating processes or from non-uniform stress inevitably introduced during the mounting process. For a Fabry-Perot cavity composed of such supermirrors, interaction can occur between two linearly polarized modes that would otherwise be orthogonal in an isotropic case. This interaction can be modeled by calculating the Jones matrix of the Fabry-Perot resonator, taking into account the birefringence and dichroism of the mirrors. The conditions for birefringence EP's are explored by determining the condition for coalescence of both the eigenvalues and eigenmodes of the Jones matrix. Furthermore, we measure the birefringence splitting by observing ringdown beating and aim to experimentally approach these EP's by controlling the birefringence and the polarization dependent loss of the supermirrors using a PZT and a knife edge.

2. Theory and results

2.1 Jones matrix of a Fabry-Perot cavity with birefringent mirrors and its EP conditions

A supermirror with a phase retardance of ϵ along two principal axes and a loss difference of μ along other orthogonal directions can be modeled as having a waveplate F and a Brewster window G in front of an ideal mirror. As seen from Fig. 1(a), assume that the fast axis of F_1 (F_2) and the direction of minimum loss of G_1 (G_2) are at angles α_1 (α_2) and β_1 (β_2) with respect to the x-axis, whose phase retardance and loss difference are ϵ_1 (ϵ_2) and μ_1 (μ_2) for mirror 1 (2), respectively. The Jones matrix R describing the reflection of the supermirror is given as follows in the first order approximation ($\epsilon_i, \mu_i \ll 1$) [1],

$$F_i = \begin{pmatrix} 1 + \frac{i\epsilon_i}{2} \cos(2\alpha_i) & \frac{i\epsilon_i}{2} \sin(2\alpha_i) \\ \frac{i\epsilon_i}{2} \sin(2\alpha_i) & 1 - \frac{i\epsilon_i}{2} \cos(2\alpha_i) \end{pmatrix}, \quad G_i = \begin{pmatrix} 1 + \frac{\mu_i}{2} \cos(2\beta_i) & \frac{\mu_i}{2} \sin(2\beta_i) \\ \frac{\mu_i}{2} \sin(2\beta_i) & 1 - \frac{\mu_i}{2} \cos(2\beta_i) \end{pmatrix},$$

$$R_i = r_i F_i G_i^2 F_i$$

where r_i is the reflection coefficient of mirror i ($= 1, 2$). After N round trips inside the cavity, as seen from Fig. 1(b), the Jones matrix of a Fabry-Perot cavity composed of two mirrors with reflection matrices R_1 and R_2 can be modeled as $T_2 \sum (R_1 R_2 e^{-2ikL})^N T_1$, where T_1 and T_2 are the transmission matrices of the coatings and substrates of the two mirrors, k is the wave number, and L is the cavity length. In a super cavity, the effect of T_1 and T_2 is negligible compared to the influence of the summation term because $N \sim 10^6$. Thus, the Jones matrix of the cavity approximately shares the common eigenstates as those of $R_1 R_2$, which is

$$R_1 R_2 = r_1 r_2 \begin{pmatrix} 1 + \mu \cos 2\beta + i\epsilon \cos 2\alpha & \mu \sin 2\beta + i\epsilon \sin 2\alpha \\ \mu \sin 2\beta + i\epsilon \sin 2\alpha & 1 - \mu \cos 2\beta - i\epsilon \cos 2\alpha \end{pmatrix},$$

where $\mu \cos 2\beta \equiv \mu_1 \cos 2\beta_1 + \mu_2 \cos 2\beta_2$ and $\epsilon \cos 2\alpha \equiv \epsilon_1 \cos 2\alpha_1 + \epsilon_2 \cos 2\alpha_2$. In other words, the Jones matrix of the Fabry-Perot cavity can be effectively considered as a combination of a single waveplate with the fast axis at an angle of α with respect to the x-axis and a Brewster window with minimum loss at an angle of β with respect to the x-axis, whose phase retardance is 2ϵ and loss difference is 2μ , respectively.

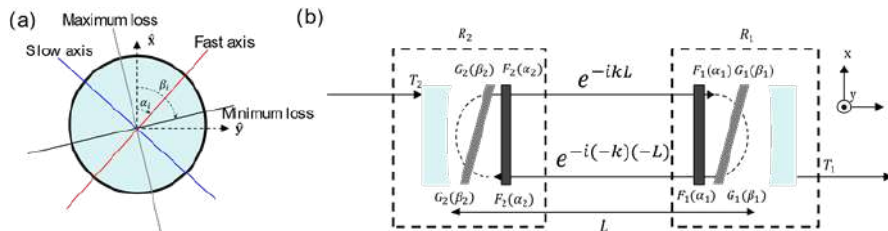


Fig. 1. Modeling of a supermirror and a Fabry-Perot cavity with birefringence and dichroism.

The eigenvalues λ_{\pm} of the $R_1 R_2$ are $\lambda_{\pm} = r_1 r_2 \left[1 \pm \sqrt{\mu^2 - \epsilon^2 + 2i\mu\epsilon \cos 2(\alpha - \beta)} \right]$. Thus, EPs appear under the

following condition:

$$\alpha = \beta + \frac{\pi}{4}(2m + 1), \quad \mu = \epsilon \quad (m \text{ is an integer}).$$

Individual mirrors can exhibit various combinations of parameters that satisfy the above condition. By independently adjusting ϵ_i , μ_i , α_i , and β_i of each mirror, it is theoretically possible to satisfy this condition.

2.2 Measurement of birefringence splitting using ringdown beating

Birefringence splitting ω_b smaller than the cavity linewidth can be measured using cavity ringdown spectroscopy. As shown in Fig. 2(a), by injecting circularly polarized light into the cavity, two eigenpolarization modes with slightly different frequencies can be excited simultaneously with a $\pi/2$ phase difference. Using an acousto-optic modulator (AOM) to switch off the light and create a ringdown signal, and then projecting it onto an analyzer, the ringdown signal follows the non-exponential decay described below, [2].

$$I(t) = e^{-t/\tau} [1 \pm \sin 2(\theta - \alpha) \sin(\omega_b t)] \approx e^{-t/\tau_{\text{eff}}} \quad (0.1)$$

In the above equation, ω_b is assumed to be sufficiently smaller than the cavity linewidth, leading to $\omega_b t \ll 1$. By

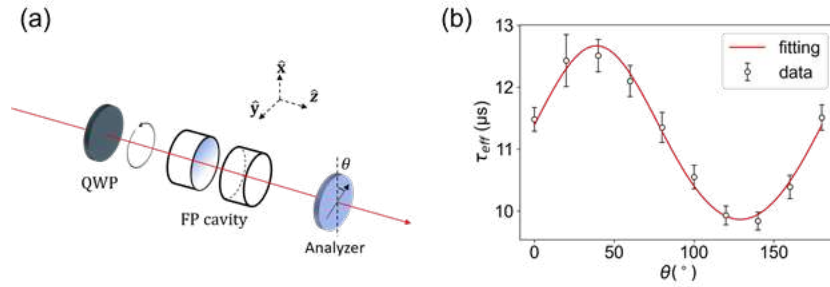


Fig. 2. Experimental scheme and the observed variation of τ_{eff} with respect to the analyzer angle.

measuring τ_{eff} as a function of the angle θ of the analyzer, ω_b and α can be obtained as fitting parameters. In Fig. 2(b), the cavity linewidth is 13 kHz, and $\omega_b/2\pi$ is measured to be 1.7(1) kHz and $\alpha = -6(1)^\circ$. We can independently adjust ϵ_1 and ϵ_2 for each mirror or modify the angles between $\alpha_{(1(2))}$ and $\beta_{(1(2))}$ by applying stress using PZT. Additionally, we can control μ_1 and μ_2 using a knife edge. By rotating the mirrors to change the angles between α_1 (β_1) and α_2 (β_2), we anticipate being able to explore the topology near the birefringence EP.

3. Summary

We studied the conditions of EP's in the non-Hermitian Jones matrix of a Fabry-Perot cavity with birefringence and dichroism in the supermirrors. By observing cavity ringdown beating and adjusting parameters using a PZT and a knife edge, we aim to observe the topology near the birefringence EP of a high-finesse Fabry-Perot cavity.

References

- [1] I. H. Huang et al., "Effects of linear birefringence and polarization-dependent loss of supermirrors in cavity ring-down spectroscopy," *Applied Optics* **47**, 3817 (2008).
- [2] A. J. Fleisher et al., "Precision interferometric measurements of mirror birefringence in high-finesse optical resonators", *Phys. Rev. A* **93**, 013833 (2016)

Spectrum of a superradiant laser with injected atomic coherence

*Junseo Ha*¹, *Seunghoon Oh*¹, *Jinuk Kim*², *Daeho Yang*³, and *Kyungwon An*^{1,*}

¹ Department of Physics and Astronomy, Seoul National University, Seoul 08826, Korea

² Quantum Technology Institute, Korea Research Institute of Standards and Science, Daejeon 34113, Korea

³ Department of Physics, Gachon University, Seongnam-si 13120, Korea

* kwan@phya.snu.ac.kr

Abstract: We measured the spectrum of a steady state superradiant laser with injected coherence using photon-counting based spectroscopy. The superradiant laser frequency matched the pump laser frequency, and its linewidth depended on the pump laser linewidth.

1. Introduction

Superradiance, first proposed by Dicke in 1953, refers to the phenomenon where correlated emitters collectively interact with light, resulting in enhanced radiation [1]. This collective emission happens at a rate proportional to the square of the number of emitters, significantly surpassing the rate of individual atomic emissions [2]. The key factor enabling superradiance is quantum coherence among the atoms.

In our experiments, an ¹³⁸Ba atomic beam passes through a nano-hole array and a pump laser before entering a high-Q cavity. The atomic state is modeled as a two-level system, with a transition wavelength of $\lambda = 791$ nm between the ¹S₀ and ³P₁ states, resonant with the cavity. The nano-hole array is fabricated using the focused ion beam (FIB) technique, with each hole measuring $0.35\lambda \times 0.25\lambda$ and spaced at 1λ intervals. This ensures that the atoms only pass through the anti-nodes of the cavity mode, thus the phases between the atom and the cavity are aligned. Our experiment was conducted in the strong coupling regime, with $(g, \gamma_a, \gamma_c)/2\pi = (334.25, 95)$ kHz, where g is the atom-cavity coupling constant, and γ_a (γ_c) is the atomic (cavity) decay linewidth (half-width). Thus, we achieve coherence by phase imprinting with a pump laser and precise positioning of the atoms using a nano-hole-array aperture, resulting in superradiance with a quadratic dependence on the number of atoms [3,4].

It is known that superradiant lasing via quantum coherence of atoms can have a narrower linewidth compared to that of conventional lasing [5]. We measured the spectrum of superradiant lasing by using the heterodyne-style photon-counting second-order correlation spectroscopy (PCSOCS) [6]. Specifically, the second-order correlation function of the heterodyne signal formed by the lasing output and a local oscillator was measured in order to obtain the autocorrelation function, and the spectrum was then obtained by performing a Fourier transform of it.

2. Results

2.1 The frequency of a superradiant laser with the pump-atom detuning

The atoms with controlled phase via a nano-hole array are prepared in a superposition state by a pump laser and then traverse a high-Q cavity. When the cavity and the pump laser are off-resonance, the atomic state can be written in the cavity rotating frame as [7]

$$|\Psi\rangle_{\text{atom}} = \prod_{i=1}^N \left[\sin(\theta/2) |g\rangle_i + \cos(\theta/2) e^{-i(\omega_p - \omega_c)t_i} |e\rangle_i \right],$$

where N is the number of atoms in the cavity, $g(e)$ represents the ground (excited) state of the atom, $\omega_p(\omega_c)$ is the (resonance) frequency of the pump laser (cavity), t_i is the arrival time of the i th atom at the cavity, and θ is the colatitude with respect to the polar axis in the Bloch sphere.

When the pump laser and the cavity are on resonance, the atomic state becomes an atomic coherent state, leading to the occurrence of superradiance. Therefore, the atomic dipole always oscillates at the atomic frequency, but due to the phase imprinted by the pump laser, enhanced radiation occurs at the pump frequency. Fig. 1a shows the results of the Quantum Trajectory Simulation (QTS) with varying pump-atom detuning $\Delta_{\text{extpa}} = \omega_p - \omega_a$ (where ω_a is the atomic frequency) when $\omega_p = \omega_c$. It can be observed that the frequency of a superradiant laser follows the pump laser. The observed spectrum of a superradiant laser is shown in Fig. 1b.

2.2 Spectral properties of a superradiant laser

Fig. 2a and 2b respectively show the superradiant laser linewidth and laser linewidth FWHM measured while varying the intracavity photon number (n) and the pump laser linewidth FWHM. Unlike the bad cavity superradiant laser, where the linewidth of the superradiant light depends on the intracavity photon number [5], we observe that the linewidth remains unchanged since atomic coherence is injected by the pump laser (Fig. 2a). When the pump laser linewidth was much narrower than the cavity linewidth, the superradiant laser linewidth was the same as the pump laser linewidth. But as the pump linewidth became larger than the cavity linewidth, the linewidth of superradiant

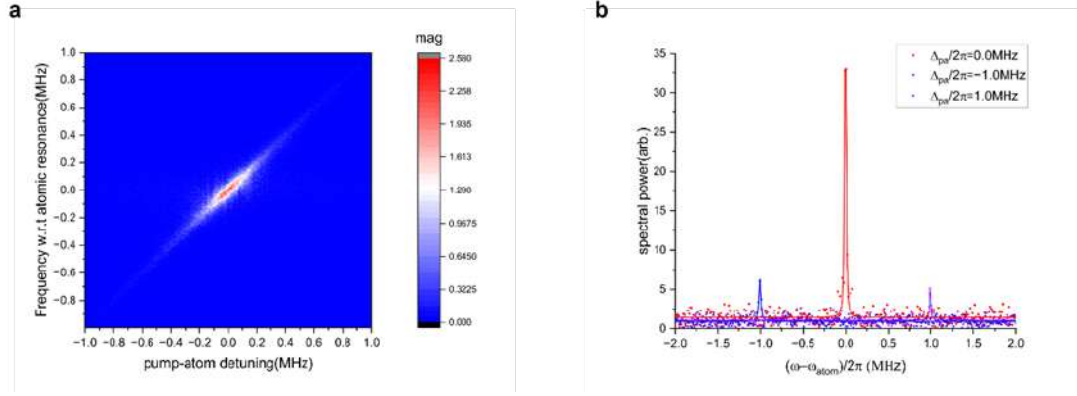


Fig. 1. Spectrum of a superradiant laser with varying pump-atom detuning. **a**, QTS results with $N_c = 20, (g, \gamma_c) 2\pi = (300, 95) \text{ kHz}, \tau = 0.1 \mu\text{s}, \omega_c = \omega_a$. Here τ is the transit time of the atoms, N_c is the number of atoms in the cavity during the cavity decay time. **b**, The measured spectrum with $\Delta_{pa} / 2\pi = 0, -1.0, +1.0 \text{ MHz}$. Symbols correspond to the data points, solid lines are the Lorentzian fitting curves.

lasing approached the cavity linewidth (Fig. 2b). This indicates that the role of the quantum coherence reservoir shifts from the atoms to the cavity photons as the pump laser linewidth increases.

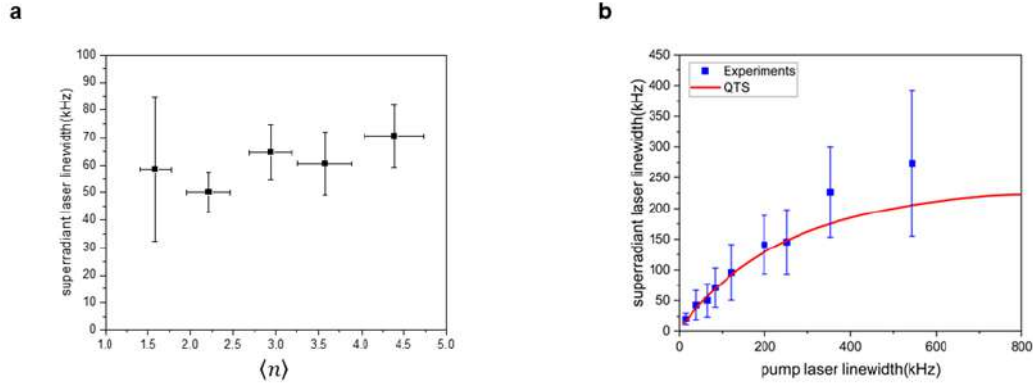


Fig. 2. The linewidth of the superradiant laser. **a**, The superradiant laser linewidth FWHM dependence on $\langle n \rangle$. Pump linewidth FWHM is 80 kHz. **b**, The superradiant laser linewidth FWHM dependence on the pump laser linewidth FWHM. The blue squares are data points from the experiments, the red solid line is the numerical solution by the QTS. In (a), (b), $\omega_a = \omega_p = \omega_c$, and error bars indicate the standard deviation from the fitting errors.

3. Summary

We measured the spectrum of a superradiant laser in a good-cavity limit. We confirmed that the frequency of the superradiant laser follows the frequency of the pump laser. We experimentally demonstrated that the linewidth of the superradiant laser depends on the linewidth of the pump laser rather than the number of atoms in the cavity. As the linewidth of the pump laser used for coherent pumping increases, the atoms lose coherence, and the role of the coherence reservoir shifts to the cavity photons.

References

- [1] Dicke, R. H., “Coherence in Spontaneous Radiation Processes,” *Physical Review* **93**, 99-110 (1954).
- [2] Gross, M. and Haroche, S., “Superradiance: An essay on the theory of collective spontaneous emission,” *Physics Reports* **93**, 301-396 (1982).
- [3] Kim, J., Yang, D., Oh, S. and An, K., “Coherent single-atom superradiance,” *Science* **359**, 662-666 (2018).
- [4] Yang, D. et al., “Realization of superabsorption by time reversal of superradiance,” *Nature Photonics* **15**, 272-276 (2021).
- [5] Bohnet, Justin G. et al., “A steady-state superradiant laser with less than one intracavity photon,” *Nature* **484**, 78-81 (2012).
- [6] Hong, H. et al., “Spectral line-shape measurement of an extremely weak amplitude-fluctuating light source by photon-counting-based second-order correlation spectroscopy,” *Optics Letters* **31**, 3182-3184 (2006).
- [7] Kim, Jinuk. et al., “A photonic quantum engine driven by superradiance,” *Nature Photonics* **16**, 707-711 (2022).

High-resolution microwave frequency identification via a hybrid microbottle cavity

Kang Xu^{1,#}, Wenyu Wang^{1,#}, Hao Wen¹, Lei Shi^{1,2,*}, and Xinliang Zhang^{1,2,3}

¹ Wuhan National Laboratory for Optoelectronics, Huazhong University of Science and Technology, Wuhan 430074, China

² Optics Valley Laboratory, Wuhan 430074, China

³ Xidian University, Xi'an 710126, China

Kang Xu and Wenyu Wang have contributed equally to this work

* lshi@hust.edu.cn

Abstract: We experimentally demonstrate a scheme for frequency identification of microwave signals via photothermal effect in a hybrid microbottle cavity. This system is capable of measuring microwave signals at frequency up to 25 GHz with a high resolution.

1. Introduction

Photonic-assisted microwave frequency identification has been extensively explored and widely applied for civil and defense applications [1]. Frequency-to-time mapping (FTTM) is one of the most commonly used measurement methods in which microwave frequencies are linearly mapped to the time delays of the spectrum. To implement a FTTM system, a narrowband and tunable optical filter is usually required, which determines the frequency resolution and range of the measurement system [2]. In this work, we demonstrate a microwave frequency identification, leveraging an ultrahigh Q microbottle cavity as an optical filter. Besides, iron oxide nanoparticles with excellent photothermal performance are coated on the end surface of the microcavity and enable a frequency sweep span of over 30 GHz by feeding the control light along the axial direction. Our work achieves a frequency measurement range of 10–25 GHz with a root-mean-squares error of 206.8 MHz and has great potential for application in future advanced microwave photonic processor.

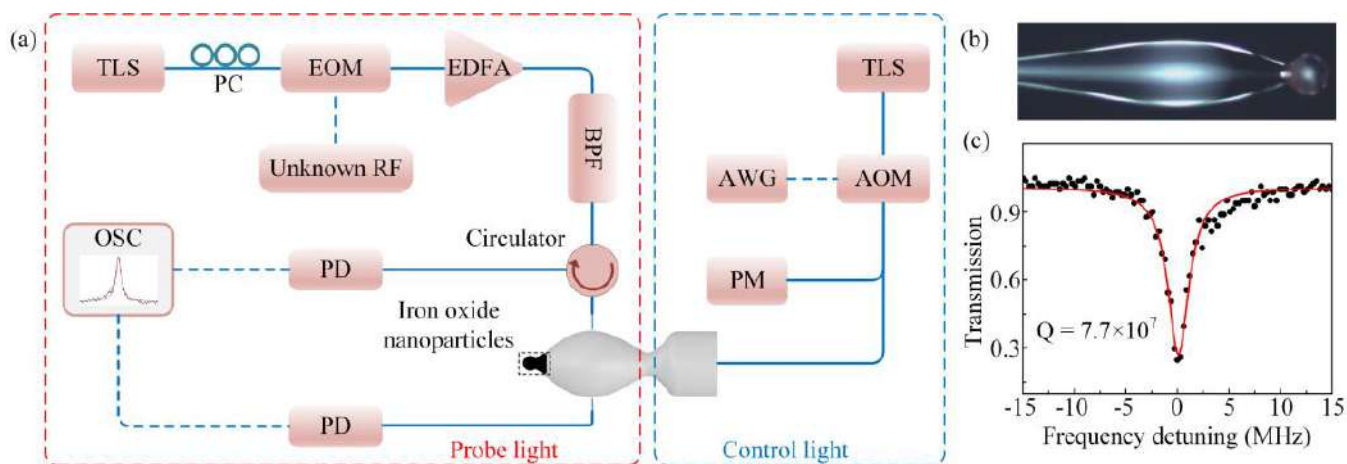


Fig. 1. Schematic of the proposed microwave frequency identification system. TLS: tunable laser source; PC: polarization controller; EOM: electro-optical modulator; BP: band-pass filter; PD: photoelectric detector; AWG: arbitrary waveform generator; AOM: acoustic-optical modulator; PM: optical power meter. (b) Optical microscope image of the hybrid microbottle cavity. (c) Measured Q factor of the microcavity in the 1550 nm band.

2. Experimental setup and results

The experimental setup is shown in Fig. 1(a), which includes two parts: the probe light branch and the control light branch. For the probe light branch, an unknown microwave signal is modulated on an optical carrier using an electro-optical modulator. The modulated optical signal is amplified by a commercial erbium-doped fiber amplifier (EDFA), and a band-pass filter is used to remove the optical carrier, negative primary sideband, and the noise of the EDFA. Then, the positive first-order sideband optical signal is coupled into the ultrahigh- Q microbottle cavity by a microfiber. In order to avoid dense modes of the microbottle cavity, we use the backscattering mode, which usually has a high Q factor. For the control light branch, the laser modulated by a sawtooth signal with a period of 500 ms is injected into the microcavity in the axial direction, resulting in a thermal tuning of the resonant frequency. Due to the high photothermal conversion efficiency of iron oxide nanoparticles, the dynamic tuning range of the microcavity

mode resonant frequency can be set as 30 GHz by feeding appropriate power of control light. When the resonant mode sweeps through the probe light signal, a resonant peak is generated. The frequency f_{RF} of the microwave signal to be measured can be expressed as:

$$f_{RF} = \frac{B}{T} \times \Delta T$$

where B and T are the frequency sweep span of the resonant mode and the period of the driving signal applied to control Light, and Δt is the measured time delay of the optical pulse. The optical microscope image of the microbottle cavity is shown in Fig. 1(b), and the Q factor is 7.7×10^7 .

The experiment result is shown in Fig. 2. We first measure the thermal tuning performance of the microcavity by varying the control optical power. The corresponding resonant frequency shift has a linear relation with the control optical power as expected, which guarantees microwave frequency to be mapped linearly to time, shown in Fig. 2(a). We verify the system performance by measuring different frequency microwave signals from 10 GHz to 25 GHz, with a step of 1 GHz. Fig. 2(b) shows the measured result and error for each input microwave signal, illustrating that the system has the ability for broadband microwave frequency identification with a root-mean-squares error of approximately 206.8 MHz.

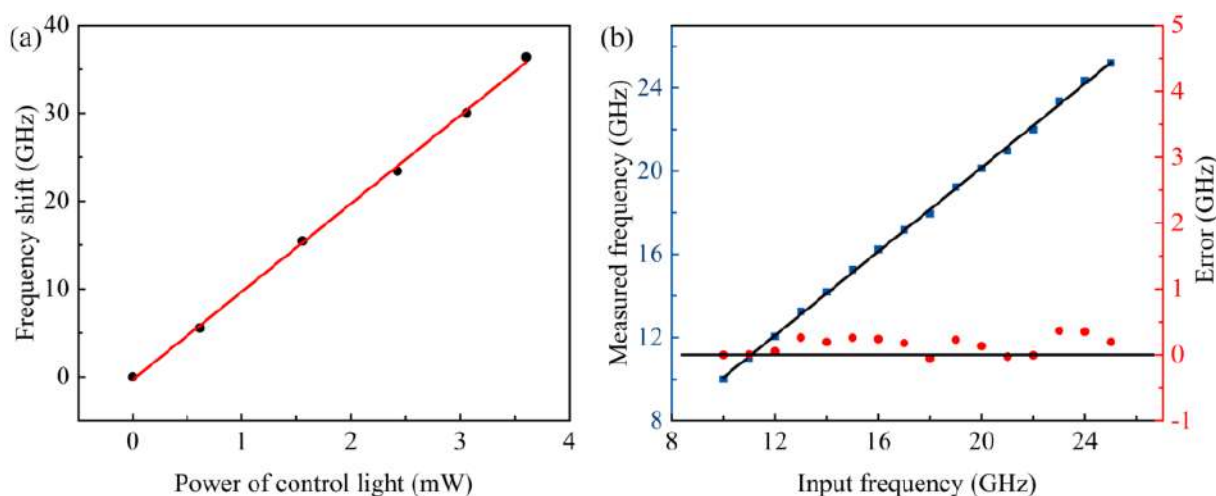


Fig. 2. (a) The resonant frequency shift of the microcavity varies with the control optical power. (b) Measurement result and error for different frequency input microwave signals.

3. Summary

High-resolution microwave frequency identification based on an ultrahigh- Q microbottle cavity is demonstrated. The photothermal effect is used to realize linear tuning of the resonance mode frequency, enabling the mapping of microwave frequency to time. The measurement system has a root-mean-square error of 206.8 MHz within the frequency range of 10 25 GHz.

References

- [1] D. Marpaung, J. Yao, J. Capmany, "Integrated microwave photonics," *Nature Photonics* 13, 80-90 (2019).
- [2] W. Zhang, H. Liu, Y. Cheng et al., "High-resolution photonic-assisted microwave frequency identification based on an ultrahigh- Q hybrid optical filter," *Optics Express* 31, 42651-42666 (2023).

Nonlinear Laser Dynamics of an Asymmetric Optical Microcavity

Maika Matogawa^{1,*}, *Yoshikazu Kuribayashi*¹, *Yuichiro Suzuki*¹, *Mengyu You*¹, *Satoshi Sunada*², *Susumu Shinohara*³, *Takahisa Harayama*¹

¹ Department of Pure & Applied Physics, Waseda University, Tokyo, Japan

² Division of Mechanical Science and Engineering, Kanazawa University, Ishikawa, Japan

³ Department of Production Systems Engineering and Sciences, Komatsu University, Ishikawa, Japan

* maikamatogawa@fuji.waseda.jp

Abstract: We studied the locking of two nearly degenerate modes in an asymmetric optical microcavity. We extend the semiclassical Lamb laser theory to describe the locking process, thereby revealing a crucial effect of an exceptional point.

1. Introduction

Non-Hermitian systems, where the interactions with the environment are not negligible, have gathered much attention recently, stemming from the feasibility of open systems in real experiments. Among such systems, two-dimensional microcavity lasers have been subjected to extensive studies of fundamental physics such as wave chaos and laser dynamics. Nonlinearities due to the lasing medium as well as cavity geometry have been investigated in terms of the locking of two or more resonance modes, often with symmetric cavities.

In addition, open cavities with no geometrical symmetries display highly non-orthogonal and nearly degenerate resonance pairs, known as chiral pairs, comprising imbalanced clockwise (CW) and counterclockwise (CCW) propagating wave components. Such asymmetric optical microcavities have much potential for the theoretical understanding of laser dynamics unique to these cavities and for practical applications such as highly sensitive gyrosensors.

This research investigates the laser dynamics of an Asymmetric Limaçon Cavity (ALC) expressed in polar form as $r = r_0 [1 + \epsilon_1 \cos(\theta) + \epsilon_2 \cos(2\theta + \delta)]$, with parameters $r_0 = 1$, $\epsilon_1 = 0.1$, $\epsilon_2 = 0.075$, and $\delta = 0.618\pi$. The cavity has no geometrical symmetries; thus, the resonances appear as chiral pairs. We particularly focused on the chiral pair for which the intensities of wave functions are localized along the triangular orbit, as shown in Fig. 1.

Furthermore, to qualitatively show the amount of CW and CCW components within the wave functions of the chiral pair, they were expanded in terms of the Bessel function to represent angular momentum distributions, as shown in Fig. 2. As can be seen, the amount of CCW components is dominant over CW components. This imbalance can further be quantified as chirality χ , ranging from 0 to 1; when $\chi = 0$, the amounts of CW and CCW components are equal, whereas when $\chi = 1$, only CCW components exist in the mode of interest.

The research aims to theoretically explain the global laser dynamics represented by the locking of those chiral pair modes and the dependence of the laser dynamics in an asymmetric cavity on the chirality and its relation to the exceptional points (EPs) in a space of two independent cavity parameters at which both complex eigenvalues and eigenstates coalesce.

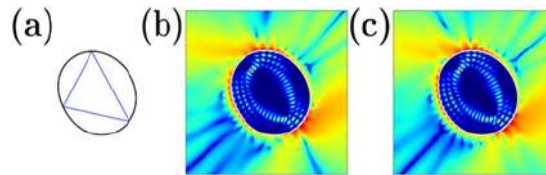


Fig. 1. Stable 3-periodic orbit inside the ALC (a) and the wave function patterns of the chiral pair (b)(c). [4]

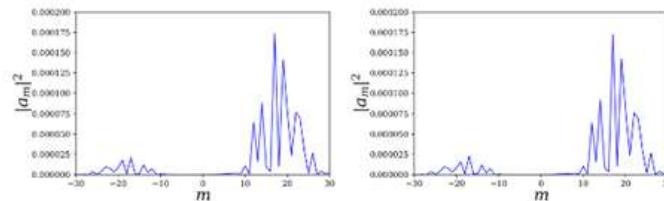


Fig. 2. The angular momentum distributions of the chiral pair with wave numbers of $k = 10.5825 - 0.0029i$ (left) and $k = 10.5826 - 0.0028i$ (right), respectively. [4]

2. Laser Numerical Simulations

Considering the nonlinear effects of the geometrical shape and the laser medium of the cavity, Maxwell-Bloch (MB) equations were solved by the Finite-Difference Time-Domain (FDTD) method. As shown in Fig.3(a) and (c), the state stabilizes to either CW or CCW stationary lasing state, depending on the initial conditions. Superpositions of the chiral pair using two different phase shifts reproduced the results of the lasing simulations as shown in Fig.3(b) and (d). Therefore, the lasing states can be described by the locking phenomenon of the chiral pair.

In addition, the laser simulations were performed under the same conditions as above except for pumping powers. Despite the dominance of CCW propagating wave components in the chiral pair mode, the intensities of CW and CCW stationary lasing states were almost the same for all the different values of pumping powers.

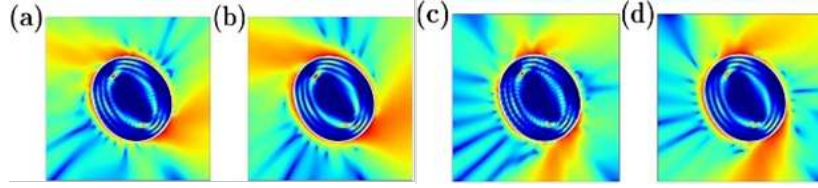


Fig. 3. A time-averaged intensity pattern in the stationary lasing regime (a)(c) and wave function patterns of the chiral pair superposed with zero (b) and π (d) phase shifts. [4]

3. Semiclassical Lamb Laser Theory

To theoretically explain the numerically observed laser dynamics, the semiclassical Lamb laser theory was introduced. The resulting laser dynamics derived by expressing the Maxwell-Bloch (MB) equations in terms of superpositions of chiral pair modes is reduced to differential equations of three variables: the electric/magnetic fields of chiral pairs, E_1 and E_2 , and the phase difference between them Φ .

Moreover, some dynamical quantities were derived analytically from the reduced equations. These quantities include the fixed points corresponding to counterclockwise (CCW) and clockwise (CW) lasing states, the basin boundary surface (BBS), which separates the basins into CW and CCW states, and the volume of the BBS.

One important implication of the reduced equations is that the laser dynamics depends on chirality. As shown in Fig. 4, the volume of the BBS of the CW lasing state decreases and eventually vanishes as χ approaches 1, corresponding to the exceptional point (EP), where only CCW components are present. This volume dependence on chirality was tested numerically and compared with analytical results.

Furthermore, the lasing intensity was analytically expressed in terms of lasing parameters and is independent of chirality. This result can be physically interpreted as the inferiority of the CW component in each chiral pair being compensated by the large growth of amplitudes E_1 and E_2 of the CW lasing mode during the mode competition.

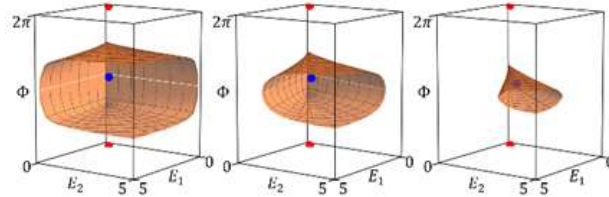


Fig. 4. Dependence of the BBS (orange) volume on χ . $\chi = 0.1, 0.5, 0.9$ from left to right. The fixed points corresponding to clockwise (CW) and counterclockwise (CCW) lasing states are indicated as blue and red dots, respectively.

4. Search for an Exceptional Point

With the aim of executing the lasing simulation and confirming the laser dynamics at this point, the search for an exceptional point was performed. Two independent cavity parameters of the Asymmetric Limaçon Cavity (ALC) were varied while the wave numbers of the chiral pair were calculated using the Boundary Element Method for each cavity shape. As a result of the search, when ϵ_1 and δ were varied, the real and imaginary parts of the wave numbers of the chiral pair displayed topological structures analogous to the Riemann surface of \sqrt{z} .

Furthermore, the chirality of each point in the parameter space was calculated. The point in the parameter space of ϵ_1 and δ of maximum chirality approximately corresponded to the values of ϵ_1 and δ at which the real and imaginary parts of the wave numbers of the chiral pair were almost degenerate. The angular momentum distributions at maximum chirality displayed only the counterclockwise (CCW) propagating wave component.

Therefore, both the eigenvalues and eigenvectors coalesced at this special point, indicating that this point is indeed an exceptional point. The maximum chirality reached as a result of the EP search with finer resolution of parameters was 0.99974016 at $(\epsilon_1, \delta; \epsilon_2) = (0.1009, 1.577; 0.075)$.

5. Summary and Future Research

The laser dynamics was theoretically described by locking of the chiral pair, revealing the dependence of its global structure on the chirality. A second-order EP was found when varying two independent cavity parameters, and its accuracy and precision are expected to improve in future research so as to be used to test the extreme laser dynamics at the EP.

References

- [1] T. Harayama and S. Shinohara, "Two-dimensional microcavity laser," *Laser & Photonics Reviews*, **5**(2): 247-271 (2011).
- [2] J. Wiersig et al., "Nonorthogonal pairs of copropagating optical modes in deformed microdisk cavities," *Phys. Rev. A*, **84**, 023845 (2011).
- [3] S. Sunada, "Enhanced response of non-Hermitian photonic systems near exceptional points," *Phys. Rev. A*, **97**, (2018).
- [4] M. Matogawa et al., "Nonlinear laser dynamics of a non-orthogonal chiral pair," *Appl. Phys. Lett.*, **123** (23): 231104 (2023).

Surface-acoustic-wave-assisted vibrational spectroscopy using an integrated microresonator

Quan-Xin Luo¹, Jia-Wei Meng¹, Zhuojun Liu¹, Qihuang Gong¹, Shui-Jing Tang¹, and Yun-Feng Xiao^{1,*}

¹ State Key Laboratory for Mesoscopic Physics and Frontiers Science Center for Nano-optoelectronics, School of Physics, Peking University, Beijing 100871, China

*yfxiao@pku.edu.cn

Abstract: We research the coupling between surface acoustic waves (SAWs) and microcavities based on-chip silicon nitride microresonator systems. This approach ensures the microcavity mode is unaffected by the sample and provides a larger sensing area. © 2024 The Author(s)

1. Introduction

Vibration of micro- and nanoparticle has always been an intriguing topic for researchers, encompassing various types of functional particles such as metallic particles, dielectric particles, magnetic particles, as well as biological particles like cells, bacteria, and viruses. Optical microresonators can tightly confine optical fields, significantly enhancing the interaction between light and matter. Researchers have utilized this property to detect particle vibrations, leading to a series of studies and advancements in this field [1–3]. Our recent work proposed a single-particle vibrational spectroscopy technique [4]. The natural vibrations of mesoscopic particles are stimulated photoacoustically by the absorption of a short laser pulse and acoustically coupled to high-Q optical resonances of the microresonator for real-time detection.

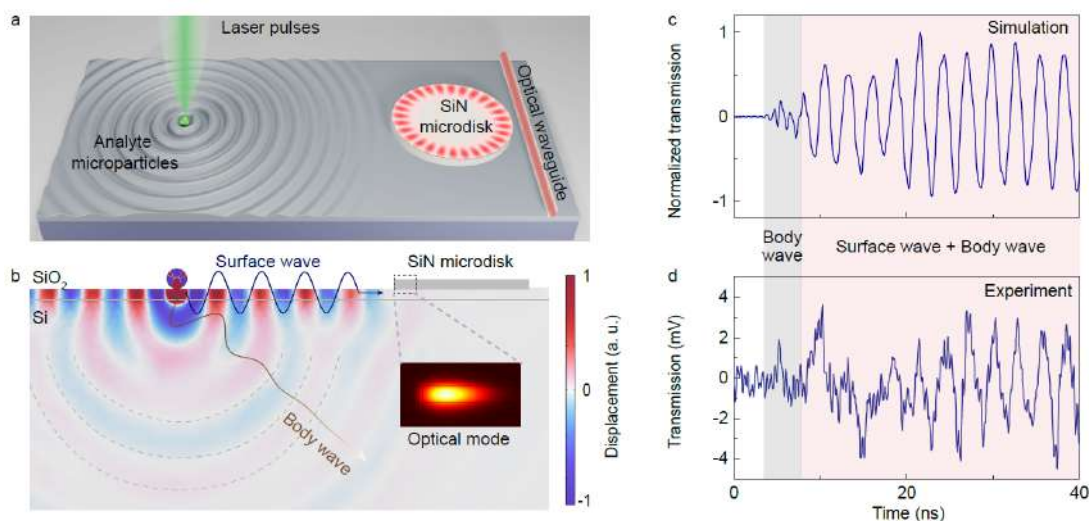


Fig. 1. (a) Natural vibrations of the particle are stimulated by a pulsed laser and generate propagation acoustic waves through the integrated optical micro-device subsequently, which couple to the whispering-gallery-mode of the micro-disk. (b) Longitudinal section view of the displacement field as acoustic waves transmit through the on-chip platform. The generated acoustic waves consist of surface waves (blue curve) and body waves (brown curve). (c) Simulation result of the acoustic signals as the particle is about $38\ \mu\text{m}$ away from the microcavity. (d) Measured acoustic signals in the time domain by monitoring the shifts of the optical transmission mode.

Here, we extend this vibrational technique to integrated microcavity systems, leveraging the characteristics of surface acoustic waves (SAWs) to achieve the far-field detection of particle vibrational spectra. We designed and fabricated an on-chip coupling system consisting of silicon nitride microcavities and waveguides, in which the quality factor (Q) of the whispering-gallery-mode (WGM) reaches 2×10^5 at the 780 nm wavelength band. The propagation properties of SAWs can be used to realize far-field detection of the natural vibrational spectra of particles. Compared with the near-field methods, this approach ensures that the microcavity mode remains unaffected by the analyte while also offering a larger sensing area.

The working principle of the SAW-assisted vibration detection is illustrated in Fig. 1(a). The particle is stimulated by a 532 nm pulsed laser (pulse width: 200 ps). The vibrations are transferred to acoustic waves propagating through the integrated micro structure. They alter the refractive index and the boundary of the microcavity, and

thereby modulate the frequency of the optical resonance. We calculate the displacements generated by acoustic waves as the particle is about $38\ \mu\text{m}$ away from the microcavity. Here, we assume that the particle vibrates in the breathing mode ($\nu_{(1,0)}$, the displacement of vibration contains only the radial component) with a specific vibrational pattern and frequency, and their driving amplitude decays exponentially over time. The signals are clearly divided into two parts as shown in Fig. 1(c): surface acoustic waves (SAWs) and bulk acoustic waves (BAWs). The velocity of BAWs is higher than that of SAWs.

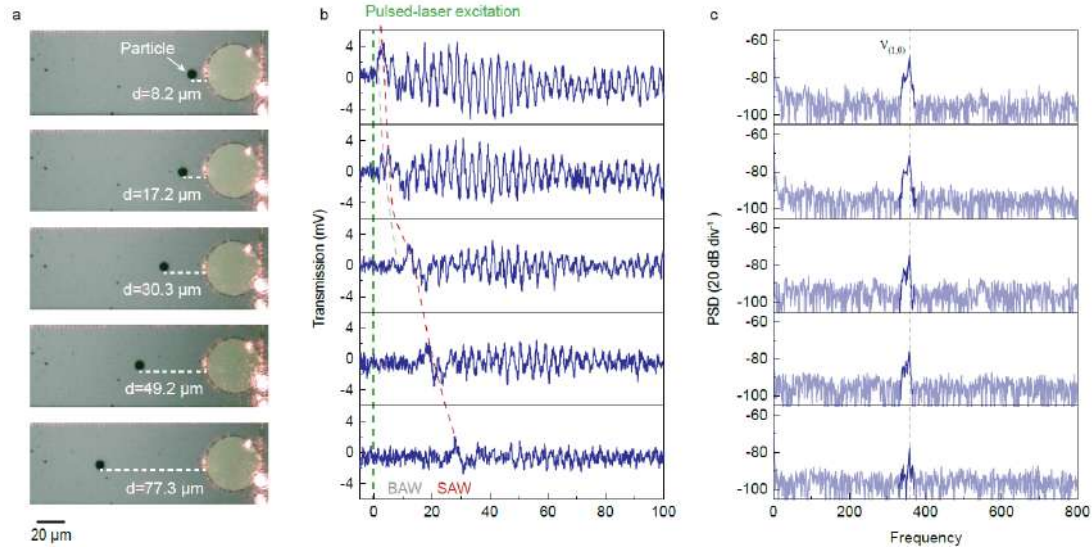


Fig. 2. (a) Microscope images of a $2.7\text{-}\mu\text{m}$ -radius PS particle at varying distances from the microdisk. (b) The temporal acoustic signals are detected by the transmitted power of the probe laser with the different distances between the particle and the microdisk, as illustrated in (a). The green dashed line marks the initial time as the laser pulse excites the particle. The grey and red dashed curves indicate the initial arriving peak signals of the BAW and the SAW, respectively. (c) The corresponding vibrational spectra derived from the signals in (b).

In our experiments, a tunable continuous laser ($780\ \text{nm}$ band) is coupled into the microdisk and is slightly detuned from the optical resonance. Real-time readout is achieved by monitoring the transmitted power modulated by acoustic waves. Varying the distance between the polystyrene (PS) particle and microcavity, mechanical vibrational signals carried by SAWs are measured experimentally (Fig. 2(b)). It is observed that the arrival time of the SAWs increases with distance, and the signal amplitude gradually decreases. Due to the significant attenuation of BAWs signals, they are obscured by system noise. The vibrational spectra are derived from the power spectral density (PSD) of the transmitted light. The signal-to-noise ratio of the breathing mode $\nu_{(1,0)}$ decreases as the distance increases.

In summary, we propose a SAW-assisted vibrational spectroscopy using an integrated microcavity. The SAWs carry the natural mechanical information of the particles, are detected by a silicon nitride microdisk. Through simulation and experimental studies, the propagation characteristics of SAWs are analyzed at various distances between the particle and the microcavity. This far-field detection method provides significant advantages in practical applications.

References

- [1] A. W. Barnard, M. Zhang, G. S. Wiederhecker, M. Lipson, and P. L. McEuen, Real-time vibrations of a carbon nanotube, *Nature* **566**(7742):89–93, 2019.
- [2] H. Chang and J. Zhang, Detecting nanoparticles by “listening”, *Frontiers of Physics* **18**(5):53602, 2023.
- [3] E. Gil-Santos, J. J. Ruz, O. Malvar, I. Favero, A. Lemaître, P. M. Kosaka, S. García-López, M. Calleja, and J. Tamayo, Optomechanical detection of vibration modes of a single bacterium, *Nature Nanotechnology* **15**(6):469–474, 2020.
- [4] S. J. Tang, M. Zhang, J. Sun, J. W. Meng, X. Xiong, Q. Gong, D. Jin, Q.-F. Yang, and Y. F. Xiao, Single-particle photoacoustic vibrational spectroscopy using optical microresonators, *Nature Photonics* **17**(11):951–956, 2023.

Precision Spectral and Spatial Optimisation of Whispering Gallery Modes in Microbubble Cavities

Ramgopal Madugani^{1,*}, Amal Jose¹, and Sile Nic Chormaic¹

¹ Okinawa Institute of Science and Technology Graduate University, Onna, Okinawa 904-0495, Japan

*ramgopal.madugani@oist.jp

Abstract: Hollow whispering gallery mode (WGM) devices, such as microbubbles, could enable spin (polarisation) and orbit interaction of light. We explore precision fabrication methods for microbubble-type hollow cavities to achieve WGM selection and their spectral and spatial isolation. Further, we aim to engineer the devices for directional emission-enhanced sensing. © 2024 The Author(s)

1. Introduction

Optical whispering gallery resonator (WGR) research has been a focus for photonics and sensing applications, due to the cavities' high Q-factors, small mode volumes, and on-chip integration possibilities [1–3]. The WGM microbubble resonator, being a special geometry with a hollow shell, offers several advantages, such as low cost of fabrication, pressure-based linear tuning of the optical modes, and *in situ* sensing with minimal environmental interference [3–5]. Furthermore, they also offer high Q-factors and low mode volumes, similar to microspheres.

The hollow shape of the microbubble could also offer a unique opportunity to observe optical spin-orbit coupling. The spin-orbit interaction of light is primarily studied in free-space optics, such as optical tweezers [6]. Very recently, spin-orbit coupling in a Fabry–Pérot microcavity has been observed [7], as polarization (spin)-resolved modes, that is, a fine structure, in close resemblance to atomic fine structure. There have been limited experimental investigations of this phenomenon in WGM-type cavities. For example, hollow-cone, three-dimensional (3D) geometry microcavities have been explored for spin-orbit coupling theoretically [8]. Experimentally, rolled-up and Möbius strip microcavities have been studied to date [9, 10]. In this work, we explore methods for the fabrication and characterisation of cone-like (i.e., axially varying diameter or effective refractive index) hollow microcavities as shown in Fig. 1 to achieve WGM optimisation and control. This may enable us to develop the next-generation of optomechanical sensors, such as accelerometers, or micro-nano particle sensors.

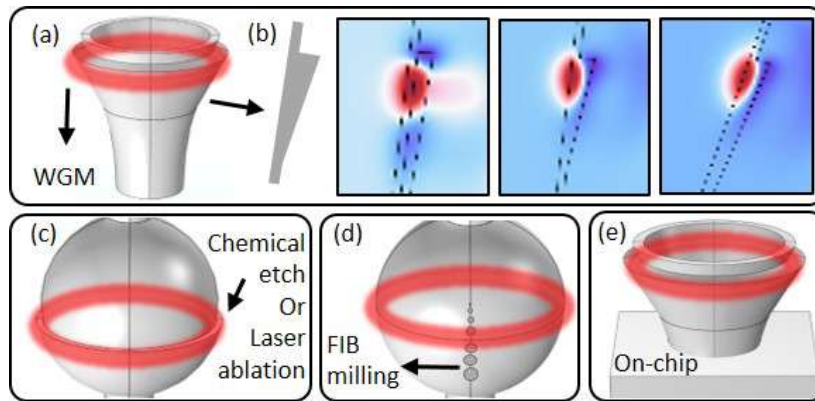


Fig. 1. Realising the spin-orbit coupling of light in hollow cone-like WGM microcavities. (a) Hollow cone-like WGM microcavity with (b) cross-section profile and mode redistribution comparison, for increased wall inclinations (or effective refractive index variation), from left to right. A cone-like profile in microbubble-like, thin wall hollow cavities by (c) HF chemical etching (or femtosecond laser ablation), (d) focussed ion beam (FIB) milling of a nano-hole pattern (to select the WGM), and (e) on-chip fabrication.

2. WGM optimisation by focussed ion beam milling

Here, we explore focussed ion beam (FIB) based processing [11] of the microbubble cavities prefabricated using a focussed CO₂ laser on tapered glass capillaries while pressurising with N₂ gas [4]. Due to the bottle shape, microbubble cavities possess a dense spectrum of WGMs with the same radial and azimuthal but different polar mode numbers (mode degeneracy lifting). To be used for sensing or trapping applications, mode isolation and optimisation may be required. As a first step, here we explored rectangular and circular shaped milling of microbubbles off-equator, as shown in Fig. 2, and observed significant mode filtering, when coupling light from a tunable 1550 nm laser to the cavity through a fibre taper. Furthermore, we milled around the equator to vary the wall thickness by writing nanolines and circles with dimensions smaller than 500 nm. Despite these modifications for spatial and spectral control, the device

sustained selected WGMs with up to 10^5 Q-factors. Further testing and fine-tuning this milling procedure may enable us to precisely control selected WGMs and induce the spin-orbit interaction.

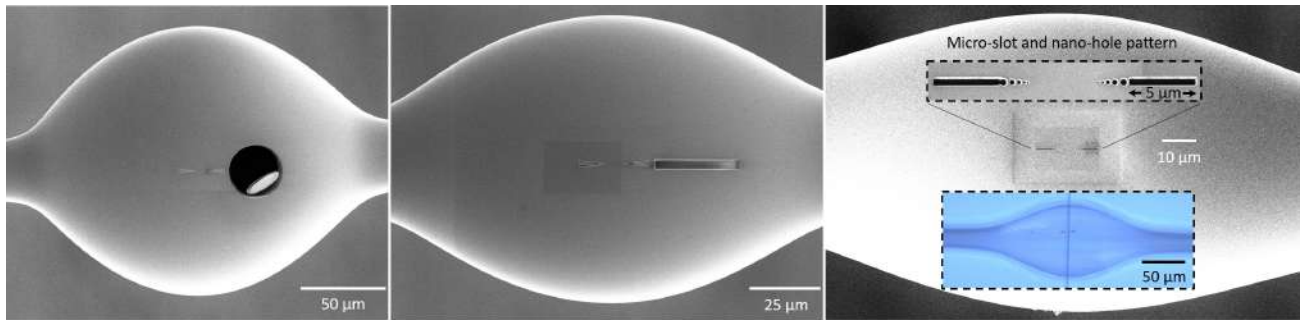


Fig. 2. FIB-based microbubble cavity modification for WGM filtering and control by off-equator circular shaped milling (left), rectangular milling (centre), and nanolines around the equator. A combination of rectangular microslot and nanocircle milling (right) with insets showing zoomed view and fibre taper coupling to the cavity to excite the WGMs

3. Conclusion

We demonstrated WGM spectral and spatial control using FIB milling on a microbubble cavity wall. Further refinement of this technique may enable us to control specific WGMs and provide spin-orbit interaction of light. The pressure-tuning ability of these devices may aid us in the near- and far-field observation of such an interaction. Furthermore, it is possible to interface the resonators with micro or nanoparticles (by filling them with liquid particle solution) to study spin-orbit-induced dynamics.

Acknowledgements

This research was supported by funding from JSPS Kakenhi (Grant 24K08290) Grant-in-Aid for Scientific Research C and by OIST Graduate University.

References

- [1] M. Aspelmeyer, T. J. Kippenberg, and F. Marquardt, "Cavity optomechanics," *Rev. Mod. Phys.* **86**, 1391 (2014).
- [2] X. Jiang, A. J. Qavi, S. H. Huang, and L. Yang, "Whispering-gallery sensors," *Matter* **3**, 371 (2020).
- [3] B. Bathish, R. Gad, F. Cheng, K. Karlsson, R. Madugani, M. Douvidzon, S. Nic Chormaic, and T. Carmon, "Absorption-induced transmission in plasma microphotonic," *Nat. Commun.* **14**, 4535 (2023).
- [4] R. Madugani, Y. Yang, V. H. Le, J. M. Ward, and S. Nic Chormaic, "Linear laser tuning using a pressure-sensitive microbubble resonator," *IEEE Photonics Technol. Lett.* **28**, 1134 (2016).
- [5] J. M. Ward, Y. Yang, F. Lei, X.-C. Yu, Y.-F. Xiao, and S. Nic Chormaic, "Nanoparticle sensing beyond evanescent field interaction with a quasi-droplet microcavity," *Optica* **5**, 674 (2018).
- [6] K. Y. Bliokh, F. J. Rodríguez-Fortuño, F. Nori, and A. V. Zayats, "Spin-orbit interactions of light," *Nat. Photonics* **9**, 796 (2015).
- [7] C. Koks, F. B. Baalbergen, and M. P. van Exter, "Observation of microcavity fine structure," *Phys. Rev. A* **105**, 063502 (2022).
- [8] J. Kreismann and M. Hentschel, "Spin-orbit interaction of light in three-dimensional microcavities," *Phys. Rev. A* **102**, 043524 (2020).
- [9] L. Ma, S. Li, V. M. Fomin, M. Hentschel, J. B. Götte, Y. Yin, M. Jorgensen, and O. G. Schmidt, "Spin-orbit coupling of light in asymmetric microcavities," *Nat. Commun.* **7**, 10983 (2016).
- [10] J. Wang, S. Valligatla, Y. Yin, L. Schwarz, M. Medina-Sánchez, S. Baunack, C. H. Lee, R. Thomale, S. Li, V. M. Fomin, and O. G. Schmidt, "Experimental observation of Berry phases in optical Möbius-strip microcavities," *Nat. Photonics* **17**, 120 (2023).
- [11] M. Ding, G. Senthil Murugan, G. Brambilla, and M. N. Zervas, "Whispering gallery mode selection in optical bottle microresonators," *Appl. Phys. Lett.* **100**, 081108 (2012).

Chaos-enhanced chirality in optical microcavities

Rui-Qi Zhang^{1,*}, Yifei Zhang¹, Qi-Tao Cao¹, and Yun-Feng Xiao¹

¹ State Key Laboratory for Mesoscopic Physics and Frontier Science Center for Nano-optoelectronics, School of Physics, Peking University, 100871, Beijing, China

² The Dodd-Walls Centre for Photonic and Quantum Technologies, New Zealand

* ruiqizhang1999@stu.pku.edu.cn

Abstract: This work finds that chaos in optical microcavities enhances local chirality. The local chirality can be transformed to the global chirality by a scatterer.

1. Introduction

Chirality is an intensively studied field in microcavity. The break of mirror symmetry in microcavity will lead to chirality—the difference in the intensities of clockwise and counterclockwise propagating light. Here, we theoretically and experimentally investigate the chaos enhanced chiral fields in optical microcavities. A small scatterer in a chaotic microcavity will induce a strong chirality. The mechanism responsible for this is that symmetry breaking is enhanced by chaotic phase space dynamics which results in the local chirality. And the local chirality can be transformed to global chirality by asymmetric scattering. By fabricating a chaotic microcavity with gain material and pumping it with pulsed light, we experimentally observe an order of magnitude enhancement of the clockwise and counterclockwise propagating light field intensity ratio. Our work reveals the principle of the chiral fields formation in chaotic microcavities and improves our understanding in the open chaotic system.

2. Some details

2.1 Research system

The chaotic microcavity with mirror symmetry is used for study. A scatterer is added in the microcavity, and the chaotic microcavity has a much stronger chirality than elliptical microcavity.

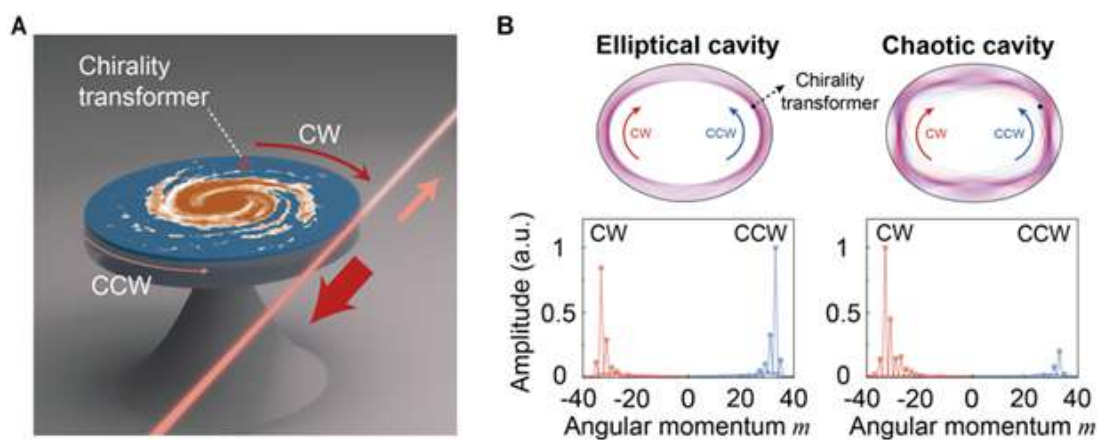


Fig. 1. Research system.

2.2 Mechanism of the formation of chirality

The chaotic microcavity breaks time reversal symmetry spontaneously and results in the local chirality. The local chirality can be transformed to global chirality by asymmetric scattering.

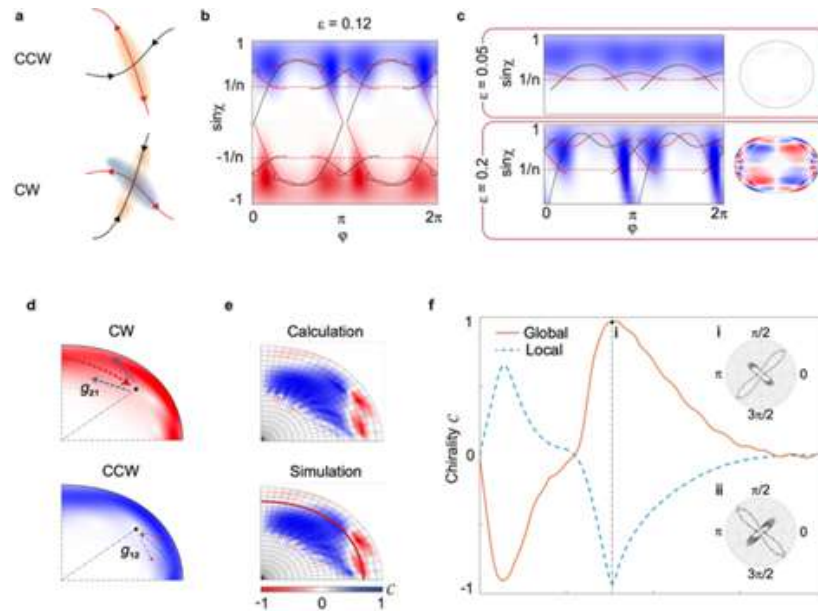


Fig. 2. Physical mechanism of the formation of the local and global chirality.

2.3 Experimental setup and maximum measured chirality

The chaotic microcavity is fabricated by photolithography and coated with gain material. The maximum ratio of the CW intensity with respect to the CCW intensity measured in the experiment is 11.48.

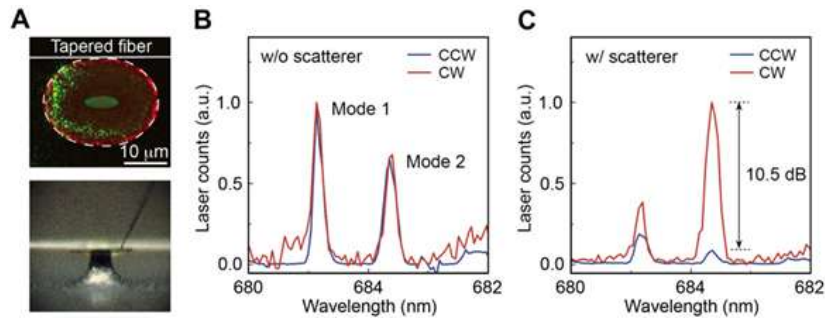


Fig. 3. Experimental setup and maximum measured chirality.

3. Summary

Our work reveals the physical mechanism of the chirality formation of chaotic microcavities and this is verified in experiment. This finding improves our understanding in the open chaotic system.

Coupling of NV centers in diamond to adiabatically tapered optical nanofibers

*Samuel Begumya*¹, *Mohammed Zia Jalaludeen*¹, *Ke Tian*¹, *Christophe Pin*¹, *Shilong Li*¹ and *Sile Nic Chormaic*¹

¹ Okinawa Institute of Science and Technology Graduate University, Japan

* s.begumya@oist.jp

Abstract: Tapered optical fibers efficiently couple with quantum emitters on their surface. We demonstrate coupling nitrogen-vacancy (NV) centers in nanodiamonds with tapered fibers, enhancing fluorescence collection for hybrid quantum devices in quantum sensing applications. © 2024 The Author(s)

1. Introduction

Tapered optical fibers as one-dimensional waveguides can provide efficient coupling between their fundamental mode and quantum emitters placed on their surface. Single nanodiamonds containing NV centers have for the past few years been integrated with optical fibers by different research groups for quantum applications through the following categories: placing diamond directly on the surface of multimode fiber [1], putting single nanodiamonds directly on the fiber endpoint or inside the fiber [2], and coupling the NV's fluorescence to the evanescent field of an optical nanofiber where NV centers are embedded in single nanodiamonds or diamond nanostructures [3]. Here we demonstrate an experimental technique for coupling nitrogen-vacancy (NV) centers in nanodiamonds with tapered fibers. The fluorescence of NV centers is collected by the fiber via the nearfield interaction between the NV centers and the tapered region of the fiber. The results will be helpful in the development of hybrid quantum devices for applications in quantum sensing.

2. Tapered fiber fabrication process

The fiber tapering process involves the application of heat as conventional fiber is stretched. As the fiber is drawn, it undergoes a reduction in diameter, adhering to the principle of mass conservation. Figure 1 illustrates the tapered optical fiber structure. When the diameter is less than 1 μm , the waist of the tapered fiber is called an optical nanofiber (ONF). Conversely, if the diameter exceeds 1 μm , the waist region is referred to as an optical microfiber (OMF).

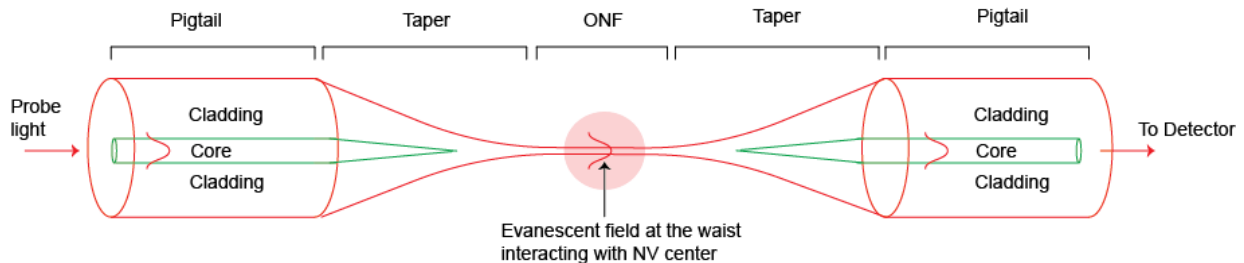


Figure 1. Schematic of a tapered optical fiber.

This fabrication method uses a hydrogen and oxygen gas flame to create the tapered optical fiber. The gas temperature is carefully regulated by adjusting the gas flow rate. The process begins by removing the jacket from a section of optical fiber, which is then securely clamped to a motorized stage. Subsequently, the oxygen-hydrogen flame is brought near the fiber and remains stationary. As the flame heats the fiber, motorized stages pull the fiber ends away from the heating direction, resulting in taper formation. For the formation of a longer taper, it is essential to heat a larger volume of the fiber uniformly. To achieve this, the two motorized stages, where the fiber is clamped, are attached to another stage, enabling the entire system to move back and forth. This makes the flame brush the fiber while creating the taper.

The taper's length and shape depend on the pull length and hot zone parameters specified during the tapering process. Fixing the hot zone parameter ensures that the taper follows an exponential profile pattern. To obtain high transmission, it is important to satisfy the adiabatic criterion (gradual tapering process to smoothly transfer optical power from the original fiber to the tapered region without causing significant loss or mode conversion), ensuring that the tapered region is small enough to allow only fundamental guided mode [4]. Figure 2 shows a scanning electron microscope (SEM) image of fabricated tapered nanofiber using a fiber tapering rig in our lab.

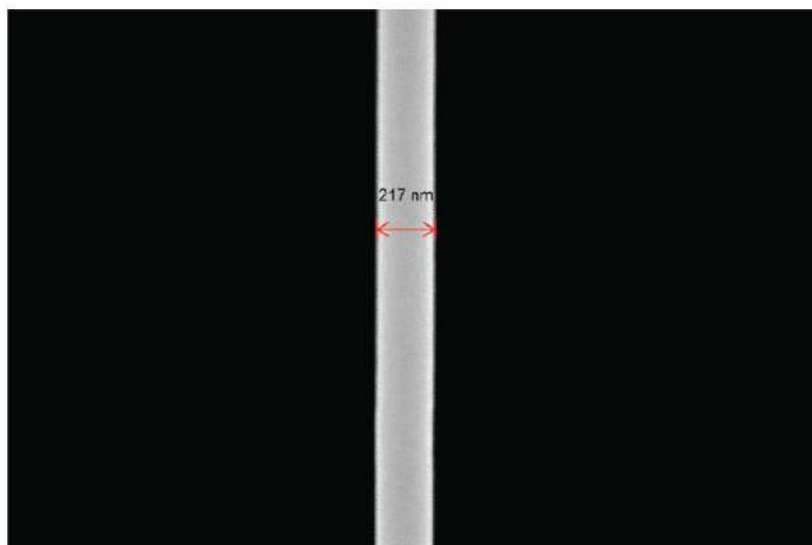


Figure 2. Scanning electron microscope (SEM) image showing tapered optical nanofiber fabricated using a fiber tapering rig in our lab.

3. Coupling of NV centers to tapered optical nanofibers

We developed the experimental procedure to manipulate and characterize the individual nanodiamonds on optical nanofibers. Nanodiamonds with NV centers are prepared on a coverslip using a spin-coating method, then picked and placed on the nanofiber deterministically using tungsten tips of a few tens of micrometers. Fluorescence signal from the NV centers is collected via the ONF and exhibited optically detected magnetic resonance by applying a microwave signal at the appropriate frequency.

References

- [1] D. Duan, G. Du, V. K. Kavatamane, S. Arumugam, Y.-K. Tzeng, H.-C. Chang, and G. Balasubramanian. “Efficient nitrogen-vacancy centers’ fluorescence excitation and collection from micrometer-sized diamond by a tapered optical fiber in endoscope-type configuration.” *Optics Express* **27**, 6734–6745 (2019).
- [2] M. Fujiwara, K. Yoshida, T. Noda, H. Takashima, A. W. Schell, N. Mizuochi, and S. Takeuchi, “Manipulation of single nanodiamonds to ultrathin fiber-taper nanofibers and control of NV-spin states toward fiber-integrated λ -systems.” *Nanotechnology* **27** 455202 (2016).
- [3] L. Shao, H. Wu, W. Fang, and L. Tong. “Twin-nanofiber structure for a highly efficient single-photon collection.” *Optics Express* **30**, 9147-9155 (2022).
- [4] P. Romagnoli, M. Maeda, J. M. Ward, V. G. Truong, and S. Nic Chormaic, Fabrication of optical nanofibre-based cavities using focussed ion-beam milling: a review, *Applied Physics B* **126**, 111 (2020).

Resonant Mode Calculation in Large-scale 3-Mirror Ring Resonators via Transformation Optics

Seongju Lee^{1,*}, *Yong-Hoon Lee*^{1,2}, *Inbo Kim*², *Sunghwan Rim*², *Tae-Yoon Kwon*³, *Muhan Choi*^{1,2}

¹ School of Electronic and Electrical Engineering, Kyungpook National University, Daegu 41566, Korea

² Digital Technology Research Center, Kyungpook National University, Daegu 41566, Korea

³ Navigation Systems R&D Team, Hanwha Aerospace, Daejeon 34101, Korea

* tpd02199@naver.com

Abstract: We propose a novel FDTD-based method for analyzing resonant modes in large-scale optical systems with lower computational memory requirements. This method efficiently divides the calculation area into subdomains and uses transformation optics to manage non-rectangular geometries. © 2024 The Author(s)

1. Introduction

To analyze the full-wave characteristics of optical resonators in devices like optical gyros or semiconductor lasers, resonant modes must be calculated using Maxwell's equations with specified boundary conditions. Numerical methods such as the finite element method (FEM) [1] and finite difference time domain (FDTD) [2] method are commonly used, but they become impractical for large-scale optical systems due to exponentially increasing computational costs. Systems with cylindrical symmetry can reduce calculation dimensions, but for extremely large systems without symmetry, obtaining optical mode properties is computationally infeasible. This paper proposes a novel FDTD-based simulation method to obtain optical modes in large-scale systems. The method involves dividing the computational area into feasible subdomains and sequentially computing fields along the light propagation direction. We validate this method by comparing FEM results in a Fabry-Pérot resonator with our FDTD results. Additionally, we demonstrate its application by calculating optical modes in a 3-mirror ring resonator, using transformation optics (TO) [3] to map non-rectangular subdomains to rectangular ones for FDTD calculations. This method aims to aid the design of large-scale optical systems by figuring out the full-wave characteristics of optical modes.

2. Methods

In this paper, we propose a novel FDTD-based approach specifically designed to overcome the high computational demands of simulating resonant modes in large-scale optical systems such as 3-mirror ring resonators. Our method significantly reduces computational memory requirements by strategically dividing the optical system into smaller, manageable subdomains, each calculated sequentially.

Conventional methods define the simulation region as encompassing the entire optical system, as shown in the gray area of Fig.1 (a), which is an inefficient approach considering the finite computational resources available. To overcome computational limit, the computation process of our method starts by segmenting the entire system into two types of subdomains based on their functionality and geometry. As shown in Fig.1 (b), subdomain A includes areas with mirrors, and Subdomain B consists of the spaces between the mirrors where light propagates freely. This division allows us to focus computational efforts where most needed, following an iterative pattern that matches the physical layout of the 3-mirror configuration.

One of the main challenges in applying the FDTD method to systems with non-orthogonal geometries, such as the 3-mirror ring resonator, is the angular disposition of the mirrors, which typically form a 60-degree angle with each other. Conventional FDTD methods rely on Cartesian grids, which are not naturally suited to handle angles that deviate from 90 degrees. To overcome this, we use transformation optics (TO) to effectively map these non-rectangular subdomains into rectangular computational domains, as shown in Fig.1 (c). This essential step involves adjusting the refractive index distribution within the subdomains to enable accurate simulations within the constraints of a Cartesian mesh. The color distribution in Fig.1 (d) represents the required refractive index distribution to map non-rectangular subdomain A into rectangular subdomain A'. Figure 1 (e) illustrates the sequential computational flow across the subdomains, where the output from one serves as the input for the next, facilitating a continuous and integrated simulation process. While the geometrical configuration within the iteration loop may seem rectangular as a result of mapping the non-rectangular subdomain into a rectangular shape, the actual configuration is triangular in practice.

3. Summary

In this study, we have proposed a novel FDTD-based simulation method designed to efficiently handle largescale optical systems. This approach significantly reduces the computational memory demands by segmenting the simulation area into manageable subdomains, utilizing transformation optics to accommodate non-rectangular geometries in systems like 3-mirror ring resonators. To validate our method, we conducted initial comparisons with traditional

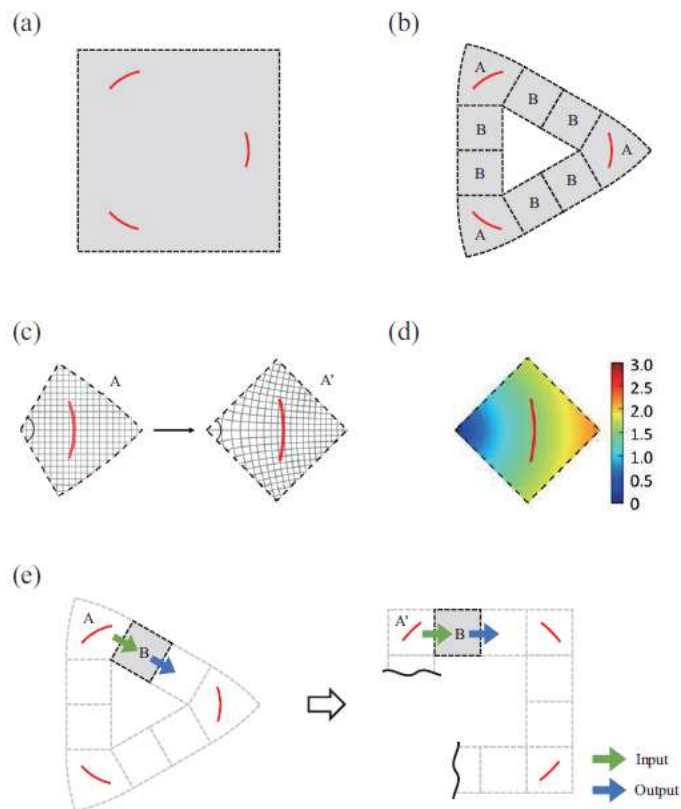


Fig. 1. Schematic of the proposed method for 3-mirror ring resonator. (a) Conventional simulation region, comprising 3-mirror system. (b) Two types of subdomains organized along the optical path with manageable size. (c) Conformal mapping of non-rectangular subdomain A to rectangular A'. (d) Refractive index distribution obtained by transformation optics. (e) The field information from the output of the previous subdomain is used as the input for the next subdomain.

FEM results obtained from COMSOL Multiphysics applied to a Fabry-Pérot resonator. Further application of our method to the more complex 3-mirror ring resonator—common in advanced ring lasers and gyro-sensors—confirmed its effectiveness. Our findings show that while drastically reducing memory requirements, our approach achieves a high fidelity in simulation outcomes, with less than a 5% deviation in the Q-factor when compared to detailed FEM simulations. This substantiates the potential of our method for broader application in optical device design, significantly advancing capabilities for modeling and analyzing intricate optical behaviors previously constrained by computational limitations.

References

- [1] Jian-Ming Jin. *The finite element method in electromagnetics*. John Wiley & Sons, 2015.
- [2] Allen Taflov, Susan C Hagness, and Melinda Picket-May. Computational electromagnetics: the finite-difference time-domain method. *The Electrical Engineering Handbook*, 3(629-670):15, 2005.
- [3] Ulf Leonhardt. Optical conformal mapping. *Science*, 312(5781):1777–1780, 2006.

Soliton Microcombs in the High-Q Lithium Niobate Microresonators

Shuai Wan^{1,*}, Pi-Yu Wang¹, Rui Ma², Fang Bo², Guang-Can Guo¹, Chun-Hua Dong¹

¹ CAS Key Lab of Quantum Information, University of Science and Technology of China, China

² MOE Key Laboratory of Weak-Light Nonlinear Photonics, TEDA Applied Physics Institute and School of Physics, Nankai University, China

* wanshuai@ustc.edu.cn

Abstract: We demonstrated a self-emerging, broadband soliton microcomb in an integrated z-cut lithium niobate microresonator. Through precise dispersion engineering, the octave soliton microcombs was realized, covering a spectral range from 130 THz to 263 THz.

1. Introduction

In recent years, dissipative Kerr solitons (DKSs) generated in the high-Q microresonators have attracted significant attention due to their remarkable advantages, which encompass compact size, minimal power consumption, and high integration[1]. The fully coherent comb lines, characterized by a high repetition rate and low noise, have found broad applications across diverse fields including quantum key distribution, precision spectroscopy, lidar, optical clocking, and optical frequency synthesis. However, accessing soliton states has traditionally been challenging due to the difficulty in capturing and maintaining them, as the abrupt power drop from the chaotic state to the soliton state can lead to the rapid cooling of the microresonator and immediately quench the soliton state.

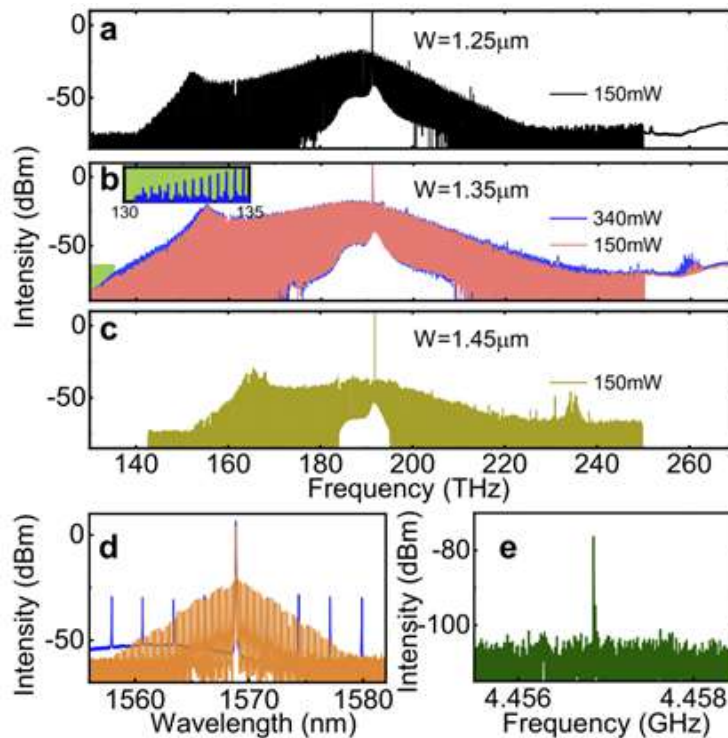


Fig. 1. (a)–(c) Optical spectra of single soliton microcombs with different widths of microring. The inset shows the zoom-in view of the spectrum. (d) Typical spectra of the electro-optic comb (orange) and the partial soliton microcomb (blue). (e) Beat note signal recorded by the ESA.

2. Some details

In this paper, we demonstrate a self-emerging, broadband soliton microcomb in an integrated z-cut lithium niobate (LiNbO_3) optical microresonator [2,3], which has the typical loaded Q factor around 0.7×10^6 . By harnessing the photorefractive effect of lithium niobate to significantly extend the soliton existence range, a spontaneous yet deterministic single-soliton formation is observed. Specifically, we show that the single soliton state is stable in the laser frequency range of 1.28 GHz and can be operated stably in the on-chip power range from 60 mW to 220 mW, demonstrating strong robustness to both frequency and power changes of the pump laser. In addition, we show the

system's ability to recover from perturbation, long-term operation up to 13 h, and turnkey soliton generation with a pre-programmed DFB laser [4]. Furthermore, through precise dispersion engineering for the soliton microresonator, the octave soliton microcomb is operated at an on-chip pump power of 340 mW, covering a spectral range from 130 THz to 263 THz. The repetition rate of the soliton microcomb is precisely measured by the EO comb generated by an x-cut LN racetrack microresonator, as shown in Fig. 1 [5], which is essential for implementing the $f - 2f$ self-referencing technique.

3. Summary

In conclusion, we demonstrate the generation of the octave soliton microcomb using a LN microring resonator based on the z-cut thin film Lithium Niobate. By introducing precise control over film thickness and etching depth, we anticipate a significant enhancement in the flexibility of dispersion engineering for soliton microcombs. Additionally, dispersion profiles can be further tailored through advanced techniques such as inverse design to mitigate phase mismatches and boost the power of comb lines, leading to a broader and more efficient spectral range.

References

- [1] I. T. J. Kippenberg, et al, "Dissipative kerr solitons in optical microresonators," *Science* 361 (2018).
- [2] Y. He, et al. "Self-starting bi-chromatic LiNbO₃ soliton microcomb," *Optica* 6, 1138 (2019).
- [3] Z. Gong, et al. "Near-octave lithium niobate soliton microcomb," *Optica* 7, 1275 (2020).
- [4] S. Wan, et al. "Photorefraction-assisted self-emergence of dissipative Kerr solitons," *Laser Photonics Reviews* 18, 2300627 (2024).
- [5] P-Y. Wang, et al. "Octave soliton microcombs in lithium niobate microresonators," *Optics Letters* 49, 1729 (2024).

Properties extraction of optical microcavity coupling system based on coupled mode theory-informed neural network

Songyi Liu¹, Xiao-chong Yu², Bing Duan¹, and Daquan Yang^{1,*}

¹ State Key Laboratory of Information Photonics and Optical Communications, and School of Information and Communication Engineering, Beijing University of Posts and Telecommunications, Beijing 100876, China

² Applied Optics Beijing Area Major Laboratory, Beijing Normal University, Beijing 100875, China

* ydq@bupt.edu.cn

Abstract: In this paper, a neural network algorithm embedded with coupled mode equations is proposed. The experimental results are in good agreement with the predicted results in the extraction of optical microcavity coupled system properties. © 2024 The Author(s)

1. Introduction

Due to their high-quality factors and small mode volumes, optical microcavities have become ideal platforms for studying coupled systems such as exceptional point [1,2], topological photonics [3,4], and optical Ising machines [5, 6]. Designing and optimizing these coupled systems require fitting a large number of spectra using coupled mode theory (CMT) equations to extract physical properties of the system, such as resonance wavelengths, losses, and coupling coefficients. This process not only consumes significant computational resources but also inevitably results in multiple sets of fitting values, making the design and optimization of microcavity coupled systems a substantial challenge. Machine learning methods have shown great potential in inverse data extraction and optical structure design [7–9]. However, traditional machine learning approaches lack physical constraints on the output parameters and perform poorly with highly nonlinear relationships and multi-parameter problems, limiting their application in complex physical issues.

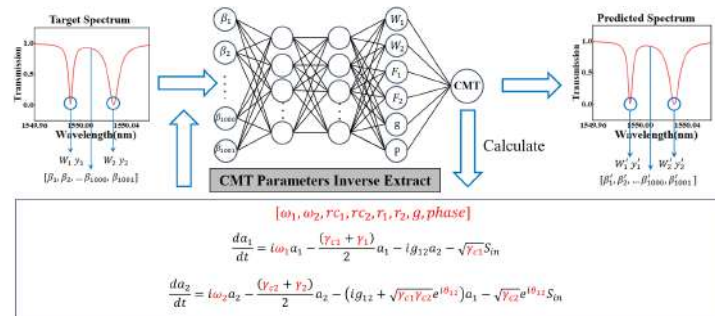


Fig. 1. Schematic diagram of CINN architecture. W and ω represent the predicted wavelength and wavelength parameters in Coupled Mode Theory (CMT); γ_c is the coupling strength between the microcavity and the incident light; γ is the microcavity's own loss; g is the coupling coefficient between the microcavities; P and θ are the predicted phase difference between the two cavities and the phase difference in CMT, respectively; F is the full width at half maximum (FWHM) of the resonant peak, which is the sum of γ_c and γ .

To address these issues, we propose a Coupled Mode Theory-informed Neural Network (CINN) architecture. This architecture accurately extracts the physical parameters of the system and overcomes the limitations of traditional machine learning methods, such as poor interpretability and limitations in strongly nonlinear and multiparameter systems. Our method meets the high-precision physical parameter extraction needs of coupled systems and provides an innovative approach to the design and optimization of optical microcavity structures.

2. Results and Discussion

To meet the design requirements, we select the transmission spectra of the microcavities as the optical response characteristics, while the structural parameters include key features such as FWHM, coupling coefficients, and resonance frequencies. The neural network learns the mapping between optical response and structural parameters to obtain predicted values of the structural parameters. Simultaneously, the predicted structural parameters are recalculated into optical responses using Coupled Mode Theory (CMT). The difference between the predicted optical response and the input optical response is then calculated and fed back to the neural network through a specially designed loss function, generating corresponding gradients for backpropagation. Two coupling scenarios in the optical microcavity coupling system are predicted. Specifically, we predict the variation of the resonant wavelength and loss corresponding

to a decrease in the coupling distance between the resonator and the fiber cone (gradually increasing γ_c) when the coupling coefficient g is 0, as shown in Fig. 2(a). Moreover, we predict the same scenario when the coupling coefficient g is nonzero, as shown in Fig. 2(b). In the figures, black squares represent the physical parameters of cavity 1, red circles represent the physical parameters of cavity 2, and green triangles represent the absolute difference in resonance wavelengths between the two cavities. To verify the feasibility of the CINN architecture, we used a system with two microsphere cavities coupled to a tapered fiber. The experimental setup is shown in Figure 2(c), and the experimental results are shown in Figure 3(d) and (e). It is worth noting that in order to ensure that g is 0, we let the distance between the two cavities be large enough, while cavity 1 always remains in the overcoupled state. Fig. 3 shows that the CINN predictions are in good agreement with the experimental results.

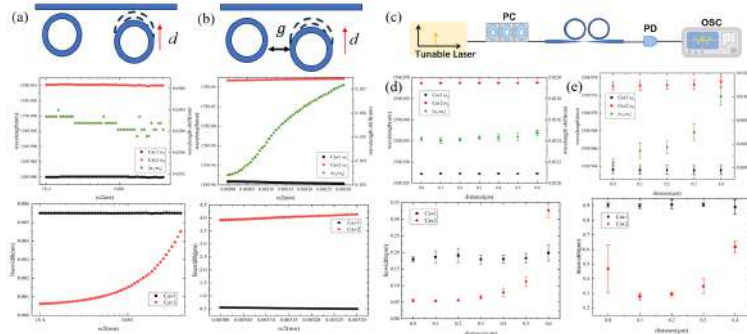


Fig. 2. (a) CINN prediction results when the coupling coefficient g is 0 and γ_{c2} gradually increases; (b) CINN prediction results when the coupling coefficient g is not 0 and γ_{c2} gradually increases; (c) Diagram of the experimental setup: PC (polarization controller), PD (photodetector), OSC (oscilloscope); (d) Experimental results when the coupling coefficient g is 0 and γ_{c2} gradually increases; (e) Experimental results when the coupling coefficient g is not 0 and γ_{c2} gradually increases.

3. Conclusion

In summary, we propose a CINN architecture for optical microcavity systems. This architecture has been experimentally validated, demonstrating its feasibility and accuracy in extracting and characterizing microcavity properties such as coupling coefficients, resonance wavelengths, and losses. The CINN addresses the limitations of traditional machine learning methods and provides an innovative approach to the design and optimization of optical microcavity structures, with potential applications in sensing and detection.

References

- [1] S. Wang, B. Hou, W. Lu, et al., "Arbitrary order exceptional point induced by photonic spin-orbit interaction in coupled resonators," *Nat. Commun* **10**, 832 (2019).
- [2] C. Wang, W. R. Sweeney, A. D. Stone, et al., "Coherent perfect absorption at an exceptional point," *Science* **373**, 1261-1265 (2021).
- [3] H. Zhao, X. Qiao, T. Wu, et al., "Non-Hermitian topological light steering," *Science* **365**, 1163-1166 (2019).
- [4] Z. Gao, H. Zhao, T. Wu, et al., "Topological quadratic-node semimetal in a photonic microring lattice," *Nat. Commun* **14**, 3206 (2023).
- [5] N. Tezak, T. Van Vaerenbergh, J. S. Pelc, et al., "Integrated coherent Ising machines based on self-phase modulation in microring resonators," *IEEE J. Sel. Top. Quantum Electron* **26**, 1-15 (2019).
- [6] L. Q. English, A. V. Zamptaki, K. P. Kalinin, et al., "An Ising machine based on networks of subharmonic electrical resonators," *Commun Phys-UK* **5**, 333 (2022).
- [7] Y. Chen, Z. Lan, Z. Su, et al., "Inverse design of photonic and phononic topological insulators: a review," *Nanophotonics* **11**, 4347-4362 (2022).
- [8] Z. Li, R. Pestourie, Z. Lin, et al., "Empowering Metasurfaces with Inverse Design: Principles and Applications," *ACS Photonics* **9**, 2178-2192 (2022).
- [9] C. C. Nadell, B. Huang, J. M. Malof, et al., "Deep learning for accelerated all-dielectric metasurface design," *Opt. Express* **27**, 27523-27535 (2019).

Enhancing Cavity Optomechanics by Magnetically-mediated Photothermal Effect

Wensong Yan¹, Lu Yao^{1,2}, Shui-Jing Tang², and Yun-Feng Xiao^{1,2,3,4,*}

¹ State Key Lab for Mesoscopic Physics and Frontiers Science Center for Nano-optoelectronics, School of Physics, Peking University, Beijing, 100871, China

² National Biomedical Imaging Center, Peking University, 100871, Beijing, China

³ Collaborative Innovation Center of Extreme Optics, Shanxi University, 030006, Taiyuan, China

⁴ Peking University Yangtze Delta Institute of Optoelectronics, Nantong, Jiangsu 226010, China

* yfxiao@pku.edu.cn

Abstract: We demonstrate high-efficiency excitation of the microresonator's vibration spectra across a wide spectrum using an intensity-modulated continuous-wave laser to excite an attached magnetic particle. Our excitation efficiency is improved by about 4 orders of magnitude compared with radiation pressure-driven methods. © 2024 The Author(s)

1. Introduction

Optical microcavities, such as microspheres or microtoroids, can support ultrahigh-Q whispering gallery modes (WGMs) [1]. These cavities also exhibit mechanical modes driven by radiation pressure [2, 3], but the low intensity of radiation pressure limits the amplitude of vibrations and restricts the variety of excited mechanical modes due to WGM symmetry. A promising method to enhance optomechanical coupling is attaching microparticles to the microcavity, where a pump laser excites acoustic waves, useful for single-particle vibrational spectroscopy [4].

We demonstrate efficient excitation of microresonator vibrations over a broad spectrum using an intensity-modulated continuous-wave laser to excite an attached magnetic particle, which exhibits a strong photothermal effect under laser irradiation. A theoretical model is developed to explain the photothermal-driven vibrations, and finite element simulations confirm the correlation with the microcavity's inherent vibration spectrum. Our method improves excitation efficiency by approximately four orders of magnitude compared to traditional radiation pressure-driven methods. This advancement represents a significant step in optomechanical sensing and phonon lasers.

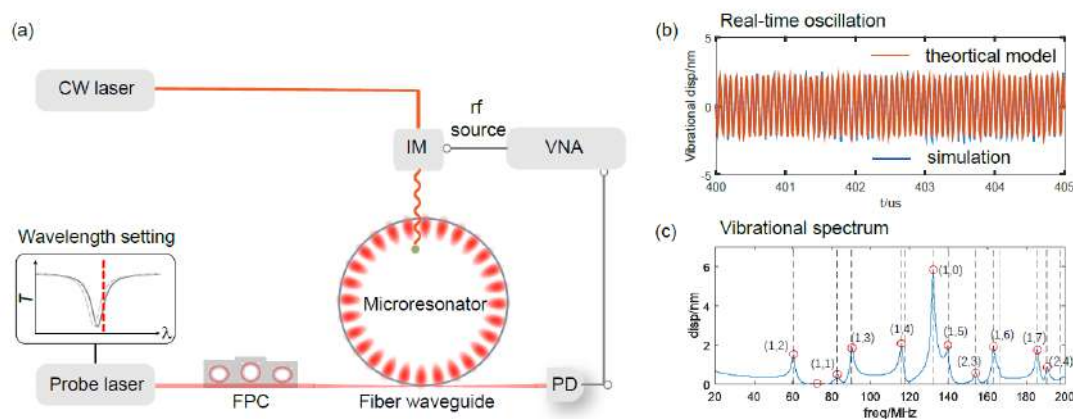


Fig. 1. Cavity optomechanics driven with photothermal effect. (a), Experimental setup. Magnetic particles deposited on the microresonator are irradiated by an intensity-modulated continuous-wave laser to stimulate their forced vibrations. Another continuous-wave laser is used to excite the optical whispering gallery mode by setting the wavelength slightly detuned from the resonance, and the optical transmission is recorded by a photodetector. (b)-(c), Real-time oscillation trace and vibrational spectrum from theoretical model and simulation.

Experimentally, we employ a silicon microsphere cavity with a polystyrene particle doped with Fe_3O_4 , which is transferred onto the surface of the microcavity. The magnetic material significantly enhances the particle's absorption of the 1550 nm laser. A continuous-wave laser excites the whispering gallery modes of the microcavity, while the intensity of another continuous-wave laser is modulated, leading to variations in its output power at a specific frequency. When the modulated pump laser irradiates the particle, it induces temperature changes and thermal expansion due to the photothermal effect. After the relaxation process, the particle exhibits vibrations that couple to the microcavity through contact. The system reaches a periodic vibrational state, known as forced vibrations. These vibrations are detected via variations in the optical modes of the microcavity. At mechanical resonance, which occurs near the mechanical modes of the microcavity, peaks are observed in the vibrational spectrum.

A theoretical model is established to analyze the system. Since the system has reached an equilibrium vibrational state, we focus only on the final state and ignore the relaxation process. Assuming the system vibrates at the same frequency as the modulation frequency, the displacement distribution takes the form:

$$u_{\text{equ}}(r, t) = u_0(r) + u_v(r) \cos(2\pi ft + \phi(r)) \quad (1)$$

where f is the modulation frequency. The results calculated by our method are consistent with transient simulation, and the calculated vibration spectrum shows the frequencies of the particle's eigenmodes, as shown in Fig. 1(b)(c).

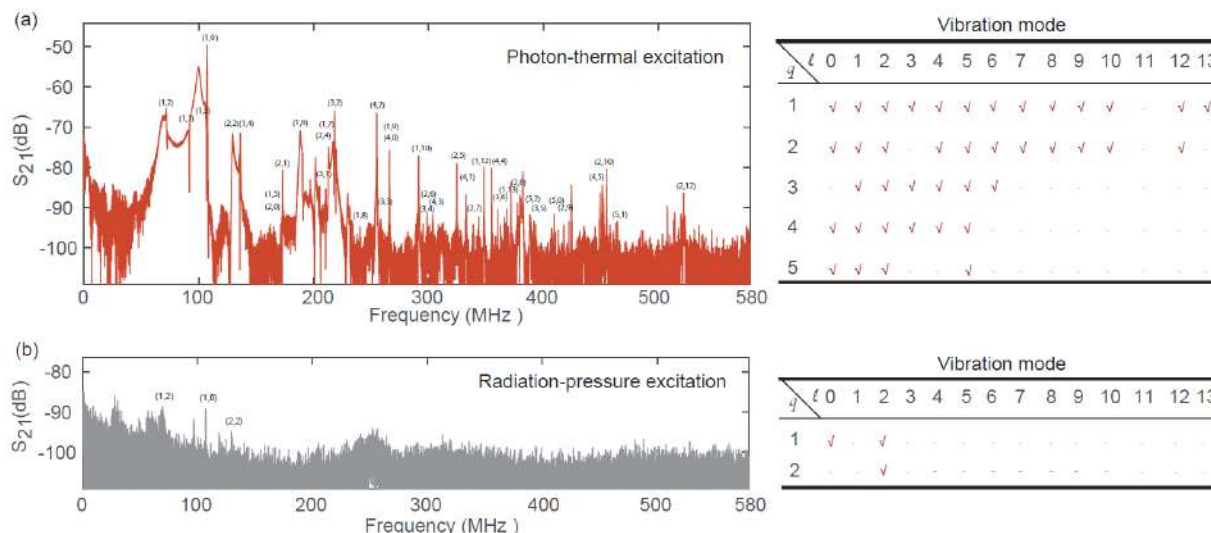


Fig. 2. Cavity Photon-thermal vibrational spectroscopy. (a), Cavity vibrational spectrum under photon-thermal excitation. (b), Cavity vibrational spectrum under radiation-pressure excitation. The mode number of the vibrational mode are marked and listed in the right side.

After frequency sweeping, we can obtain the vibrational spectrum and compare it with the spectrum under the effect of pure radiation pressure, as shown in Fig. 2. Compared to the traditional radiation pressure excitation method, our photon-thermal excitation method can significantly enhance the vibrational amplitude, with an increase of up to four orders of magnitude. By comparing the peaks of vibrational spectrum and the calculated frequencies of eigenmodes, the types of modes excited by the two methods are given in the table. Our method can achieve almost full-mode excitation, whereas the radiation pressure method typically has difficulty exciting modes with odd l values.

References

- [1] Vahala K J. Optical microcavities[J]. *nature*, 2003, 424(6950): 839-846.
- [2] Kippenberg T J, Rokhsari H, Carmon T, et al. Analysis of radiation-pressure induced mechanical oscillation of an optical microcavity[J]. *Physical Review Letters*, 2005, 95(3): 033901.
- [3] Ma R, Schliesser A, Del'Haye P, et al. Radiation-pressure-driven vibrational modes in ultrahigh-Q silica microspheres[J]. *Optics letters*, 2007, 32(15): 2200-2202.
- [4] Tang S J, Zhang M, Sun J, et al. Single-particle photoacoustic vibrational spectroscopy using optical microresonators[J]. *Nature Photonics*, 2023, 17(11): 951-956.

Single-Molecule Optofluidic Microsensor with Interface Whispering Gallery Modes

Xiao-Chong Yu^{1,2,*}, *Shui-Jing Tang*^{3,4}, *Wenjing Liu*^{3,4}, *Yinglun Xu*^{3,4}, *Qihuang Gong*^{3,4}, *You-Ling Chen*⁵, and *Yun-Feng Xiao*^{3,4,6,7,8}

¹ School of Physics and Astronomy, Beijing Normal University, Beijing 100875, China

² Applied Optics Beijing Area Major Laboratory, Beijing Normal University, Beijing 100875, China

³ State Key Laboratory for Mesoscopic Physics, School of Physics, Peking University, Beijing 100871, China

⁴ Frontiers Science Center for Nano-optoelectronics, Peking University, Beijing 100871, China

⁵ State Key Laboratory on Integrated Optoelectronics, Institute of Semiconductors, Chinese Academy of Sciences, Beijing 100083, China

⁶ Collaborative Innovation Center of Extreme Optics, Shanxi University, Taiyuan 030006, China

⁷ Yangtze Delta Institute of Optoelectronics, Peking University, Nantong 226010, China

⁸ National Biomedical Imaging Center, Peking University, Beijing 100871, China

* yuxc@bnu.edu.cn

Abstract: We report an ultrasensitive optofluidic biosensor with high- Q interface whispering gallery modes in a microbubble cavity. And the single molecule detection is demonstrated by further utilizing the plasmonic hybridization. © 2024 The Author(s)

1. Introduction

Optical microresonators have emerged as promising platforms for label-free detection of molecules. However, approaching optimum sensitivity is hindered due to the weak tail of evanescent fields. In this work, we demonstrate an ultrasensitive optofluidic microbubble biosensor by exploiting the whispering gallery modes (WGMs) peaked at the interface between the optical resonator and the analyte solution, which are termed as the interface modes. Previously, the microbubble resonator has been widely used for measuring refractive index, biomolecule concentration, and single nanoparticle generally by the mode localized in the liquid core. Here, we tune the WGM field profile by varying the wall thickness, and the maximum of the field intensity is drawn onto the interface. Compared with conventional evanescent sensors, the present scheme utilizing interface modes promises maximum sensitivity for interfacial molecular analysis, pushing the detection limit down to 0.3 pg/cm^2 . Furthermore, the single molecule detection is demonstrated with a plasmonic-enhanced interface mode. Naturally integrated into a microfluidic system, the sensor with single-molecule sensitivity exhibits ultrasmall sample consumption down to 10 pL , providing an automatic platform for biomedical analysis.

2. Experimental Results

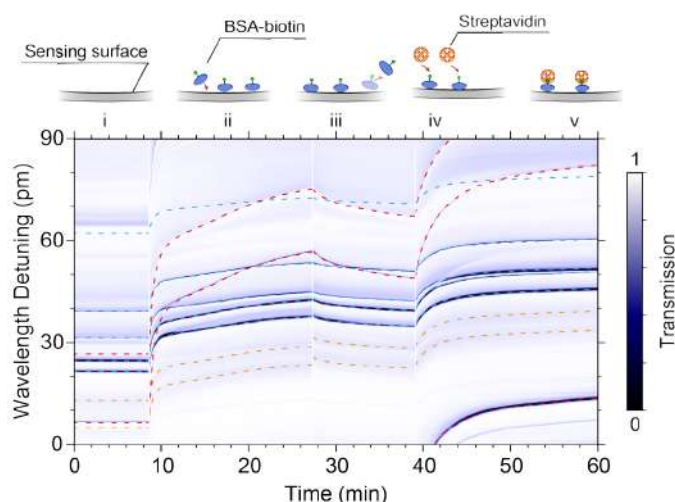


Fig. 1. Resonance shifts of the wall modes (blue dashed curves), interface modes (red dashed curves) and core modes (orange dashed curves) during the sequential addition of citrate buffer (i), biotinylated BSA molecules in citrate buffer (ii), citrate buffer (iii), and streptavidin proteins in citrate buffer (iv and v).

Experimentally, a microbubble resonator with a wall thickness of about $1 \mu\text{m}$ is fabricated from a microcapillary by CO_2 laser irradiation. WGMs are excited by a tunable laser via a side-coupled tapered fiber, and the transmission spectrum is monitored in real time. The sensing capabilities of different modes are then characterized by microfluidic experiments

with two kinds of analytes, biotinylated bovine serum albumin (BSA-biotin) molecules and streptavidin proteins. As 1 μM BSA-biotin molecules gradually enter the microfluidic channel, all WGMs experience red shifts (Fig. 1, ii) due to the molecular adsorption onto the hydroxylated silica surface. After removing the surplus BSA-biotin molecules with citrate buffer rinsing (Fig. 1, iii), streptavidin proteins with concentrations down to 50 nM are then delivered into the microbubble cavity. Further red shifts occur due to specific binding between the two kinds of molecules (Fig. 1, iv). This specific interaction is also confirmed by the control experiments without BSA-biotin molecule functionalization, which shows no evident adsorption signal.

Further enhancement of the interface mode via plasmonic hybridization is also demonstrated. With a gold nanorod adsorbed onto the inner surface of a microbubble, numerical simulation predicts a field enhancement factor $\gamma_p = 2500$ at the hotspot. An additional plasmonic enhancement factor γ_e in the range of 10^1 to 10^2 has been reported owing to the surface roughness of the gold nanorod or the ion layer around the molecules in the aqueous environment. The intrinsic Q factor of the fundamental interface mode before and after gold nanorod adsorption is 2.6×10^8 and 8.6×10^6 , respectively. Single-strand DNA molecules are then delivered into the Au-decorated microsensor. The resonant wavelengths of three representative modes are traced, as presented in Fig. 2. Transient steps and spikes are observed on the trace of the fundamental interface mode, corresponding to the adsorption and the transient movements of single DNA molecules, respectively. Statistical analysis shows that a single-strand DNA molecule with $m \approx 8$ kDa can induce the resonance shift up to ~ 70 fm. In contrast, on the trace of the wall mode and the core mode, single-molecule signals are buried in the frequency noises and difficult to be resolved. The noise levels are 3.1 and 23 fm for the high- Q interface mode with $\Delta\lambda = 0.2$ pm and low- Q core mode with $\Delta\lambda = 2.5$ pm, respectively.

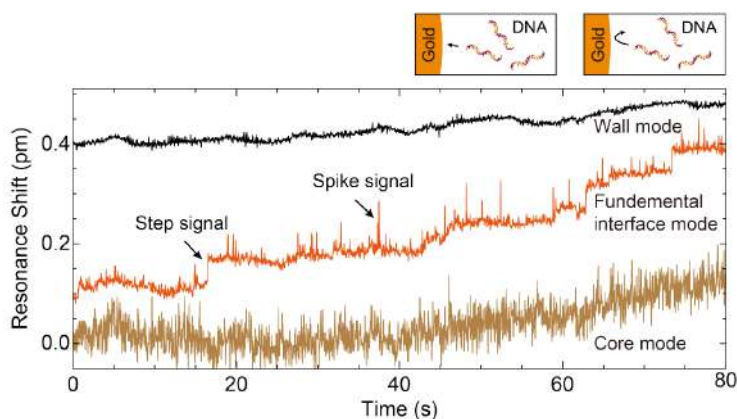


Fig. 2. Resonance shift induced by a single DNA oligo of a fundamental interface mode (orange curve), a wall mode (black curve), and a core mode (brown curve) with plasmonic enhancement.

3. Summary

In conclusion, we proposed an optofluidic biosensor with the interface modes in a microbubble resonator. The interface mode features both the peak field intensity at the sensing surface and high- Q factors, enabling a detection limit as low as 0.3 pg/cm^2 . Furthermore, the proposed scheme can be directly incorporated with other SNR enhancement methods, enabling multifold sensitivity enhancement. As an example, single-molecule detection was demonstrated with the plasmonic-enhanced interface mode.

References

- [1] X.-C. Yu, S.-J. Tang, W. Liu, Y. Xu, Q. Gong, Y.-L. Chen, Y.-F. Xiao, "Single-molecule optofluidic microsensor with interface whispering gallery modes," *Proc. Natl. Acad. Sci. USA* **119**, e2108678119 (2022).

Microwave-rate dark pulse microcombs in integrated LiNbO₃ microresonators

Xiaomin Lv^{1,2,†}, *Binbin Nie*^{1,†}, *Chen Yang*^{1,†,*}, *Rui Ma*³, *Ze Wang*¹, *Yanwu Liu*¹, *Xing Jin*¹, *Zhenyu Chen*³, *Du Qian*¹, *Guanyu Zhang*¹, *Guowei Lv*¹, *Qihuang Gong*^{1,4,5}, *Fang Bo*^{3,*}, and *Qi-Fan Yang*^{1,2,*}

¹ State Key Laboratory for Artificial Microstructure and Mesoscopic Physics and Frontiers Science Center for Nano-optoelectronics, School of Physics, Peking University, Beijing, 100871, China

² Hefei National Laboratory, Hefei, 230088, China

³ Nankai University, Tianjin, 300071, China

⁴ Collaborative Innovation Center of Extreme Optics, Shanxi University, Taiyuan, 030006, China

⁵ Peking University Yangtze Delta Institute of Optoelectronics, Nantong, 226010, China

† These authors contributed equally to this work.

* ycoptics@pku.edu.cn; bofang@nankai.edu.cn; leonardoyoung@pku.edu.cn

Abstract: We demonstrate the generation of dark pulse microcombs with 25 GHz comb spacing and near 200 nm spectral span in an integrated LiNbO₃ microresonator. © 2024 The Author(s)

1. Introduction

The realization of optical frequency combs in microresonators (microcombs) [1] has enabled compact spectrometers [2], miniaturized optical clocks [3], and high-capacity data links [4]. These advances are primarily attributed to the rapid development of microresonator technology, notably the enhancement of quality factors and the expansion of material options. Up to date, mode-locked microcombs have been demonstrated in a broad selection of material platforms such as silica, Si₃N₄, and MgF₂ [5].

LiNbO₃ has become a key infrastructure for photonic applications due to its diverse optical nonlinearities. The most renowned Pockels and Kerr effect has enabled microcombs in LiNbO₃ microresonators [6]. Other nonlinearities such as the photorefractive effect have also facilitated comb formation. However, the crystal structure of LiNbO₃ indicates strong Raman responses within several narrow frequency bands, often hindering the generation of Kerr microcombs. These challenges become more prevalent for microresonators with smaller free spectral ranges (FSRs), where optical mode pairs are more prone to resonate with Raman phonons.

2. Microcomb demonstration

Here, we introduce dissipation engineering to mitigate the impact of the Raman effect on comb formation in an integrated LiNbO₃ microresonator. Notably, we report the first observation of dark pulse microcombs in these resonators, with the repetition rate down to 25 GHz. Figure 1(a) shows the images of our device, which is fabricated on a 570 nm thick z-cut LiNbO₃-on-insulator wafer. The radius of the resonator is 817 μm, corresponding to a free spectral range (FSR) of 24.803 GHz. The top width and the etching depth of the microring are 2.2 μm and 300 nm, respectively. This geometry gives normal group velocity dispersion at the telecommunication C band, which is confirmed through measurement (Fig. 1(b)). The concept of dissipation engineering is implemented using a pulley coupler. By precisely tuning the phase matching conditions between the bus waveguide and the microring, a stronger coupling is realized at Raman-active wavelengths. This wavelength-dependent dissipation modulation effectively elevates the power requirements for Raman lasing beyond the parametric threshold, which opens up the possibility of microcomb formation.

The microresonator is pumped by an amplified continuous-wave laser, generating microcomb spectra as presented

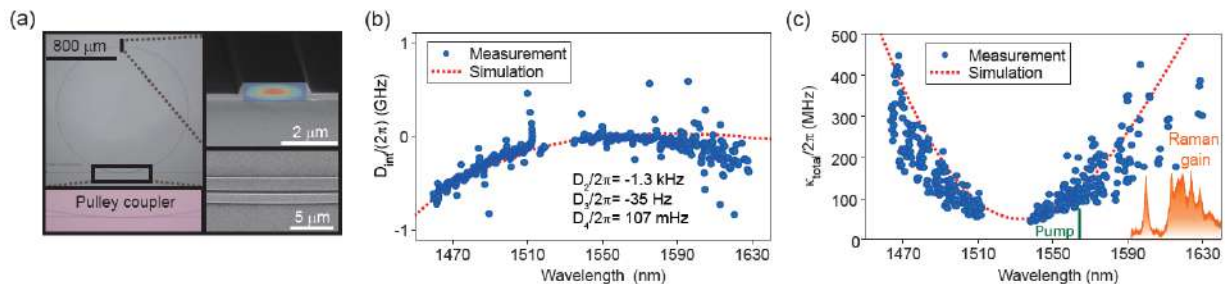


Fig. 1. (a) Optical microscope images (left) and scanning-electron-microscopy images (right) of the LiNbO₃ resonator. (b) Mode family dispersion of the microresonator. The fitted dispersion parameters to the simulated results are also provided. (c) Measured and simulated total dissipation rates of the LiNbO₃ microresonator as a function of wavelength.

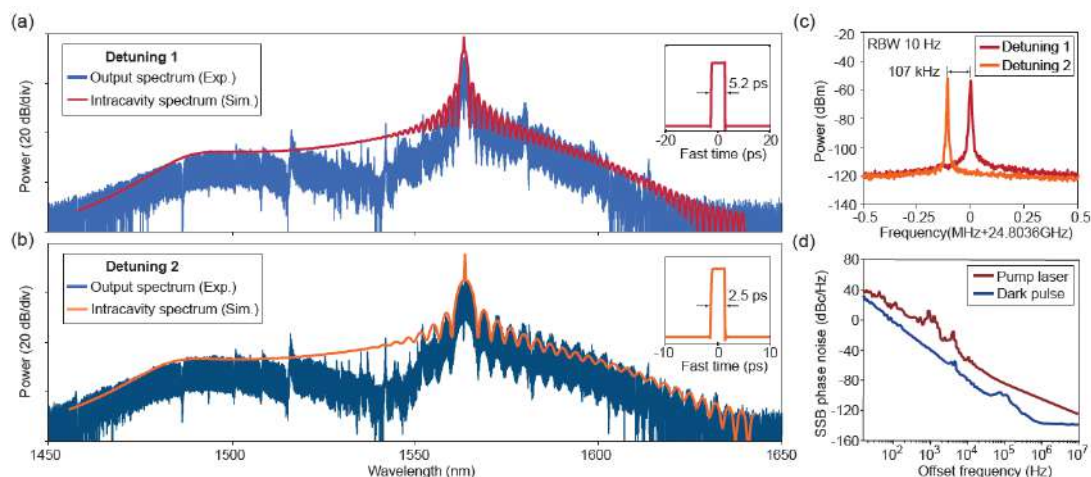


Fig. 2. (a)(b) Optical spectra of dark pulse microcombs. Insets show the simulated intracavity waveform. (c) Electrical beatnotes showing the repetition rates of the microcomb. (d) Representative phase noise spectrum of the pump laser and the repetition rate of the microcomb.

in Fig. 2. By adjusting the detuning between the pump and resonance, we access distinct microcomb states. These spectra, spanning nearly 200 nm, exhibit characteristic modulations akin to dark pulse microcombs reported by Xue et al. [7]. To fit the spectra, we perform numerical simulations using the Lugiato-Lefever equations and inputs from experimental parameters. The deviation between the simulated intracavity spectra and the experimental results is attributed to wavelength-dependent coupling. For example, the dips observed in the experimental spectra near 1540 nm align with the weakly coupled regime shown in Fig. 1(c). This fitting allows for the reconstruction of intracavity waveforms. Flat-top pulses are found to form in the microresonator, whose pulse width varies from 5.2 ps to 2.5 ps depending on the detuning. The coherence of the microcombs is assessed by measuring their electrical beatnotes, which shows a monotone radiofrequency peak with over 70 dB signal-to-noise ratio at 10-Hz resolution bandwidth (Fig. 2(c)). The beatnotes can be tuned over a range of 107 kHz by adjusting the pump-resonator detuning. Using a phase noise analyzer, we measure the phase noise of the beatnotes, which achieve -80 dBc/Hz at a 10 kHz offset frequency. This represents a notable reduction of approximately 35 dB from the phase noise of the pump laser, providing further evidence of mode locking in the microcomb.

In conclusion, we have demonstrated the viability of generating dark pulse microcombs in strong Raman active media such as LiNbO₃. The resulting microwave-rate dark pulses can be further augmented by the Pockels effect in LiNbO₃, enabling high-speed electro-optic tunability [8] and spectral translations into the visible wavelengths [6].

References

- [1] T. J. Kippenberg, R. Holzwarth, and S. A. Diddams, "Microresonator-based optical frequency combs," *Science* **332**, 555–559 (2011).
- [2] M.-G. Suh, Q.-F. Yang, K. Y. Yang, X. Yi, and K. J. Vahala, "Microresonator soliton dual-comb spectroscopy," *Science* **354**, 600–603 (2016).
- [3] Z. L. Newman, V. Maurice, T. Drake, J. R. Stone, T. C. Briles, D. T. Spencer, C. Fredrick, Q. Li, D. Westly, B. R. Ilic et al., "Architecture for the photonic integration of an optical atomic clock," *Optica* **6**, 680–685 (2019).
- [4] P. Marin-Palomo, J. N. Kemal, M. Karpov, A. Kordts, J. Pfeifle, M. H. Pfeiffer, P. Trocha, S. Wolf, V. Brasch, M. H. Anderson et al., "Microresonator-based solitons for massively parallel coherent optical communications," *Nature* **546**, 274 (2017).
- [5] T. J. Kippenberg, A. L. Gaeta, M. Lipson, and M. L. Gorodetsky, "Dissipative Kerr solitons in optical microresonators," *Science* **361** (2018).
- [6] Y. He, Q.-F. Yang, J. Ling, R. Luo, H. Liang, M. Li, B. Shen, H. Wang, K. Vahala, and Q. Lin, "Self-starting bichromatic LiNbO₃ soliton microcomb," *Optica* **6**, 1138–1144 (2019).
- [7] X. Xue, Y. Xuan, Y. Liu, P.-H. Wang, S. Chen, J. Wang, D. E. Leaird, M. Qi, and A. M. Weiner, "Mode-locked dark pulse Kerr combs in normal-dispersion microresonators," *Nat. Photon.* **9**, 594–600 (2015).
- [8] Y. He, R. Lopez-Rios, U. A. Javid, J. Ling, M. Li, S. Xue, K. Vahala, and Q. Lin, "High-speed tunable microwave-rate soliton microcomb," *Nat. Commun.* **14**, 3467 (2023).

Microresonator-referenced soliton microcombs with zeptosecond-level timing noise

Xing Jin^{1,†}, Zhenyu Xie^{1,†}, Hanfei Hou^{1,†}, Fangxing Zhang², Xuanyi Zhang¹, Qihuang Gong^{1,2,3}, Qi-Fan Yang^{1,3,*}

¹ State Key Laboratory for Artificial Microstructure and Mesoscopic Physics and Frontiers Science Center for Nano-optoelectronics, School of Physics, Peking University, Beijing 100871, China.

² Peking University Yangtze Delta Institute of Optoelectronics, Nantong, Jiangsu 226010, China.

³ Collaborative Innovation Center of Extreme Optics, Shanxi University, 030006, Taiyuan, China.

[†] These authors contributed equally to this work.

* leonardoyoung@pku.edu.cn

Abstract: Using a MgF₂ microresonator as the frequency reference and a Si₃N₄ microresonator for comb generation, we synthesize ultralow-noise 25-GHz microwaves with -141 dBc/Hz phase noise at 10 kHz offset frequency via optical frequency division. © 2024 The Author(s)

Microwaves with low noise and exceptional time stability are essential for various applications, including telecommunications [1] and metrology [2]. So far, the purest microwaves are synthesized using photonic approaches, particularly optical frequency division (OFD) technology [3]. The key components of an OFD setup are frequency references and optical frequency combs. However, the systems are typically very bulky due to the use of ultrastable resonators in vacuum and table-top optical frequency combs [4, 5], which restrict their application within laboratories. Replacing these key components with compact photonic devices has become the research focus over the past years. For example, ultrahigh-Q whispering-gallery-mode optical microresonators [6] could provide high-performance optical references for laser stabilization. Additionally, miniature optical frequency combs have been developed in nonlinear microresonators as soliton microcombs [7]. Combining these technologies has the potential to create compact OFD systems for broader applications beyond laboratories [8, 9]. In this work, we use an MgF₂ microresonator (Fig. 1(a)) with quality factors exceeding 3 billion as the frequency reference and a Si₃N₄ microresonator [10] (Fig. 1(b)) for comb generation to synthesize K-band microwaves via OFD. The resulting phase noise of a 25-GHz-rate microwave reaches -141 dBc/Hz at 10 kHz offset frequency.

The schematic diagram of our OFD system is shown in Fig. 1(c). Two fiber lasers with wavelengths of 1540 nm and 1560 nm are stabilized to the same MgF₂ disk microresonator via Pound-Drever-Hall (PDH) locking. This scheme, known as two-point OFD, has the advantage of not requiring an octave-spanning, self-referenced optical frequency comb. Therefore, the soliton microcomb used here only needs to cover 1540 nm - 1560 nm, which can be readily generated by pumping the Si₃N₄ microresonator at 1550 nm. The soliton microcomb is amplified and then combined with the reference lasers in two photodetectors. The frequencies of the two beatnotes are $\Delta_1 = f_A - f_p - n f_r$ and $\Delta_2 = f_B - f_p - m f_r$, with f_A and f_B the reference laser frequencies, f_p the pump laser frequency, f_r the microcomb repetition rate, and m, n the extracted comb line numbers. The two beatnotes are down-mixed to $\Delta = f_B - f_A - (m - n) f_r$, which is stabilized to a local oscillator (f_{LO}) by feedback to the pump laser of the soliton microcomb via a phase-locked loop. As a result, the microcomb repetition rate is stabilized to $f_r = (f_B - f_A - f_{LO}) / (m - n)$, whose noise is expected to be reduced from the frequency difference between optical references by a factor of $(m - n)^2$. In the experiment, the soliton microcomb has a repetition rate of 25 GHz, providing a division ratio of 100 as well as 40 dB noise suppression (Fig. 1(d)). To achieve a large locking bandwidth, all lasers used in the experiment are implemented with an acousto-optic frequency shifter.

We first characterize the relative phase noise of the reference lasers using a multi-frequency delayed self-heterodyne interferometer [11]. In this setup, both reference lasers are guided into an unbalanced Mach-Zehnder interferometer with a 1 km delay fiber coil installed in one arm and an acousto-optic frequency shifter in the other. At the output, the laser pair and their frequency-shifted counterparts are separated by a fiber Bragg grating and detected by two photodetectors, yielding two beatnotes containing the phase fluctuation of the respective reference lasers. The phases of the beatnotes are extracted simultaneously using two methods: Hilbert transform of oscilloscope traces and IQ demodulation with a datalogger. Such a combination allows for noise measurement bandwidth from 10 Hz to 1 MHz. The relative phase noise shown in Fig. 1(e) is already very low due to the excellent thermal stability of MgF₂, and the expected phase noise of the divided signals are projected to be 40 dB lower. We then detect the repetition frequency of the soliton microcomb using a fast photodetector and measure its phase noise using a phase noise analyzer. In sharp contrast to its free-running condition, the soliton microcomb locked to the references exhibits a repetition frequency strictly following the noise performance of the divided reference lasers at offset frequencies up to 10 kHz. Remarkably, a phase noise level of -141 dBc/Hz at 10 kHz offset frequency is achieved, corresponding to timing noise of 547 zs Hz^{-1/2},

which is competitive in recent OFD involving microcombs [8, 9, 12, 13].

In conclusion, we demonstrated an OFD system utilizing microresonators as key optical components. Such compact, ultralow-noise microwave oscillators have the potential to advance high-speed wireless communications, high-resolution radars, and space-based radio astronomy.

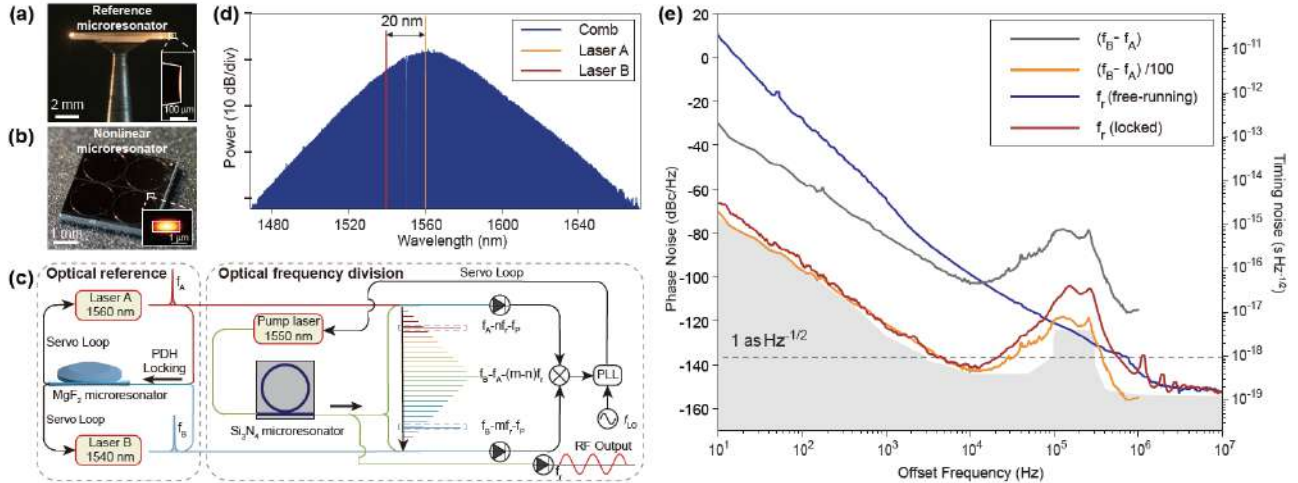


Fig. 1. Summary of microresonator-based optical frequency division. (a) Photograph of the MgF₂ reference microresonator. (b) Photograph of the Si₃N₄ nonlinear microresonator. (c) Schematic diagram for microresonator-based OFD. (d) Optical spectra of the soliton microcomb and reference lasers. (e) Phase noise of the repetition rate of free-running soliton microcomb (blue), locked soliton microcomb (red), relative phase noise between reference lasers (gray), and the phase noise of the divided signal projected from the reference lasers (orange). The dashed black line indicates the timing jitter level of 1 as Hz^{-1/2}. The gray shaded area represents the noise floor of the phase noise analyzer during the measurement.

References

- [1] S. Koenig, D. Lopez-Diaz, J. Antes, F. Boes, R. Henneberger, A. Leuther, A. Tessmann, R. Schmogrow, D. Hillerkuss, R. Palmer et al., "Wireless sub-THz communication system with high data rate," *Nat. Photonics* **7**, 977–981 (2013).
- [2] P. Ghelfi, F. Laghezza, F. Scotti, G. Serafino, A. Capria, S. Pinna, D. Onori, C. Porzi, M. Scaffardi, A. Malacarne et al., "A fully photonics-based coherent radar system," *Nature* **507**, 341–345 (2014).
- [3] Y. Yao, Y. Jiang, and L. Ma, "Optical frequency division," *National Sci. Rev.* **7**, 1801–1802 (2020).
- [4] T. M. Fortier, M. S. Kirchner, F. Quinlan, J. Taylor, J. Bergquist, T. Rosenband, N. Lemke, A. Ludlow, Y. Jiang, C. Oates et al., "Generation of ultrastable microwaves via optical frequency division," *Nat. Photonics* **5**, 425–429 (2011).
- [5] X. Xie, R. Bouchand, D. Nicolodi, M. Giunta, W. H. Hansel, M. Lezius, A. Joshi, S. Datta, C. Alexandre, M. Lours et al., "Photonic microwave signals with zeptosecond-level absolute timing noise," *Nat. Photonics* **11**, 44–47 (2017).
- [6] K. J. Vahala, "Optical microcavities," *Nature* **424**, 839–846 (2003).
- [7] T. J. Kippenberg, A. L. Gaeta, M. Lipson, and M. L. Gorodetsky, "Dissipative Kerr solitons in optical microresonators," *Science* **361**, eaan8083 (2018).
- [8] S. Sun, B. Wang, K. Liu, M. W. Harrington, F. Tabatabaei, R. Liu, J. Wang, S. Hanifi, J. S. Morgan, M. Jahanbozorgi et al., "Integrated optical frequency division for microwave and mmwave generation," *Nature* **627**, 540–545 (2024).
- [9] I. Kudelin, W. Groman, Q.-X. Ji, J. Guo, M. L. Kelleher, D. Lee, T. Nakamura, C. A. McLemore, P. Shirmohammadi, S. Hanifi et al., "Photonic chip-based low-noise microwave oscillator," *Nature* **627**, 534–539 (2024).
- [10] Z. Ye, H. Jia, Z. Huang, C. Shen, J. Long, B. Shi, Y.-H. Luo, L. Gao, W. Sun, H. Guo et al., "Foundry manufacturing of tight-confinement, dispersion-engineered, ultralow-loss silicon nitride photonic integrated circuits," *Photonics Res.* **11**, 558–568 (2023).
- [11] D. Jeong, D. Kwon, I. Jeon, I. H. Do, J. Kim, and H. Lee, "Ultralow jitter silica microcomb," *Optica* **7**, 1108–1111 (2020).
- [12] S. Sun, M. W. Harrington, F. Tabatabaei, S. Hanifi, K. Liu, J. Wang, B. Wang, Z. Yang, R. Liu, J. S. Morgan, S. M. Bowers, P. A. Morton, K. D. Nelson, A. Beling, D. J. Blumenthal, and X. Yi, "Kerr optical frequency division with integrated photonics for stable microwave and mmwave generation," *arXiv preprint arXiv:2402.11772* (2024).
- [13] Q.-X. Ji, W. Zhang, P. Liu, W. Jin, J. Guo, J. Peters, L. Wu, A. Feshali, M. Paniccia, V. Ilchenko et al., "Dispersive-wave-agile optical frequency division," *arXiv preprint arXiv:2403.00973* (2024).

Microresonator-based Vortex Spectroscopy

Yanwu Liu^{1,*}, *Chenghao Lao*^{1,2,*}, *Min Wang*^{2,3}, *Yinke Cheng*^{1,2}, *Shiyao Fu*⁴, *Chunqing Gao*⁴, *Jianwei Wang*^{1,5}, *Bei-Bei Li*^{2,6}, *Qihuang Gong*^{1,5,7}, *Yun-Feng Xiao*^{1,5,7,†}, *Wenjing Liu*^{1,5,†}, and *Qi-Fan Yang*^{1,5,†}

¹State Key Laboratory for Artificial Microstructure and Mesoscopic Physics and Frontiers Science Center for Nano-optoelectronics, School of Physics, Peking University, Beijing, 100871, China

²Beijing National Laboratory for Condensed Matter Physics, Institute of Physics, Chinese Academy of Sciences, Beijing, 100190, China

³University of Chinese Academy of Sciences, Beijing 100049, China

⁴School of Optics and Photonics, Beijing Institute of Technology, Beijing, 100081, China

⁵Collaborative Innovation Center of Extreme Optics, Shanxi University, Taiyuan, 030006, China

⁶Songshan Lake Materials Laboratory, Dongguan, 523808, Guangdong, China

⁷Peking University Yangtze Delta Institute of Optoelectronics, Nantong, Jiangsu, 226010, China

*These authors contributed equally to this work.

†e-mail addresses: yfxiao@pku.edu.cn; wenjingl@pku.edu.cn; leonardoyoung@pku.edu.cn

Abstract: By correlating frequency and orbital angular momentum (OAM) dimensions with the integrated vortex soliton microcomb, we performed a proof-of-concept experiment demonstrating a one-shot diagnosis of high-dimensional OAM states using conventional spectroscopy. © 2024 The Author(s)

1. Introduction

Combining optical frequency comb (OFC) [1] generation and OAM beam emission functions [2–4] into a standalone microresonator, we generate a multi-frequency beam that carries multiple OAM states, with a one-to-one correspondence between the OAM and the frequencies. This new type of beam, coined the "vortex soliton microcomb," introduces powerful measurement tools in the frequency domain to the OAM dimension. The one-to-one correspondence between the OAM and frequencies exhibits a high extinction ratio of over 18.5 dB, enabling precision spectroscopy of optical vortices using conventional spectroscopy techniques. We conducted a proof-of-concept experiment to measure the OAM response using an optical spectrum analyzer (OSA).

2. Vortex spectroscopy

The profile of the vortex soliton microcomb at its cross-section can be expressed as

$$A(r, \theta, t) = \sum_l a_l F_l(r) \exp(il\theta - il\omega_r t - i\omega_0 t), \quad (1)$$

where a_l and $F_l(r)$ are the complex amplitude and the normalized radial distribution of the photon carrying $l\hbar$ OAM, respectively. The frequency of the comb line with $l = 0$ is denoted by ω_0 . This formula manifests the bijective connection between the frequency and the OAM. After modulated by an object, whose phase pattern could be expressed as the summation of different topological charges given by $\sum_l b_l \exp(il\theta)$, the output vortex soliton microcomb becomes:

$$A_M(r, \theta, t) = \sum_l \sum_{l'} a_l b_{l'} F_l(r) \exp[i(l + l')\theta - i\omega_l t]. \quad (2)$$

After being Fourier transformed, the exterior part of the beam is blocked by an aperture, such that components with $l \neq 0$ are prohibited from transmitting. Therefore, the transmitted optical spectrum should only contain components with $l = 0$. The power readings of comb lines on a spectrometer are indeed indicators of the weight of pattern topological charges.

3. Experiment results

The scanning electron microscopy (SEM) images of our device are shown in Fig. 1a. With an appropriate grating design, the Q factor is maintained at 1.79 million (Fig. 1b). The OAM spectrum of a soliton state is shown in Fig. 1c, where each pattern corresponds to an individual comb line. A spatial light modulator (SLM) is used to emulate the target such as the turbulent air vortices in a free-space communication channel [5], and the OAM beams are then utilized to detect these SLM patterns. The results for two different phase patterns are shown in Fig. 1b, and the measurement results are in good agreement with the preset values. All weight information is collected in a single-shot

diagnosis using an OSA. Although this demonstration provides only singularity weights, phase information can also be recovered through coherent detection of the vortex soliton microcomb by heterodyning with a local OFC. In this process, the optical signals are converted into an array of electrical beatnotes [6–9].

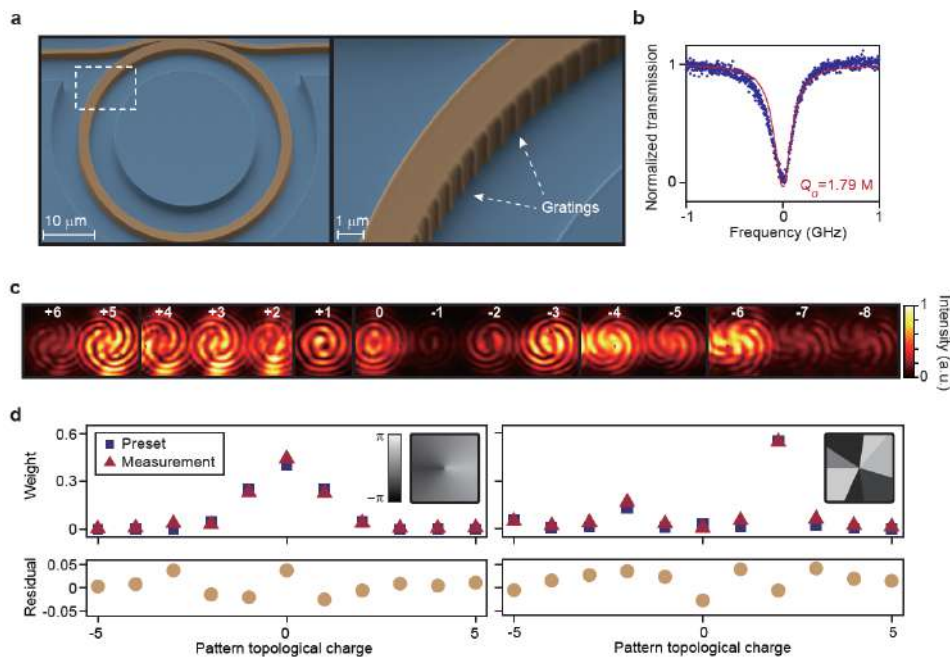


Fig. 1. (a), Scanning-electron-microscopy images of Si₃N₄ microresonator vortex emitter. (b), Transmission spectra and Q factor of a mode. (c), Optical spectra of a single-soliton microcomb. (d), Weight of topological charges on designated patterns. The preset and measured results are indicated in blue and red respectively, and their difference is plotted as residual errors in the panels below.

References

- [1] Diddams, S. A., Vahala, K. & Udem, T. Optical frequency combs: Coherently uniting the electromagnetic spectrum. *Science* **369**, eaay3676 (2020).
- [2] Allen, L., Beijersbergen, M. W., Spreeuw, R. J. C. & Woerdman, J. P. Orbital angular momentum of light and the transformation of Laguerre-Gaussian laser modes. *Phys. Rev. A* **45**, 8185–8189 (1992).
- [3] Yao, A. M. & Padgett, M. J. Orbital angular momentum: origins, behavior and applications. *Adv. Opt. Photon.* **3**, 161–204 (2011).
- [4] Cai, X. et al. Integrated compact optical vortex beam emitters. *Science* **338**, 363–366 (2012).
- [5] Chen, S. et al. Demonstration of 20-gbit/s high-speed Bessel beam encoding/decoding link with adaptive turbulence compensation. *Optics Letters* **41**, 4680–4683 (2016).
- [6] Suh, M.-G., Yang, Q.-F., Yang, K. Y., Yi, X. & Vahala, K. J. Microresonator soliton dual-comb spectroscopy. *Science* **354**, 600–603 (2016).
- [7] Dutt, A. et al. On-chip dual-comb source for spectroscopy. *Sci. Adv.* **4**, e1701858 (2018).
- [8] Yang, Q.-F. et al. Vernier spectrometer using counterpropagating soliton microcombs. *Science* **363**, 965–968 (2019).
- [9] Picqué, N. & Hänsch, T. W. Frequency comb spectroscopy. *Nat. Photon.* **13**, 146–157 (2019).

Self-organized formation of nonlinear scar modes

Yoshikazu Kuribayashi^{1,*}, *Shunsuke Nakamura*¹, *Mengyu You*¹, *Susumu Shinohara*², *Satoshi Sunada*³, *Takahisa Harayama*¹

¹ Department of Applied Physics, Waseda University, Tokyo, Japan

² Department of Production Systems Engineering and Sciences, Komatsu University, Ishikawa, Japan

³ Faculty of Mechanical Engineering, Kanazawa University, Ishikawa, Japan

* y.kuri1023@fuji.waseda.jp

Abstract: Numerically simulating the lasing of a fully chaotic billiard laser with selective pumping along an unstable periodic orbit, we show self-organized formation of a “nonlinear scar mode” whose intensity localizes along the unstable periodic orbit.

1. Introduction

For a partially chaotic billiard laser, it has been demonstrated that lasing modes localized along a stable periodic orbit can be selectively excited by forming a pumped region along the orbit [1]. This is possible because the passive cavity (i.e., the cavity without gain) have underlying resonant modes whose intensities are distinctly localized along the stable periodic orbit [2]. Meanwhile, a fully chaotic billiard has no stable periodic orbit, and all of its periodic orbits are unstable. For such a billiard, strong localization of a resonant mode along an unstable periodic orbit has never been reported in previous studies, although weak localization of a resonant mode along an unstable periodic orbit is rarely observed. Such a mode is named a scar mode [3]. Here, we numerically demonstrate that strong localization along an unstable periodic orbit can be observed for a lasing mode of a fully chaotic billiard laser with a partial pumping region formed along the unstable periodic orbit. By a systematic study of relevant resonant modes, we concluded that the localized lasing mode is formed by the nonlinear interaction of multiple resonant modes, either of which does not necessarily exhibit obvious signs of localization along the unstable periodic orbit. Therefore, the scarring is generated in a self-organized manner as a result of nonlinear interaction of multiple resonant modes. We call this type of a localized lasing mode a nonlinear scar mode.

2. Model and Results

We numerically simulate the lasing of the stadium billiard laser by using the Schrödinger-Bloch (SB) model [4]. The stadium billiard is a well-known example of a fully chaotic billiard [5], and the SB model describes the nonlinear interaction between the light field and a gain medium. We focus our attention on the three types of unstable periodic orbit, the diamond orbit (period-four), the v-shaped orbit (period-four), and the horizontal orbit (period-two), and examined the partial pumping along these unstable periodic orbits. In all cases, we observed the formation of a nonlinear scar mode. We confirmed that the superposition of multiple resonant modes can well reproduce the spatial pattern of the nonlinear scar modes. This result indicates that the nonlinear scar mode can be understood as a frequency-locking state of multiple resonant modes [4].

3. Summary

A fully chaotic billiard generally does not have resonant modes whose intensities strongly localize along periodic orbits. However, here we numerically demonstrate that such a billiard is with a gain medium and partially pumped along a periodic orbit, the lasing mode exhibits strong localization along the periodic orbit, which we called a nonlinear scar mode. This lasing mode is explained by the frequency-locking of multiple resonant modes, either of which does not necessarily show obvious signs of localization along the periodic orbit. We can interpret this result as a self-organization for utilizing the gain maximally.

References

- [1] S. Shinohara, T. Harayama, T. Fukushima, M. Hentschel, T. Sasaki, and E. E. Narimanov, “Chaos-assisted directional light emission from microcavity lasers,” *Phys. Rev. Lett.* **104**, 163902 (2010).
- [2] H. E. Türeci, H. G. L. Schwefel, A. D. Stone, and E. E. Narimanov, “Gaussian-optical approach to stable periodic orbit resonances of partially chaotic dielectric micro-cavities,” *Opt. Express* **10**, 752-776 (2002).
- [3] E. J. Heller, “Bound-state eigenfunctions of classically chaotic Hamiltonian systems: Scars of periodic orbits,” *Phys. Rev. Lett.* **53**, 1515-1518 (1984).
- [4] T. Harayama, S. Sunada, and K. S. Ikeda, “Theory of two-dimensional microcavity lasers,” *Phys. Rev. A* **72**, 013803 (2005).
- [5] L. A. Bunimovich, “On the ergodic properties of nowhere dispersing billiards,” *Commun. Math. Phys.* **65**, 295-312 (1979).

Graphene-assisted mode locking of optomechanical combs in a microresonator

Yupei Liang^{1, #}, Hao Zhang^{1, #}, Shi-Da Wen², Yan-Wu Liu², Yanhong Guo¹, Teng Tan^{1, *}, Yunjiang Rao¹, Yun-Feng Xiao², Qi-Fan Yang^{2, *}, Baicheng Yao^{1, *}

¹ Key Laboratory of Optical Fibre Sensing and Communications (Education Ministry of China), University of Electronic Science and Technology of China, Chengdu, China.

² State Key Laboratory for Mesoscopic Physics and Frontiers Science Center for Nano-optoelectronics, School of Physics, Peking University, Beijing, China.

* yaobaicheng@uestc.edu.cn, leonardoyoung@pku.edu.cn, taurus_tan@uestc.edu.cn

Mode locking is a significant process in which resonant modes establish stable synchronization through non-linear interactions [1]. This self-organization enables photonic and electronic sources to deliver coherent pulsed waveforms and underlies scientific applications. In recent years, the realization of soliton mode locking in high-Q microresonators remarkably reduces the device size, opening the technology of microcombs [2]. Recently, dissipative optomechanical solitons have been found in microcavities [3]. Here, we report the deterministic excitation of mode-locked optomechanical microcombs in a graphene-covered silica microresonator. The circulating optical field triggers mechanical oscillations, which in turn modulate the light wave. Once the periodic modulation is strong enough, graphene nonlinear absorption-based modulation enables a localized coherent mechanical wavepacket, leading to deterministic mode-locking with a 7.6 MHz repetition rate, demonstrating a sech^2 spectral envelope and phase noise down to -108 dBc/Hz at a 1 Hz offset, suggesting ultrahigh-precision photonic time-frequency standards for applications such as sensing. This work bridges optomechanics and two-dimensional material optoelectronics, initiating a new physical paradigm with high convenience, reliability, and controllability.

Figure 1a shows the conceptual design of our graphene-assisted silica microresonator for generating optomechanical mode-locked frequency combs. A silica microsphere with a diameter of approximately $610 \mu\text{m}$ supports both optical and mechanical modes. The graphene nanolayer is positioned 10°C above the equator plane (Fig. 1b). The mechanical mode situated at 7.6 MHz has a quality factor of 7480, which agrees well with the simulated result (Figs. 1c and 1d). The measured optical Q factor of this device is approaching 10^8 . Considering Pauli blocking in graphene, with continuous tuning of the pump laser into resonance, sharp phase-locked pulses are excited from a flat background.

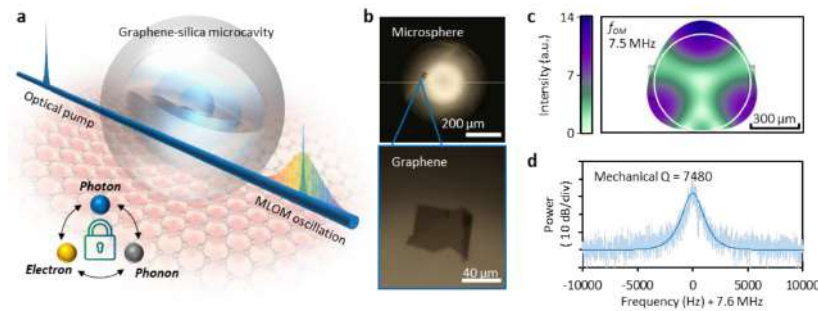


Fig. 1. Conceptual design and mechanism of the optomechanical mode in a graphene-assisted silica microresonator. **a**, Schematic diagram. By detuning a pump laser into an optical mode, the increasing intracavity optical power excites optomechanical oscillations via ‘photon-phonon’ interactions. The optomechanical oscillations are then localized and locked by the graphene due to the blocking of ‘photon-electron’ interactions. **b**, Device pictures. The diameter of the silica microsphere is $610 \mu\text{m}$, and the graphene size is $60 \times 40 \mu\text{m}^2$. **c**, Passive transmission of the graphene-assisted microresonator. The group FSR is ≈ 91.6 GHz and contains 126 mode resonances. By zooming in on the transmission, we measure that a typical Q factor of the optical modes is approaching 10^8 . **d**, Measured mechanical resonance, showing a mechanical Q = 7480. The dark blue curve represents Lorentz fitting.

Fig. 2a demonstrates the experimental setup. We use a tunable continuous-wave laser diode as the pump and fix its output power at 200 mW, while another tunable laser is used to beat the signal down to radio frequency. The frequency difference between these two lasers is set to be 2 GHz, and it remains fixed during the scanning process, using an electronic synchronizer. Fig. 2b shows the measured evolution trace of the microcavity’s output during laser scanning. With a scanning speed of 2.5 GHz/s, starting from 1550.321 nm, the range covered in this process is 5 GHz, including the entire resonance, considering thermal effects. During the pump scanning, the optomechanical oscillation traverses four states in sequence: sinusoidal, chaotic, cnoidal, and mode locking (Fig. 2c and 2d). When the intracavity power is high enough, the system enters a regime in which only coherent pulses remain (state iv). The device outputs a

quasi- sech^2 shaped spectrum in the frequency domain, with a stable 7.6 MHz repetition rate and a 3 dB-bandwidth of approximately 0.18 GHz. In Fig. 2e, we zoom in on a single pulse of state iv in Fig. 2c, showing the pulse duration and internal structure of the measured pulse. In Fig. 2f, the single-sideband phase noise (SSB-PN) of the mode-locked state reaches -39 dBc/Hz at 1 Hz offset, and approaches -108 dBc/Hz at 1 kHz offset. The phase noise curve of the optomechanical comb fits the $f^{-2.3}$ trend, suggesting that its noise is primarily determined by white noise.

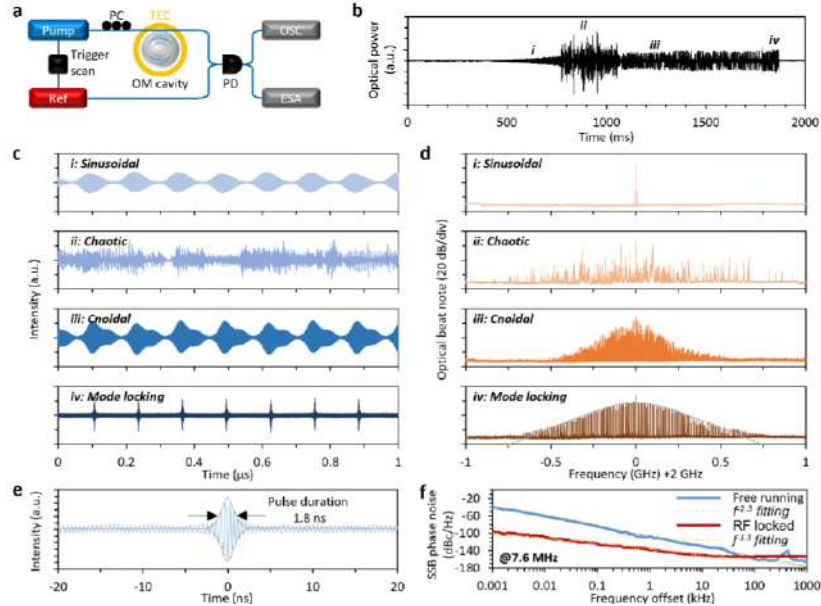


Fig. 2. Optomechanical evolution and time-frequency measurements. **a**, Experimental setup. PC: polarization controller, PD: photodetector, OSC: oscilloscope, ESA: electrical spectral analyzer. **b**, Evolution of the optomechanical oscillation in a resonance located at 1550.321 nm. The speed of the pump frequency scanning is 2.5 GHz/s. The optomechanical wave evolves through periodic, chaotic, cnoidal, and single mode locking states (i-v). **c & d**, Temporal and spectral measurements in state i to state iv. The resonant mechanical waves exhibit comb-like spectra, corresponding to stable pulses with a repetition rate of 7.6 MHz and a pulse period of 131.58 ns. **e**, Measured single pulse of the mode-locked state, showing the pump-reference beating oscillation within. Pulse duration: 1.8 ns. **f**, Measured phase noise of the mode-locked repetition frequency, showing free-running operation (blue curve) and feedback-stabilized operation (red curve).

In summary, we report the formation of optomechanical solitons in a graphene-assisted microresonator. The stable mechanical mode-locking pulses are generated by the mutually coupling process of three waves, namely cavity-confined photons, mechanical-related phonons, and graphene-carried electrons. The optomechanical backaction and saturable optoelectrical energy conversion work in synergy, forming a mode-locking resonant standing wave. The optomechanical mode-locking comb contains 7.6 MHz and harmonics, demonstrating a uniform sech^2 shape spectrally, and delivers stable nanosecond pulses temporally, with phase noise down to -110 dBc/Hz @ 1 Hz. The capability to localize phonons through the graphene-based optoelectronic locking in a micro-nano geometry opens up a new avenue for microcavity-based optomechanical applications, such as acoustic comb formation, radio-frequency clocks, gyroscopes, and high-precision sensing[4].

References

- [1] Haus, H. A. Mode-locking of lasers. *IEEE J. Sel. Top. Quantum Electron.* **6**, 1173–1185 (2000).
- [2] Kippenberg, T. J., Holzwarth, R. & Diddams, S. A. Microresonator-Based Optical Frequency Combs. *Science* **332**, 555–559 (2011).
- [3] Zhang, J. et al. Optomechanical dissipative solitons. *Nature* **600**, 75–80 (2021).
- [4] Tan, T. et al. Multispecies and individual gas molecule detection using Stokes solitons in a graphene over-modal microresonator. *Nat. Commun.* **12**, 6716 (2021).

Large-scale cluster quantum microcombs

*Ze Wang*¹, *Kangkang Li*^{1,*}, *Yue Wang*¹, *Xin Zhou*², *Yinke Cheng*^{1,2}, *Boxuan Jing*¹, *Fengxiao Sun*¹, *Jincheng Li*², *Zhilin Li*², *Qihuang Gong*^{1,3,4}, *Qiongyi He*^{1,3,4,*}, *Bei-Bei Li*^{2,*}, and *Qi-Fan Yang*^{1,3,4,*}

¹ State Key Laboratory for Artificial Microstructure and Mesoscopic Physics and Frontiers Science Center for Nano-optoelectronics, School of Physics, Peking University, Beijing, 100871, China

² Beijing National Laboratory for Condensed Matter Physics, Institute of Physics, Chinese Academy of Sciences, Beijing, 100190, China

³ Collaborative Innovation Center of Extreme Optics, Shanxi University, Taiyuan, 030006, China

⁴ Peking University Yangtze Delta Institute of Optoelectronics, Nantong, Jiangsu, 226010, China

* kangkangli@pku.edu.cn; qiongyihe@pku.edu.cn; libeibei@iphy.ac.cn; leonardoyoung@pku.edu.cn

Abstract: We propose and generate cluster quantum microcombs within an on-chip optical microresonator driven by chromatic lasers. Through resonantly enhanced four-wave mixing processes, we deterministically establish quantum correlations among the continuous quantum variables of 60 modes. © 2024 The Author(s)

Entanglement is indispensable for quantum technologies spanning sensing and computation. If entanglement is established among many elements, they form a cluster state that unlocks novel paradigms such as one-way quantum computing [1] and unconditional quantum teleportation [2]. Recent advances in squeezed light have enabled deterministic preparation of cluster states through time [3], frequency [4, 5], and spatial multiplexing [6].

The recent development of high-Q optical microresonators provides a compact and scalable resolution for generating squeezed light [8–10]. In contrast with table-top optical parametric oscillators, the large free spectral range (FSR) of the microresonator allows for resolving individual qumodes. Bi-partite squeezing has been demonstrated in a monochromatically pumped microresonator via Kerr nonlinearity, in which the qumodes are equidistantly spaced to form a comb-like structure termed as squeezed quantum microcomb [10]. However, realization of CV cluster states involving numerous frequency qumodes remains a challenge for microresonators, primarily due to parasitic losses during collection and detection of squeezed light.

In this work, we entangle over 60 qumodes in a microresonator and obtain continuous variables cluster quantum microcomb. The cluster structures can be reconfigured into one- and two-dimensional lattices by adjusting the pump lasers. The experimental configuration is shown in Fig. 1(a). A silica microresonator with an intrinsic quality factor over 300 M and an FSR of 25 GHz is pumped by bi-chromatic lasers, which are tuned resonant with two optical modes. Entanglement is established between qumodes via degenerate and non-degenerate four-wave mixing (FWM), and to equalize the nonlinear coupling we intentionally set the power of one pump (at mode -1) to 1/4 of the other (at mode 0). The entanglement between qumode pairs is interrogated via homodyne detection using an electro-optic comb derived from the same pump laser that drives the microresonator. With a total detection efficiency of 67%, we have directly measured 3.1 dB bi-partite squeezing for monochromatic pumping (not shown), a record-high value demonstrated in on-chip devices.

Two-mode squeezing is characterized by evaluating the noise variance of $\hat{x}_m + \hat{x}_n$ (Fig. 1(b)). As expected, squeezing is observed for the qumodes (17, -17) and (16, -17), directly resulting from the squeezing operations. The quadrature noise variance for the qumodes (18, -17) and (15, -17), although above the shot noise limit, also varies periodically with the applied phase modulation. This quantum correlation arises from Bragg scattering. While Bragg scattering does not directly induce squeezing, it synergizes with two-mode squeezing operations between the qumodes $(k, -k)$ and $(k, -k - 1)$ to induce effective squeezing between otherwise uncorrelated $(k, -k + 1)$ and $(k, -k - 2)$ pairs.

We also measure the quadrature noise variances for three qumodes and observe quantum interference with respect to their phase relations (Fig. 1(c)). When their phases are aligned, the quadrature yields $\hat{x}_{-17} + \frac{(\hat{x}_{17} + \hat{x}_{16})}{2}$. Significant raw squeezing is achieved for appropriate phase relations between these qumodes, which vanishes if their phases are altered. Notably, the maximum three-mode raw squeezing (1.29 ± 0.10 dB) surpasses that of any related two-mode squeezing (< 1 dB), indicating tri-mode entanglement.

Figure 1(d) shows two-mode squeezing measurements for selected pairs of qumodes. Consistent with our theoretical predictions, squeezing is observed exclusively for qumode pairs with indices summing to 0 and -1. Each qumode is entangled with two others, forming a one-dimensional lattice. The fully-connected cluster quantum microcomb extends from qumode ± 6 to ± 35 , encompassing 60 qumodes. The raw squeezing for selected qumode pairs is summarized in Fig. 1(e), typically ranging from 0.5 dB to 0.9 dB, showing a relatively even distribution over the spectrum. The maximum raw squeezing observed is 1 dB.

In conclusion, we have demonstrated cluster quantum microcombs with up to 60 qumodes using a single microresonator, which can be further engineered via more complex pumping strategies. Leveraging frequency qumodes offers significant simplification in the experimental setup and theoretically allows for infinite elements. Our protocol can potentially provide large-scale cluster states for exploring quantum many-body physics and accomplishing advanced quantum tasks.

References

[1] N. C. Menicucci, P. Van Loock, M. Gu, C. Weedbrook, T. C. Ralph, and M. A. Nielsen, “Universal quantum computation with continuous-variable cluster states,” *Phys. Rev. Lett.* **97**, 110501 (2006).

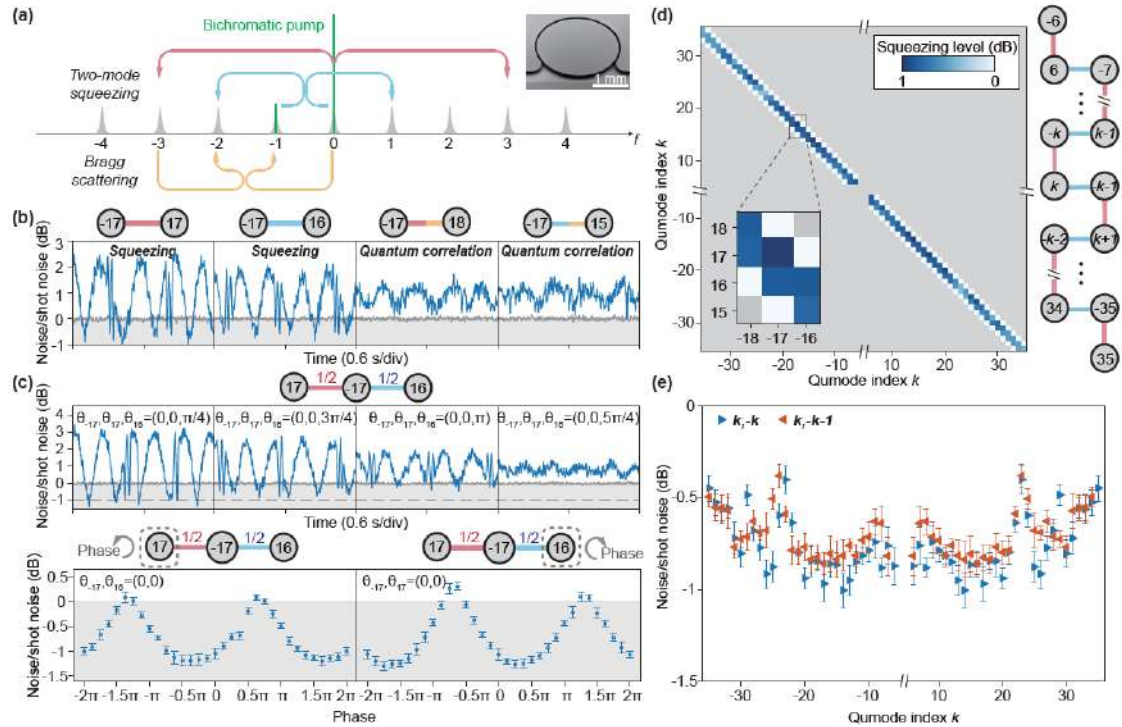


Fig. 1. Cluster quantum microcombs generated by bichromatic pump lasers. (a) Pumping scheme and FWM processes. The power ratio of the pump lasers launched at modes 0 and -1 is 1:0.2. (b) Electrical spectra showing 2-mode quadrature noise variance (blue) relative to shot noise (gray) for representative qumode pairs. (c) Upper panel: Electrical spectra showing 3-mode quadrature noise variance (blue) relative to shot noise (gray). Lower panel: Minimal quadrature noise variance normalized to shot noise when varying the phases of a mode in the LO. (d) Maximal two-mode raw squeezing. Measurements in the gray shades are not taken. The right panel shows the graph structure. (e) Maximal two-mode raw squeezing for qumode pairs $(k, -k)$ and $(k, -k-1)$.

- [2] A. Furusawa, J. L. Sørensen, S. L. Braunstein, C. A. Fuchs, H. J. Kimble, and E. S. Polzik, “Unconditional quantum teleportation,” *Science* **282**, 706–709 (1998).
- [3] S. Yokoyama, R. Ukai, S. C. Armstrong, C. Sornphiphatphong, T. Kaji, S. Suzuki, J.-i. Yoshikawa, H. Yonezawa, N. C. Menicucci, and A. Furusawa, “Ultra-large-scale continuous-variable cluster states multiplexed in the time domain,” *Nat. Photon.* **7**, 982–986 (2013).
- [4] M. Pysher, Y. Miwa, R. Shahrokhshahi, R. Bloomer, and O. Pfister, “Parallel generation of quadripartite cluster entanglement in the optical frequency comb,” *Phys. Rev. Lett.* **107**, 030505 (2011).
- [5] J. Roslund, R. M. De Araujo, S. Jiang, C. Fabre, and N. Treps, “Wavelength-multiplexed quantum networks with ultrafast frequency combs,” *Nat. Photon.* **8**, 109–112 (2014).
- [6] S. Armstrong, J.-F. Morizur, J. Janousek, B. Hage, N. Treps, P. K. Lam, and H.-A. Bachor, “Programmable multimode quantum networks,” *Nat. Commun.* **3**, 1026 (2012).
- [7] L. S. Madsen, F. Laudenbach, M. F. Askarani, F. Rortais, T. Vincent, J. F. Bulmer, F. M. Miatto, L. Neuhaus, L. G. Helt, M. J. Collins et al., “Quantum computational advantage with a programmable photonic processor,” *Nature* **606**, 75–81 (2022).
- [8] A. Dutt, K. Luke, S. Manipatruni, A. L. Gaeta, P. Nussenzevig, and M. Lipson, “On-chip optical squeezing,” *Phys. Rev. Appl.* **3**, 044005 (2015).
- [9] Y. Zhao, Y. Okawachi, J. K. Jang, X. Ji, M. Lipson, and A. L. Gaeta, “Near-degenerate quadrature-squeezed vacuum generation on a silicon-nitride chip,” *Phys. Rev. Lett.* **124**, 193601 (2020).
- [10] Z. Yang, M. Jahanbozorgi, D. Jeong, S. Sun, O. Pfister, H. Lee, and X. Yi, “A squeezed quantum microcomb on a chip,” *Nat. Commun.* **12**, 4781 (2021).

Efficient second and third harmonic generation in dual-layer lithium niobate resonator

Zhenzhong Hao, Xiao Wu, Qiang Luo, Zhang Li, Rui Ma, Fang Bo*, Feng Gao, Guoquan Zhang, and Jingjun Xu

MOE Key Laboratory of Weak-Light Nonlinear Photonics, TEDA Institute of Applied Physics and School of Physics, Nankai University, Tianjin 300457, China

*bofang@nankai.edu.cn

Abstract: Lithium niobate thin film frequency doubler has extensive applications in the preparation of classical and quantum sources. In this study, we successfully fabricated microdisk resonators with a quality factor of 2.2×10^5 in reverse-polarization dual-layer x-cut lithium niobate for the first time. Based on the modal phase matching condition, efficient second harmonic generation with a record normalized conversion efficiency of $\sim 56000\% \text{ W}^{-1}$ and cascaded third harmonic generation with an efficiency of $\sim 6500\% \text{ W}^{-2}$ were obtained in the microdisk resonator. Compared with the periodically poled lithium niobate microcavity, the complex domain structure preparation processes are avoided. Our work provides a scheme for achieving highly efficient second-order nonlinear effects in non-periodically poled microcavities.

Design and fabrication

By applying the dispersion engineering and finite element analysis, we could obtain two modes marked as $\text{TE}_{00,\text{FF}}$ and $\text{TE}_{01,\text{SH}}$ that fulfill the MPM condition. The effective mode refractive indexes of the two modes and the effective nonlinear coefficient along with θ , are given in Figure 1(a) and (b). Figure 1(c) and (d) are the mode field distribution of $\text{TE}_{00,\text{FF}}$ and $\text{TE}_{01,\text{SH}}$, respectively. The inset in Figure 1(d) is the sketch of the dual-layer lithium niobate microdisk.

Due to the lack of symmetry in the z direction of mode $\text{TE}_{01,\text{SH}}$, the spatial overlap between $\text{TE}_{00,\text{FF}}$ and

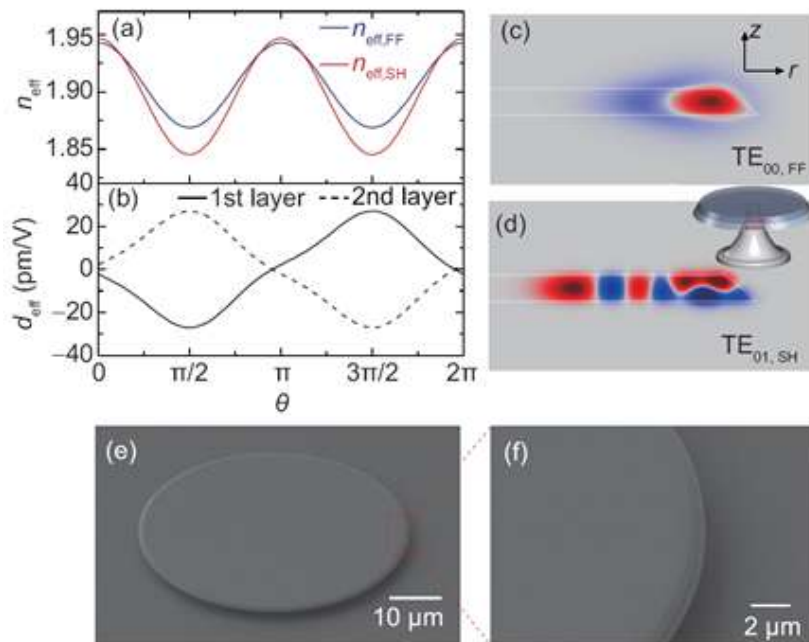


Fig. 1. Design and characterizations of the microdisk on reverse-polarization dual-layer x-cut LNTF. (a) Effective mode refractive indexes of $\text{TE}_{00,\text{FF}}$ and $\text{TE}_{01,\text{SH}}$ along with θ . (b) Effective nonlinear coefficient varies with θ for the first layer and the second layer. (c), (d) Mode field distribution of the $\text{TE}_{00,\text{FF}}$ and $\text{TE}_{01,\text{SH}}$, and the inset represents the schematic diagram of the dual-layer microdisk. (e) The SEM image of the microdisk resonator. (f) Detailed SEM image of the edge of the microdisk.

$\text{TE}_{01,\text{SH}}$ could be very low. By introducing reverse-polarization dual-layer thin film lithium niobate structure, the nonlinear coupling strength between $\text{TE}_{01,\text{SH}}$ and $\text{TE}_{00,\text{FF}}$ can be dramatically improved. The theoretical conversion efficiency of the dual-layer LNTF is $230000\% \text{ W}^{-1}$, which is three orders of magnitude higher than $126\% \text{ W}^{-1}$ of the single-layer LNTF. The nonlinear coupling strength g between $\text{TE}_{00,\text{FF}}$ and $\text{TE}_{01,\text{SH}}$ in dual-layer LNTF can be maximized by finely scanning the geometric structure parameters of the microdisk.

References

- [1] X. Wu, Z. Hao, L. Zhang, D. Jia, R. Ma, C. Tao, F. Gao, F. Bo, G. Zhang, and J. Xu, "Second-harmonic generation with a 440000% $W-1$ conversion efficiency in a lithium niobate microcavity without periodic poling," *Laser Photonics Rev.* 18, 2300951 (2024).
- [2] X. Wu, L. Zhang, Z. Hao, Y. Zhang, S. Kang, R. Ma, F. Gao, F. Bo, G. Zhang, and J. Xu, "Efficient cascaded third-harmonic generation in sampled-grating periodically-poled lithium niobate waveguides," *Laser Photonics Rev.* 18, 2300953 (2024).
- [3] Z. Hao, X. Wu, Q. Luo, Z. Li, R. Ma, F. Bo, F. Gao, G. Zhang, and J. Xu, "Efficient second and third harmonic generation in dual-layer lithium niobate microdisk resonator," *Sci. China. Phys. Mech.* 67, 1-6 (2024).

Desynchronisation dynamics of ultrashort dissipative Raman solitons

Zongda Li^{1,2,†}, *Yiqing Xu*^{1,2}, *Stéphane Coen*^{1,2}, *Stuart G. Murdoch*^{1,2} and *Miro Erkintalo*^{1,2}

¹ Department of Physics, University of Auckland, Auckland 1010, New Zealand

² The Dodd-Walls Centre for Photonic and Quantum Technologies, New Zealand

† zongda.li@auckland.ac.nz

Abstract: In this work, we numerically show that ultrashort dissipative Raman solitons can exist under conditions of continuous-wave driving, and we use this fact to elucidate the solitons' desynchronisation dynamics in pulse-driven systems.

1. Introduction

Over the past decade, a wide variety of temporally localised structures have been observed and studied in coherently driven passive Kerr resonators. Arguably the most famous of these is the bright temporal cavity soliton (CS) [1], but some other examples include dark solitons [2], parametrically driven cavity solitons [3,4] and Stokes solitons [5]. The significant interest in these nonlinear structures is motivated not only by their fascinating nonlinear dynamics but also their potential for practical applications. In particular, the frequency domain representation of these structures corresponds to broadband Kerr (microresonator) frequency combs that have found applications in fields ranging from communications to atomic clocks [1].

One notable recently discovered nonlinear structure is the ultrashort dissipative Raman soliton [6,7]. Such Raman solitons arise due to an interplay between dispersion, Kerr nonlinearity and stimulated Raman scattering, resulting in a surprisingly broad soliton spectral bandwidth when compared to conventional CSs under comparable cavity parameters, with Raman solitons as short as 50 fs experimentally realised in a metre-long cavity composed of commercially available optical fibre. Raman solitons also exhibit several other advantageous features, including spontaneous turn-key formation that greatly reduces the complexity of generation, and the ability to operate with zero or low linear detuning that considerably improves driving efficiency.

In Ref. [7], it was experimentally demonstrated that the driving pulse desynchronisation — given by the mismatch between the driving pulse repetition rate and the cavity roundtrip time — is a key parameter that determines the existence and characteristics of the Raman solitons. While the role of desynchronisation can be qualitatively described by considering the phase-matching and group-velocity-matching conditions that underpin the solitons' existence, this analysis does not provide a prediction for the range of desynchronisation over which the solitons exist, nor does it reveal the mechanism through which desynchronisation influences the soliton properties.

In this work, we demonstrate through extensive numerical simulations that pulse-driving is not a critical requirement for the existence of Raman solitons, but that they can also exist in continuous-wave (CW) driven cavities. Furthermore, by examining the properties and existence of CW-driven Raman solitons, we reveal the mechanism through which desynchronisation influences the soliton characteristics in pulse-driven systems. In addition to elucidating the solitons' desynchronisation dynamics, our analysis yields an explanation for the range of desynchronisation over which the solitons exist [8].

2. Results

We begin by numerically demonstrating that Raman solitons can exist even under conditions of CW driving. The solid orange curves in Fig. 1(a) and (b) show the temporal and spectral profile of a stable Raman soliton driven by a CW beam. Interestingly, this CW-driven soliton possesses near identical temporal and spectral characteristics to a Raman soliton driven by pulse train [solid blue curves] for one particular value of the desynchronization. The similarity between the two solitons, despite drastic differences in their driving conditions, highlights an important feature of Raman solitons: while the formation of the Raman soliton is facilitated by time-delayed stimulated Raman scattering, the characteristics of the individual solitons are underpinned by the instantaneous background power experienced by the soliton. To further illustrate this point, Fig. 1(c) compares the evolution of the peak power and spectral bandwidth of CW- and pulse-driven Raman solitons as a function of background power. Two conclusions can be drawn from these results: (1) consistent with our expectation, the characteristics of the solitons under the two driving conditions are nearly identical for all background powers; (2) each background power value provides the soliton with a unique set of characteristics.

The second conclusion is particularly important: there exists a one-to-one mapping between the background power and soliton drift velocity. As demonstrated in Fig. 1(d), the drift velocity of the CW-driven soliton (in the natural reference frame of the cavity) monotonically decreases with increasing background power. Leveraging the observations above, one can construct an explanation for the role of desynchronisation in pulse-driven systems. Specifically, each

temporal position along the background envelope is associated with a set of soliton characteristics. For the soliton to remain stationary atop the background envelope (a necessary condition for achieving steady-state), the soliton is attracted toward the temporal position associated with a critical background power that provides a drift velocity that exactly cancels the desynchronisation. A change in desynchronisation demands a new steady-state drift velocity (and, thus, critical power), leading to a shift in the temporal position of the soliton and giving it a new set of pulse characteristics.

The hypothesis above is corroborated by results illustrated in Fig. 1(e). Here, we performed multiple simulations, each starting with an initial condition that is a steady-state Raman soliton (shown in the upper panel) displaced temporally by various amounts from its stationary position. Then, the evolutions of the soliton position are recorded and depicted in the lower panel as the solid curves. To assist visualisation, the corresponding steady-state background envelope is also depicted as the dashed blue curve. As we can see, the solitons are attracted toward the original steady-state position (i.e., temporal position with the critical power) as expected.

The drift velocity curve [Fig. 1(d)] can be used for the prediction of soliton steady-state position. Specifically, we found the predicted critical power for the given desynchronisation, and the temporal position that is associated with it is marked by the yellow diamond. This point is found to be close to the actual steady-state position of the soliton. This observation can be extended to predict the Raman soliton existence range as a function of desynchronisation, with the minimum desynchronisation given by minimum background power that can sustain Raman soliton, while the maximum desynchronisation is given by the peak power of the background envelope.

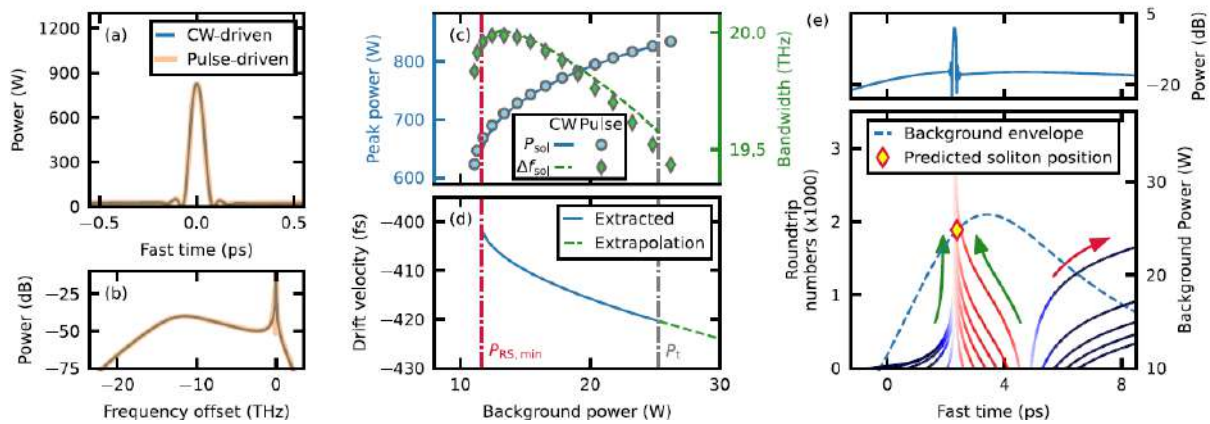


Fig. 1. Comparison of simulated (a) temporal and (b) spectral profiles of Raman solitons driven by CW-beam (solid orange) and train of pulses (solid blue). (c) Solid blue and dashed green curves show Raman soliton peak power (left axis) and bandwidth (right axis) as a function of background power. The solid curves and markers denote results from CW- and pulse-driven simulations, respectively. (d) Raman soliton temporal drift velocity as a function of background power. (e) Simulated responses of the Raman soliton shown in the upper panel when temporally displaced by various amounts. Solid lines in the lower panel indicate the evolution of the soliton's temporal position. The dashed curve shows the steady-state background envelope prior to the significant growth of the Raman signal. The yellow diamond indicates the predicted trapping position.

3. Summary

In conclusion, we have demonstrated that Raman solitons can exist within CW-driven cavities. By examining the existence and properties of the CW-driven Raman soliton, we have revealed the mechanism through which desynchronisation influences the Raman soliton characteristics. This has also enabled us to qualitatively predict the soliton steady-state position and thus the soliton existence range as a function of desynchronisation [8].

References

- [1] T. J. Kippenberg et al., ‘Dissipative Kerr solitons in optical microresonators’, *Science*, 2018.
- [2] X. Xue et al., ‘Mode-locked dark pulse Kerr combs in normal-dispersion microresonators’, *Nat. Photon.*, 2015.
- [3] N. Englebort et al., ‘Parametrically driven Kerr cavity solitons’, *Nat. Photon.*, 2021.
- [4] G. Moille et al., ‘Parametrically driven pure-Kerr temporal solitons in a chip-integrated microcavity’, *Nat. Photon.*, 2024.
- [5] Q.-F. Yang, X. Yi, K. Y. Yang, and K. Vahala, ‘Stokes solitons in optical microcavities’, *Nat. Phys.*, 2017.
- [6] Y. Xu et al., ‘Frequency comb generation in a pulse-pumped normal dispersion Kerr mini-resonator’, *Opt. Lett.*, 2021.
- [7] Z. Li et al., ‘Ultrashort dissipative Raman solitons in Kerr resonators driven with phase-coherent optical pulses’, *Nat. Photon.*, 2024.
- [8] Z. Li et al., ‘Continuous-wave driving elucidates the desynchronisation dynamics of ultrashort dissipative Raman solitons generated in dispersive Kerr resonators’, *Opt. Lett.*, 2024.

List of Participants

Name	Surname	Affiliation	Country
Amal	Jose	OIST Graduate University, Okinawa	Japan
Andrew	Poon	Hong Kong University of Science & Technology	Hong Kong
Andrey	Matsko	NASA Jet Propulsion Laboratory, Pasadena, California	USA
Anna	Petersen	The University of Otago, Dunedin	New Zealand
Beibei	Li	Chinese Academy of Sciences, Beijing	China
Binbin	Nie	Peking University, Beijing	China
Chengcai	Tian	The University of Otago, Dunedin	New Zealand
Christophe	Pin	OIST Graduate University, Okinawa	Japan
Dmitry	Strekalov	The University of Otago, Dunedin	New Zealand
Fangxing	Zhang	Peking University, Beijing	China
Farhan	Azeem	The University of Otago, Dunedin	New Zealand
Florian	Lorenz	Technische Universität Dresden, Dresden	Germany
Florian	Sedlmeir	The University of Otago, Dunedin	New Zealand
Guoping	Lin	Harbin Institute of Technology, Shenzhen	China
Hammad	Khalid	The University of Otago, Dunedin	New Zealand
Harald	Schwefel	The University of Otago, Dunedin	New Zealand
Hugo	Girin	C2N, Université Paris-Saclay, Palaiseau	France
Hui	Cao	Yale University, New Haven, Connecticut	USA
James	Luxon	The University of Otago, Dunedin	New Zealand
Jan	Wiersig	Otto von Guericke University Magdeburg, Magdeburg	Germany
Jordan	Wise	The University of Auckland, Auckland	New Zealand
Josh	Christensen	The University of Otago, Dunedin	New Zealand
Julius	Kullig	Otto von Guericke University Magdeburg, Magdeburg	Germany
Juman	Kim	Seoul National University, Seoul	RO Korea
Junseo	Ha	Seoul National University, Seoul	RO Korea
Kang	Xu	Huazhong University of Science and Technology, Wuhan	China
Keiji	Sasaki	Hokkaido University, Hokkaido	Japan
Kerry	Vahala	Caltech, Pasadena, California	USA
Kyungwon	An	Seoul National University, Seoul	RO Korea
Li	Ge	City University of New York, New York	USA
Linjie	Shao	The University of Otago, Dunedin	New Zealand
Luke	Trainor	The University of Otago, Dunedin	New Zealand

Maika	Matogawa	Waseda University, Tokyo	Japan
Mallika	Suresh	The University of Otago, Dunedin	New Zealand
Matthew	Macnaughtan	The University of Auckland, Auckland	New Zealand
Matthew	Seo	Seoul National University, Seoul	RO Korea
Mengjie	Yu	University of Southern California, Los Angeles, California	USA
Min	Wang	Chinese Academy of Sciences, Beijing	China
Miro	Erkintalo	The University of Auckland, Auckland	New Zealand
Jalaludeen	Mohammed	OIST Graduate University, Okinawa	Japan
Muhan	Choi	Kyungpook National University, Daegu	RO Korea
Nicholas	Lambert	The University of Otago, Dunedin	New Zealand
Peigen	Ni	Natural Science Foundation of China, Beijing	China
Qi-Fan	Yang	Peking University, Beijing	China
Qi-Tao	Cao	Peking University, Beijing	China
Quan-Xin	Luo	Peking University, Beijing	China
Ramgopal	Madugani	OIST Graduate University, Okinawa	Japan
Rui-Qi	Zhang	Peking University, Beijing	China
Ruokai	Zheng	Peking University, Beijing	China
Samuel	Begumya	OIST Graduate University, Okinawa	Japan
Scott	Papp	NIST, Maryland	USA
Seongju	Lee	Kyungpook National University, Daegu	RO Korea
Shuai	Wan	University of Science and Technology of China, Hefei	China
Shui-Jing	Tang	Peking University, Beijing	China
Shuqi	Chen	Nankai University, Tianjin	China
Síle	Nic Chormaic	OIST Graduate University, Okinawa	Japan
Songyi	Liu	Beijing University of Posts and Telecommunications, Beijing	China
Stuart	Murdoch	The University of Auckland, Auckland	New Zealand
Suwan	Sun	Shanghai University, Shanghai	China
Takahisa	Harayama	Waseda University, Tokyo	Japan
Takao	Aoki	Waseda University, Tokyo	Japan
Takasumi	Tanabe	Keio University, Yokohama	Japan
Timothy	Newman	The University of Sydney, Sydney, NSW	Australia
Vahid	Sandoghdar	Max Planck Institute for the Science of Light, Erlangen	Germany
Wang	Liao	The University of Auckland, Auckland	New Zealand
Warwick	Bowen	The University of Queensland, St. Lucia, Queensland	Australia
Wenjie	Wan	Shanghai Jiao Tong University, Shanghai	China
Wensong	Yan	Peking University, Beijing	China
Xi	Yang	University of Electronic Science & Technology of China, Chengdu	China

Xiaochong	Yu	Beijing Normal University, Beijing	China
Xiaomin	lv	Peking University, Beijing	China
Xing	Jin	Peking University, Beijing	China
Yanne	Chembo	University of Maryland, Maryland	USA
Yanwu	Liu	Peking University, Beijing	China
Yicheng	Zhu	Shanghai Jiao Tong University, Shanghai	China
Yongyong	Zhuang	Xi'an Jiaotong University, Xi'an	China
Yoshikazu	Kuribayashi	Waseda University, Tokyo	Japan
Youling	Chen	Chinese Academy of Sciences, Beijing	China
Ze	Wang	Peking University, Beijing	China
Zhen	Shen	University of Science and Technology of China, Hefei	China
Zhi-Gang	Hu	Chinese Academy of Sciences, Beijing	China
Zongda	Li	The University of Auckland, Auckland	New Zealand

Biographies of Invited Speakers



Prof. Andrew Wing On Poon

Professor at the Department Electronic and Computer Engineering
The Hong Kong University of Science and Technology

Biography: Prof. Andrew Wing On Poon received his B.A. (Hons.) degree from The University of Chicago, Illinois, USA in 1995, and his M. Phil and Ph. D. degrees from Yale University, Connecticut, USA, in 1998 and 2001, all in Physics. In 2001, he joined the Department of Electronic and Computer Engineering, The Hong Kong University of Science and Technology, as an assistant professor. Since then, he has risen through the ranks and is now a professor. Since 2002, Prof. Poon and his students at HKUST have been spearheading diverse research directions in optical microcavities leveraging wafer-level silicon nanofabrication processes. The Poon group is among the early players of the now global silicon photonics community in academia and industry. He is a Senior Editor of the IEEE Photonics Technology Letters. He was the General Chair of the 6th International Workshop on Microcavities and Their Applications (WOMA) 2022, Hong Kong. In 2022, Prof. Poon was elected a Fellow of Optica.



Dr Andrey B. Matsko

Group Leader

NASA Jet Propulsion Laboratory, Pasadena, California, USA

Biography: Dr. Andrey Matsko leads the Frequency and Timing Advanced Instrument Development Group of Jet Propulsion Laboratory supporting the Deep Space Network's Time and Frequency System as well as Deep Space Atomic Clock developments and other edge cutting time and frequency projects. Prior to that he worked at OEwaves Inc., where he took positions of Principal Engineer and, later, Chief Technology Officer. He was responsible for the business development, program management, and R&D research in the fields of timing, frequency and control, RF photonics, quantum and nonlinear optics. He contributed to the development of technology involving crystalline whispering gallery mode resonators, optical fibers, and atomic vapor cells; including electro-optical modulators, RF photonic receivers, optical and RF photonic filters, delay lines, clocks, magnetometers, gyroscopes, oscillators, and lasers. He is the author of more than 200 peer reviewed articles and a co-inventor in 50 U.S. patents. Dr. Matsko is a Fellow of the APS, Optica, IEEE, and SPIE.



Prof. Baicheng Yao

Professor of Information Science

University of Electronic Science and Technology of China (UESTC), Chengdu, China

Biography: Prof. Yao received his Ph.D. in 2016 (co-educated at UESTC, CHN and the University of California, Los Angeles, USA) and worked as a research associate at the University of Cambridge (UK) from 2017-2018. Currently a full professor at UESTC, he is a senior member of Optica, COS and IEEE. His research focuses on microcavity frequency combs and related sensing technologies. Prof. Yao's group has published over 80 papers in scientific journals such as Nature, Nature Photonics, Nature Communications, Science Advances and Physical Review Letters. He has also delivered more than 30 invited talks at conferences including CLEO, OFS and ACP. He serves as the director of the Young Editorial Board of Photonic Sensors, and the Young Editor of Light: Science & Applications.



A/Prof. Beibei Li

Associate Professor at Institute of Physics
Chinese Academy of Sciences (CAS), Beijing, China

Biography: Beibei Li is an associate professor at the Institute of Physics, Chinese Academy of Sciences (CAS). She obtained her Bachelor's degree from Tianjin University in 2009 and Ph.D degree from Peking University in 2014. Following this, she pursued postdoctoral research at the University of Queensland in Australia from 2014 to 2018. Since October 2018, she has been working at the Institute of Physics, CAS. Dr. Li's research primarily focuses on high-quality optical microcavities and their applications in precision sensing and nonlinear optics, ranging from ultrasound sensing, magnetometry, Brillouin lasers, and microcomb, etc. She has published over 40 papers, which have been cited more than 2700 times. In addition, Dr. Li has been invited to serve as an assistant editor for Photonics Research, The Innovation, and Photonic Sensors, as well as a reviewer for various journals. In recognition of her achievements, she was awarded the "Raoyutai fundamental Optics Prize" and received the "Excellent Young Scientist fund of NSFC" in 2022.



Dr Dmitry V. Srekalov

Researcher at Resonant Optics Lab

University of Otago, Dunedin New Zealand

Biography: Dr. Dmitry V. Srekalov completed his M.S. degree at Moscow State University in 1994, and Ph.D. at University of Maryland in 1997, specializing in nonlinear and quantum optics. He received postdoctoral experience at New York University and at Rice University in 1997-2000 where he conducted experimental research with cold atoms and BEC. Since 2000 he is a researcher at the Quantum Science and Technology group of Jet Propulsion Lab of Caltech. The main field of his current scientific interests is the optics of whispering gallery mode resonators. Working in this field, Dr. Srekalov maintains close collaborations with the Max Planck Institute for Physics of Light in Erlangen, Germany, through extended Humboldt Fellowship, and with the University of Otago, New Zealand, through the Royal Academy of sciences' Catalyst Fellowship. Dr. Srekalov published over 90 peer-reviewed physics papers cited in more than 5000 other articles. He also authored several popular articles in Optics and Photonics News and Nature Photonics and book chapters, as well as nine US patents. Besides the scientific research, Dr. Srekalov's JPL responsibilities include software development and data analysis for several NASA missions, attracting research funds, and project management.



Dr Gabriella Gardosi

Research Fellow at Aston Institute of Photonic Technologies (AIPT)

Aston University, Birmingham, United Kingdom

Biography: Dr Gabriella Gardosi is a research fellow at the Aston Institute of Photonic Technologies, where she has been advancing high-precision microresonator fabrication on the SNAP (Surface Nanoscale Axial Photonics) platform since 2017 under Prof. Misha Sumetsky. Previously an artist, Gabriella transitioned into photonics, where her artistic background strongly influences her approach to scientific innovation, merging technical precision with creativity. She completed her PhD in Photonics at Aston University in 2022, where she developed a 'slow-cooking' technique for picometre-level control in microresonator fabrication, enabling applications in optical circuit devices and optofluidic sensing. In 2023, she began her Leverhulme Early Career Fellowship, focusing on sensor development for sustainable and food-safe packaging.

Recognized as one of *Electro Optics* magazine's *Photonics 100* in 2023, Dr. Gardosi has contributed to multiple conferences and workshops. She is also committed to diversity in STEM, founding the WEST society (Women in Engineering, Science, and Technology) at Aston University, and recently organizing the FreQomb workshop, which brings together international experts on frequency comb technology.



A/Prof. Guoping Lin

Associate Professor at School of Science
Harbin Institute of Technology, Shenzhen, China

Biography: Guoping Lin, Ph.D., is an Associate Professor at the School of Science, Harbin Institute of Technology (Shenzhen). He received his bachelor's from Xiamen University and joint doctoral degrees in optics and physics from Xiamen University and École Normale Supérieure of Paris in 2010. He conducted four years of postdoctoral research at NASA's Jet Propulsion Laboratory and FEMTO-ST Institute in France. He then joined Huazhong University of Science and Technology, contributing to laser system development for future space-based gravitational wave detection for four years. His research interests lie in nonlinear optical frequency conversion and light-matter interactions exploiting crystalline high-Q whispering gallery mode resonators.



Prof. Hui Cao

John C. Malone Professor of Applied Physics, Professor of Physics, and Professor of Electrical Engineering
Department of Applied Physics, Yale University, New Haven, CT, USA

Biography: Hui Cao is the John C. Malone Professor of Applied Physics, a Professor of Physics, and a Professor of Electrical Engineering at Yale University. She received her Ph.D. degree in Applied Physics from Stanford University in 1997. Prior to joining the Yale faculty in 2008, she was on the faculty of Northwestern University for ten years. Her technical interests and activities are in the areas of mesoscopic physics, complex photonic materials and devices, nanophotonics, and biophotonics. Cao is a Fellow of IEEE, AAAS, APS and OSA, and an elected member of the National Academy of Sciences, and the American Academy of Arts and Sciences.



Prof. Jan Wiersig

Professor of Theoretical Physics

Department of Theory of Condensed Matter, Otto-von-Guericke-Universität Magdeburg, Magdeburg, Germany

Biography: Dr Jan Wiersig is a full professor of theoretical physics at Otto-von-Guericke-Universität Magdeburg, Germany. He received his Ph.D. degree in theoretical physics from Universität Bremen in 1998. He was a Postdoctoral Fellow of theoretical physics at Queen Mary and Westfield college (London), MPI für Physik komplexer systeme (Dresden) and Universität Bremen from 1998-2008. He has 156 peer-reviewed publications in PRL, Nature, PNAS, etc. Since 2023 he is a fellow of Optica (formerly OSA). His research interests include quantum optics, wave chaos and non-Hermitian effects in optical systems, and light-matter interaction in semiconductor micro- and nanostructures.



Prof. Keiji Sasaki

Professor Emeritus at Research Institute for Electronic Science
Hokkaido University, Hokkaido, Japan

Biography: Keiji Sasaki is a Professor Emeritus of Research Institute for Electronic Science (RIES), Hokkaido University. He received PhD degree in Applied Physics from Osaka University in 1986. He held a Professor position of RIES since 1997 and worked as a Director of RIES (2005-2009) and a Head of Nanotechnology Research Center (2009-2015). His research interests are in nanophotonic, plasmonics and quantum optics. He is the General Chair of the 4th International Workshop on Microcavities and Their Applications (WOMA2015), Sapporo, Japan.



Prof. Kerry J. Vahala

Professor of Applied Physics

Department of Applied Physics and Materials Science, Caltech, California, USA

Biography: Kerry Vahala is Professor of Applied Physics at Caltech and holds the Jenkins Chair in Information Science and Technology. His research on chip-based high-Q optical resonators and related nonlinear optical devices has advanced miniature frequency and time systems, microwave sources, parametric oscillators, astrocombs and gyroscopes. Vahala also made early contributions to the subject of cavity optomechanics and demonstrations of chip-based devices to cavity QED phenomena. A member of the National Academy of Engineering and Fellow of the IEEE and Optica, he received the IEEE Sarnoff Medal for research on quantum-well laser dynamics, the Alexander von Humboldt award and MPQ Distinguished Scholar Award for work on ultra-high-Q optical microcavities, a NASA achievement award for application of microcombs to exoplanet detection, and the Optica Paul F. Forman Team Engineering Excellence Award for a 2-photon optical clock. Vahala is also the Executive Officer of the Department of Applied Physics and Materials Science at Caltech.



Prof. Kyungwon An

Professor of Physics

Department of Physics & Astronomy, Seoul National University, Seoul, Republic of Korea

Biography: Kyungwon An received his BS and MS in physics from Seoul National University, and his Ph.D. from Massachusetts Institute of Technology working with Michael S. Feld on realizing the first single-atom laser. He stayed at MIT as a postdoc and then a research scientist until 1998. He then moved to Korea Advanced Institute of Science and Technology and stayed there as Professor of Physics until 2001. Since then, he has been Professor of Physics at Seoul National University, performing various experiments on nonclassical field generation in an atom-cavity system as well as quantum chaos and non-Hermitian physics in microcavity lasers. He received Vinci d'Excellence Award in 1995 and Young Scientist Award from the Korean Ministry of Science and Technology in 1999 for the development of the first single-atom laser. He received Atomic and Molecular Physics Award from the Korean Physical Society in 2018, Sung-Do Optical Science Award from the Korean Optical Society as well as National Academy of Sciences Award in 2021 for his work on the coherent single-atom superradiance. Kyungwon An started the WOMA in 2009 and served as co-chair of the second WOMA in 2011.

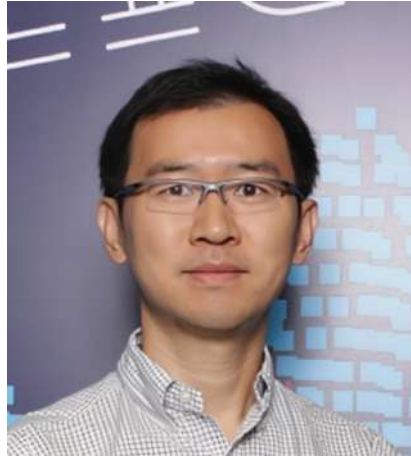


Prof. Lan Yang

Edwin H. & Florence G. Skinner Professor of Engineering

Electrical & Systems Engineering, Washington University in St. Louis, Missouri, USA

Biography: Lan Yang is the Edwin H. and Florence G. Skinner professor in the Electrical and Systems Engineering Department at Washington University in St. Louis, USA. She is also the editor-in-chief of *Photonics Research*. She received her M.S. in materials science in 2000 and Ph.D. in applied physics at Caltech in 2005. She enjoys investigating physics in photonic resonators and exploring their diverse applications, including communication, quantum technologies, sensing, spectroscopy, and imaging, etc. Her research in parity-time-symmetry and non-Hermitian physics in resonators has led to a series of discoveries for unconventional control of light transport in photonic structures. She received the NSF CAREER Award in 2010 for her work on nanoparticle detection and sizing using on-chip optical resonators. She also received the 2010 Presidential Early Career Award for Scientists and Engineers (PECASE). She is a Fellow of Optica, the Institute of Electrical and Electronics Engineers (IEEE), the American Physical Society (APS), the American Association for the Advancement of Science (AAAS), and the American Institute for Medical and Biological Engineering (AIMBE).



Prof. Li Ge

Professor at College of Staten Island and The Graduate Center
City University of New York, NY, USA

Biography: Li Ge received his PhD in Physics from Yale University in 2010, with his thesis focusing on laser physics in complex and disordered media, including wave-chaotic lasers and random lasers. Before joining the City University of New York in 2013, he was a postdoctoral associate in the Department of Electrical Engineering at Princeton University. His current research interests include nonlinear and non-Hermitian phenomena in optics and photonics. Li Ge has published more than 150 journal articles and conference proceedings in top scientific journals such as Science, Nature, Nature Physics, Nature Photonics, and PRL, with a total citation of over 10000 with an h-index of 43. He has been on the editorial boards and/or a guest editor for PRB, Photonics Research, APL, and PNAS. He is a Fellow of Optica since 2024.



Prof. Martina Hentschel

Professor of Theoretical Physics of Complex Dynamical Systems

Institute of Physics, TU Chemnitz, Chemnitz, Germany

Biography: Prof. Martina Hentschel holds a professorship for Theoretical Physics of Complex Dynamical Systems at TU Chemnitz, Germany, performing research on mesoscopic physics in optical and condensed matter systems such as microresonators and graphene. After studying physics in Dresden and London, she obtained her PhD in 2001, followed by Postdocs at Duke University, Regensburg University, and at ATR Labs Kyoto. From 2006 to 2012 she was leading an Emmy-Noether research group at MIPKS Dresden and was appointed a professor for Theoretical Physics at TU Ilmenau from 2012 to 2020, when she moved to Chemnitz.

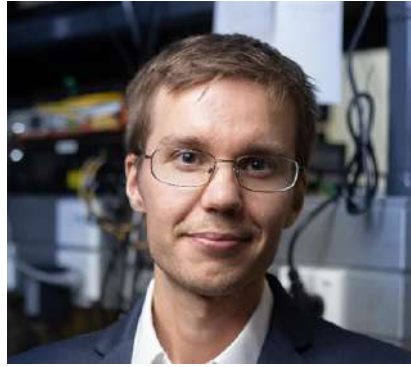


Asst. Prof. Mengjie Yu

Gabilan Assistant Professor

Department of Electrical and Computer Engineering, University of Southern California, USA

Biography: Mengjie Yu is Gabilan Assistant Professor of Department of Electrical and Computer Engineering at the University of Southern California, and will be an Assistant Professor of Electrical Engineering and Computer Science and Weber Family Engineering Faculty Fellow at the University of California, Berkeley starting Jan 2025. She received her Ph.D. degree in Electrical and Computer Engineering in 2018 from Cornell University and held research staff associate position in Applied Physics and Mathematics at Columbia University from 2015-2018. She is a postdoctoral fellow in the John A. Paulson School of Engineering and Applied Sciences at Harvard University from 2018-2021. Her research group focuses on developing nanoscale nonlinear and quantum photonics devices for optical communication, computing, sensing, and metrology. She serves on the Early Career Editorial Advisory Board for APL Photonics. She is the 2020 the Optica (formerly OSA) Ambassador, the Caltech 2019 Young Investigator Lecturer and received DARPA Young Faculty Award at 2023.



A/Prof. Miro Erkintalo

Associate Professor in Physics

Faculty of Science, University of Auckland, Auckland, New Zealand

Biography: Miro was born and educated in Finland, obtaining the degree of Doctor of Science in Technology in 2012. He has been working at The University of Auckland in New Zealand since 2012 in various roles. He is currently an Associate Professor in Physics, conducting experimental and theoretical research on coherently driven nonlinear optical resonators.



Prof. Muhan Choi

Professor at School of Electronics Engineering
Kyungpook National University (KNU), Daegu, Korea

Biography: Muhan Choi is a full professor at the School of Electronics Engineering at Kyungpook National University (KNU). He received his Ph.D. in physics from Sogang University, South Korea, in 2003. From 2005 to 2008, he was a postdoctoral researcher at the Advanced Telecommunications Research Institute International (ATR) in Kyoto, Japan. Before joining KNU, he worked as a senior researcher at the Electronics and Telecommunications Research Institute (ETRI). His main research interests are in the investigating and advancing micro/nano photonic devices based on metamaterials and transformation optics. He has published papers on these topics in major journals, including Nature, Nature Photonics, Nature Materials, etc.



Asst. Prof. Qi-Fan Yang

Assistant Professor and PI at Laboratory of Integrated Photonics and Precision Measurement

State Key Laboratory for Artificial Microstructure and Mesoscopic Physics and Frontiers Science Center for Nano-optoelectronics, School of Physics, Peking University, Beijing, China

Biography: Qi-fan Yang, an assistant professor at Peking University, is committed to the study of high-quality nonlinear optical microresonators. He has developed miniaturized optical frequency combs, namely integrated microcombs, which can be integrated on photonic chips using standard CMOS techniques. His research focuses on developing devices and applications of integrated microcombs. Yang had a keen interest in photonics while he was an undergrad, so during his Ph.D., he joined the research group of Professor Kerry Vahala, a leader in the field of optical microresonators, at the California Institute of Technology, and chose integrated microcombs as his research direction. After receiving his Ph.D. in 2019, Yang set himself on a research direction that focuses on the realization of chip-level fully integrated microcombs. In November 2020, he returned to his alma mater, Peking University, to set up a laboratory and work as an assistant professor. His main research direction is to develop photonic chips related to integrated microcombs and provide commercial-available high-performance coherent laser sources for integrated optoelectronics.



Dr Scott B. Papp

Senior Investigator at Time and Frequency division
National Institute of Standards and Technology, Boulder, Colorado, USA

Lecturer at Department of Physics
University of Colorado, Boulder, Colorado, USA

Biography: Scott B. Papp received the Ph.D. degree from the University of Colorado, Boulder, CO, USA, in 2008 for experiments on long-sought beyond mean-field physics in Bose-Einstein condensates. He is a Physicist in the NIST Time and Frequency Division and a Lecturer with the University of Colorado, Boulder. From 2008 to 2010, he worked with Caltech as a Postdoctoral Fellow at the Center for the Physics of Information on atomic ensemble quantum memories and multipartite entanglement. Since 2010, he has been working with NIST, leading investigations of Kerr frequency combs, and other integrated-photonics devices.



Asst. Prof. Shui-Jing Tang

Assistant Professor at the National Biomedical Imaging Center
Peking University, Beijing, China

Biography: Dr Shui-Jing Tang is an Assistant Professor at the National Biomedical Imaging Center at Peking University. She earned her PhD and completed her postdoctoral training at the School of Physics, Peking University, before joining the National Biomedical Imaging Center at the College of Future Technology, Peking University, in 2024. Her lab focuses on the development of micro-nanoscale optical probes, including microcavity-based optical sensors and intracellular lasers, for applications in mechanobiological spectroscopy and microscopy.



Prof. Síle Nic Chormaic

Professor and PI at Light-Matter Interactions for Quantum Technologies (LMI-QT) Unit
Okinawa Institute of Science and Technology (OIST) Graduate University, Okinawa, Japan

Biography: Síle is an atomic and laser physicist and heads the Light-Matter Interactions for Quantum Technologies Unit at OIST since 2011. Having studied and worked in Ireland, England, France, Austria, Australia, Germany, and Japan, she's passionate about travel and using her international experience and viewpoint to improve the status of women in academia.

Aside from her research in basic physics, she exploits her knowledge to develop optics-based tools for a range of topics that branch across to other disciplines, such as neuro-imaging and environmental monitoring. In her spare time, when not travelling overseas, she enjoys exploring the many islands of the Ryukyu Archipelago in Japan by foot or bicycle; 2020 was a particularly fruitful year for this pastime due to the COVID pandemic.

In recent years, Síle has been running a programme that allows displaced students from Ukraine and Russia to continue their scientific studies on Okinawa. She considers this island paradise to be a perfect place for healing, since nature and living in harmony with the seasons play an important daily role for everyone on it. She is an active member of two professional societies, Optica and SPIE, and recently joined the latter's committee on equity, diversity and inclusion.

She hopes her main legacy will be the opportunities she has provided to students from diverse socio-economic and geographical backgrounds to be empowered through education and research for the betterment of society.



A/Prof. Stuart Murdoch

Associate Professor of Physics, PI at Laser Lab
Faculty of Science, University of Auckland, New Zealand

Biography: Stuart Murdoch is an Assoc. Professor in Physics at the University of Auckland, New Zealand. His current research interests include nonlinear optics and optical microresonators.

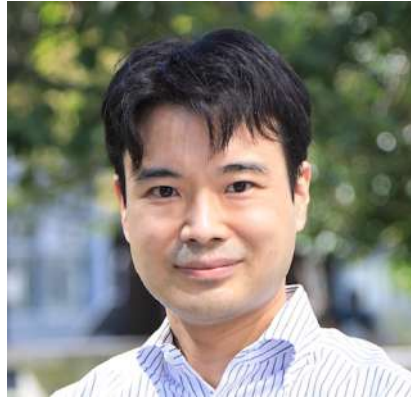


Prof. Takahisa Harayama

Professor at Faculty of Science and Engineering

School of Advanced Science and Engineering, Waseda University, Tokyo, Japan

Biography: Takahisa Harayama received the Ph. D. degree in physics from Waseda University, Tokyo, Japan, in 1993. He worked as a Research Associate with Waseda University until 1995. He joined ATR Optical and Radio Communications Research Laboratories in 1995. In 1996, he joined ATR Adaptive Communications Research Laboratories. In 2004, he joined ATR Wave Engineering Research Laboratories, where he was the Head of the Department of Nonlinear Science. In 2009, he joined NTT Communication Science Laboratories, where he was a Research Specialist. In 2011, he joined Toyo University, where he was a Professor in the Department of Mechanical Engineering. In 2014, he joined Waseda University, where he is a Professor in the Department of Applied Physics. Dr. Harayama is a member of the Physical Society of Japan.



Prof. Takao Aoki

Head of the Quantum Optics Group

Department of Applied Physics, Waseda University, Japan

Biography: Prof. Takao Aoki is the head of the Quantum Optics Group at Department of Applied Physics, Waseda University in Japan, and the Chief Scientific Officer at the quantum hardware startup Nanofiber Quantum Technologies, Inc. He earned BEng, MEng, and PhD in Department of Applied Physics, School of Engineering, The University of Tokyo. His research focuses on quantum technologies based on cavity quantum electrodynamics with optical nanofibers and laser-cooled atoms.



Prof. Takasumi Tanabe

Professor at Department of Electronics and Electrical Engineering
Keio University, Tokyo, Japan

Biography: He received his B.S. in Electronics and Electrical Engineering from Keio University, Yokohama, Japan, in March 2000, and his M.S. and Ph. Design Engineering from the same institution in September 2001 and March 2004, respectively. He was a research associate of the 21st Century Center of Excellence (COE) program in optical and electronic device technology for access networks at Keio University from November 2002 to March 2004. He received a Certificate for Distinguished Activity as Research Assistant at Keio Information, Electronics, and Electrical Engineering Field COE. On April 2004, he joined NTT Basic Research Laboratories, NTT Corporation, in Atsugi, Japan. On April 2010, he moved to Electronics and Electrical Engineering at Keio University, where he is currently a professor. He received Scientific American 50 Award in 2007, and the Commendation for Science and Technology by the Minister of Education, Culture, Sports, Science and Technology, The Young Scientists' Prize in 2010. Dr. Tanabe is a member of the Optical Society, IEEE Photonics Society, SPIE, the Japan Society of Applied Physics, the Laser Society of Japan, and the Institute of Electronics, Information, and Communication Engineers. He is currently a Senior Editor for the IEEE Journal of Selected Topics in Quantum Electronics and Associate Editor for AIP Advances (APS) and Scientific Reports (NPG). He is also serving as a conference committee member in various conferences, including the general chair for CLEO:2022, program chair for CLEO:2020 and ALPS2023, vice-program chair for ICNN, sub-committee chair for CLEO:2018/2019 and CLEO Pacific Rim 2022, the committee in Optica Congress, LEOS, ALPS, APLS, ICO-24, ICNN, WOMBAT, LSJ, and JSAP.



Prof. Vahid Sandoghdar

Director

Max Planck Institute for the Science of Light, Erlangen, Germany

Biography: Born 1966 in Tehran, Iran. Bachelor of Science in Physics from the University of California in Davis (1987), Ph.D. in Physics (supervisors: E. A. Hinds and S. Haroche) from Yale University (1993), Postdoctoral Fellow at École Normale Supérieure (group of S. Haroche) in Paris. Head of the Nano-Optics group and habilitation in Physics at University of Konstanz (Chair of J. Mlynek). Professorship at Eidgenössischen Technischen Hochschule (ETH) Zurich (2001-2011). Recipient of an ERC Advanced Grant (2010). Alexander von Humboldt Professorship at Friedrich-Alexander-Universität Erlangen-Nürnberg and Director and Scientific Member at the Max Planck Institute for the Science of Light in Erlangen since 2011. Fellow of the Optical Society (OSA). Founder of the Max-Planck-Zentrum für Physik und Medizin, a joint research center that aims to address questions in fundamental medical research with physical and mathematical methods.



A/Prof. Wenjie Wan

Associate Professor and PI at Nonlinear Photonics Group

State Key Laboratory of Advanced Optical Communication Systems and Networks, University of Michigan-Shanghai
Jiao Tong University Joint Institute, Shanghai, China

Biography: Wenjie Wan received the B.E. from the Hong Kong University of Science and Technology in 2004 and Ph.D from at Princeton University in 2010, both in Electrical Engineering. After one year postdoctoral training at Yale University, he joint UM-JI as Assistant Professor and jointly appointed by Department of Physics , SJTU. Dr. Wan's publications include Science, Nature Physics, Nature Photonics and Physical Review Letters. He is the recipient of the 2009 Chinese Government Award for Outstanding Self-Financed Students Abroad. In 2011, he is awarded "1000 people's plan (youth)" by Chinese Government.



Prof. Yanne Chembo

Professor at the Department of Electrical and Computer Engineering
University of Maryland, Maryland, USA

Biography: Yanne K. Chembo received a Ph.D. in nonlinear dynamics from the University of Yaounde I, Cameroon (2001-2005), and a Ph.D. degree in photonics from the University of the Balearic Islands, Palma de Mallorca, Spain (2002-2006). He has been a postdoctoral fellow at CNRS in France (2007-2009), and at the NASA/Caltech Jet Propulsion Lab in California (2009-2010). He was a Research Director for the CNRS in France before joining the University of Maryland in 2019, where is currently Professor in the Department of Electrical and Computer Engineering, and Director of the Institute for Research in Electronics and Applied Physics (IREAP). He is a Fellow of SPIE, OPTICA and APS.



Prof. Youling Chen

Professor in Key Laboratory of Optoelectronic Materials and Devices
Institute of Semiconductors, Chinese Academy of Sciences, Beijing, China

Biography: Youling Chen is a professor in Key Laboratory of Optoelectronic Materials and Devices, Institute of Semiconductors, Chinese Academy of Sciences. Youling received her Bachelor's degree and Master's degree from University of Science and Technology of China (USTC), and the Doctor's degree from Peking University. Her research interests include electrically pumped semiconductor microresonators, silicon microresonators with ultra-high-quality factors, and their applications for lasing, ultrasensitive sensing and nonlinear optics.



Asst. Prof. Zaijun Chen

Research Assistant Professor and PI at The Laboratory of Intelligent and Quantum Photonics

Ming Hsieh Department of Electrical and Computer Engineering, University of Southern California, California, USA

Biography: Zaijun Chen received his Ph.D. in Physics with the highest distinction from the Max-Planck Institute of Quantum Optics and the Ludwig Maximilian University of Munich in 2019, for his work on frequency-comb based precision metrology and optical sensing. Before joining USC, he was a postdoctoral fellow in the Quantum Photonics Group at MIT, where he developed photonic AI accelerators and neuromorphic devices using integrated photonics and co-packaged optics.

He is a recipient of the 2023 Optica Foundation Challenge Award, the 2023 SPIE Artificial Intelligence and Machine Learning Award, the OECC/PSC 2022 Best Paper Award, the 2022 Sony Faculty Award, and the 2018 Rao Prize for the best student talk at the international symposium of molecular spectroscopy. He serves on the Early Career Editorial Board for Advanced Photonics. He is a principle investigator for the DARPA NaPSAC program in developing the next-generation AI processors and co-PI for DARPA INSPIRED program for on-chip quantum sensing.

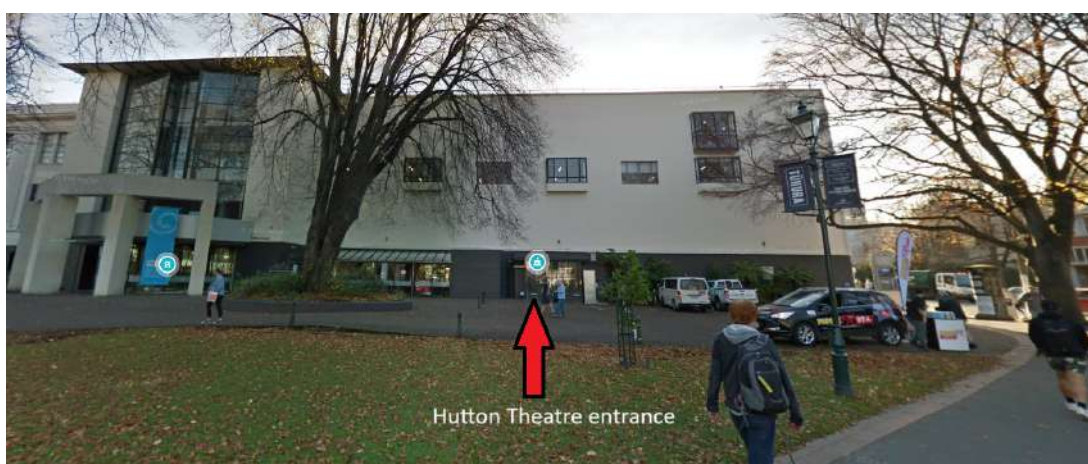
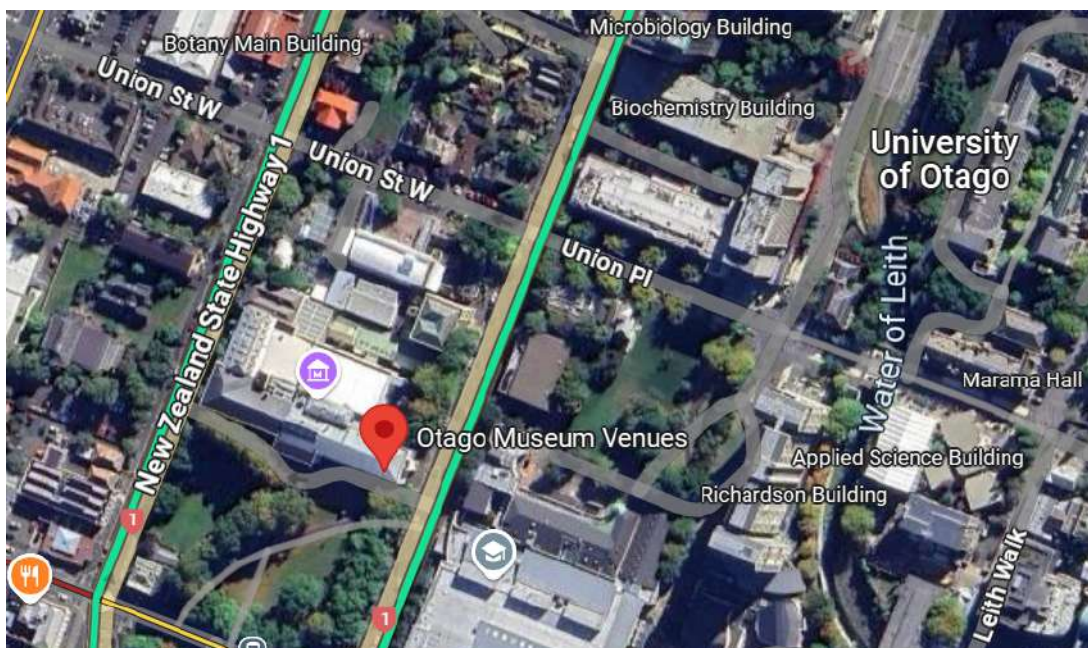
Useful Information

All the **conference talks** will take place at "Hutton Theatre" located on the ground floor in Tūhura Otago Museum. Full address of the venue is:

Otago Museum Venues, Tūhura Otago Museum, 416 Great King Street North, Dunedin North, Dunedin 9016.

Coordinates for the venue are -45.86581112994699, 170.51122695346243.

Google maps hyperlink: <https://maps.app.goo.gl/5jfTzzczeU3yFDqYa8>



Catering, i.e., tea and lunch breaks & Poster Sessions will also take place at Hutton Theatre.

Wi-Fi will be available during the conference.

Conference dinner will take place at "*Larnach Castle*" with buses departing at 18:00 from Tūhura Otago Museum bus stops on Albany Street.

Partner Institutions & Sponsors

